Microfluidics of sugar transport in plant leaves and in biomimetic devices

Rademaker, Hanna

Publication date:
2016

Document Version
Publisher's PDF, also known as Version of record

DTU Physics
Department of Physics

Ph.D. thesis

Microfluidics of sugar transport in plant leaves and in biomimetic devices

Hanna Rademaker

14 September 2016

Supervised by Tomas Bohr and Kaare Hartvig Jensen

Cover image:
Light microscopy image of a *Coleus blumei* leaf. The image shows the natural color.

Microfluidics of sugar transport in plant leaves and in biomimetic devices

Typeset using LaTeX and Ti*k*Z.

Abstract

The physical mechanisms underlying vital plant functions constitute a research field with many important, unsolved problems. Some of these research topics gaining attention in recent years are concerned with the fluid transport in plants.

Plants photosynthesize sugars in their leaves for energy production and growth. These sugars are taken up into the veins of the leaf and then transported efficiently to other parts of the plant via the vascular system. The vascular system of plants has two types of tissue: the *xylem* brings water from the roots up to the leaves, and the *phloem* transports sugars from the sources in the leaves to the sinks in roots, fruits and regions of growth. The transport of sugar solution in the phloem is driven by an osmotic pumping mechanism. The uptake of water from the xylem into the phloem generates a hydrostatic pressure difference between sources and sinks which results in a bulk flow of sugar solution. It is not clear where in the leaf this bulk flow starts, especially in plants that have intercellular connections (*plasmodesmata*) between the phloem and the cells surrounding the veins. In these plants bulk flow could be involved in the process of sugar loading into the veins.

We studied the physics of two basic mechanisms for sugar loading: the *polymer trap* and *passive loading*. The polymer trap is an active mechanism, which is characterized by an elevated concentration of sugars inside the veins compared to the rest of the leaf. This is achieved with the help of enzymes combining sucrose molecules entering the vein through plasmodesmata into larger sugar molecules. These molecules are then too large to move back out of the vein. In order for this system to work, the plasmodesmata have to act as extremely precise filters. Microscopy studies show that these plasmodesmata are very small, in fact they are too small to resolve their exact cross section available to transport. In our theoretical model, we approximated the plasmodesmata as cylindrical slit pores and investigated whether the pores could be small enough to fulfill the filtering function, and at the same time large enough to allow for sufficient transport of sucrose. We found that this mechanism is indeed feasible. We could further conclude that sugar is not only transported by diffusion, but is partly advected through the plasmodesmata by a bulk flow. This bulk flow is actually enough to drive the export from the leaf, meaning that no additional water has to be taken up into the phloem in order to drive the flow.

In plants that use passive loading instead, the concentration of sugars inside the veins is lower than in the surrounding tissue, and the plasmodesmata connecting the phloem with the cells surrounding the veins are larger than in the polymer trap case. We suspected, that in passive loading the advective transport contribution to sugar loading could be even more important than in the polymer trap. We demonstrated advective loading of sugars in experiments with biomimetic devices, modeling the leaf as a system of three compartments: phloem, xylem and sugar producing tissue. We further developed a theoretical model of passive loading, enabling us to identify the key parameters that determine the sugar uptake into the phloem. Assuming values typically found in plants for the three key parameters sugar concentration, interface areas between the three compartments and pore size of the plasmodesmata, the uptake

of sugar can be dominated by either advection or diffusion. Of these key parameters, the pore size has the largest influence on the ratio of advective to diffusive loading.

The next step in the transport of sugars is the export from the leaf. We studied the case of conifer needles, which are linear leaves with unbranched venation. Most conifer leaves are not longer than 6 cm, which is rather short compared to broad leaves with sizes spanning from millimeters to meters. In order to understand this limitation we modeled the phloem conduits in linear leaves as cylindrical, osmotic pipes running from the tip to the base of the needle. Using a simple analytical model we calculated the sugar export rate from these conduits assuming a constant concentration of sugars along the pipe. We found that in needles longer than a characteristic length the fluid close to the tip becomes stagnant and sugars can no longer be exported efficiently. This means, that very little output can be gained from making a leaf longer than the efficient leaf length. Our prediction for an efficient leaf length matches well with the mean needle lengths from a data set comprising 519 of the 629 currently known conifer species.

We further calculated the energy dissipated by the export of sugar solution from linear osmotic pipes. There are two main contributions to the dissipation of energy, one due to the resistance of membrane pores and one due to Poiseuille resistance inside the pipe. We found simple and general analytical solutions for flow rates and dissipation of energy for single pipes, generalizing the normal Poiseuille expression and showing that the driving force is not only the pressure, but the "water potential", which is a combination of concentration and pressure. We also treated a system of coupled parallel pipes with a power law distribution of lengths, as found in linear leaves. The results for the system of coupled pipes are surprisingly similar to the single pipe solutions, and likewise show the emergence of the stagnant zone for leaves longer than the effective length.

Resumé (Danish)

De fysiske mekanismer, som ligger til grund for de vitale plantefunktioner, er et forskningsområde med mange vigtige uløste problemer. Nogle af disse problemer, som har fået større opmærksomhed i de senere år, knytter sig til væsketransport i planter.

Planter producerer sukker i deres blade ved hjælp af fotosyntese. Sukkeret, som bruges som energi- og vækstkilde optages i bladets ledningsstrenge, som så transporterer dem effektivt til andre dele af planten via karsystemet. Planternes karsystem har to typer af væv: *xylemet*, der bringer vand fra rødderne op til bladene, og *phloemet*, der transporterer sukker fra kilderne i bladene til drænene i rødder, frugter og vækstområder. Transporten af sukkeropløsningen i phloemet drives af en osmotisk pumpemekanisme: Optagelsen af vand fra xylemet ind i phloemet frembringer en hydrostatisk trykforskel mellem kilder og dræn, som medfører en strømning af sukkeropløsning. Det er ikke forstået, hvor i bladet strømningen starter, især i de planter, der har intercellulære forbindelser (*plasmodesmata*) mellem phloemet og cellerne omkring ledningsstrengene. I disse planter er strømningen sandsynligvis involveret i optagelsen (*loading*) af sukker ind i ledningsstrengene.

Vi har undersøgt fysikken bag to grundlæggende mekanismer for loading af sukker: *polymerfælden* og *passiv loading*. Polymerfælden er en aktiv mekanisme, der er karakteriseret ved en forøget koncentration af sukker i ledningsstrengene i forhold til resten af bladet. Dette opnås ved hjælp af enzymer, der sammensætter sukrosemolekyler, som kommer ind i ledningsstrengen gennem plasmodesmata, til større sukkermolekyler. Molekylerne er derefter for store til at komme ud af ledningsstrengen igen, de er fanget i en "fælde". For at systemet kan virke, skal plasmodesmata fungere som ekstremt præcise filtre. Mikroskopiske undersøgelser viser, at disse plasmodesmata er meget små. De er faktisk så små, at det ikke har været muligt nøjagtigt at bestemme det tværsnitsareal, som kan bruges til transporten. Vi har modelleret plasmodesmata som cylindriske porer, blokeret i midten af en uigennemtrængelig cylinder. Vi undersøgte derefter med vores teoretiske model, om porerne kunne være små nok til at udføre filtreringsfunktionen, og samtidig store nok til at tillade tilstrækkelig transport af sukrose. Vi fandt at mekanismen faktisk er gennemførlig. Derudover kunne vi konkludere at sukker, udover diffusion, transporteres ved hjælp af advektion gennem plasmodesmata. Strømningen er faktisk tilstrækkelig til at drive eksporten ud af bladet, som betyder, at der ikke behøves optagelse af ekstra vand i phloemet for at drive strømningen.

I planter, der bruger passiv loading, er koncentrationen af sukker i ledningsstrengene lavere end i det omliggende væv og plasmodesmata, som forbinder phloemet med cellerne omkring ledningsstrengene, er større end i planter, der anvender polymerfælden. Vi formodede, at strømningens bidrag til loading af sukker kunne være endnu vigtigere i passiv loading end i polymerfælden og vi har også vist advektiv loading af sukker i eksperimenter med biomimetiske enheder. Her modelleres bladet som et system med tre kamre: phloemet, xylemet og det sukkerproducerende væv. Herudover udviklede vi en teoretisk model af passiv loading, som gjorde det muligt for os at identificere de nøgleparametre, der bestemmer optagelsen af sukker i phloemet.

På basis af de værdier, man typisk finder i planter for de tre nøgleparametre, som er koncentrationen af sukker, kontaktflader mellem de tre kamre og størrelsen af porerne i plasmodesmata, kan optagelsen af sukker både være domineret af advektion og diffusion. Det er størrelsen af porerne som har den største indflydelse på forholdet mellem advektiv og diffusiv loading.

Det næste trin af sukkertransporten er eksporten ud af bladet. Vi har specielt studeret grannåle, som er lineære blade med uforgrenede ledningsstrenge. De fleste af disse nåle er ikke længre end 6 cm, som er rimelig kort, når man sammenligner det med løvtræernes blade, hvis størrelser spænder fra millimeter til meter. For at forstå denne begrænsning modellerede vi phloem-karrene i nålene som cylindriske, osmotiske rør, der løber fra spidsen til foden af nålen. Vi anvendte en simpel analytisk model til at udregne eksporten af sukker fra karrene, hvor vi forudsatte en konstant koncentration af sukker langs røret. Vi fandt at hvis nålen er længere end en karakteristisk længde, bliver væsken ude ved spidsen af nålen stillestående og sukkeret derfra eksporteres ikke effektivt. Den karakteristiske ("effektive") længde, som vi bestemte, passer godt sammen med den gennemsnitlige nålelængde, som vi har fundet fra et stort datasæt med 519 ud af de 625 kendte arter af nåletræer.

Vi beregnede derudover energidissipationen som følge af sukkeropløsningens strømning. Der er to væsentlige bidrag til dette energiforbrug: én på grund af modstanden af membranporer og én på grund af Poiseuille modstand indenfor røret. Tilsammen danner disse et totalt energiforbrug, der har et forbavsende simpelt udtryk, som generaliserer det kendte udtryk for en Poiseuillestrømning, men viser at drivkraften ikke er trykket alene, men "vandpotentialet", som er en kombination af koncentration og tryk. Vi studerede også et system af koblede parallelle rør med en potenslovsfordeling af rørlængderne, som i en grannål. Resultaterne er forbavsende tæt på, hvad vi fandt for de enkelte rør, og igen finder man en stillestående område ude ved spidsen for nåle længere end den effektive længde.

Preface

This thesis is submitted as partial fulfilment of the requirements for obtaining the degree of Doctor of Philosophy (Ph.D.) at the Technical University of Denmark (DTU). The Ph.D. project was carried out at the Department of Physics at DTU, and as a member of the Complex Motion in Fluids Group, during a three year period from 15 September 2013 to 14 September 2016. I gratefully acknowledge funding support from DTU Physics, from the Danish Council for Independent Research under grant no. 12-126055 and a travel grant from the Otto Mønsteds Fond.

The theoretical work and experiments on biomimetic devices were carried out at DTU Physics. All microscopy studies on plant material were conducted at the Center for Advanced Bioimaging (CAB) and in collaboration with the Department of Plant and Environmental Sciences at the University of Copenhagen.

Three years ago, all I knew about plants was what I had learned in school. I was excited to start this Ph.D. and am grateful to my supervisor, Tomas Bohr, for giving me the opportunity to dive into this fascinating subject and to discover something new about life. Tomas trusted me with my work and in best Danish tradition made me feel like his colleague rather than his student. He infected me with his enthusiasm and gave me the freedom to follow my own path.

I benefitted greatly from the fresh ideas Kaare Hartvig Jensen brought into my Ph.D. project after returning to DTU and becoming my co-supervisor. I am grateful to him for guiding me in practical issues about the experimental part of my project, and also in organizing my research more efficiently.

It was a great pleasure to receive additional supervision from Alexander Schulz, who not only taught me all I needed to know about phloem anatomy and physiology, but was also there for me, whenever I needed help while sitting at the microscope.

I am grateful to Helle Juel Martens for assistance during my microscopy studies and for welcoming me in her office, whenever I worked at CAB. Thanks also to Johannes Liesche for introducing me to the photoactivation experiments, to Catherine Nielsen for support in the histology lab, and to Piotr Binczycki, the master of ultrathin sections.

Thanks to Kirstine Berg-Sørensen and Anders Andersen for helping me out with equipment from their labs. I would also like to thank Erik Hansen and Poul Erik Andersen at the workshop for their fast and reliable work.

I thank Tomas, Julia and Navish for carefully reading drafts and providing helpful feedback.

Finally, I thank my friends and family for their continuous encouragement and support.

Kongens Lyngby, 14 September 2016

Hanna Rademaker

Table of Contents

List of abbreviations

Abbreviation	Description
BSC	bundle sheath cell
CA	cyanoacrylate (super glue)
CC	companion cell
CLSM	confocal laser scanning microscopy
FM	fluorescence microscopy
IC	intermediary cell
PD(s)	plasmodesma(ta): intercellular pore(s)
PEEK	polyether ether ketone (material for tubing)
ROI	region of interest (in microscopy)
SE	sieve element
TEM	transmission electron microscopy
UV	ultraviolet (wavelengths of 10 nm to 380 nm)

List of symbols

Symbol	Description
∂_t	partial derivative with respect to t
∇	vector differential operator
$\boldsymbol{v}$	velocity field
u	radially averaged flow velocity
Q	volume bulk flow
J	flux of fluid or solute
Φ	solute flux
Γ	sugar loading, sugar export
L_p	membrane permeability
σ	reflection coefficient
ω	mobility
H, W	diffusive and convective hindrance factors
η	dynamic viscosity
$\boldsymbol{g}$	gravitational acceleration
p	hydrostatic pressure
ρ	mass density
R	gas constant
T	temperature
c	concentration of solute
μ	chemical potential
Π	osmotic pressure
Ψ	water potential
D	diffusion coefficient
L	length
r	radius
A	area
d	membrane thickness, pore length
U_0	characteristic velocity scale
T_0	characteristic time scale
L_0	characteristic length scale
P_0	characteristic pressure scale
M, Mü	Münch number
Re	Reynolds number
Pe	Peclet number

List of original papers

Paper I: Julia Dölger, Hanna Rademaker, Johannes Liesche, Alexander Schulz, and Tomas Bohr. Diffusion and bulk flow in phloem loading: a theoretical analysis of the polymer trap mechanism for sugar transport in plants. *Physical Review E*, 90(4): 042704, 2014.

Paper II: Hanna Rademaker, Katrine E Villumsen, Jean Comtet, Tomas Bohr, and Kaare H Jensen. Diffusion and bulk flow in passive phloem loading. *Manuscript under preparation.*

Paper III: Hanna Rademaker, Maciej A Zwieniecki, Tomas Bohr, and Kaare H Jensen. On the size of conifer needles. *In revision. Target journal: PNAS.*

Paper IV: Hanna Rademaker, Kaare H Jensen, and Tomas Bohr. Osmotically driven flows and maximal transport rates in systems of long, linear porous pipes. *Manuscript under preparation. Target journal: Journal of Fluid Mechanics.*

1 Introduction

Why study plants?

It seems fair to say, that life on Earth depends heavily on plants, as they provide the oxygen we breathe and almost all the food we eat. On top of that, imagine a world without wood, coal and biofuels, or even just the recreational value plants add to our life, like in parks and gardens.

There are 300,000 different plant species in the world [Christenhusz and Byng, 2016], and one could ask, how is it possible for them to exist next to each other and be successful with their individual strategy, with all their different heights, leaf shapes, textures and colors? The variation seems endless, but in fact it is not. What looks so diverse from the outside, follows the same basic principles inside. The leaves, stem and roots of any higher plant rely on a vascular system comprised of two types of pipes, one for transporting water and one for sugar solution. The mechanism of fluid transport is basically the same, whether comparing 420 million years old horsetails with modern, flowering plants, or a small herb with a tall tree.

In order to secure life as we know it on our planet, we have to understand what makes a plant species efficient and suited for certain environmental conditions. Overall plant efficiency boils down to the effective distribution of photosynthetically produced sugars from the production sites in the leaf to other parts of the plant like roots, fruits and regions of growth. This is a research field where simple, mechanistic models, which treat the plant as a microfluidic system, can give a good understanding of the transport related optimization parameters.

Sugar transport in plants

The first theoretical and experimental models of sugar transport in plants were conceived in the 1930s by Ernst Münch. The *Münch hypothesis* is that the driving force which moves sugars from sources to sinks in a plant is an osmotically created pressure difference [Münch, 1930]. These models have since been further developed [Horwitz, 1958; Eschrich et al., 1972; Christy and Ferrier, 1973]. They were mostly concerned with systemic transport inside the microfluidic conduits. In the last decade, these models were refined and used to explain some experimental observations and e.g. make predictions about the conduit radius [Jensen et al., 2012a], leaf sizes [Jensen and Zwieniecki, 2013], sugar concentration [Jensen et al., 2013] etc. However, there are still surprisingly many, basic open questions about the sugar transport in plants.

Water has many purposes and destinations inside the leaf: it is needed for photosynthesis in all sugar producing cells, creating the osmotic pressure to export sugar from the leaf, and a large portion evaporates from the lower side of the leaf. At the same time, sugar has to enter the vein from all the surrounding cells. How does the plant accomplish this logistic masterpiece? How is sugar loaded into and unloaded from the transport system?

These questions address the transport into and out of the conduits, and transport inside cells as well as around cells, using the cell wall or intercellular spaces as a transport pathway. We need to zoom in on certain parts of the leaf and the root and address fundamental questions about osmosis and solute transport through narrow pores.

In order to achieve this, we also have to study the structural features, physical properties and physiological conditions of different plant cell types. It was only this year that the 80 years old Münch hypothesis on sugar transport could be supported directly by an experiment in plants [Knoblauch et al., 2016], after the necessary suitable pressure probes had been developed [Knoblauch et al., 2014]. On a similar note we are lacking basic data on structural details like the sizes, numbers and bifurcations of conduits inside the veins of a leaf or a root, the internal structure of intercellular pores, or even solute concentrations in different cell types. All these data are important to estimate local fluid flows.

Microfluidics of sugar loading

This thesis focuses on sugar transport inside the leaf, where sugars are taken up into the veins in order to be exported to other parts of the plant. To achieve this sugar loading, there are three different, basic mechanisms, which are distinguished according to whether sugars are loaded through intercellular pores or over the cell membrane, and whether proteins are involved in the loading step. For none of the three mechanisms the underlying physics is well understood.

It is in the nature of the problem, that sugar transport in plants cannot be studied separately from water transport, and there is at least as much mystery about the pathway of water inside the leaf as there is about sugar loading. This is especially true when sugar loading occurs through intercellular pores whereby the transport of sugar and water is strongly coupled.

My point of view is mostly a microfluidic one, concerning the pressures, flow rates, feasibility and efficiency of the leaf's cellular and vascular system. Part of my work is from a more biological perspective though, looking at the internal structure of veins and their bifurcations.

Lastly, I am interested in how the transport principles used in plants can be transferred to artificial, biomimetic systems, and in how we can use artificial systems to gain new insights into plants.

Approach

Defining the research questions of this Ph.D. thesis has been a collaborative effort. The projects presented in this thesis would not have been possible without the numerous and fruitful discussions with my supervisors Tomas Bohr and Kaare Hartvig Jensen at DTU Physics and our coworkers Alexander Schulz and Helle Juel Martens at the Section for Transport Biology at the University of Copenhagen.

We developed theoretical models of sugar loading for two of the three mechanisms mentioned above – the so-called polymer trap (Sec. 4.1, 5.1, and 6.1) and passive loading (Sec. 4.2, 5.2, and 6.2). The passive loading project was supplemented with experiments on biomimetic devices designed for this study.

Going one step further along the transport path, we studied the export of sugars from the leaf, looking at the simplest leaves found in nature – the linear leaves of conifers (Sec. 4.3, 5.3, and 6.3). This was again a theoretical study, comparing to literature data of conifer needle lengths. During this project we also went deeper into the fundamental problem of osmotic pipe flow, which has consequences for the leaf venation, some of which we discuss in our most recent paper (Sec. 4.4, 5.4, and 6.4).

The theoretical studies were accompagnied by microscopy studies (Sec. 6.5), giving valuable insight into the geometric features of leaf venation. State-of-the-art methods and expertise was available thanks to Alexander and Helle, and the facilities at the Center for Advanced Bioimaging (CAB) associated with the University of Copenhagen. We have a plan to publish some of these results in a joint article with Alexander and Helle, complemented with results from their Master student Signe Randi Andersen.

The interdisciplinarity of this project is reflected in the range of conferences to which I could contribute during the past three years: The EMBO workshop on "Intercellular communication via plasmodesmata", the Plant Biomechanics Conference, the European Fluid Mechanics Conference, and the European Conference on Mathematical and Theoretical Biology.

2 Plant biology background

Plants are important for life on Earth in many ways, providing oxygen, food, energy and raw materials. All these assets go back to the ability of plants to do photosynthesis, converting carbon dioxide and water into oxygen and sugars. Yet, for a plant to work efficiently it is not enough to produce the sugars, it is also important that sugars and water can be distributed effectively throughout the plant. Higher plants use a vascular system to direct fluid flow. Despite the astonishing diversity found in the morphology of plants, there are some common features of these vascular systems, which we can use to develop simplified models to understand the working principles of these transport processes.

This chapter gives a brief introduction to the biological background relevant for the transport of sugar and water in vascular plants. The first part describes the vascular system and gives typical values of conduit sizes, time scales and pressures found in these systems.

The second part focuses on transport processes inside the leaf. Intercellular transport of sugars and water is facilitated by pores and semi-permeable membranes. On a higher level, transport is guided by the veins which can form complex venation patterns.

In the third part of this chapter the different mechanisms of uptake of photosynthetized sugars into the veins are introduced and compared.

The fourth part introduces the reader to the Münch mechanism and models of long-distance transport, which is closely connected to the topic of sugar loading.

2.1 The vascular system of plants

A vascular system is key to efficient transport within multicellular organisms. The first vascular plants (tracheophytes, or "higher plants") emerged around 420 million years ago [Boyce, 2005]. The extant tracheophytes are comprised of clubmosses, horsetails, ferns and the two most recently evolved groups: *angiosperms* with about 250,000 different species and *gymnosperms* with about 700 species [Taiz et al., 2015]. Angiosperms are all flowering plants including herbs, shrubs and broad-leaved trees, while the evolutionary older gymnosperms comprise mostly needle or scale bearing species like conifers, with some exceptions like ginkgo. All tracheophytes show two distinct types of vascular tissue, the *xylem* for transporting water and the *phloem* for transporting photoassimilates (sugars or sugar alcohols) and signaling molecules.

The systemic fluid transport in vascular plants is driven by two mechanisms: Firstly, *evaporation* of water from the leaves creates a tension in the conduits of the xylem, which together with intermolecular forces brings up more water from the roots ("cohe-

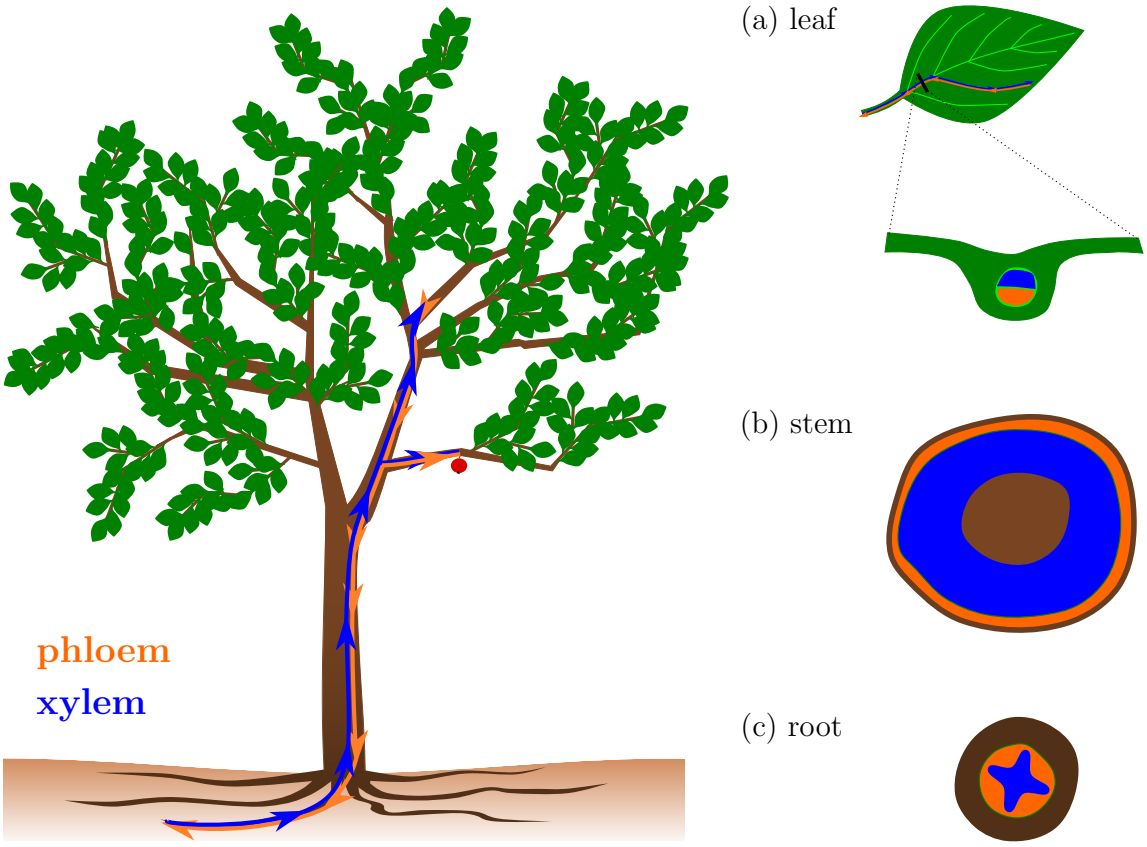

Figure 2.1: Sugar conducting phloem (orange) and water conducting xylem (blue) tissue in a vascular plant. Left: Phloem and xylem conduits run in parallel and close proximity throughout the whole plant. Water is taken up into the roots and transported upwards to the leaves. Photoassimilates like sugars are produced in mature leaves and distributed to storage places, e.g. roots or fruits, and regions of growth, e.g. young leaves. Right: Arrangement of phloem and xylem tissue in cross sections of the plant organs (a) leaf, (b) stem and (c) root as found in a woody angiosperm.

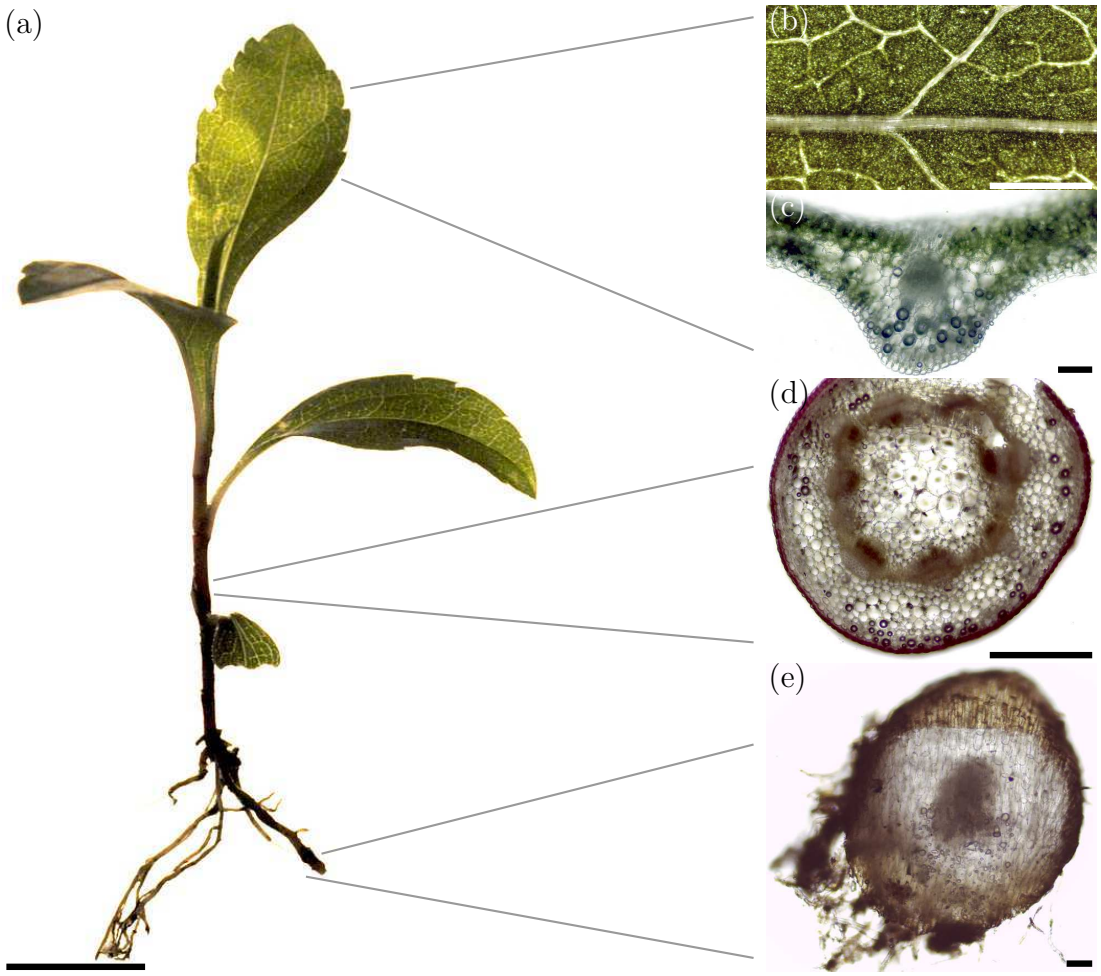

Figure 2.2: (a) Whole plant. (b) Leaf venation as seen from the lower side of the leaf. (c) Cross section through the leaf at the mid-vein. (d) Cross section of the stem. (e) Cross section of the largest root. Scale bars: (a): 1 cm, (b) and (d): 1 mm, (c) and (e): 100 µm.

	phloem transports photoassimilates and signaling molecules		xylem transports water and minerals	
transport	*sieve elements* living, with reduced cytoplasm		*tracheary elements* dead, lignified wall thickenings	
	(A) *sieve tubes* with *companion cells*	(G) *sieve cells* with *Straßburger cells*	(A) *vessels, tracheids*	(G) *tracheids*
	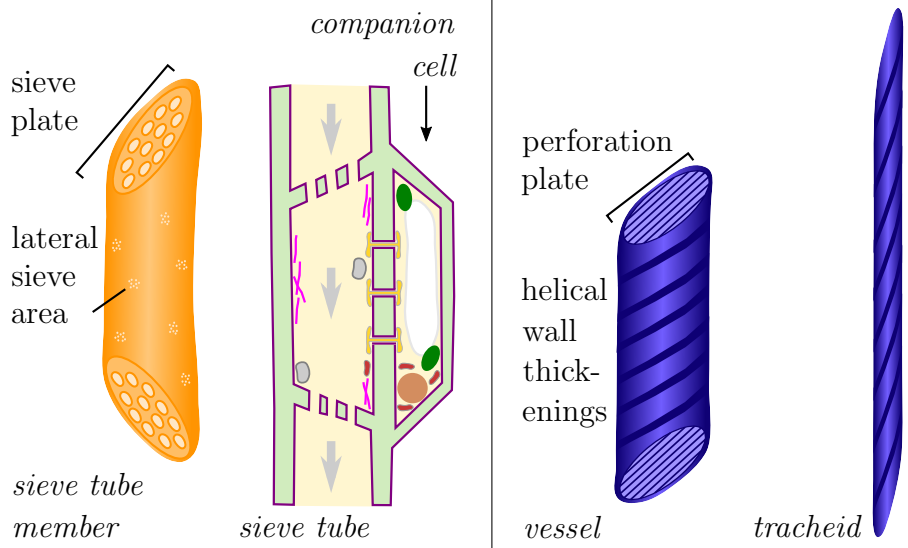			
support	*fibers, sclereids*		*fibers*	
storage	*parenchyma*		*parenchyma*	

Table 2.1: Cell types inside the phloem and xylem tissue in angiosperms (A) and gymnosperms (G) for the basic functions transport, support and storage. Mature conducting cells are either dead (tracheary elements in the xylem) or have reduced cytoplasm (sieve elements in the phloem) in order to reduce resistance to flow. Compiled using information from Taiz et al. [2015]; Schulz and Thompson [2009]; Raven et al. [2005].

sion-tension theory", see e.g. Stroock et al. [2014]). Secondly, the high concentrations of sugars inside the leaves lead to uptake of water into the phloem by *osmosis*, and the resulting pressure is used to export sugar sap to other parts of the plant. The uptake of sugars into the phloem (*phloem loading*) and the mechanism of osmotically driven flows in long-distance transport, known as the Münch mechanism [Münch, 1930], are discussed in Sec. 2.3 and Sec. 2.4.

The exact arrangement of phloem and xylem inside leaves, stems and roots varies between species (e.g. dicots vs. monocots), however, the conducting phloem and xylem are always in close proximity throughout the entire plant (Figs. 2.1 and 2.2), only separated by a few cell layers. Nevertheless, their physical conditions are very different: the sap in the phloem is under positive pressure, typically between 6 and 14 bars in trees and around 20 bars in herbs [Turgeon, 2010a], while the negative pressure, or *tension*, in the xylem is typically between -5 and -20 bars for plants growing in moist habitats. Negative pressures up to -80 bars have been measured in the xylem of plants living under more demanding conditions e.g. in deserts or at the sea shore [Scholander et al., 1965].

Xylem cells are equipped with thickened, lignified cell walls which enable them to withstand these huge tensions. In order to reduce resistance to flow, mature conducting xylem cells are actually dead and stripped of all inner organelles including the cell membrane. While phloem cells also have thicker cell walls, they are living cells. To improve conductivity, mature conducting phloem cells only retain a few organelles (endoplasmic reticulum, mitochondria, modified plastids) and are otherwise dependent on their companion cells (angiosperms) or Straßburger cells (gymnosperms) (Table 2.1) [Taiz et al., 2015].

Sizes of phloem and xylem cells vary between species, and also between leaf, stem and root of a plant. However, phloem cells are always smaller than xylem cells. Sieve tubes in angiosperms and sieve cells in gymnosperms are typically 15 to 40 µm in diameter in the stem [Jensen et al., 2012b]. Xylem vessels in angiosperms can be anything between 15 and 500 µm in diameter in the stem [Olson and Rosell, 2013]. Tracheids in gymnosperms are smaller being up to 70 µm in diameter in the stem [Pittermann and Sperry, 2003].

Typical fluid flow speeds in the stem were found to be 0.5 to 5.0 mm/s in the xylem of angiosperm herbs [Windt et al., 2006]. In the phloem 0.2 to 0.4 mm/s were measured in angiosperm herbs [Windt et al., 2006], while the average flow speed is lower in trees, namely 0.16 mm/s in angiosperm trees, and 0.06 mm/s in gymnosperm trees [Liesche et al., 2015].

2.2 The leaf

The leaf is a fascinating plant organ. It is here plants can "breathe" - meaning the exchange of gases with their environment. Water can evaporate from leaves through pores in the leaf surface (*stomata*). It is through the same pores, plants take up carbon dioxide from the surrounding air, enabling the photosynthetic production of sugars.

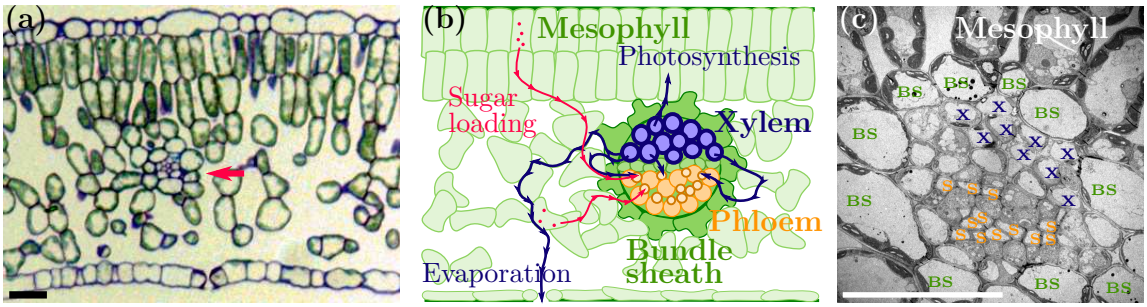

Figure 2.3: Cross section of a leaf. (a) Bright field image of an apple leaf (*Malus sylvestris*). The red arrow points to a small vascular bundle (vein). (b) Schematic view, indicating different transport processes in the leaf. Sugars produced in the mesophyll cells by photosynthesis are loaded into the phloem to be transported to other parts of the plant (red arrows). Water from the xylem is used for photosynthesis, but is also taken up into the phloem by osmosis to drive the flow in the phloem. The largest portion of the water is lost due to evaporation through the pores (stomata) in the epidermis. (c) TEM image of a vein cross section of an apple leaf. BS: bundle sheath cells, X: xylem vessels, S: sieve elements in the phloem. Scale bars (a,c): 20 µm.

Looking at the cross section of a leaf (Fig. 2.3), we find the sugar and water conducting tissue (phloem and xylem) inside the veins, surrounded by a cell layer called the *bundle sheath*. The bundle sheath is impermeable to gasses and shields the cells in the vein from the air spaces. The surrounding tissue, which makes up the largest portion of the leaf, is the mesophyll. Typically, these cells form one or two tighter layers (palisade mesophyll) at the upper side of the leaf, since their main function is photosynthesis. Towards the lower side of the leaf, they are arranged with more air spaces between them (spongy mesophyll), facilitating gas exchange through the stomata, which are found mostly in the bottom surface of the leaf.

2.2.1 Transport processes inside the leaf

The different tissues inside the leaf need to communicate and transport sugars and water between them. There are different routes to take, and the main distinction is, whether the transport takes place directly from cell to cell, inside the cell lumen (*symplasmic*), or along (inside) the cell walls, outside the plasma membrane (*apoplastic*) (Fig. 2.4).

The symplasmic intercellular transport makes use of connections called plasmodesmata (PDs). They are about 50 to 70 nm in diameter [Fisher, 1999; Robinson-Beers and Evert, 1991], but most of their inner volume is occluded by endoplasmic reticulum (ER), a cell organ forming flattened sacs or tube-like structures reaching from one cell into the next. The slit between the ER-membrane and the plasma membrane is

thought to be between 2 and 4 nm wide [Robinson-Beers and Evert, 1991; Ding et al., 1992], but most likely there is still a more complex inner structure made of proteins etc. inside this slit. The details of the inner structure of PDs, their development and selectivity are still subjects of ongoing investigation [Burch-Smith and Zambryski, 2012; Knox et al., 2015; Faulkner et al., 2013]. The transport is often assumed to be unspecific, meaning that all molecules of a size smaller than the slit-width can pass the PD. On the other hand, there is evidence of symplasmic transport of macromolecules like virus-RNA, clearly larger than this assumed slit-width. It is suspected that viruses can alter the slit-width of the PD [Lucas and Gilbertson, 1994].

The apoplastic transport takes place inside the cell walls, which are complex structures in themselves: cellulose microfibrils, coated with hemi-cellulose and embedded in a pectin matrix. Together they form a hydrogel of high mechanical stability [Taiz et al., 2015]. Water can move from symplast to apoplast via aquaporins, which are pore-forming proteins inside the plasma membrane, specifically transporting water molecules [Maurel, 1997]. Also photoassimilates like sugars can cross the plasma membrane, they do so with the help of specific transporters, for example sucrose in the apoplastic loading mechanism as discussed in Sec. 2.3.1 [Chen et al., 2012].

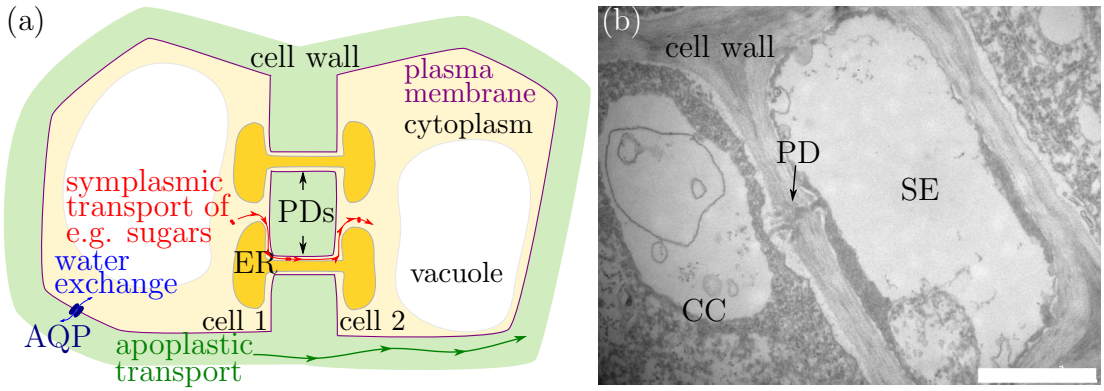

Figure 2.4: (a) Schematic drawing of symplasmic and apoplastic transport in plant tissue. The symplasm, that is the volume inside the plasma membrane, of one cell can be directly connected to the symplasm of a neighboring cell via plasmodesmata (PDs). PDs are small channels which allow for a continuous endoplasmic reticulum (ER) between cells. Symplasmic, intercellular transport of e.g. sugars is assumed to take place in the free slit between ER and plasma membrane. On the other hand, diffusive transport inside the cell wall and outside the plasma membrane is also possible, and is termed apoplastic transport. The osmotic water permeability of the plasma membrane is due to aquaporins (AQP), which are transmembrane proteins. (b) Transmission electron microscopy image of a sieve element (SE) and a companion cell (CC) symplasmically connected by plasmodesmata (PD). Scale bar: 1 µm.

2.2.2 Leaf venation patterns

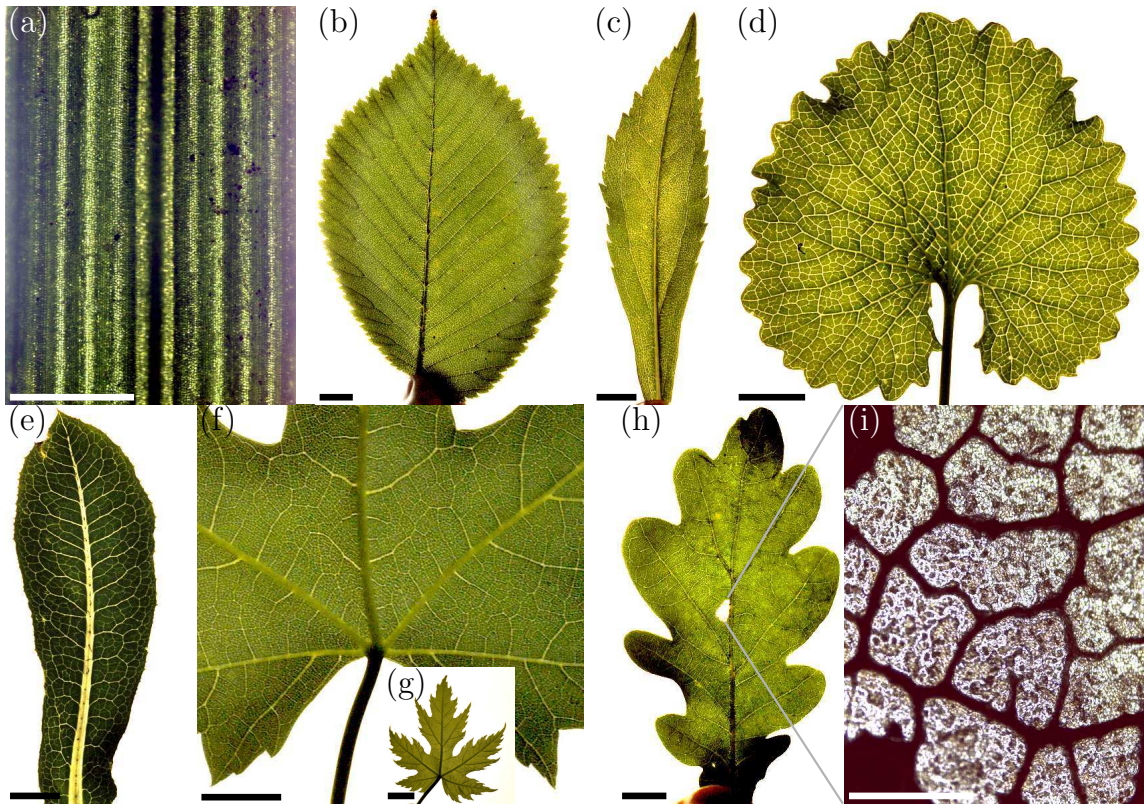

Figure 2.5: Photographs/microscopy images of leaf venation patterns. (a) Parallel venation in a grass. (b)-(h): Reticulated venation in different leaf shapes. A small part of the oak leaf in (h) has been "cleared" by a herbivore, which reveals details of the smallest veins (i). Scale bars: (a,i): 1 mm, (b)-(h): 1 cm.

The topological and geometrical arrangement of venation in the leaf is quite diverse (Fig. 2.5). The simplest form is *parallel* or striate venation (Fig. 2.5(a)), which is mostly found in linear leaves like e.g. conifer needles or grasses.

The more complex, *reticulated* venation establishes a hierarchy of veins (Fig. 2.6). The mid-vein or primary vein enters the leaf from the petiole at the base of the leaf blade. There can be several primary veins, as in the leaves in Fig. 2.5(f) and (g). The secondary veins branch from the primary vein, tertiary veins from secondary veins and so on. There are typically 6 or more vein classes in angiosperm leaves [Nelson and Dengler, 1997]. The veins of the first three classes are also referred to as *major* veins, while class four and above are called *minor* veins.

The major veins are already established when the young leaf unfolds from the bud, while the minor veins develop during the growth of the leaf [Turgeon, 1989]. Major veins are usually easily seen from the outside, as they protrude from the lower side of

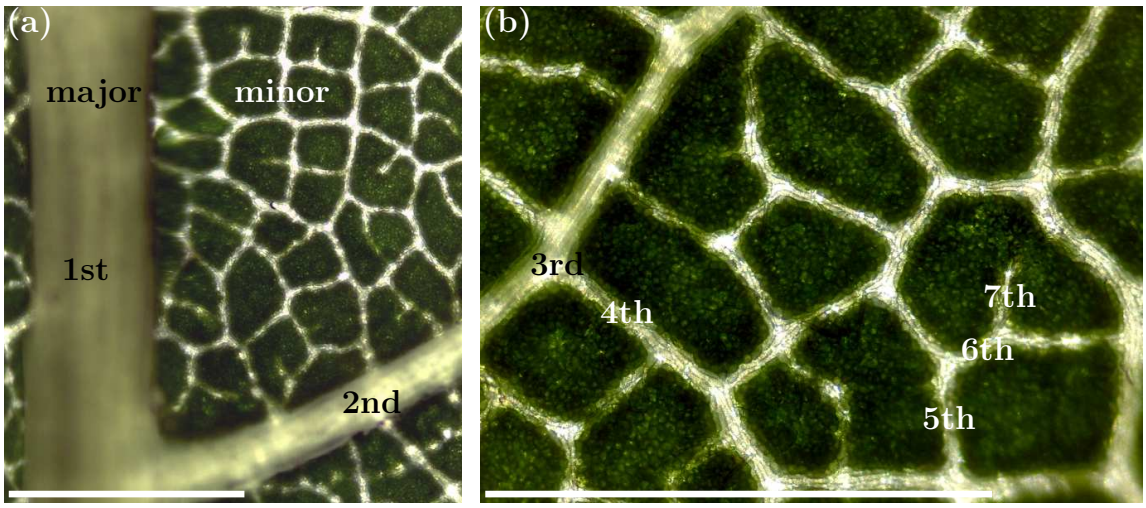

Figure 2.6: Major and minor veins. Sugar loading takes place in the minor veins of a leaf, which are of class 4 and higher. The major veins – class 1 to 3 – are mainly for transport and for mechanical stability of the leaf. Scale bars (a,b): 1 mm.

the leaf, whereas minor veins are embedded in the mesophyll cells [Nelson and Dengler, 1997]. There are different functions associated with the vein classes. The uptake of sugars into the veins takes primarily place at the minor veins, and the phloem within is consequently called *collection phloem*. Major veins provide mechanical stability to the leaf [Kawai and Okada, 2015], and the phloem within is referred to as *transport phloem* [Evert, 2006].

2.3 Phloem loading

Phloem loading is the process of taking up sugars (or other photoassimilates) into the sieve element-companion cell complex, in order to transport them efficiently over long distances. In general one can distinguish between symplasmic and apoplastic loading. In symplasmic loading sugars are transported inside the cytoplasm from the production sites in the mesophyll cells to the sieve elements via plasmodesmata connecting the cells. In contrast apoplastic loading allows sugars to travel inside the cell walls and the final uptake into the phloem conduits necessitates crossing the plasma membrane back into the cytoplasm.

Another classification is active vs. passive loading. In active loading, energy is consumed in the loading process, since proteins facilitate sugar transport against the concentration gradient and/or over the plasma membrane. Passive loading does not require the help of these proteins and sugar moves “downhill”, along the concentration gradient. Active loading thus results in elevated sugar concentration inside the phloem compared to the surrounding mesophyll, while passive loading leads to higher

concentrations in the mesophyll. This can be used to determine the loading type experimentally: Leaf disks are exposed to radiolabeled carbon dioxide and subsequently pressed against x-ray film. Locations with higher concentrations of photosynthesized sugars cause stronger illumination of the film and result in darker coloring of the obtained image. In the case of active loading, the veins will therefore appear dark, while for passive loading, the veins are brighter than or indistinguishable from the mesophyll (for details see e.g. [Weisberg et al., 1988]).

Rennie and Turgeon [2009] distinguish three loading types, as described in the following paragraphs: active apoplastic, active symplasmic and passive symplasmic loading (Fig. 2.7). Although some plants seem to use only one of the loading mechanisms, e.g. gray poplar (*Populus alba* var. *canescens*), which is a passive symplasmic loader [Zhang et al., 2014], more and more examples of mixed loaders are being discovered. One of the first examples (tropical spiderwort, *Commelina benghalensis*) was found by Van Bel et al. [1988]. Recently, also trees with mixed loading have been discovered, for example ash (*Fraxinus excelsior*) uses active as well as passive loading [Öner-Sieben and Lohaus, 2014].

Biologists have distinguished apoplastic and symplasmic loading by the absence or presence of plasmodesmata for decades [Gamalei, 1974, 1989] and the categorization into three basic loading mechanisms has been used for several years now [Rennie and Turgeon, 2009]. Nevertheless, the physics of all three loading types is not well understood. It is a central part of this Ph.D. thesis to contribute new findings to the physical understanding of sugar loading.

2.3.1 Active apoplastic loading

In the active apoplastic loading mechanism (Fig. 2.7(a)), bundle sheath cells and companion cells are not connected by plasmodesmata. Instead, sugars are released into the apoplast by so called "SWEET proteins" and taken up into the phloem by the proton-coupled sucrose transporter SUT1 [Chen et al., 2012]. These transporter proteins are located in the plasma membrane of the companion cell, which in apoplastic loaders is called a *transfer cell* and typically shows cell wall ingrowths increasing its surface area. Because of the lack of symplasmic connection of the phloem with the mesophyll in apoplastic loading, plants using this mechanism can have very high concentration of sugars in the phloem sap, up to 1.8 M in potato (*Solanum tuberosum*) [Pescod et al., 2007].

Active apoplastic loading is mostly found in small angiosperms, like herbs [Gamalei, 1991]. This is somewhat surprising, as one could suspect the tallest plants like trees to have the highest sugar concentrations and therefore the largest driving force for their phloem transport.

Apoplastic loading has recently been studied analytically and numerically in a complex model taking into account the reaction rates of six protein states during the sucrose-proton symport over the plasma membrane of the transfer cell [Sze et al., 2013, 2014].

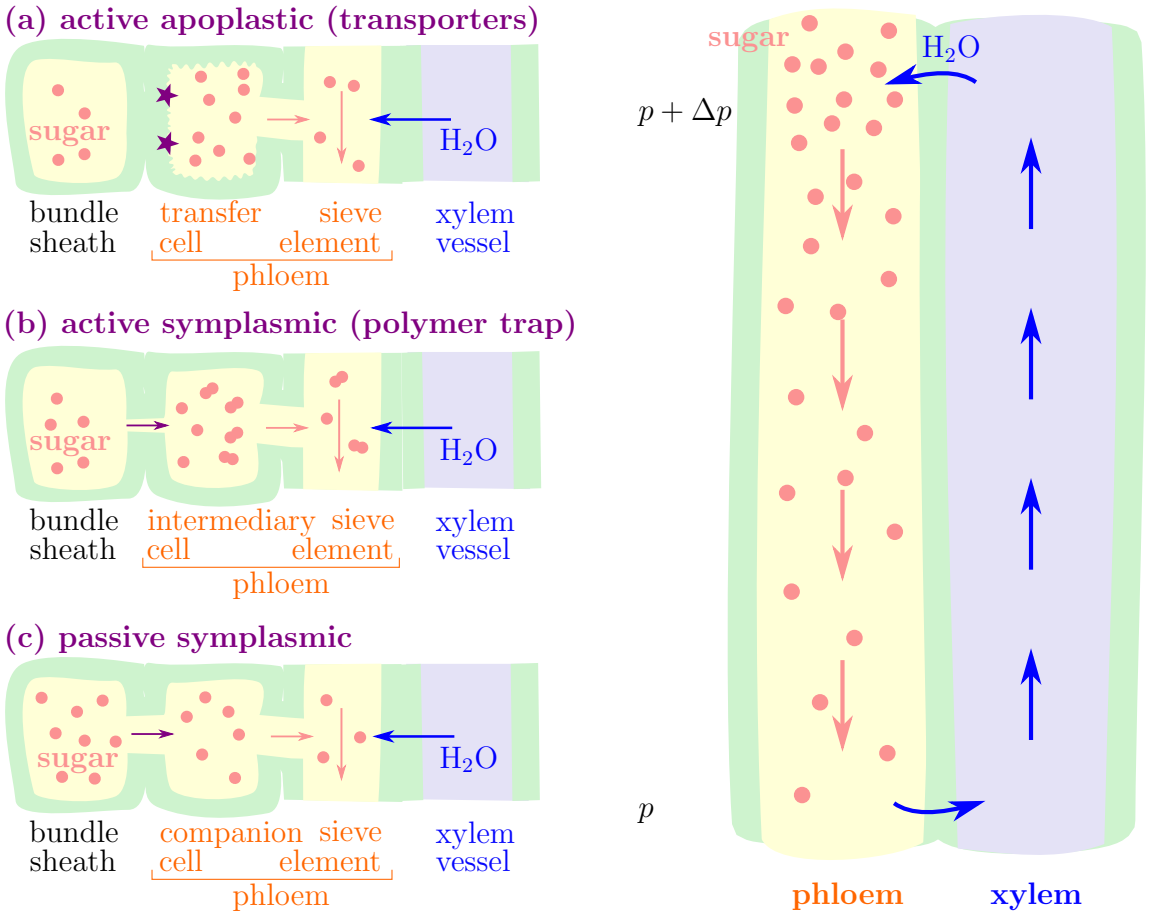

Figure 2.7: Left: Three basic loading mechanisms: (a) active apoplastic (sucrose transporters), (b) active symplasmic (polymer trap) and (c) passive symplasmic. Inspired by Rennie and Turgeon [2009]. Right: Long-distance transport is facilitated by pressure differences between sources (mature leaves) and sinks (young leaves, roots, fruits etc.). These pressure differences are generated by the osmotic uptake of water into the sieve elements of the phloem. The mechanism was first described by Münch [1930].

2.3.2 Active symplasmic loading

In active symplasmic loading (Fig. 2.7(b)), sucrose from the bundle sheath can enter the companion cells (in this mechanism also called *intermediary cells*) via plasmodesmata, where it is enzymatically converted to larger sugar molecules like raffinose and stachyose. These polymers are then too large to diffuse back through the PDs towards the bundle sheath. They are trapped inside the phloem, which is why active symplasmic loading is also called the *polymer trap* mechanism.

Famous polymer trap species are squash (*Cucurbita pepo*) [Turgeon and Hepler, 1989], cucumber (*Cucumis sativus*) [Pharr and Sox, 1984], melon (*Cucumis melo*) [Haritatos et al., 1996], pumpkin (*Cucurbita maxima*) [Webb and Burley, 1964] and *Coleus blumei* [Rennie and Turgeon, 2009]. Their phloem sap contains a mixture of sucrose and oligomers in varying fractions. The average sugar concentration is higher than in the mesophyll, and can be similarly high as in the apoplastic loading case [Turgeon, 2010b].

The polymer trap mechanism is quite interesting from a physics perspective. Firstly, oligomerizing the sucrose molecules to larger sugars reduces the osmolarity of the sap, and it is not at all obvious whether and how this is beneficial for the export efficiency. Secondly, the PDs between bundle sheath cell and intermediary cell must be tuned in size very precisely, as they can discriminate between sucrose (disaccharide) and raffinose and stachyose (trisaccharide and tetrasaccharide). Since the open slit in these very special PDs is so small, it also poses the question of feasibility of the mechanism: Is it possible, that these PDs still allow for enough sucrose to diffuse into the phloem? Is this transport enhanced by a bulk flow from bundle sheath cell to intermediary cell? Our paper [Dölger et al., 2014], summarized in Sec. 4.1, gives a detailed physical analysis of these questions.

2.3.3 Passive symplasmic loading

Plants using the passive symplasmic loading (Fig. 2.7(c)) have "ordinary" companion cells, which are connected to the bundle sheath by numerous PDs. In mature leaves, the concentration of sugars is highest in the mesophyll cells and sugar follows a downhill gradient into the phloem. This process has sometimes not even been considered as loading, as the title of the paper by Turgeon and Medville [1998] indicates ("The absence of phloem loading in willow leaves"), but will nonetheless lead to export of sugar from the leaf.

The concentration of sugars in the phloem sap of plants that load passively is the lowest, around 15% wt/wt on average as compared to 21% wt/wt for active loading species [Jensen et al., 2013]. Most of these plants are trees, e.g. willow (*Salix spp.*), common beech (*Fagus slyvatica*) and sugar maple (*Acer saccharum*) [Rennie and Turgeon, 2009]. Loading in all gymnosperms is less well understood. Since there are no indications for an active loading mechanism, they are currently assumed to load passive symplasmically [Liesche et al., 2011].

At first glance, the physics of passive loading seems straightforward: sucrose diffuses

from the mesophyll into the phloem, water is osmotically taken up from the xylem and drives the bulk flow. What discriminates passive loading from the active mechanisms though, is that there is no clear loading step, and no increase in concentration when entering the phloem. So where does the water neccessary to drive the flow enter the phloem? With the highest concentration in the mesophyll, the uptake of water might happen along the pre-phloem pathway, and water and sugar could enter the phloem together as a bulk flow. This would mean, that sugar is not diffusing into the phloem, but being advected with the incoming water, with possibly important consequences for the efficiency of the loading process. We study the interplay of diffusion and advection in detail in our paper, introduced in Sec. 4.2.

2.4 Long-distance transport and the Münch mechanism

This thesis focuses on the transport of sugars and water inside the leaf. Nevertheless, we have to consider the long-distance transport from the leaves to the rest of the plant in order to choose the right boundary conditions, e.g. the pressure at the base of the leaf.

Already in 1930 Münch understood that the osmotic uptake of water from the xylem into the phloem creates a hydrostatic pressure difference, which drives the sugar transport to roots, fruits and regions of growth. Münch in particular pointed out that a concentration potential inside the plant not only leads to diffusion, but also to a bulk flow of sugar solution [Münch, 1930].

One simplistic type of model, which already gives valuable insights, is the one-dimensional hydraulic resistor [Jensen et al., 2011, 2012b]. These models study one isolated conduit running through the whole plant. The conduit is divided into three parts where sugar is loaded, transported and unloaded, corresponding to leaf, stem and root. These models predict an optimal conduit radius which maximizes the flow rate for given lengths of leaf, stem and root. The optimal radius exists due to a balance of resistance for transport of fluid inside the tube and for uptake/release of fluid over the membrane wall in the loading/unloading zone. The relation of radius and lengths of leaf, stem and root resulting from the one-dimensional hydraulic resistor model fits surprisingly well to field measurements in angiosperms and gymnosperms [Jensen et al., 2012b].

Other predictions made from simplistic models include the limits of leaf sizes [Jensen and Zwieniecki, 2013] and optimal sugar concentration, maximizing sugar mass flux [Passioura, 1976; Jensen et al., 2013].

Mathematically more demanding models are based on the Aldis flow [Aldis, 1988] (see Sec. 3.4) and can capture details like the effect of small variations between concentration at the wall and the mean concentration in an osmotic tube [Haaning et al., 2013].

A subcategory of these models are based on the Münch-Horwitz equations [Horwitz, 1958], which use radially averaged concentration and axial flow speed making use of the lubrication approximation. This approximation is valid, if the radius is much

smaller than the length of the conduit, which is of course very reasonable for phloem tubes. Besides numerical solutions of concentration and flow velocity for steady state [Christy and Ferrier, 1973] and transient behavior [Thompson and Holbrook, 2003a], there are also analytical solutions for time-dependent models [Jensen et al., 2009] and for stationary equations [Thompson and Holbrook, 2003b; Jensen et al., 2011, 2012a], assuming e.g. a constant sugar concentration in the leaf.

The constant sugar concentration in the leaf is a good approximation, if the system is limited by transport as opposed to limited by loading. To include cases limited by loading, one can use a target concentration, where the local loading is proportional to the concentration difference to a target value [Lacointe and Minchin, 2008; Jensen et al., 2012a].

3 Microfluidics background

Modeling the fluid flows inside the conduits of the phloem means entering a certain domain of fluid mechanics. Fluid flow inside these conduits is slow and laminar, as the diameters of the conduits are small, in the range of 1 to 40 µm (see Sec. 2.1).

The first section of this chapter, takes us from the governing equations of fluid mechanics to one fundamental and well known solution: the slow, steady, pressure-driven flow through a cylindrical pipe.

In the second section we see how diffusion influences the transport of solutes in these slow flows and understand, why it was so important for plants to develop a vascular system.

The third section discusses osmotically driven fluid flow over a membrane and introduces the concept of hindrance factors. These components are important in order to understand the water balance and symplasmic transport between plant cells.

Finally, the fourth section presents the derivation of the flow field in an osmotic pipe, known as Aldis flow, and ends with the radially averaged flow velocity in such a pipe, which is the starting point for our analyses in the papers presented in this thesis.

3.1 From Navier-Stokes to slow, pressure-driven pipe flow

The two governing equations in fluid mechanics are the *continuity equation*, which is the conservation of mass

$$\partial_t \rho = -\boldsymbol{\nabla} \cdot (\rho \boldsymbol{v}) \tag{3.1}$$

and the *Navier-Stokes equation*, which describes the conservation of momentum

$$\rho \left[\partial_t \boldsymbol{v} + (\boldsymbol{v} \cdot \boldsymbol{\nabla})\boldsymbol{v}\right] = -\boldsymbol{\nabla} p + \eta \boldsymbol{\nabla}^2 \boldsymbol{v} + \beta\eta \boldsymbol{\nabla}(\boldsymbol{\nabla} \cdot \boldsymbol{v}) + \rho \boldsymbol{g} + \rho_{\text{el}} \boldsymbol{E}, \tag{3.2}$$

where ρ is the density and $\boldsymbol{v}$ the velocity of the fluid, p the pressure, η the dynamic viscosity, $\boldsymbol{g}$ the gravitational accelaration, ρ_{el} the electric charge density, $\boldsymbol{E}$ the external electric field and β a dimensionless viscosity ratio [Bruus, 2008]. In the work of this thesis, no external electrical fields are present, so the last term in the Navier-Stokes equation drops out. Further, fluid velocities in plants are slow, so that the fluid can be treated as incompressible ($\partial_t \rho = 0$). With this assumption, the continuity equation and the Navier-Stokes equation simplify to

$$\boldsymbol{\nabla} \cdot \boldsymbol{v} = 0 \tag{3.3}$$

$$\rho \left[\partial_t \boldsymbol{v} + (\boldsymbol{v} \cdot \boldsymbol{\nabla})\boldsymbol{v}\right] = -\boldsymbol{\nabla} p + \eta \nabla^2 \boldsymbol{v} + \rho \boldsymbol{g}. \tag{3.4}$$

The force contribution due to gravity $\rho \boldsymbol{g} = -\rho g \boldsymbol{e}_z$ is balanced by the hydrostatic pressure difference $p_{\mathrm{hs}} = -\rho g z$, thus from now on the gravity contribution is left out of Eq. (3.4) and p denotes the pressure without p_{hs}.

In slow flows, the non-linear term $(\boldsymbol{v} \cdot \boldsymbol{\nabla})\boldsymbol{v}$ can be neglected, as can be seen when expressing velocity and pressure as dimensionless quantities, using their characteristic scales U_0 and P_0:

$$\tilde{\boldsymbol{v}} = \frac{\boldsymbol{v}}{U_0} = \frac{T_0}{L_0}\,\boldsymbol{v} \tag{3.5}$$

$$\tilde{p} = \frac{p}{P_0} = \frac{L_0}{\eta U_0}\,p. \tag{3.6}$$

This is assuming that the system is characterized by only one typical length scale L_0 and one time scale T_0. With these scalings the non-dimensional form of the Navier-Stokes equation is

$$\mathrm{Re}\left[\tilde{\partial}_t \tilde{\boldsymbol{v}} + (\tilde{\boldsymbol{v}} \cdot \tilde{\boldsymbol{\nabla}})\tilde{\boldsymbol{v}}\right] = -\tilde{\boldsymbol{\nabla}}\tilde{p} + \tilde{\nabla}^2 \tilde{\boldsymbol{v}} \tag{3.7}$$

where Re is the *Reynolds number*, comparing inertial and viscous forces:

$$\mathrm{Re} \equiv \frac{L_0 U_0 \rho}{\eta}, \tag{3.8}$$

It becomes clear from Eq. (3.7), that for low Reynolds numbers the viscous term $\tilde{\nabla}^2\tilde{\boldsymbol{v}}$ dominates, while the inertial term $(\tilde{\boldsymbol{v}} \cdot \tilde{\boldsymbol{\nabla}})\tilde{\boldsymbol{v}}$ is most important for large Reynolds numbers. In the slow flows observed in plants, the Reynolds number is on the order of

$$\mathrm{Re}_{\mathrm{phloem}} \approx \frac{1..10 \cdot 10^{-6}\,\mathrm{m} \cdot 10^{-4}\,\mathrm{m/s} \cdot 10^{3}\,\mathrm{kg/m^3}}{10^{-3}\,\mathrm{Pa\,s}} = 10^{-4}..10^{-3} \tag{3.9}$$

Thus, to describe the flow in the phloem, only the low Reynolds number case is important. The reduced Navier-Stokes equation with $\mathrm{Re} \to 0$ is also called *Stokes equation*:

$$\boldsymbol{\nabla} p = \eta \nabla^2 \boldsymbol{v}. \tag{3.10}$$

One basic solution of the Stokes equation is the so called *Poiseuille flow*, the slow, pressure-driven, steady state flow in a channel, which is particularly important to describe the flow inside the conduits of plants. This solution is a parabolic flow profile, due to the no-slip boundary condition at the channel walls. For a circular cross-section of the channel, with the x-direction being the direction of flow, the solution for the velocity profile in cartesian and cylindrical coordinates is

$$v_x(y,z) = \frac{\Delta p}{4\eta L}\left(r_0^2 - y^2 - z^2\right) \tag{3.11}$$

$$v_x(r,\phi) = \frac{\Delta p}{4\eta L} r_0^2 (1 - r^2) \tag{3.12}$$

This solution is based on a constant pressure gradient $\partial_x p$, and therefore a linear pressure profile of the form

$$p(\boldsymbol{r}) = \frac{\Delta p}{L}(L - x) + p^* \tag{3.13}$$

so that $p_0 = p^* + \Delta p$ and $p(L) = p^*$. The volume flow rate, constant along the channel, is found by integrating the velocity v_x over the cross-section:

$$Q = \int v_x(y, z)\, dy\, dz = r_0^2 \int_0^{2\pi} d\phi \int_0^1 dr\, r\, v_x(r, \phi) = \frac{\pi r_0^4}{8\eta L}\Delta p. \tag{3.14}$$

With Δp the pressure potential and Q the resulting volume flow rate, we understand the ratio

$$R_{\text{Poiseuille}} = \frac{\Delta p}{Q} = \frac{8\eta L}{\pi r_0^4} \tag{3.15}$$

as the hydrodynamic resistance of a cylindrical channel, given in $\mathrm{Pa\,s\,m^{-3}}$. As the pressure gradient is linear, we can write $\Delta p/L = -\partial p/\partial x$, which gives *Darcy's law*:

$$\frac{\partial p}{\partial x} = -\frac{8\eta}{\pi r_0^4} Q. \tag{3.16}$$

3.2 The interplay of advection and diffusion

Solutes present in the fluid can be transported by advection and diffusion. Looking at a solute of concentration c, the advection-diffusion equation is

$$\partial_t c + \boldsymbol{v} \cdot \boldsymbol{\nabla} c = D \nabla^2 c \tag{3.17}$$

where D is the diffusion coefficient. Similar to the Reynolds number, which compares inertial and viscous forces, there is a non-dimensional number, which compares advective and diffusive transport velocity. It is the Peclet number and defined as

$$\mathrm{Pe} \equiv \frac{L_0 U_0}{D}. \tag{3.18}$$

where again U_0 is a typical velocity and L_0 a typical length. In the high Peclet number regime, advective transport is much faster than diffusive transport, while diffusion dominates for small Peclet numbers.

A system which has more than one typical length scale, can have different Peclet numbers assigned. For example in a cylindrical cell, a radial Peclet number Pe_r compares radial diffusion with a radial flow velocity, e.g. an osmotic flow over the membrane wall. Pe_r then could be used to estimate the importance of a diluted boundary layer due to the inflow of water. The same cell can also have an axial Peclet number Pe_a, comparing diffusion and advection along the cell, e.g. to estimate how fast bulk

flow has to be to outrun diffusive transport. And sometimes even "mixed" Peclet numbers are used, comparing e.g. radial diffusion with axial advection. This could be used to determine, if radial diffusion of loaded sugars is fast enough to replenish the sugars flushed away by the bulk flow.

In the phloem conduits of plant leaves, comparing the advective transport along the conduits with radial diffusion, the Peclet number is on the order of

$$\mathrm{Pe}_{\mathrm{phloem}} \approx \frac{1..10 \cdot 10^{-6}\,\mathrm{m} \cdot 10^{-4}\,\mathrm{m/s}}{10^{-10}\,\mathrm{m^2/s}} = 1..10. \tag{3.19}$$

3.3 Osmotic membrane flow

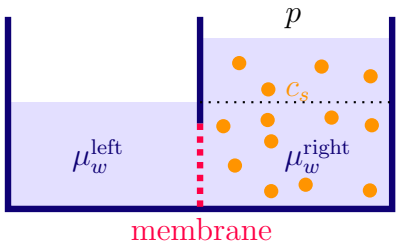

Figure 3.1: Two compartments separated by a semi-permeable membrane. The higher concentration of solute c_s on the right side leads to a lower water potential μ_w on the right side, and thus a flow of water from left to right. The equilibrium is reached, when the hydrostatic pressure p reaches the osmotic pressure of the solution.

A membrane is a porous boundary between two volumes. If the pores are short and wide, the resistance for fluid to pass the membrane is low. Longer, more narrow pores lead to a significant resistance, or reduced permeability. The permeability (sometimes also termed *conductivity*) is usually denoted as L_p, which is given in $\mathrm{m\,s^{-1}\,Pa^{-1}}$.

Osmosis The term *osmosis* was established by Graham [1854], while the phenomenon had already been discovered and described about a hundred years earlier by Nollet [1752]: Nollet closed an alcohol filled flask using a piece of bladder as a cap and immersed it in water, in order to avoid contact with air. Coming back a few hours later, he noticed with surprise that the bladder was stretched and bulged outwards, and he concluded that water must have entered the flask. The bladder acted as a semi-permeable membrane where water could go through, but alcohol could not.

In this case, the bulk flow of fluid is not due to a hydrostatic pressure potential Δp, but due to an entropic effect, depending on the difference in concentration of solute Δc across the membrane. In analogy to Δp, this potential is called *osmotic pressure*.

The osmotic pressure is derived from the chemical potential μ_j, which is the free energy per mole of a chemical species j [Nobel, 2009]. In an aquaeous solution of

sucrose there are two chemical species – water (the solvent) and sucrose (the solute). Experimental evidence suggests a logarithmic relation of the chemical potential μ_j to the activity a_j:

$$\mu_w = \mu_w^* + RT \ln a_w = \mu_w^* + RT \ln(\gamma_w N_w) \tag{3.20}$$
$$\mu_s = \mu_s^* + RT \ln a_s = \mu_s^* + RT \ln(\gamma_s c_s) \tag{3.21}$$

where R is the gas constant, T the temperature, γ_j the activity coefficient ($\gamma = 1$ for ideal solutions and $\gamma < 1$ in real solutions), c_s the concentration of sucrose, and N_w is the mole fraction of water. The chemical potential is expressed relative to an arbitrary reference level μ_j^*, which cancels out when looking at differences of the chemical potential. Eqs. (3.20) and (3.21) neglect effects of hydrostatic pressure, electrical interactions and gravity. The mole fraction of water is defined as

$$N_w \equiv \frac{n_w}{n_w + n_s} = 1 - \frac{n_s}{n_w + n_s} \tag{3.22}$$

with n_w and n_s the number of moles of water and sucrose. In dilute solutions, the number of moles of sucrose is much less than that of water ($n_s \ll n_w$) and the chemical potential of water can be simplified by using

$$\ln a_w = \ln N_w = \ln\left(1 - \frac{n_s}{n_w + n_s}\right) \approx -\frac{n_s}{n_w + n_s} \approx -\frac{n_s}{n_w}. \tag{3.23}$$

Let us now consider two compartments separated by a semi-permeable membrane as in Fig. 3.1. The left compartment contains pure water and is at atmospheric pressure, while in the right compartment the concentration of sucrose is $c_s > 0$. Water is taken up into the right compartment, leading to a hydrostatic pressure p. The chemical potential of the water in the left and the right compartment is then

$$\mu_w^{\text{left}} = \mu_w^* \tag{3.24}$$
$$\mu_w^{\text{right}} = \mu_w^* + \bar{V}_w p + RT \ln a_w \tag{3.25}$$

where $\bar{V}_w$ is the partial molal volume of water. An equilibrium is reached, when the chemical potential on the two sides is the same:

$$\begin{aligned} \mu_w^{\text{left}} &= \mu_w^{\text{right}} \\ \Rightarrow \bar{V}_w p &= -RT \ln a_w \\ p &= -\frac{RT}{\bar{V}_w} \ln a_w \approx -\frac{RT}{\bar{V}_w}\left(-\frac{n_s}{n_w}\right) = RT\frac{n_s}{\bar{V}_w n_w} = RTc_s \equiv \Pi. \end{aligned} \tag{3.26}$$

where we used the approximation for dilute solutions (Eq. (3.23)). The pressure reached in equilibrium is the osmotic pressure Π.

Eq. (3.26) is known as the Van't Hoff relation. Van't Hoff won the first Nobel prize in chemistry in 1901 in recognition of "the extraordinary services he has rendered by

the discovery of the laws of chemical dynamics and osmotic pressure in solutions“ [Nob, 2014; Van't Hoff, 1887].

The water flux J_w over a membrane hence depends in general on both hydrostatic and osmotic pressure difference across the membrane:

$$J_w = L_p(\Delta p - \Delta\Pi) \equiv L_p \Delta\Psi. \tag{3.27}$$

This difference between hydrostatic and osmotic pressure potential $\Delta\Psi$ is termed *water potential* [Nobel, 2009].

Hindered diffusion and advection In the situation above, the case of a perfectly selective membrane, or semi-permeable membrane, was described. For solutes smaller than the pores of the membrane, the osmotic pressure will be reduced, as some of the molecules will be able to pass the membrane. One can multiply the osmotic pressure Π with a *reflection coefficient* σ to quantify this reduction of the osmotic pressure. It was Kedem and Katachalsky, who described the flux of water J_w and solute J_s over a porous membrane with the following equations [Kedem and Katchalsky, 1958]:

$$J_\mathrm{w} = L_p(\Delta p - \sigma RT\Delta c) \tag{3.28}$$

$$J_\mathrm{s} = \omega RT\Delta c + (1-\sigma)\bar{c}J_\mathrm{w} \tag{3.29}$$

where $\bar{c}$ is the mean solute concentration, ω is the mobility of the solute and σ is the reflection coefficient. If the membrane is ideally semi-permeable, then $\sigma = 1$ and $\omega = 0$. In the other extreme, the membrane is non-selective and the solute moves unhindered, meaning that $\sigma = 0$ and ω is directly proportional to the free diffusion coefficient ($\omega = \frac{A}{dRT} D_\mathrm{free}$, with A and d the area and thickness of the membrane, and assuming a constant concentration gradient).

In a more mechanistic approach, Dechadilok and Deen [2006] review the theory of hydrodynamic hindrance of uncharged, spherical particles in long pores of uniform cross-section, in particular cylindrical and parallel-plate (slit) channels. Part of this hindrance is purely steric, meaning due to spatial contraints. In the case of a spherical solute, the fraction of the cross-sectional area of the pore, that is accessible to the sphere center, is

$$(1-\lambda)^2 \qquad \text{(cylindrical pores)} \tag{3.30}$$

$$(1-\lambda) \qquad \text{(slit pores)}, \tag{3.31}$$

where λ is the ratio of the radii of the solute and the pore:

$$\lambda = \frac{r_\mathrm{solute}}{r_\mathrm{pore}}. \tag{3.32}$$

There are no simple analytical expressions for the overall hindrance factors H (diffusion) and W (convection). Currently, the best estimates obtained by cross-sectional averaging are given as series expansions in λ [Dechadilok and Deen, 2006]. H and W

are parameters used instead of σ and ω to express diffusive and convective hindrance. W is connected to the reflection coefficient simply as

$$W = 1 - \sigma, \tag{3.33}$$

while H directly relates the free and the hindered diffusion coefficient as

$$D_{\text{hind.}} = \gamma H D_{\text{free}}, \tag{3.34}$$

where γ is the pore covering fraction of the membrane. Written in terms of H and W, Eqs. (3.28) and (3.29) become

$$J_{\text{w}} = L_p(\Delta p - (1 - W)RT\Delta c) \tag{3.35}$$

$$J_{\text{s}} = \frac{A}{d} D_{\text{hind.}} \Delta c + W c J_{\text{w}}. \tag{3.36}$$

In this mechanistic picture considering pores of definite length d, the concentration c is the local concentration, not the average of the two sides.

3.4 Aldis flow

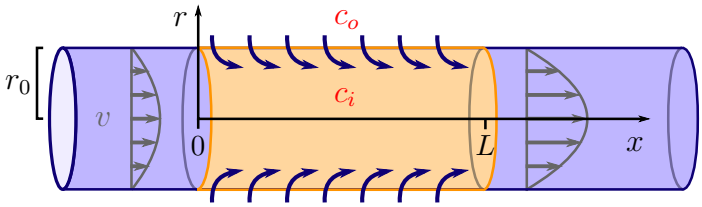

Figure 3.2: Aldis flow in a partly osmotic, cylindrical pipe. The arrows indicate water flow. The difference in concentration $\Delta c = c_i - c_o$ drives an osmotic uptake of water over the semi-permeable membrane part of length L.

Aldis [1988] derived the flow field inside a cylindrical pipe, the walls of which are permeable to water along a length L (Fig. 3.2). The concentration of solute is higher inside the pipe (c_i) than outside (c_o), thus water is taken up into the pipe. Upstream and downstream of the osmotic section, there is a parabolic flow profile, as given by the Poiseuille solution.

Starting from the Stokes equations - assuming low Reynolds number flow - the velocity field inside this pipe can be derived as follows (see [Aldis, 1988; Jensen et al., 2016]):

$$\boldsymbol{\nabla} p = \eta \nabla^2 \boldsymbol{v} \tag{3.37}$$

as given in Eq. (3.10). In cylindrical coordinates (x, r, ϕ), this set of equations is

$$\frac{\partial p}{\partial x} = \eta \left[\frac{\partial^2 v_x}{\partial r^2} + \frac{1}{r^2}\frac{\partial^2 v_x}{\partial \phi^2} + \frac{\partial^2 v_x}{\partial x^2} + \frac{1}{r}\frac{\partial v_x}{\partial r} \right] \tag{3.38}$$

$$\frac{\partial p}{\partial r} = \eta \left[\frac{\partial^2 v_r}{\partial r^2} + \frac{1}{r^2}\frac{\partial^2 v_r}{\partial \phi^2} + \frac{\partial^2 v_r}{\partial x^2} + \frac{1}{r}\frac{\partial v_r}{\partial r} - \frac{2}{r^2}\frac{\partial v_\phi}{\partial \phi} - \frac{v_r}{r^2} \right] \tag{3.39}$$

$$\frac{1}{r}\frac{\partial p}{\partial \phi} = \eta \left[\frac{\partial^2 v_\phi}{\partial r^2} + \frac{1}{r^2}\frac{\partial^2 v_\phi}{\partial \phi^2} + \frac{\partial^2 v_\phi}{\partial x^2} + \frac{1}{r}\frac{\partial v_\phi}{\partial r} - \frac{2}{r^2}\frac{\partial v_r}{\partial \phi} - \frac{v_\phi}{r^2} \right]. \tag{3.40}$$

The flow is assumed to be axis-symmetric (no ϕ-dependence) and of the form

$$\boldsymbol{v} = v_x \boldsymbol{e}_x + v_r \boldsymbol{e}_r + 0 \cdot \boldsymbol{e}_\phi. \tag{3.41}$$

With these assumptions, the Stokes equations become

$$\frac{\partial p}{\partial x} = \eta \left[\frac{\partial^2 v_x}{\partial r^2} + \frac{1}{r}\frac{\partial v_x}{\partial r} + \frac{\partial^2 v_x}{\partial x^2} \right] \tag{3.42}$$

$$\frac{\partial p}{\partial r} = \eta \left[\frac{\partial^2 v_r}{\partial r^2} + \frac{1}{r}\frac{\partial v_r}{\partial r} - \frac{v_r}{r^2} + \frac{\partial^2 v_r}{\partial x^2} \right] \tag{3.43}$$

and the continuity equation $\boldsymbol{\nabla} \cdot \boldsymbol{v} = 0$ (Eq. (3.3)) for this velocity field is

$$\frac{\partial v_x}{\partial x} + \frac{v_r}{r} + \frac{\partial v_r}{\partial r} = 0. \tag{3.44}$$

The boundary conditions are that the radial flow component vanishes at the center line, there is a no-slip condition for the axial flow component at the wall, and the radial flow component at the wall is the inward osmotic inflow velocity v_0 due to the difference in water potential across the membrane:

$$v_r(x, 0) = 0 \tag{3.45}$$

$$\frac{\partial}{\partial r} v_x(x, 0) = 0 \tag{3.46}$$

$$v_x(x, r_0) = 0 \tag{3.47}$$

$$v_r(x, r_0) = -v_0(x) \tag{3.48}$$

where

$$v_0(x) = L_p[RT(c_i(x, r_0) - c_o) - (p_i(x, r_0) - p_o)]. \tag{3.49}$$

To analyze the importance of the different terms in the governing equations, the vari-

ables are scaled as

$$X = \frac{x}{L} \tag{3.50}$$

$$R = \frac{r}{r_0} \tag{3.51}$$

$$V_x = \frac{v_x}{v_x^*} = \frac{v_x}{Q/\pi r_0^2} \tag{3.52}$$

$$V_r = \frac{v_r}{v_r^*} = \frac{v_r}{Q/2\pi L r_0} = \frac{2L}{r_0}\frac{v_r}{v_x^*} \tag{3.53}$$

$$P = \frac{r_0^2}{\eta v_x^* L}\, p \tag{3.54}$$

where v_x^* is a scale for the bulk flow and v_r^* a scale for the osmotic inflow. The velocity scales are connected by the surface to volume ratio of the pipe, that is $v_x^* = 2\frac{L}{r_0}v_r^*$, as indicated in Eqs. (3.52) and (3.53).

The scaled Eqs. (3.42)-(3.44) are

$$\frac{\partial P}{\partial X} = \frac{r_0^2}{L^2}\frac{\partial^2 V_x}{\partial X^2} + \frac{1}{R}\frac{\partial V_x}{\partial R} + \frac{\partial^2 V_x}{\partial R^2} \tag{3.55}$$

$$\frac{2L^2}{r_0^2}\frac{\partial P}{\partial R} = \frac{r_0^2}{L^2}\frac{\partial^2 V_r}{\partial X^2} + \frac{1}{R}\frac{\partial V_r}{\partial R} + \frac{\partial^2 V_r}{\partial R^2} - \frac{V_r}{R^2} \tag{3.56}$$

$$0 = 2\frac{\partial V_x}{\partial X} + \frac{V_r}{R} + \frac{\partial V_r}{\partial R} \tag{3.57}$$

and the scaled boundary conditions are

$$V_r(X,0) = 0 \tag{3.58}$$

$$\frac{\partial}{\partial R}V_x(X,0) = 0 \tag{3.59}$$

$$V_x(X,1) = 0 \tag{3.60}$$

$$V_r(X,1) = -V_0(X). \tag{3.61}$$

From these scaled equations arises a simplification in the case of a long, narrow pipe with $r_0 \ll L$, the so-called *lubrication approximation*. In the sieve tubes of the phloem this approximation is certainly valid. In this limit, terms with $\frac{r_0^2}{L^2}$ can safely be neglected. Thus the radial pressure gradient is very small, we can disregard Eq. (3.56), and are left with

$$\frac{\partial P}{\partial X} = \frac{1}{R}\frac{\partial V_x}{\partial R} + \frac{\partial^2 V_x}{\partial R^2} = \frac{1}{R}\frac{\partial}{\partial R}\left(R\frac{\partial V_x}{\partial R}\right) \tag{3.62}$$

$$0 = 2\frac{\partial V_x}{\partial X} + \frac{V_r}{R} + \frac{\partial V_r}{\partial R} = 2\frac{\partial V_x}{\partial X} + \frac{1}{R}\frac{\partial}{\partial R}\left(RV_r\right). \tag{3.63}$$

Darcy's law (Eq. (3.16)) relates the pressure gradient with the volume flow taken up by osmosis, here expressed as the integral over the inflow velocity up to position X:

$$\frac{\partial P}{\partial X} = -8\int_0^X V_0(X')dX' \tag{3.64}$$

Inserting this into Eq. (3.62) and using the ansatz $V_x(R,X) = f(R)\frac{r_0}{2}\int_0^X V_0(X')dX'$, we find an ordinary differential equation for $f(R)$, and its solution:

$$-\frac{16}{r_0} = \frac{1}{R}\frac{\partial}{\partial R}\left(R\frac{\partial f(R)}{\partial R}\right) \tag{3.65}$$

$$\Rightarrow f(R) = \frac{4}{r_0}\left(1-R^2\right), \tag{3.66}$$

fulfilling the boundary conditions Eqs. (3.59) and (3.60). Thus the solution for the axial velocity is

$$V_x(R,X) = 2(1-R^2)\int_0^X V_0(X')dX'. \tag{3.67}$$

Inserting this solution into Eq. (3.63), we now find the solution for the radial velocity, fulfilling the boundary conditions Eqs. (3.58) and (3.61):

$$V_r(R,X) = \left(R^3 - 2R\right)V_0(X). \tag{3.68}$$

Going back to dimensional variables, the solutions for the flow field components are

$$v_x(x,r) = \left[1-\frac{r^2}{r_0^2}\right]\frac{4}{r_0}\int_0^x v_0(\xi)d\xi \tag{3.69}$$

$$v_r(x,r) = \left[\frac{r^3}{r_0^3} - 2\frac{r}{r_0}\right]v_0(x). \tag{3.70}$$

The flow components of the Aldis flow field (Eqs. (3.69) and (3.70)) for the case of constant concentration along the wall ($v_0(x) = v_0$) are displayed in Fig. 3.3.

Often we are only interested in the radially averaged velocity $u(x) = \langle v_x\rangle_r$ and concentration profile $c(x) = \langle c\rangle_r$ along the pipe, assuming that the solution is well-stirred. The bulk flow entering the pipe up to postion x is the integrated inflow velocity (Eq. (3.49)):

$$Q(x) = 2\pi r_0\int_0^x v_0(x')dx' \tag{3.71}$$

The radially averaged change in flow velocity in the pipe is then

$$\frac{\partial u}{\partial x} = \frac{1}{\pi r_0^2}\frac{\partial Q}{\partial x} = \frac{2}{r_0}v_0(x) = \frac{2L_p}{r_0}(RT\Delta c(x) - \Delta p(x)). \tag{3.72}$$

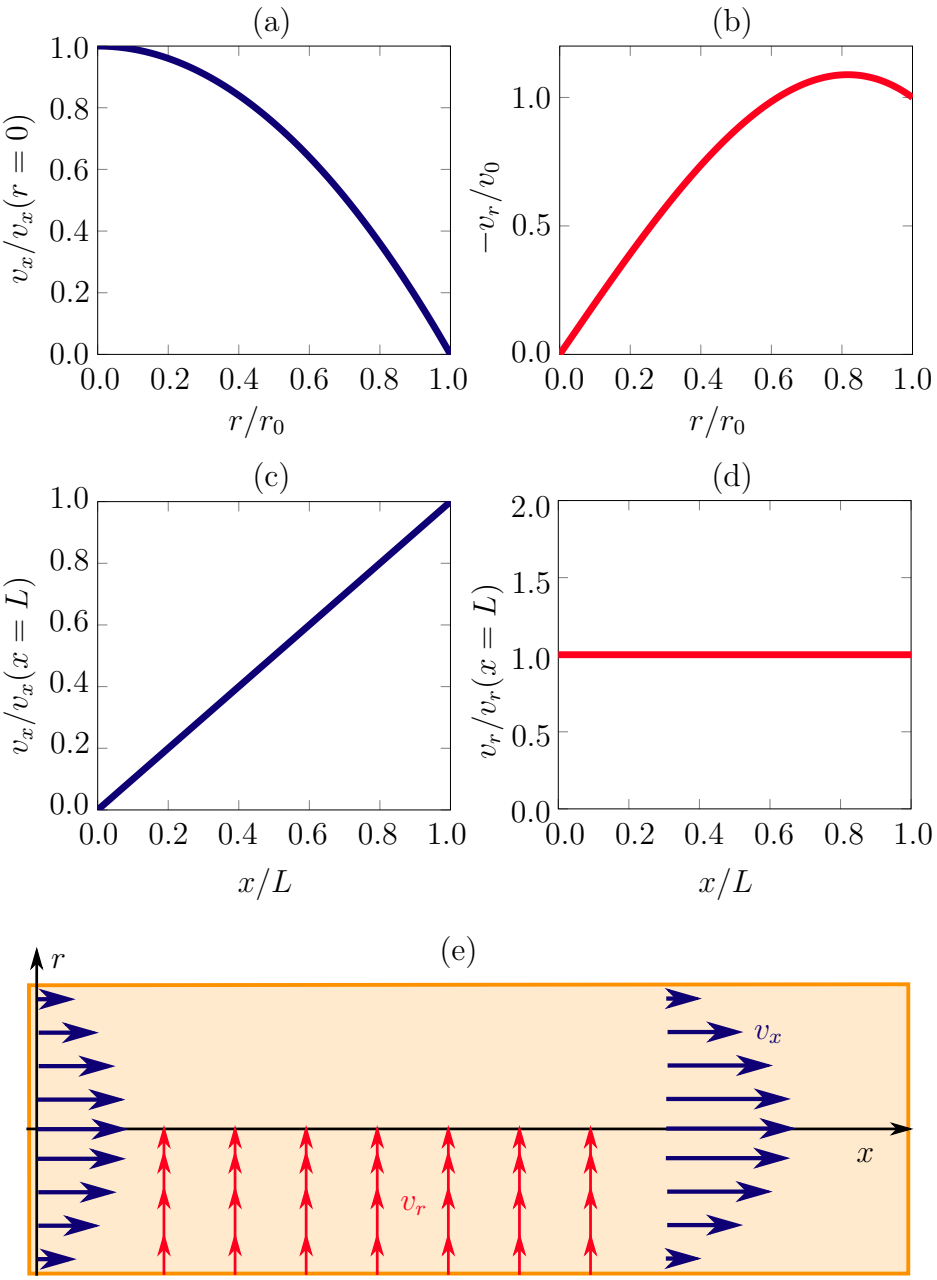

Figure 3.3: Aldis flow field components $v_x(r)$ and $v_r(r)$, here for the case of constant concentration along the wall ($c(x, r = r_0) = \text{const.} \Rightarrow v_0(x) = v_0$). (a) Axial velocity v_x is highest at the centerline and reaches zero at the wall (no-slip BC). (b) Radial velocity v_r is equal to v_0 at the wall by definition and goes to zero at the centerline. (c) Axial velocity increases linearly along the centerline, due to the assumption of constant concentration along the wall. (d) Radial velocity at a fixed radial distance is constant, again due to the assumption of constant concentration along the wall. (e) Qualitative visualization of axial (blue) and radial (red) flow components v_x and v_r.

4 Summary of the results

This chapter gives a summary of the four original research papers which are part of this Ph.d. thesis, in the order in which they appear in Chapter 5. Additional comments, experiments and results for each paper are appended in Chapter 6, following the same order.

4.1 Paper I: Theoretical analysis of the polymer trap mechanism

Biologists have categorized the loading of photosynthesized sugars into the phloem transport system of the plant into three basic mechanisms (see Sec. 2.3). These categories were based on structural and experimental observations, however, the physics are not well understood. Of these three mechanisms, the polymer trap is particularly interesting from a physics point of view. Like in passive loaders, there is a symplasmic connection from mesophyll cells to phloem cells via plasmodesmata (PDs), yet it is an active mechanism, that makes use of enzymes to trap and concentrate sugars in the phloem by oligomerization. This description of active symplasmic loading raises several questions:

Firstly, is the mechanism *feasible* from a physics perspective at all? This includes the issue, that the plasmodesmal pores in this loading type have to act as very precisely tuned filters, which can retain raffinose in the phloem, while allowing for sufficient uptake of sucrose. It further includes the question, whether we can find a set of reasonable values for pressures, concentrations and flow rates, comparing to values found in plants.

Secondly, what is the route of water uptake and transport along the pre-phloem pathway? Where does the water necessary to drive the flow enter into the phloem? If water does not enter over the plasma membrane of the sieve elements or companion cells, but via the plasmodesmata along with the sugar, this has consequences for the sugar loading step as well. How large are the proportions of advectively and diffusively loaded sucrose?

We studied the water and sugar transport in the polymer trap mechanism with a theoretical model, focusing on the two interfaces bundle sheath/intermediary cell and intermediary cell/sieve element (Fig. 4.1). Our analytical model describes steady-state situations using the Kedem-Katchalsky equations [Kedem and Katchalsky, 1958] combined with hindrance factors for diffusive and advective transport in pores [Dechadilok and Deen, 2006] (see also Sec. 3.3). Literature values for morphological and physiological parameters are scarce, thus we picked one relatively well described, active

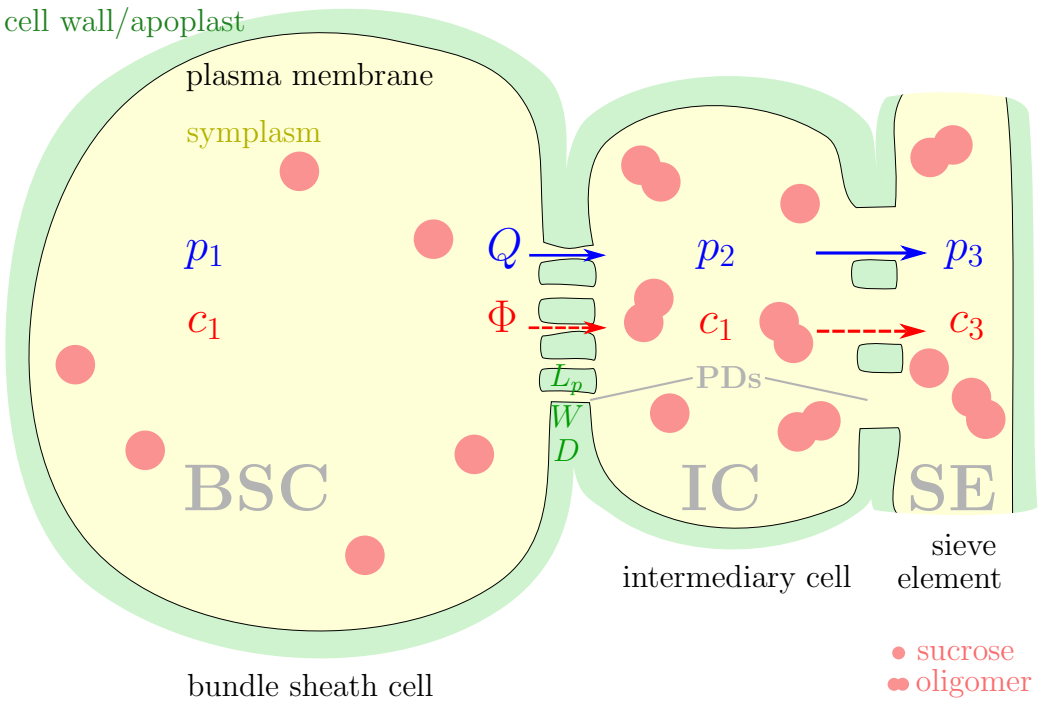

Figure 4.1: A mechanistic model of the polymer trap mechanism. Sucrose entering the intermediary cell from the bundle sheath is enzymatically converted into slightly larger oligomers. Due to the very narrow plasmodesmata between these cells, the oligomers are trapped in the intermediary cell. Looking at pressures p and concentrations of sugars c, we study the feasibility of this mechanism as well as the advective and diffusive contributions of sugar uptake Φ over the bundle sheath / intermediary cell interface.

symplasmic loading species (musk melon, *Cucumis melo*), and we calculate the sugar and water fluxes for some special cases.

Looking at a purely diffusive sugar loading situation as a first special case, we conclude that there exists a range of pore sizes which allows for sufficient sucrose transport, while retaining raffinose in the phloem. The general situation with diffusive and advective sugar transport can become quite complicated due to many unknown parameters (pressures, bulk flows), and can be simplified by assuming equal sugar concentrations in the intermediary cell (IC) and the sieve element (SE). This assumption is reasonable, because IC and SE are well connected by larger PDs. In this second special case, we find that the polymer trap mechanism is feasible for the values measured in musk melon and that the sugar loading from bundle sheath cell (BSC) into intermediary cell is mostly diffusive with advection contributing about 15%.

Even though the advective contribution is not dominating the sugar uptake, we notice that the plant does not need to take up more water osmotically into the phloem in order to drive the flow. This is also confirmed in the third special case where we again allow for different concentrations in IC and SE, but demand that all sieve elements along the vein have the same pressure and sugar concentration. This condition comprises, that no additional water can be taken up over the SE plasma membrane from the apoplast. Also in this case the pressures and concentrations resulting from our calculations give a consistent picture.

4.2 Paper II: Diffusion and bulk flow in passive phloem loading

Even in modern textbooks [Taiz et al., 2015], passive symplasmic loading (see Sec. 2.3.3) is described as a purely diffusive process. However, the symplasmic connection of the mesophyll cells to the phloem opens the possibility of an advective component of sugar transport in the pre-phloem pathway, just like in the polymer trap mechanism. A significant advective contribution to the sugar uptake in passively loading plants could help explain how these plants can compete with active loaders, which have an advantage due to their higher concentrations in the phloem.

With the assumption that passive loading has potentially two contributions – advective and diffusive – we analyze under which conditions the advective contribution becomes important. We demonstrate the advective sugar loading component in 3d-printed, biomimetic devices. We further study advective and diffusive transport contributions in a theoretical model, describing sugar export from a system with three compartments corresponding to xylem (X), mesophyll (M) and phloem (P) tissue, taking the functions of water reservoir, sugar reservoir and sugar export tissue, respectively (Fig. 4.2). From our analytical model, we can identify relevant parameters which determine the rate of sugar export and the proportions of advective and diffusive transport contributions.

In the experiments, the compartments are arranged in the order XMP, so that wa-

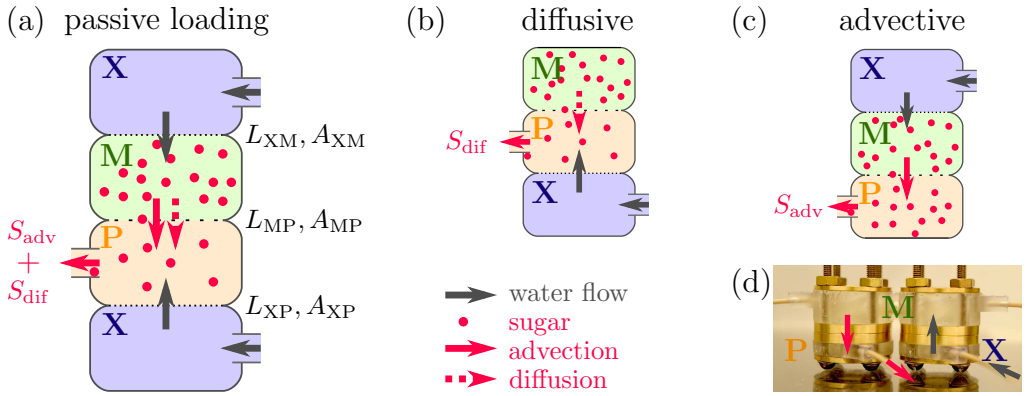

Figure 4.2: Diffusive and advective component in passive phloem loading. (a) In passive symplasmic loading, the mesophyll (M) and phloem (P) tissue are well connected via intercellular channels. Water can be taken up by osmosis from the xylem (X) into the phloem either directly or via the mesophyll. As a consequence the uptake of sugars from the mesophyll into the phloem has a diffusive component S_{dif} and an advective component S_{adv}. These components can be analyzed separately (b,c). (d) Biomimetic device used to demonstrate the advective configuration. A leaky membrane is used to model the intercellular channels between M and P, whereas X and M are separated by an osmotic membrane. The device is about 5 cm in height.

ter entering the mesophyll from the xylem can advect sugar into the phloem. This is a purely advective device once steady-state is reached, since then the concentration in mesophyll and phloem will be the same. In a purely diffusive situation, the compartments would be arranged in the order MPX, so that sugar and water enter the phloem over different interfaces. A full model, allowing for both advective and diffusive loading, would be realized as a XMPX configuration.

We find that the size of the pores connecting mesophyll and phloem, the interface areas, as well as the sugar concentration are the key parameters to determine sugar uptake into the phloem. Of these, the pore size has the largest influence on the ratio of advective to diffusive loading in the parameter ranges relevant for plants.

4.3 Paper III: On the size of conifer needles

After loading sugars into the phloem conduits, they are exported from the leaf by the osmotically driven bulk flow. In this paper we study the export of sugars from phloem venation of the simplest geometry: parallel, unbranched conduits, as they are found e.g. in conifer needles.

It has recently been revealed, that while the diversity of plant leaves is astonishing, extant species cover only a small portion of the available morphological and physiological trait-space [Díaz et al., 2016; Kunstler et al., 2016]. This confinement can

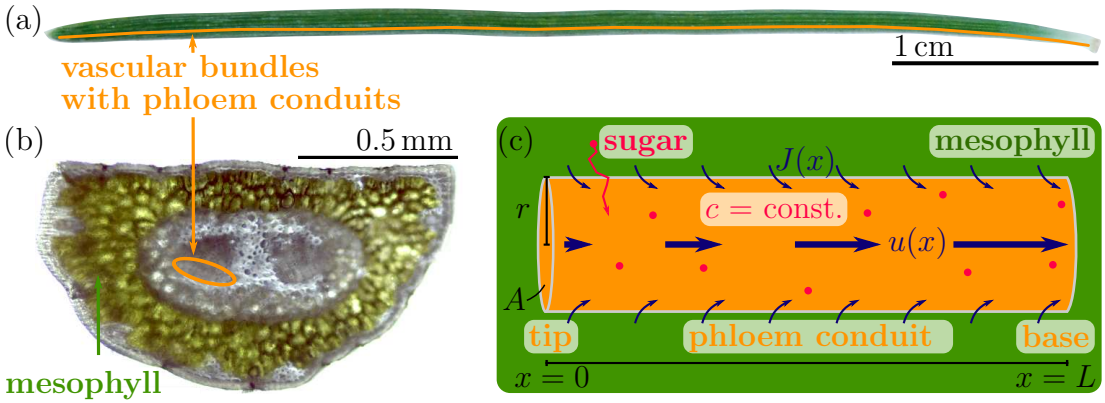

Figure 4.3: Model of sugar export from a needle. (a,b) The bottom view and cross section of a conifer needle show the vascular bundles running in parallel close to the center axis of the needle. The location of the phloem tissue is marked in orange. (c) We model one file of sieve elements as a single cylindrical pipe with radius r and length L. We assume a constant sugar concentration inside the conduit. The export of sugars from the needle is driven by the osmotic uptake of water $J(x) = L_p(RTc - p(x))$. The velocity inside the tube increases from $u(0) = 0$ at the tip to $u(L)$ at the base of the needle.

be observed in the different size ranges of conifer leaves (needles or scale-like leaves) and broad leaves of angiosperms. Looking at literature data from 519 conifer species, we find that the majority (75%) of these species has leaves shorter than 6 cm, while lengths of broad leaves span 3 orders of magnitude, from millimeters to meters. The reason for this confinement of lengths of conifer leaves is not known.

In this paper we explore, if the physics of sugar export can help explain the limited lengths of conifer leaves. We develop a theoretical model for the export of sugars from a cylindrical osmotic pipe, corresponding to a single sieve element running from the tip to the base of the leaf (Fig. 4.3). In our model, we assume a constant concentration of sugar inside the conduit, and water is taken up osmotically over the membrane surface. The transported fluid experiences two resistances: the Poiseuille resistance to moving fluid inside the conduit from the tip to the base and the resistance to fluid entering the conduit over the membrane. The ratio of these resistances is the Münch number $M = 16\eta L_p L^2/r^3$, where η is the viscosity, L_p the membrane permeability, L the length and r the radius of the conduit.

Our analysis shows the emergence of an inactive zone of stagnant fluid towards the needle tip for leaves longer than a length $L_{\text{eff}} = L/\sqrt{M}$. The stagnant zone is an intrinsic feature of the osmotically driven pipe flow. We assume that there is a biological limit to the sugar concentration, and in this case the constant concentration profile results in the largest export rate possible. As a consequence, it is in general not economic for the plant to invest in needles much longer than the effective length,

which is reflected in the data of leaf lengths of the 519 conifer species.

So why are angiosperms then able to produce much longer leaves than conifers? First of all, our model is for linear venation only, and cannot capture any benefits reticulated venation might have. Secondly, while we have only very few data on phloem conduit sizes, both for angiosperms with parallel venation and for conifers, these examples indicate that angiosperms are able to construct wider phloem conduits than conifer species. Furthermore, phloem conduits in leaves of angiosperms could be tapered (no data available to our knowledge), while a study on four conifer species showed that their conduits are uniform along the needle [Ronellenfitsch et al., 2015b].

Our model of sugar export from the leaf is simplified with respect to several potentially important processes (like sugar production and loading), and effiency in sugar export is only one among many factors possibly influencing leaf size. Thus needles longer than our predicted leaf length L_{eff} can exist, although we expect them to be the exception. However, the predicted leaf length correlates with the median of conifer leaf lengths. This intrinsic limitation of the length of phloem conduits due to the osmotic pumping mechanism has not been described before.

4.4 Paper IV: Osmotically driven flows in systems of long porous pipes

Studying the fluid flow in the branched network of blood vessels Murray [1926] found that the power dissipation of the fluid circulation is minimized, if the cube of the parent channel radius is equal to the sum of the cubes of the daughter channel radii. Experimental data from different biological transport systems indicate that Murray's law is a useful approximation to describe the branching hierarchy, as discussed in the paper by LaBarbera [1990]. Recently, Stephenson and Lockerby [2016] presented a generalized law which is valid for asymmetric branching, arbitrary cross-sectional shapes, and a range of fluidic models including turbulent and non-Newtonian fluid flow.

Murray's law seems to hold for the larger xylem conduits (i.e. in petiolules, petioles and shoots) [McCulloh et al., 2003], yet the minor vein phloem inside the leaf could behave quite differently. One major difference is that the internal fluid volume is not conserved due to the osmotic uptake of water over the conduit membrane. In fact, there are still many open questions concerning osmotically driven flows. There has been some confusion in the literature on how to calculate the energy dissipation of an osmotic pipe system, or even just a single osmotic pipe.

We therefore study the flow through an osmotic pipe in more detail. Again we assume constant concentration, and show that this is the concentration profile that leads to the largest export flow rate. We derive an expression for the energy dissipation in a slender osmotic pipe (Fig. 4.4(a)) with two main contributions: a Poiseuille contribution from moving fluid along the inside of the pipe and a membrane contribution due to the uptake of water over the surface of the pipe (Fig. 4.4(b)). Here we consider the

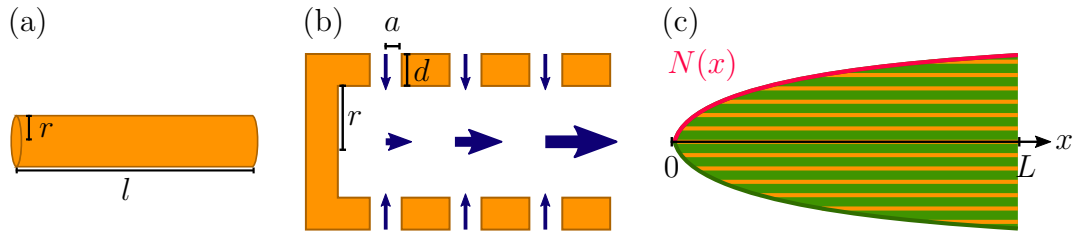

Figure 4.4: Osmotically driven flows in linear pipes. (a) We study systems where the radius r is much smaller than the length l of each pipe. (b) In slow, laminar flows through osmotic pipes energy is dissipated due to the resistance of the pores in the membrane, and due to the Poiseuille resistance of moving fluid along the inside of the pipe. (c) A system of coupled osmotic pipes in a parallel arrangement as it is found in linear leaves like conifer needles or grasses. The number of pipes follows a distribution $N(x)$ from the tip ($x = 0$) to the base ($x = L$).

pores of the membrane as cylindrical channels of finite length. We find quite simple and general expressions for the flow rates and dissipation, independent of material parameters. These expressions differ from the standard Poiseuille expressions for flows with conserved fluid volume, and show that the driving force is not just the pressure, but the water potential, which is a combination of concentration and pressure.

As a next step we look at linear systems of coupled osmotic pipes running in parallel, their lengths following a power law distribution (Fig. 4.4(c)), as it is found e.g. in linear leaves. The system is coupled in the sense that the flow velocity and pressure at any position along the linear system is unique for all pipes, as treated in Zwieniecki et al. [2006]. We find analytical solutions for flow rates and energy dissipation in these coupled systems. The solutions found for the coupled system look surprisingly similar to the ones for a single pipe. In particular, they also show the stagnant zone at the tip of long leaves.

Under the above stated assumptions (constant concentration, cylindrical membrane pores) our results indicate that the energy dissipation can not be minimized by a certain choice of the power law exponent. This differs from results of earlier work, where an exponent of 1/2 was found to minimize viscous energy dissipation or pressure dissipation, supported by experimental data on conduit length distribution [Zwieniecki et al., 2006; Ronellenfitsch et al., 2015b]. It will be an interesting future problem to conciliate these results.

5 Original papers

These are the original research papers, completed to different degrees (published, in revision, under preparation). A summary of these papers can be found in Chapter 4, additional comments, experiments and results are appended in Chapter 6, following the same order.

5.1 Diffusion and bulk flow in phloem loading: A theoretical analysis of the polymer trap mechanism for sugar transport in plants

Paper published in Physical Review E. (2014)

PHYSICAL REVIEW E **90**, 042704 (2014)

Diffusion and bulk flow in phloem loading: A theoretical analysis of the polymer trap mechanism for sugar transport in plants

Julia Dölger,[1,3] Hanna Rademaker,[1] Johannes Liesche,[2] Alexander Schulz,[2] and Tomas Bohr[1]
[1]*Department of Physics and Center for Fluid Dynamics, Technical University of Denmark, Kgs. Lyngby, Denmark*
[2]*Department of Plant and Environmental Sciences, University of Copenhagen, Copenhagen, Denmark*
[3]*Institute for Condensed Matter Physics, Darmstadt University of Technology, Darmstadt, Germany*
(Received 3 June 2014; revised manuscript received 11 August 2014; published 8 October 2014)

Plants create sugar in the mesophyll cells of their leaves by photosynthesis. This sugar, mostly sucrose, has to be *loaded* via the bundle sheath into the phloem vascular system (the sieve elements), where it is distributed to growing parts of the plant. We analyze the feasibility of a particular loading mechanism, *active symplasmic loading*, also called the *polymer trap* mechanism, where sucrose is transformed into heavier sugars, such as raffinose and stachyose, in the intermediary-type companion cells bordering the sieve elements in the minor veins of the phloem. Keeping the heavier sugars from diffusing back requires that the *plasmodesmata* connecting the bundle sheath with the intermediary cell act as extremely precise filters, which are able to distinguish between molecules that differ by less than 20% in size. In our modeling, we take into account the coupled water and sugar movement across the relevant interfaces, without explicitly considering the chemical reactions transforming the sucrose into the heavier sugars. Based on the available data for plasmodesmata geometry, sugar concentrations, and flux rates, we conclude that this mechanism can in principle function, but that it requires pores of molecular sizes. Comparing with the somewhat uncertain experimental values for sugar export rates, we expect the pores to be only 5%–10% larger than the hydraulic radius of the sucrose molecules. We find that the water flow through the plasmodesmata, which has not been quantified before, contributes only 10%–20% to the sucrose flux into the intermediary cells, while the main part is transported by diffusion. On the other hand, the subsequent sugar translocation into the sieve elements would very likely be carried predominantly by bulk water flow through the plasmodesmata. Thus, in contrast to apoplasmic loaders, all the necessary water for phloem translocation would be supplied in this way with no need for additional water uptake across the plasma membranes of the phloem.

DOI: 10.1103/PhysRevE.90.042704 PACS number(s): 87.16.dp, 47.63.−b, 47.56.+r

I. INTRODUCTION

Leaves maintain an extremely delicate balance between water and sugar translocation to ensure the outflow and eventual evaporation of water from the *xylem* cells simultaneously with the inflow of water and sugar to the *phloem* cells nearby. Xylem and phloem are the two long distance pathways in vascular plants, where the former conducts water from the roots to the leaves and the latter distributes the sugar produced in the leaves. The sugar which is loaded into the *sieve elements*, the conducting cells of the phloem, is generated in the chloroplasts of the *mesophyll cells* outside the *bundle sheath*, a layer of tightly arranged cells around the vascular bundle, which protects the veins of both xylem and phloem from the air present in the space between the mesophyll cells and the *stomata*. The latter are specialized cells that control the air flow in and out of the leaf by adjusting the size of pores in the epidermis. The water which leaves the xylem is under negative pressure (up to −80 bars have been reported [1]), whereas the water in the phloem a few micrometers away is under positive pressure, typically around +10 bars [2]. On the other hand, the sugar concentration is close to 0 in the xylem and up to 1 molar in the phloem, where the *Münch mechanism* [3] is believed to be responsible for the flow: the large sugar concentrations in the phloem cells of the mature "source" leaves will by osmosis increase the pressure and drive a bulk flow towards the various "sinks," where sugar is used.

The water flow from the xylem has two important goals: most of it evaporates, presumably from the walls of the mesophyll cells, maintaining the negative pressures in the xylem necessary to draw water from the roots, but a small part of it passes across the plasma membranes into the mesophyll cells and takes part in the photosynthesis and the subsequent translocation of the sugars through the bundle sheath towards the sieve elements of the phloem. This loading process is not understood in detail, but several important characteristics are known and plants have been divided into rough categories [4] depending on their loading mechanisms. Many trees are so-called "passive loaders," which means that the sugar concentration is largest in the mesophyll and decreases towards the sieve cells. This implies that sugar could simply diffuse from mesophyll cells to sieve elements without any active mechanism.

In other plants the concentrations are reversed, with the largest concentration occurring in the phloem, which then involves some active mechanism. An interesting class of plants is believed to make use of the so-called "active symplasmic" loading or "polymer trap" mechanism [4] which is illustrated in Fig. 1. Here high concentrations, and thus efficient sugar translocation in the sap, are achieved actively, by transforming the sucrose generated in the mesophyll and transported into the bundle sheath into heavier sugars, the oligosaccharides raffinose and stachyose, which are too large to diffuse back.

The flow into the phloem can follow two pathways, either through the *symplasm* (the interior of the cells) or through the *apoplast* (the space outside the plasma membranes, e.g., cell walls). In symplasmic loaders abundant plasmodesmata, i.e., membrane-surrounded channels through the cell walls, provide continuity of the loading pathway, and therefore the sugar does not have to pass the plasma membranes as shown

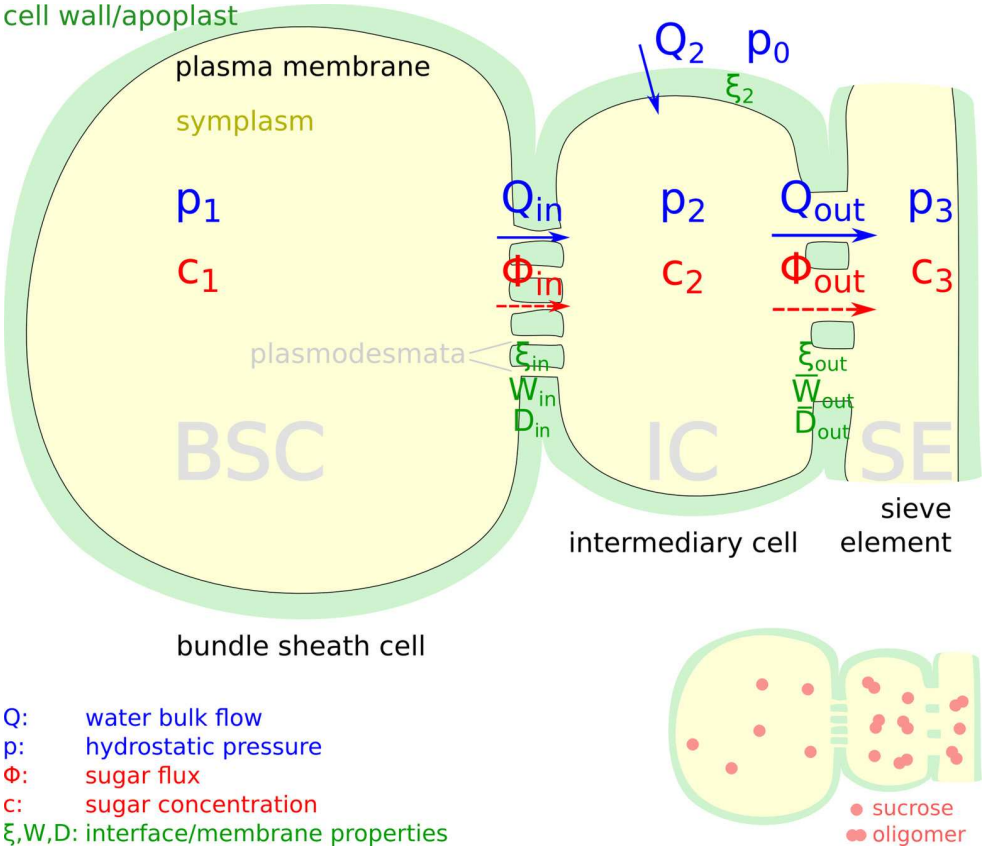

FIG. 1. (Color online) The polymer trap model with diffusion and bulk flow. The water flow rates Q through the cell interfaces and IC membrane are depicted with blue (full) arrows, the sugar flow rates Φ as red (dashed) arrows. These flows depend on the pressures p as well as on sucrose and oligomer concentrations c inside and outside the cells on the loading pathway. The semipermeable cell interfaces are characterized by the permeability ξ, the bulk hindrance factor W, and the effective diffusion coefficient D with subscripts "in" and "out." Bundle sheath cell (BSC), intermediary cell (IC), and sieve element (SE) are numbered according to the loading steps. The IC and SE are both part of the phloem and are well connected via wide contacts called *pore plasmodesma units*. The BSC-IC interface is characterized by narrow plasmodesmata (PDs) which prevent the oligomers from diffusing back into the bundle sheath.

in Fig. 1. It has recently been pointed out that the polymer trap mechanism would require plasmodesmata with very specific filtering properties allowing sufficient amounts of sucrose to pass while blocking the heavier sugars [5].

We analyze this question in the present paper including both sugar diffusion and bulk water flow in our model without explicitly considering the chemical reactions transforming the sucrose into the heavier sugars. We restrict the scope of our model to the part of the leaf where the loading of sugar into the phloem transport system takes place. We therefore only include one bundle sheath cell (BSC), intermediary cell (IC), and sieve element (SE) and their interfaces in our study. We also restrict the model to a steady-state situation in which flows, concentrations and pressures are constant. We derive and solve general equations for this setup and check their plausibility and implications with the help of the most complete set of measured values that we could find (for *Cucumis melo*). The phloem cells in the leaf need water for sugar translocation, and they need to build up sufficient pressure (p_3 in Fig. 1) to generate efficient bulk movement of the phloem sap. On the other hand, the pressure cannot be too high in cells which are exposed to the xylem. Otherwise they would lose water across the water permeable plasma membrane towards the apoplast. If sugar is loaded only via diffusion without any significant water flow, the sieve element has to draw in the water from the surroundings across its plasma membrane. This requires a sufficiently low *water potential* $\Psi = p - RTc$ in the phloem, i.e., a hydrostatic pressure p significantly lower than the osmotic pressure RTc. If, on the other hand, enough water flows along with the sugar through the plasmodesmata, i.e., symplasmically, the plant does not have to draw in water across the plasma membrane of the phloem cells (sieve element plus intermediary cells) and the hydrostatic pressure can therefore be greater, leading to more efficient vascular flow. In the following we shall point out a likely scenario (see Sec. V B), in which the polymer trap mechanism can function. We stress that this conclusion is based on very limited experimental information. There is a severe lack of precise knowledge on the anatomy of the plasmodesmata, the precise sugar concentrations (taking sufficient account of the distribution of the sugars inside the compartments of the cells), and, as the most severe problem, an almost total lack of pressure measurements. The latter reflects the fact that determination of the pressure in a functioning (living)

phloem is at present not feasible. From our analysis, however, some important features of this special and fascinating loading mechanism has become clear. Analyzing simple equilibrium configurations with the use of irreversible thermodynamics (Kedem-Kachalsky equations) and the theory of hindered transport, we show that diffusion can in fact, despite claims to the contrary [5], be sufficient to load the sucrose through narrow plasmodesmata into the phloem of a polymer trap plant, while efficiently blocking the back flow of larger sugars. The simultaneous water flow can also be of importance not only to support the sugar flux but also to achieve advantageous pressure relations in the leaf and thus to preserve the vital functions of the strongly interdependent phloem and xylem vascular systems. We show that the bulk water entering the symplasm of pre-phloem cells already outside the veins can effectively suffice to drive the Münch flow, although the same flow does only contribute a minor part to the loading of sugar into the intermediary cells of the phloem.

II. THE POLYMER TRAP MODEL

The polymer trap loading mechanism was postulated for angiosperm taxa, for example, cucurbits, and is shown in Fig. 1. Most of the concrete values which are used in our calculations, i.e., the sugar concentrations in the cells of the loading pathway [6], the surface and interface areas of the cells [7], and the total leaf sugar export [8], were measured in muskmelon (*Cucumis melo*). The cytosolic concentration of sucrose is around 200 mM [6] in the mesophyll and bundle sheath cells (BSCs) taking into account the intracellular compartmentation. Sucrose passes symplasmically through narrow plasmodesmata (PDs) into the companion cells of the phloem, which are called *intermediary cells* (ICs) in this special loading type. In the ICs the sucrose is converted to larger oligomers, also called raffinose family oligosaccharides (RFOs), which pass through relatively wide PDs into the sieve element (SE). The tetrasaccharide stachyose is the most abundant sugar oligomer in the phloem of *Cucumis melo*. The sucrose and stachyose concentrations in the phloem *cytosol*, i.e., in the cell sap outside of the vacuole, were measured to be about 132 mM and 335 mM, respectively [6]. These two sugars represent together about 87% of the total sugar concentration in the phloem, which, with a value of 539 mM, is more than twice as large as the concentration in the bundle sheath cytosol [6].

On the contrary, almost no RFOs have been found outside the SE-IC complex, and since no evidence for active sucrose transporters in the bundle sheath membranes of RFO-transporting plants have been found, it seems that the narrow plasmodesmatal pores in the BSC-IC interface must provide the delicate filtering effect letting the smaller sucrose molecules pass from the bundle sheath while retaining the oligomers in the phloem [4]. For this task, the effective pore widths must be similar to the diameters of the sugar molecules i.e., around 1 nm. Such small widths seem at least not in conflict with evidence from electron microscopy, where parts of the plasmodesmata found in the IC wall look totally obstructed [9], but where one can hardly resolve patterns of sizes below 1 nm. Schmitz *et al.* measured the total export rate in leaves of *Cucumis melo* [8], from which a sugar current density $J_{\text{in}} \approx 9.7 \times 10^{-7}$ mol m^{-2} s^{-1} across the BSC-IC interface can be calculated [5].

The explanation of the functioning of the polymer trap given by Turgeon and collaborators [4] is that the sucrose diffuses along a downhill concentration gradient into the phloem while the oligomers, which are synthesized by enzymatic reactions at this location, are blocked by the specialized narrow PDs in the IC wall from diffusing back into the bundle sheath. This simple picture was questioned by Liesche and Schulz [5], who considered quantitatively the hindered diffusion across the BSC-IC interface. In the present paper, we present an extended model, relating the transport coefficients to the structure and density of PDs in the cellular interfaces, and including explicitly the water flow. Based on the available experimental data, we show that pure diffusion *can* create a large enough sugar export in *Cucumis melo* while blocking the oligosaccharides, but since the pores are of the dimension of the sugar molecules, osmotic effects across the cell interfaces are unavoidable and probably important. Thus, the resulting water flows may be crucial for building up the bulk flow in the phloem vascular system. We calculate the hydrostatic pressures created in the cells, and to compute a possible water intake across the cell membranes, we have to compare the resulting water potentials to that of the apoplast outside the cell membranes. We expect the pressures in the apoplast to be close to the (negative) values in the xylem, which are unfortunately not known for this particular species. However, we assume the value in muskmelon to be close to that in maize, which has a typical xylem pressure of around -4 bar [10]. The (positive) so-called turgor pressure for well-hydrated living cells should be large enough to keep the fairly elastic plasma membrane tight against the rigid cell wall. Since there are, as far as we know, no data available for the leaf cell pressures in *Cucumis melo* we assume them to be larger than and close to the ambient pressure similar to the mesophyll turgor pressures measured in *Tradescantia virginiana* [11]. We use the lower limit 1 bar as a reasonable value for the bundle sheath pressure in our numerical calculations. With this assumption the pressure in the phloem thus builds up to values of close to 10 bars, which is a typical value quoted for the phloem pressure [2,12].

A. Transport equations for the polymer trap model

Our model (see Fig. 1) considers diffusion and bulk flow through the plasmodesmata of the BSC-IC and IC-SE cell interfaces and furthermore takes into account a possible osmotic water flow across the IC-plasma membrane. For simplicity we assume here that, in the IC, two sucrose molecules are oligomerized to one tetrasaccharide, corresponding to a stachyose molecule in *Cucumis melo*. The volume and sugar flows across the two cell interfaces can be written using the Kedem-Katchalsky equations [13] for membrane flows in the presence of multiple components. The volumetric water flow rates (measured, e.g., in m^3 s^{-1}) into and out of the IC can be expressed as

$$\begin{aligned} Q_{\text{in}} &= \xi_{\text{in}} \left[\left(c_2^{\text{s}} - c_1^{\text{s}}\right)\left(1 - W_{\text{in}}^{\text{s}}\right) RT + c_2^{\text{o}} RT - (p_2 - p_1) \right] \\ &= \xi_{\text{in}} \left[\Psi_1 - \Psi_2 + W_{\text{in}}^{\text{s}} \Delta c_{\text{in}}^{\text{s}} RT \right], \end{aligned} \tag{1}$$

$$Q_{\rm out} = \xi_{\rm out}\left[\left(c_3^{\rm s}-c_2^{\rm s}\right)\left(1-W_{\rm out}^{\rm s}\right)RT+\left(c_3^{\rm o}-c_2^{\rm o}\right)\right.$$
$$\left.\times\ \left(1-W_{\rm out}^{\rm o}\right)RT-(p_3-p_2)\right]$$
$$=\xi_{\rm out}\left[\Psi_2-\Psi_3+W_{\rm out}^{\rm s}\left(c_2^{\rm s}-c_3^{\rm s}\right)RT\right.$$
$$\left.+\ W_{\rm out}^{\rm o}\left(c_2^{\rm o}-c_3^{\rm o}\right)RT\right], \qquad (2)$$

where the subscripts number the cells in the sequence BSC, IC, SE, and $\Delta c_{\rm in}^{\rm s}=c_1^{\rm s}-c_2^{\rm s}$. The superscripts denote the molecule species, sucrose (s) and oligomer (o). The water potentials are defined as $\Psi_i=p_i-RTc_i$. Note that the water can flow through the plasmodesmata from a lower to a higher water potential because of the different osmotic effects of the sugar species. The coefficients W are the bulk hindrance factors $W=1-\sigma$, where σ is the reflection coefficient used by Kedem and Katchalsky. Thus, if $W=0$ for a given molecule, it cannot get through the membrane and creates a full osmotic pressure, while $W=1$ means that the molecule passes as easily as the water molecules. We use the universal gas constant $R=8.314\ \mathrm{J\,mol^{-1}\,K^{-1}}$ and the absolute temperature $T=300$ K.

The corresponding sugar flow rates (e.g., in $\mathrm{mol\,s^{-1}}$) can then be written as

$$\Phi_{\rm in}=Q_{\rm in}c_1^{\rm s}W_{\rm in}^{\rm s}+\frac{A_{\rm in}}{d}D_{\rm in}^{\rm s}\Delta c_{\rm in}^{\rm s}, \qquad (3)$$

$$\Phi_{\rm out}=Q_{\rm out}\left[c_2^{\rm s}W_{\rm out}^{\rm s}+c_2^{\rm o}W_{\rm out}^{\rm o}\right]$$
$$+\ \frac{A_{\rm out}}{d}\left[D_{\rm out}^{\rm s}\left(c_2^{\rm s}-c_3^{\rm s}\right)+D_{\rm out}^{\rm o}\left(c_2^{\rm o}-c_3^{\rm o}\right)\right]. \qquad (4)$$

Here D is a diffusion coefficient related to the diffusive mobility ω used by Kedem and Katchalsky as $D=d\omega RT$. A is an interfacial area and d is the diffusion distance, i.e., the thickness of the intermediary cell wall. The two terms in Φ describe, respectively, the advective contribution (proportional to Q) and the diffusive one (proportional to the concentration differences). The interface coefficients are computed in the next section, based upon the geometry of the PDs.

If we introduce average interface coefficients $\bar{W}_{\rm out}=(x^{\rm s}W_{\rm out}^{\rm s}+x^{\rm o}W_{\rm out}^{\rm o})$ and $\bar{D}_{\rm out}=(x^{\rm s}D_{\rm out}^{\rm s}+x^{\rm o}D_{\rm out}^{\rm o})$ with the sucrose and oligomer proportions $x^{\rm s(o)}=c_2^{\rm s(o)}/c_2=c_3^{\rm s(o)}/c_3$ in the phloem, the expressions (2) and (4) for the outflows can be simplified to

$$Q_{\rm out}=\xi_{\rm out}[(c_3-c_2)(1-\bar{W}_{\rm out})RT-(p_3-p_2)]$$
$$=\xi_{\rm out}[\Psi_2-\Psi_3+(c_2-c_3)\bar{W}_{\rm out}RT], \qquad (5)$$

$$\Phi_{\rm out}=Q_{\rm out}c_2\bar{W}_{\rm out}+\frac{A_{\rm out}}{d}\bar{D}_{\rm out}(c_2-c_3), \qquad (6)$$

where we assume that the sucrose and oligomer proportions are the same in the SE and the IC. There might also be an osmotic water flow Q_2 across the IC membrane, which builds a connection to the apoplast, where we expect a (negative) hydrostatic pressure p_0, probably close to the xylem pressure. This transmembrane flow can be written using the permeability coefficient ξ_2 and the van't Hoff equation for an ideally semipermeable IC membrane as

$$Q_2=\xi_2[RTc_2-(p_2-p_0)]=\xi_2[p_0-\Psi_2]. \qquad (7)$$

For a water flow $Q_2>0$ into the intermediary cell the water potential $\Psi_2=p_2-RTc_2$ has to be less (more negative) than the pressure p_0 in the apoplast. The flows into and out of the IC are related by conservation laws for water and sugar in the form

$$Q_{\rm in}+Q_2=Q_{\rm out}, \qquad (8)$$

$$\Phi_{\rm in}=(x^{\rm s}+2x^{\rm o})\Phi_{\rm out}, \qquad (9)$$

where Eq. (9) is derived from the mass conservation $M^{\rm s}\Phi_{\rm in}=\frac{1}{c_2}(M^{\rm s}c_2^{\rm s}+M^{\rm o}c_2^{\rm o})\Phi_{\rm out}$ of sugar molecules in the intermediary cell with the molar masses related by $M^{\rm o}=2M^{\rm s}$ used in our approximate model.

III. ESTIMATES OF THE COEFFICIENTS AND CONCENTRATIONS

The cell interfaces are modeled as porous membranes. From detailed electron microscopic investigations [7,9] the PDs at this specific interface are generally branched towards the IC. However, the detailed substructure is not known, in particular the shape and area of the *cytoplasmic sleeve* connecting the cytosol of the cells. For our modeling we simplify these channels as circular slits (see Fig. 2), as suggested in Ref. [17], with average radius $r_{\rm PD}$, half-width $h\leqslant 1$ nm, and length d equal to the thickness of the part of the cell wall belonging to the IC.

From the slit geometry together with the density $n_{\rm PD}$ of plasmodesmata and the interface areas $A_{\rm in(out)}$ (see Table I) the interface coefficients can be calculated using the hindrance factors H and W for diffusion and convection in narrow pores, which were recently analyzed by Deen and Dechadilok [18]. For spherical particles these hindrance factors have been estimated as polynomials in the relative solute size $\lambda=r_{\rm solute}/h$. The following expressions are valid for $0\leqslant\lambda\leqslant 0.8$ (H) and $0\leqslant\lambda\leqslant 0.95$ (W):

$$H(\lambda)=1+\tfrac{9}{16}\lambda\ln\lambda-1.19358\lambda+0.4285\lambda^3$$
$$-\ 0.3192\lambda^4+0.08428\lambda^5, \qquad (10)$$

$$W(\lambda)=1-3.02\lambda^2+5.776\lambda^3-12.3675\lambda^4+18.9775\lambda^5$$
$$-\ 15.2185\lambda^6+4.8525\lambda^7. \qquad (11)$$

For $\lambda\geqslant 1$ the solute should be totally blocked by the plasmodesmatal pores. In this case both hindrance factors are set to zero. Plots of the hindrance factors as functions of λ are shown in Fig. 3. The bulk hindrance factor $W_{\rm in(out)}^{\rm s(o)}$ enters our equations directly as one of the three interface coefficients. The diffusive hindrance factor $H_{\rm in(out)}^{\rm s(o)}$ is used together with the pore covering fraction $\gamma_{\rm in(out)}$ to compute the effective diffusion coefficients $D_{\rm in(out)}^{\rm s(o)}$ appearing in (3) and (4) as

$$D_{\rm in(out)}^{\rm s(o)}=\gamma_{\rm in(out)}H_{\rm in(out)}^{\rm s(o)}D^{\rm s(o)}. \qquad (12)$$

Here the covering fraction $\gamma_{\rm in(out)}$ is given as the ratio of free slit-space to total cell-interface area, i.e.,

$$\gamma_{\rm in(out)}=4\pi r_{\rm PD}h_{\rm in(out)}n_{\rm PD}, \qquad (13)$$

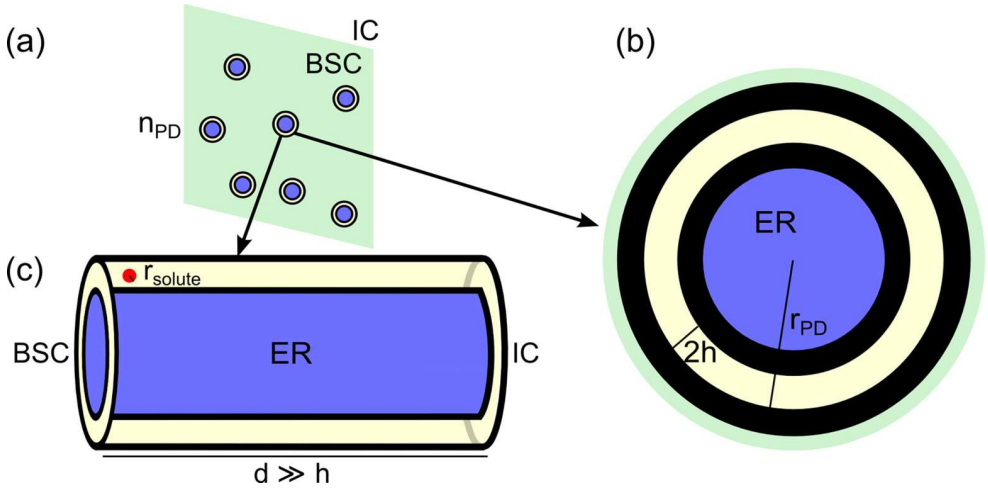

FIG. 2. (Color online) Three perspectives of the plasmodesmata modeled as slit pores. Part of the cell wall between BSC and IC with PD density n_{PD} is sketched in (a). The assumed substructure of a PD is shown in cross section (b) and three dimensionally (c). The cytoplasmic sleeve (light yellow) available for water and sugar transport is restricted by the desmotubule of the endoplasmic reticulum [ER, blue (gray)] and electron-dense particles (black) attached to the membrane, and is assumed to take the form of a circular slit with radius r_{PD}, half-width h, and length d.

where n_{PD} is the density of plasmodesmata in the IC wall, and the unobstructed sleeve is assumed to be very narrow ($h_{in(out)} \ll r_{PD}$). The free diffusion coefficient $D^{s(o)}$ of the respective solutes in cytosol can be written using the Einstein relation for diffusing spherical molecules as

$$D^{s(o)} = \frac{kT}{6\pi \eta_{cyt} r^{s(o)}} f^{s(o)} \tag{14}$$

with the hydrodynamic radii $r^{s(o)}$ of the solutes, the cytosolic viscosity η_{cyt}, and the Boltzmann constant k related to the universal gas constant $R = N_A k$ by the Avogadro constant $N_A = 6 \times 10^{23}$ mol^{-1}. The shape factor f accounts for the deviation from the Einstein relation primarily due to the nonspherical shape of the molecule. In our modeling we use a three-dimensional (3D) structural model to compute the radii $r^{s(o)}$ for hydrated molecules [5] and thus include shape factors of the order of unity (see Table I). The permeability coefficient

TABLE I. Parameter values characterizing the loading pathway in *Cucumis melo*, estimated from the given references.

Variable	Measured as	Value	Unit	Reference
A_{in}	Interface area between IC and BSC	10^{-9}	m^2	[7]
A_{out}	Interface area between IC and SE	0.2×10^{-9}	m^2	[7]
A_2	Surface area of the IC	10^{-9}	m^2	[7]
r^s	Hydrodynamic radius of sucrose from 3D model	4.2×10^{-10}	m	[5]
r^o	Hydrodynamic radius of stachyose from 3D model	6.0×10^{-10}	m	[5]
$D^s = 1/2\, D^s_{water}$	Free cytosolic diffusion coefficient for sucrose	2.3×10^{-10}	m^2 s^{-1}	[14]
$D^o = 1/2\, D^o_{water}$	Free cytosolic diffusion coefficient for stachyose	1.9×10^{-10}	m^2 s^{-1}	[15]
f^s	Shape factor for hydrated sucrose molecules	0.88		
f^o	Shape factor for hydrated stachyose molecules	1.04		
η_{cyt}	Dynamic viscosity of cytosol	2×10^{-3}	Pa s	[5]
h_{in}	Half-slit width of PDs in the IC wall	$<10^{-9}$	m	[9,16]
h_{out}	Half-slit width of "normal" PDs	10^{-9}	m	[16]
r_{PD}	Average radius of PDs in plant cell walls	2.5×10^{-8}	m	[9,16]
d	Thickness of the IC wall	10^{-7}	m	[7]
n_{PD}	Density of PDs in the IC wall	10^{13}	m^{-2}	[7]
$c_1 = c^s_1$	Cytosolic sucrose concentration in mesophyll and bundle Sheath	200	mol m^{-3}	[6]
c_2	Total cytosolic sugar concentration in the IC-SE complex	500	mol m^{-3}	[6]
c^s_2	Cytosolic sucrose concentration in IC-SE complex	140	mol m^{-3}	[6]
$\Delta c^s_{in} = c^s_1 - c^s_2$	Sucrose concentration difference between BSC- and IC-cytosol	60	mol m^{-3}	[5,6]
p_1	Hydrostatic pressure in the bundle sheath	$\sim 10^5$	Pa	[11]
p_0	Xylem and apoplast pressure (from maize)	-4×10^5	Pa	[10]
$J_{in} = \Phi_{in}/A_{in}$	Sugar current density through BSC-IC interface, from total leaf export rate	9.7×10^{-7}	mol m^{-2} s^{-1}	[8]

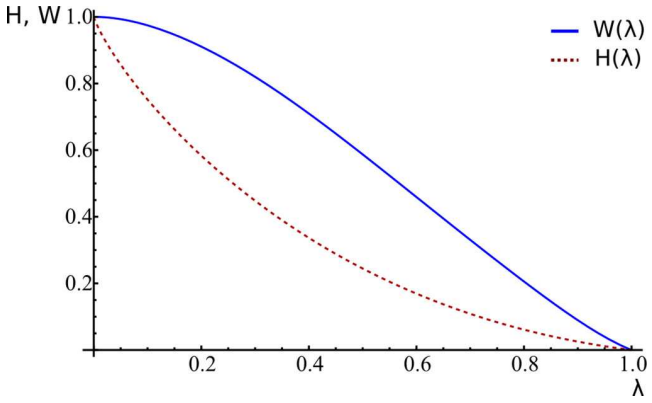

FIG. 3. (Color online) Diffusive and convective hindrance factors H (blue, solid) and W (red, dashed) in circular slit pores as function of the relative solute size λ. Both approximations given by Ref. [18] decrease smoothly from 1 to 0 for an increasing solute size, where a hindrance factor of zero corresponds to total blockage of the respective molecule. The convective hindrance factor W is in the whole range larger than the diffusive hindrance factor H. Above $\lambda = 0.8$ the curves should be regarded as extrapolations.

$\xi_{\mathrm{in(out)}}$ for the BSC-IC and IC-SE interface is estimated using a pressure-driven Poiseuille flow Q_{slit} through narrow rectangular channels of height $2h$ and width $2\pi r_{\mathrm{PD}}$, where $h_{\mathrm{in(out)}} \ll r_{\mathrm{PD}}$, i.e.,

$$A_{\mathrm{in(out)}} n_{\mathrm{PD}} Q_{\mathrm{slit}} = A_{\mathrm{in(out)}} n_{\mathrm{PD}} \frac{4\pi r_{\mathrm{PD}} h_{\mathrm{in(out)}}^3}{3\eta_{\mathrm{cyt}} d} \Delta p = \xi_{\mathrm{in(out)}} \Delta p \tag{15}$$

$$\Rightarrow \xi_{\mathrm{in(out)}} = A_{\mathrm{in(out)}} n_{\mathrm{PD}} \frac{4\pi r_{\mathrm{PD}} h_{\mathrm{in(out)}}^3}{3\eta_{\mathrm{cyt}} d}. \tag{16}$$

The cytosolic viscosity is estimated with a value twice as large as the viscosity of water, i.e., $\eta_{\mathrm{cyt}} = 2 \times 10^{-3}$ Pa s. The characteristic cell-wall thickness d as well as the plasmodesmata radius r_{PD} have been estimated from TEM images [7,19]. Based on the measurements by Volk *et al.*, the density n_{PD} of plasmodesmata in the IC wall is fixed to a value of around 10 μm^{-2} [7]. For the BSC-IC interface we assume that the PDs are very narrow and have a half-width between the hydrodynamic radius of sucrose $r^{\mathrm{s}} \approx 0.42$ nm and of stachyose $r^{\mathrm{o}} \approx 0.60$ nm, since stachyose should be totally blocked from going back to the bundle sheath. We shall choose $h_{\mathrm{in}} = r^{\mathrm{o}} = 0.6$ nm as a standard value since it is the largest value for which we are certain that $W_{\mathrm{in}}^{\mathrm{o}} = H_{\mathrm{in}}^{\mathrm{o}} = 0$ (see, however, the final section on raffinose hindrance). The hydrodynamic radii r^{s} and r^{o} have been computed using the 3D-structural models of hydrated sucrose and stachyose molecules accounting in particular for the cylindrical molecule forms [5]. For the IC-SE interface, the PDs are wider and we use a "normal" slit-width $h_{\mathrm{out}} = 1$ nm [16]. The interface coefficients for this configuration are listed in Table II.

The sucrose and total sugar concentrations in the IC are fixed to the values 140 mM and 500 mM, respectively (see Table I), based on the measured concentrations from Ref. [6].

TABLE II. Calculated interface coefficients for the half-slit widths $h_{\mathrm{in}} = 0.6$ nm and $h_{\mathrm{out}} = 1$ nm.

Coefficient	Value	Unit
$W_{\mathrm{in}}^{\mathrm{s}}$	0.33	
$W_{\mathrm{out}}^{\mathrm{s}}$	0.69	
$W_{\mathrm{out}}^{\mathrm{o}}$	0.46	
$D_{\mathrm{in}}^{\mathrm{s}}$	4.71×10^{-14}	m^2 s^{-1}
$D_{\mathrm{out}}^{\mathrm{s}}$	2.29×10^{-13}	m^2 s^{-1}
$D_{\mathrm{out}}^{\mathrm{o}}$	1.01×10^{-13}	m^2 s^{-1}
ξ_{in}	1.13×10^{-21}	m^3 Pa^{-1} s^{-1}
ξ_{out}	1.05×10^{-21}	m^3 Pa^{-1} s^{-1}

IV. DIMENSIONLESS EQUATIONS AND THEIR SOLUTION

To nondimensionalize we scale the used variables with the factors stated in Table III based on the concentration c_1 in the BSC and the properties of the BSC-IC interface. The dimensionless flows can be written as

$$\begin{aligned}\hat{Q}_{\mathrm{in}} &= \hat{\xi}_{\mathrm{in}} \left[\hat{c}_2^{\mathrm{o}} - \left(1 - W_{\mathrm{in}}^{\mathrm{s}}\right)\Delta\hat{c}_{\mathrm{in}}^{\mathrm{s}} - (\hat{p}_2 - \hat{p}_1)\right] \\ &= \hat{\xi}_{\mathrm{in}} \left[\hat{\Psi}_1 - \hat{\Psi}_2 + W_{\mathrm{in}}^{\mathrm{s}} \Delta\hat{c}_{\mathrm{in}}^{\mathrm{s}}\right], \end{aligned} \tag{17}$$

$$\begin{aligned}\hat{Q}_{\mathrm{out}} &= \hat{\xi}_{\mathrm{out}}[(1 - \bar{W}_{\mathrm{out}})(\hat{c}_3 - \hat{c}_2) - (\hat{p}_3 - \hat{p}_2)] \\ &= \hat{\xi}_{\mathrm{out}}[\hat{\Psi}_2 - \hat{\Psi}_3 + \bar{W}_{\mathrm{out}}(\hat{c}_2 - \hat{c}_3)], \end{aligned} \tag{18}$$

$$\hat{Q}_2 = \hat{\xi}_2[\hat{c}_2 - (\hat{p}_2 - \hat{p}_0)] = \hat{\xi}_2[\hat{p}_0 - \hat{\Psi}_2], \tag{19}$$

$$\hat{\Phi}_{\mathrm{in}} = W_{\mathrm{in}}^{\mathrm{s}} \hat{Q}_{\mathrm{in}} + \hat{D}_{\mathrm{in}}^{\mathrm{s}} \Delta\hat{c}_{\mathrm{in}}^{\mathrm{s}}, \tag{20}$$

$$\hat{\Phi}_{\mathrm{out}} = \bar{W}_{\mathrm{out}} \hat{Q}_{\mathrm{out}} \hat{c}_2 + \hat{A}_{\mathrm{out}} \bar{\hat{D}}_{\mathrm{out}} (\hat{c}_2 - \hat{c}_3). \tag{21}$$

In addition we have the conservation laws (8) and (9), which are unchanged, i.e.,

$$\hat{Q}_{\mathrm{in}} + \hat{Q}_2 = \hat{Q}_{\mathrm{out}}, \tag{22}$$

$$\hat{\Phi}_{\mathrm{in}} = (x^{\mathrm{s}} + 2x^{\mathrm{o}})\hat{\Phi}_{\mathrm{out}}. \tag{23}$$

The dimensionless sugar inflow corresponding to the experimentally determined sugar current density $J_{\mathrm{in}} = 9.7 \times 10^{-7}$ mol m^{-2} s^{-1} [8] in *Cucumis melo* is

$$\hat{\Phi}_{\mathrm{in}}^{\mathrm{exp}} = \hat{J}_{\mathrm{in}} = \frac{J_{\mathrm{in}} A_{\mathrm{in}}}{\xi^* RT c_1^2} = 0.025. \tag{24}$$

TABLE III. Scaling factors for the nondimensionalization.

Variable	Scaling factor	Value
A	A_{in}	10^{-9} m^2
c	c_1	200 mol m^{-3} (200 mM)
p	RTc_1	5×10^5 Pa (5 bar)
Ψ	RTc_1	5×10^5 Pa
ξ	$\xi^* = \xi_{\mathrm{in}}(h_{\mathrm{in}} = r^{\mathrm{s}})$	4×10^{-22} m^3 Pa^{-1} s^{-1}
D	$RTd\xi^* c_1 / A_{\mathrm{in}}$	2×10^{-14} m^2 s^{-1}
Q	$\xi^* RTc_1$	2×10^{-16} m^3 s^{-1}
Φ	$\xi^* RTc_1^2$	4×10^{-14} mol s^{-1}
J_{in}	$\xi^* RTc_1^2 / A_{\mathrm{in}}$	4×10^{-5} mol m^{-2} s^{-1}

The scaled permeability $\hat{\xi}_{\mathrm{in(out)}}$ and effective diffusion coefficients $\hat{D}^{\mathrm{s(o)}}_{\mathrm{in(out)}}$ take the form

$$\hat{D}^{\mathrm{s(o)}}_{\mathrm{in(out)}} = \frac{H^{\mathrm{s(o)}}_{\mathrm{in(out)}} f^{\mathrm{s(o)}}}{\left(\lambda^{\mathrm{s}}_{\mathrm{in(out)}}\right)^3 N^{\mathrm{s(o)}}_{\mathrm{in(out)}}}, \tag{25}$$

$$\hat{\xi}_{\mathrm{in}} = \left(\lambda^{\mathrm{s}}_{\mathrm{in}}\right)^{-3}, \tag{26}$$

$$\hat{\xi}_{\mathrm{out}} = \hat{A}_{\mathrm{out}}\left(\lambda^{\mathrm{s}}_{\mathrm{out}}\right)^{-3}. \tag{27}$$

Here the definitions from Sec. III and the scaling factors from Table III were used, and the relative solute size in the slits of half-width $h_{\mathrm{in(out)}}$ is defined as $\lambda^{\mathrm{s(o)}}_{\mathrm{in(out)}} = r^{\mathrm{s(o)}}/h_{\mathrm{in(out)}}$. The expression $N^{\mathrm{s(o)}}_{\mathrm{in(out)}} = N_{\mathrm{A}} c_1 2\pi (r^{\mathrm{s(o)}})^3 (\lambda^{\mathrm{s(o)}}_{\mathrm{in(out)}})^{-2}$ can be understood as the average number of sucrose molecules in the BSC in a small volume $2\pi (r^{\mathrm{s(o)}})^3 (\lambda^{\mathrm{s(o)}}_{\mathrm{in(out)}})^{-2}$ of the dimension of the sugar molecules. Inserting the dimensionless coefficients in the scaled flows, these can be rewritten as

$$\hat{Q}_{\mathrm{in}} = \left(\lambda^{\mathrm{s}}_{\mathrm{in}}\right)^{-3}\left[\hat{\Psi}_1 - \hat{\Psi}_2 + W^{\mathrm{s}}_{\mathrm{in}}\Delta\hat{c}^{\mathrm{s}}_{\mathrm{in}}\right], \tag{28}$$

$$\hat{Q}_{\mathrm{out}} = \left(\lambda^{\mathrm{s}}_{\mathrm{out}}\right)^{-3}\hat{A}_{\mathrm{out}}[\hat{\Psi}_2 - \hat{\Psi}_3 + (\hat{c}_2 - \hat{c}_3)\bar{W}_{\mathrm{out}}], \tag{29}$$

$$\begin{aligned}\hat{\Phi}_{\mathrm{in}} &= W^{\mathrm{s}}_{\mathrm{in}}\hat{Q}_{\mathrm{in}} + \left(\lambda^{\mathrm{s}}_{\mathrm{in}}\right)^{-3}\left(N^{\mathrm{s}}_{\mathrm{in}}\right)^{-1} H^{\mathrm{s}}_{\mathrm{in}} f^{\mathrm{s}}\Delta\hat{c}^{\mathrm{s}}_{\mathrm{in}} \qquad (30)\\ &= \left(\lambda^{\mathrm{s}}_{\mathrm{in}}\right)^{-3} W^{\mathrm{s}}_{\mathrm{in}}[\hat{\Psi}_1 - \hat{\Psi}_2] + \left(\lambda^{\mathrm{s}}_{\mathrm{in}}\right)^{-3}\\ &\quad\times\left(\left(W^{\mathrm{s}}_{\mathrm{in}}\right)^2 + \left(N^{\mathrm{s}}_{\mathrm{in}}\right)^{-1} H^{\mathrm{s}}_{\mathrm{in}} f^{\mathrm{s}}\right)\Delta\hat{c}^{\mathrm{s}}_{\mathrm{in}}, \qquad (31)\end{aligned}$$

$$\begin{aligned}\hat{\Phi}_{\mathrm{out}} &= \bar{W}_{\mathrm{out}}\hat{Q}_{\mathrm{out}}\hat{c}_2 + \hat{A}_{\mathrm{out}}\left(\lambda^{\mathrm{s}}_{\mathrm{out}}\right)^{-3}\left(\bar{N}_{\mathrm{out}}\right)^{-1}\\ &\quad\times\bar{H}_{\mathrm{out}}\bar{f}[\hat{c}_2 - \hat{c}_3] \qquad (32)\\ &= \left(\lambda^{\mathrm{s}}_{\mathrm{out}}\right)^{-3}\hat{A}_{\mathrm{out}}\bar{W}_{\mathrm{out}}[\hat{\Psi}_2 - \hat{\Psi}_3]\hat{c}_2 + \left(\lambda^{\mathrm{s}}_{\mathrm{out}}\right)^{-3}\hat{A}_{\mathrm{out}}\\ &\quad\times\left(\bar{W}^2_{\mathrm{out}}\hat{c}_2 + \left(\bar{N}_{\mathrm{out}}\right)^{-1}\bar{H}_{\mathrm{out}}\bar{f}\right)[\hat{c}_2 - \hat{c}_3]. \qquad (33)\end{aligned}$$

The bar over a variable always denotes an average quantity, calculated with the proportions of the two different sugars in the phloem, e.g., $\bar{W}_{\mathrm{out}} = x^{\mathrm{s}} W^{\mathrm{s}}_{\mathrm{out}} + x^{\mathrm{o}} W^{\mathrm{o}}_{\mathrm{out}}$ using the proportions $x^{\mathrm{s}} = c^{\mathrm{s}}_2/c_2$ and $x^{\mathrm{o}} = 1 - x^{\mathrm{s}}$ of sucrose and oligomer molecules in the phloem.

We can use, for example, $\Delta\hat{c}^{\mathrm{s}}_{\mathrm{in}}, x^{\mathrm{o}}, \hat{\Psi}_1, \hat{Q}_{\mathrm{out}}$ and $\hat{Q}_2$ as independent variables and calculate the other quantities. The sucrose and oligomer concentrations in the intermediary cell can be calculated from the concentration difference $\Delta\hat{c}^{\mathrm{s}}_{\mathrm{in}}$ between the BSC and the IC, and the oligomer proportion x^{o} in the phloem using, e.g., $\hat{c}^{\mathrm{s}}_2 = 1 - \Delta\hat{c}^{\mathrm{s}}_{\mathrm{in}}$, $x^{\mathrm{s}} = 1 - x^{\mathrm{o}}$, $\hat{c}_2 = \hat{c}^{\mathrm{s}}_2/x^{\mathrm{s}}$. The concentration $\hat{c}_3$ in the sieve element can then be determined from the volume and sugar conservation equations (22) and (23) with the use of expressions (30) and (32) for the sugar flow rates, i.e.,

$$\begin{aligned}\hat{c}_3 = \hat{c}_2 &+ \frac{(x^{\mathrm{s}} + 2x^{\mathrm{o}})\hat{c}_2\bar{W}_{\mathrm{out}} - W^{\mathrm{s}}_{\mathrm{in}}}{(x^{\mathrm{s}} + 2x^{\mathrm{o}})\hat{A}_{\mathrm{out}}\bar{H}_{\mathrm{out}}\bar{f}}\left(\lambda^{\mathrm{s}}_{\mathrm{out}}\right)^3\bar{N}_{\mathrm{out}}\hat{Q}_{\mathrm{out}}\\ &+ \frac{W^{\mathrm{s}}_{\mathrm{in}}}{(x^{\mathrm{s}} + 2x^{\mathrm{o}})\hat{A}_{\mathrm{out}}\bar{H}_{\mathrm{out}}\bar{f}}\left(\lambda^{\mathrm{s}}_{\mathrm{out}}\right)^3\bar{N}_{\mathrm{out}}\hat{Q}_2\\ &- \frac{1}{(x^{\mathrm{s}} + 2x^{\mathrm{o}})\hat{A}_{\mathrm{out}}}\frac{H^{\mathrm{s}}_{\mathrm{in}} f^{\mathrm{s}}\left(\lambda^{\mathrm{s}}_{\mathrm{out}}\right)^3\bar{N}_{\mathrm{out}}}{\bar{H}_{\mathrm{out}}\bar{f}\left(\lambda^{\mathrm{s}}_{\mathrm{in}}\right)^3 N^{\mathrm{s}}_{\mathrm{in}}}\Delta\hat{c}^{\mathrm{s}}_{\mathrm{in}}. \qquad (34)\end{aligned}$$

Finally, using the expressions for the water flows (28), (29), and (19), the water potentials $\hat{\Psi}_2$, $\hat{\Psi}_3$, and $\hat{\Psi}_0$ and corresponding hydrostatic pressures $\hat{p}_i$ inside and outside the cells of the loading pathway can be calculated (with the interface coefficients from Table II and the geometry as fixed in Table I) as

$$\hat{\Psi}_2 = \hat{p}_2 - \hat{c}_2 = \hat{\Psi}_1 - \left(\lambda^{\mathrm{s}}_{\mathrm{in}}\right)^3(\hat{Q}_{\mathrm{out}} - \hat{Q}_2) + W^{\mathrm{s}}_{\mathrm{in}}\Delta\hat{c}^{\mathrm{s}}_{\mathrm{in}}, \tag{35}$$

$$\hat{\Psi}_3 = \hat{p}_3 - \hat{c}_3 = \hat{\Psi}_2 - \left(\lambda^{\mathrm{s}}_{\mathrm{out}}\right)^3\hat{A}^{-1}_{\mathrm{out}}\hat{Q}_{\mathrm{out}} + \bar{W}_{\mathrm{out}}[\hat{c}_2 - \hat{c}_3], \tag{36}$$

$$\hat{\Psi}_0 = \hat{p}_0 = \frac{\hat{Q}_2}{\hat{\xi}_2} + \hat{\Psi}_2. \tag{37}$$

V. SPECIAL CASES

A. Pure diffusion

In this subsection we first investigate whether pure diffusion through plasmodesmata can transport enough sugar into the phloem, and, subsequently, whether this special case with no bulk flow through the plasmodesmata represents a likely loading situation in real plants. Assuming that the sucrose is transported into the IC by pure diffusion without a supporting bulk flow, we get

$$\hat{\Phi}_{\mathrm{in}} = \hat{D}^{\mathrm{s}}_{\mathrm{in}}\Delta\hat{c}^{\mathrm{s}}_{\mathrm{in}} = \frac{H^{\mathrm{s}}_{\mathrm{in}} f^{\mathrm{s}}}{N^{\mathrm{s}}_{\mathrm{in}}\left(\lambda^{\mathrm{s}}_{\mathrm{in}}\right)^3}\Delta\hat{c}^{\mathrm{s}}_{\mathrm{in}}. \tag{38}$$

This is in agreement with Fick's first law of diffusion. Taking $r^{\mathrm{s}} = 0.42$ nm gives $f^{\mathrm{s}} = 0.88$. The sugar current depends on the half-slit width h_{in} of the PDs in the BSC-IC interface through the relative solute size $\lambda^{\mathrm{s}}_{\mathrm{in}}$, which also appears as variable in the diffusive hindrance factor $H^{\mathrm{s}}_{\mathrm{in}} = H(\lambda = \lambda^{\mathrm{s}}_{\mathrm{in}})$.

Figure 4 shows that even for slits which are only slightly larger than the oligomers, the back flow into the bundle

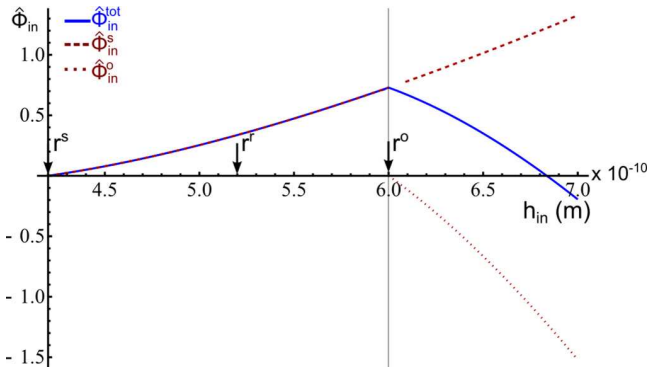

FIG. 4. (Color online) Sugar flow rate $\hat{\Phi}_{\mathrm{in}}$ into the IC as function of the PD-half-slit width h_{in} in the purely diffusive case. The sugar flow rate is composed by the sucrose flow rate $\Phi^{\mathrm{s}}_{\mathrm{in}}$ (red, dashed) given by Eq. (38) and the hypothetical negative oligomer flow rate $\Phi^{\mathrm{o}}_{\mathrm{in}}$ (red, dotted), which would occur when h_{in} is larger than the oligomer radius r^{o}. For the concentration differences measured in *Cucumis melo* the flow rate $\hat{\Phi}^{\mathrm{o}}_{\mathrm{in}}$ of oligomers back into the bundle sheath would cause the total sugar flow rate $\hat{\Phi}^{\mathrm{tot}}_{\mathrm{in}}$ (blue, solid) to vanish at slit widths only about one tenth larger than these molecules. The diffusive sucrose flow rate $\hat{\Phi}^{\mathrm{s}}_{\mathrm{in}}$, however, gives a sufficient overall flux rate in the case of total blockage of the modeled oligomers (i.e., $h_{\mathrm{in}} = r^{\mathrm{o}}$) and even for smaller slits totally blocking raffinose molecules (i.e., $h_{\mathrm{in}} = r^{\mathrm{r}}$; see Sec. V D).

sheath due to diffusion would exceed the sucrose flux in the opposite direction. With our standard half-slit width of $h_{\mathrm{in}} = r^{\mathrm{o}}$ equal to the hydrodynamic radius of the stachyose molecules, corresponding to a relative sucrose size of $\lambda^{\mathrm{s}}_{\mathrm{in}} = 0.7$, the tetrasaccharides in our model are blocked completely. For the sucrose flow rate we get $\hat{\Phi}_{\mathrm{in}} = 0.73$, which is about 30 times larger than the experimental value from Ref. [8]. This shows that, in *Cucumis melo*, diffusion through the narrow plasmodesmatal pores can be sufficient to achieve the measured sugar current into the phloem, and in fact the large value that we obtain probably means that the pores are even narrower than the size of the stachyose molecules. Indeed, the pores also have to be able to block the back flow of raffinose, which is around 10% smaller than stachyose. We discuss that in Sec. V D.

We found that pure diffusion is sufficient to export enough sugar into the phloem of RFO-transporting plants. On the other hand, the long-distance transport in the phloem system is based on a bulk flow for which water has to enter the symplasm at some point. Since in this special case we ruled out any bulk flow through the plasmodesmata between BSC and IC, the water has to go across the membrane of either the intermediary cell or the sieve element. We now calculate the pressures, concentrations, and water potentials in these cells to see if this is a possible and even advantageous situation for the plant, i.e., if the water potentials are low enough for water from the xylem to be drawn in. The condition of purely diffusive sugar loading implies that the hydrostatic and osmotic pressure differences across the BSC-IC interface must be balanced in order to achieve zero bulk flow. From this boundary condition, i.e., $\hat{Q}_{\mathrm{in}} = 0$, the water potential $\hat{\Psi}_2$ and hydrostatic pressure $\hat{p}_2$ in the intermediary cell can be calculated for a fixed potential $\hat{\Psi}_1$ in the bundle sheath. With $\hat{Q}_{\mathrm{in}} = 0$ Eq. (35) is reduced to

$$\hat{\Psi}_2 = \hat{\Psi}_1 + W^{\mathrm{s}}_{\mathrm{in}} \Delta \hat{c}^{\mathrm{s}}_{\mathrm{in}}. \tag{39}$$

For a water potential of $\hat{\Psi}_1 = -0.8$, corresponding to $p_1 = 1$ bar in the bundle sheath, a value $\hat{\Psi}_2 = -0.70$ results in the IC which corresponds to $\Psi_2 = -3.5$ bar. To avoid inflow of water from the BSC, the intermediary cell thus has to build up a large hydrostatic pressure of $p_2 = 9.0$ bar. If the water needed in the phloem enters as $\hat{Q}_2 > 0$ across the membrane of the intermediary cell, the pressure in the apoplast has to be larger than the water potential $\hat{\Psi}_2$ in the IC, i.e., $p_0 = Q_2/\xi_2 + \Psi_2 > -3.5$ bar. As mentioned above we assume the xylem pressure p_0 to be around -4 bar [10], and thus such a water uptake would not be feasible. For pressures $p_1 > 1$ bar this conclusion is even more justified. Now we consider the case $\hat{Q}_2 = 0$ where the flow through the PDs into the sieve element also vanishes, i.e., $\hat{Q}_{\mathrm{out}} = \hat{Q}_{\mathrm{in}} + \hat{Q}_2 = 0$. In this situation, the water from the xylem must flow in across the membrane of the sieve element. The concentration in the SE can be calculated with Eq. (34), which simplifies for pure diffusion at both interfaces to

$$\hat{c}_3 = \hat{c}_2 - \frac{1}{(x^{\mathrm{s}} + 2x^{\mathrm{o}})\hat{A}_{\mathrm{out}}} \frac{H^{\mathrm{s}}_{\mathrm{in}} f^{\mathrm{s}} \left(\lambda^{\mathrm{s}}_{\mathrm{out}}\right)^3 \bar{N}_{\mathrm{out}}}{\bar{H}_{\mathrm{out}} \bar{f} \left(\lambda^{\mathrm{s}}_{\mathrm{in}}\right)^3 N^{\mathrm{s}}_{\mathrm{in}}} \Delta \hat{c}^{\mathrm{s}}_{\mathrm{in}}. \tag{40}$$

The resulting concentration $\hat{c}_3 = 2.2$ in the sieve element is lower than the IC-sugar concentration because a downhill gradient to the SE is essential for diffusion. The water potential $\hat{\Psi}_3$ is calculated with Eq. (36) for zero water outflow $\hat{Q}_{\mathrm{out}} = 0$ as

$$\hat{\Psi}_3 = \hat{\Psi}_2 + \bar{W}_{\mathrm{out}}[\hat{c}_2 - \hat{c}_3], \tag{41}$$

and we obtain a value of $\hat{\Psi}_3 = -0.5$ corresponding to $\Psi_3 = -2.7$ bar and $p_3 = 8.3$ bar. To generate osmotic water flow into the SE, the xylem pressure has to be larger than Ψ_3, i.e., $p_0 > -2.7$ bar, which makes it even more difficult for the water to flow directly into the sieve element than into the IC. Thus the water potential in both of the phloem cells (IC and SE) will probably be too high to allow sufficient water intake across the cell membrane from the xylem system. Furthermore pure diffusion across the IC-SE interface requires that the sugar concentration decreases into the SE [as seen in Eq. (40)] which presumably is a disadvantage for efficient sugar translocation. In both respects the situation improves, when we allow for water flow through the PD pores in the BSC-IC interface as we show below.

B. Equal concentrations in SE and IC

The general case with both diffusion and water flow across both cell interfaces is complicated as seen, for example, from Eq. (34), and one has to deal with many unknown variables, mainly pressures, bulk flows, and the SE concentration. In this subsection we shall therefore treat the special case, where the concentrations in the intermediary cell and sieve element are equal, i.e., $c_2 = c_3$, which is likely due to the well-connected IC-SE complex. Compared to pure diffusion into the SE this has the advantage that the concentration of sugar in the phloem sap is higher and therefore the sugar flow will be larger. As a consequence of the equal concentrations in the phloem, the sugar from the IC will be transported by pure bulk flow from the intermediary cell into the sieve element. Using (30) and (32), the sugar flows are then expressed as

$$\hat{\Phi}_{\mathrm{in}} = W^{\mathrm{s}}_{\mathrm{in}} \hat{Q}_{\mathrm{in}} + \frac{H^{\mathrm{s}}_{\mathrm{in}} f^{\mathrm{s}}}{N^{\mathrm{s}}_{\mathrm{in}} \left(\lambda^{\mathrm{s}}_{\mathrm{in}}\right)^3} \Delta \hat{c}^{\mathrm{s}}_{\mathrm{in}}, \tag{42}$$

$$\hat{\Phi}_{\mathrm{out}} = \bar{W}_{\mathrm{out}} \hat{Q}_{\mathrm{out}} \hat{c}_2. \tag{43}$$

Using the volume conservation (22) we can determine the volume flow $\hat{Q}_{\mathrm{out}}$ and sugar flow $\hat{\Phi}_{\mathrm{out}}$ from the sugar conservation (23) with a given transmembrane flow $\hat{Q}_2$ as functions of the concentration $\hat{c}_2$ in the phloem, i.e.,

$$\hat{Q}_{\mathrm{out}} = \frac{H^{\mathrm{s}}_{\mathrm{in}} f^{\mathrm{s}} \left(\lambda^{\mathrm{s}}_{\mathrm{in}}\right)^{-3} (N^{\mathrm{s}}_{\mathrm{in}})^{-1} \Delta \hat{c}^{\mathrm{s}}_{\mathrm{in}} - W^{\mathrm{s}}_{\mathrm{in}} \hat{Q}_2}{(x^{\mathrm{s}} + 2x^{\mathrm{o}}) \bar{W}_{\mathrm{out}} \hat{c}_2 - W^{\mathrm{s}}_{\mathrm{in}}}, \tag{44}$$

$$\hat{\Phi}_{\mathrm{out}} = \frac{H^{\mathrm{s}}_{\mathrm{in}} \bar{W}_{\mathrm{out}} f^{\mathrm{s}} \left(\lambda^{\mathrm{s}}_{\mathrm{in}}\right)^{-3} (N^{\mathrm{s}}_{\mathrm{in}})^{-1} \Delta \hat{c}^{\mathrm{s}}_{\mathrm{in}} \hat{c}_2 - W^{\mathrm{s}}_{\mathrm{in}} \bar{W}_{\mathrm{out}} \hat{Q}_2 \hat{c}_2}{(x^{\mathrm{s}} + 2x^{\mathrm{o}}) \bar{W}_{\mathrm{out}} \hat{c}_2 - W^{\mathrm{s}}_{\mathrm{in}}}. \tag{45}$$

Here the proportions x^{s} and x^{o} and consequently the average bulk hindrance factor $\bar{W}_{\mathrm{out}}$ at the IC-SE interface also depend on $\hat{c}_2$. The corresponding inflows are subsequently determined by the conservation laws. The higher we choose the oligomer

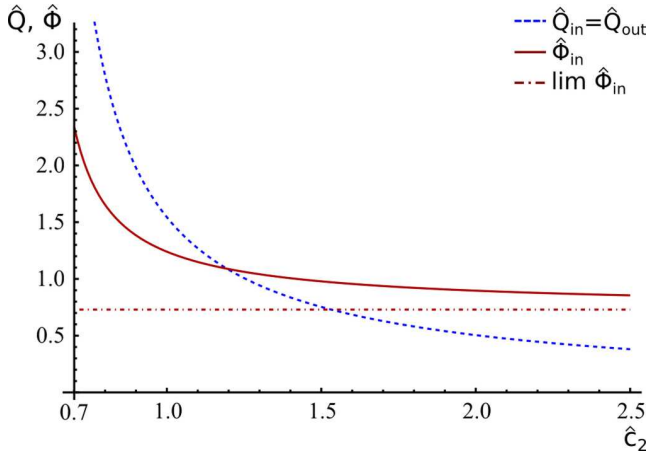

FIG. 5. (Color online) Water and sugar flow rates $\hat{Q}_{\rm in} = \hat{Q}_{\rm out}$ (blue, dashed) and $\hat{\Phi}_{\rm in}$ (red) as functions of the total sugar concentration $\hat{c}_2$ in the case where the concentrations in IC and SE are equal ($c_2 = c_3$). The flow rates are shown for no transmembrane flow, i.e., $\hat{Q}_2 = 0$, only the oligomer concentration $\hat{c}_2^{\rm o}$ in the phloem is varied while the sucrose concentration is fixed to $\hat{c}_2^{\rm s} = 0.7$. The diffusive flow rate into the IC retains its constant value $\lim \hat{\Phi}_{\rm in} \propto \Delta\hat{c}_{\rm in}^{\rm s}$ (dot-dashed), while for an increasing oligomer concentration the advective contribution to the sugar flow decreases with the water flow which is limited by the conservation laws.

concentration for a fixed sucrose concentration $\hat{c}_2^{\rm s}$ the lower are the resulting flows, approaching the limits

$$\lim_{\hat{c}_2\to\infty} \hat{Q}_{\rm out} = 0, \tag{46}$$

$$\lim_{\hat{c}_2\to\infty} \hat{\Phi}_{\rm in} = \frac{H_{\rm in}^{\rm s} f^{\rm s}}{\left(\lambda_{\rm in}^{\rm s}\right)^3 N_{\rm in}^{\rm s}} \Delta\hat{c}_{\rm in}^{\rm s} - W_{\rm in}^{\rm s} \hat{Q}_2. \tag{47}$$

The contribution of the bulk flow to the inflowing sugar current decreases for high IC concentrations, if there is no runoff of pure water from the IC into the apoplast that would prevent the dilution of the concentrated phloem solution. Since the diffusive contribution stays constant due to the fixed sucrose gradient, the total sugar inflow decreases together with the water flow for a more concentrated phloem solution as seen in Fig. 5.

We do not know values for the permeability of the plasma membranes on the loading pathway. Depending on the abundance of *aquaporins*, i.e., water-conducting proteins, it can vary by several orders of magnitude between $L_{\rm p,2} = \xi_2/A_2 = 2\times10^{-14}\,{\rm m\,s^{-1}\,Pa^{-1}}$ and $L_{\rm p,2} = 10^{-11}\,{\rm m\,s^{-1}\,Pa^{-1}}$ as measured by Maurel in plant cells [20]. We assume here, however, that the permeability $L_{\rm p,2}$ of the IC-plasma membrane is much smaller than the permeabilities $L_{\rm p,in(out)} = \xi_{\rm in(out)}/A_{\rm in(out)} \sim 10^{-12}\,{\rm m\,s^{-1}\,Pa^{-1}}$ of the plasmodesmata, and we thus neglect $\hat{Q}_2$ in the following. For this case, Fig. 5 shows the behavior of the volume and sugar flows $\hat{Q}_{\rm in} = \hat{Q}_{\rm out}$ and $\hat{\Phi}_{\rm in}$ as functions of $\hat{c}_2$ as in Eqs. (44) and (45). For the measured IC concentration of $\hat{c}_2 = 2.5$ in muskmelon [6] the bulk flow contributes to the sugar inflow only by 15%. Also for $\hat{Q}_2 = 0$, we have $\hat{Q}_{\rm in} = \hat{Q}_{\rm out}$ and the water potentials in the phloem can then be determined as

$$\hat{\Psi}_2 = \hat{p}_2 - \hat{c}_2 = \hat{\Psi}_1 - \left(\lambda_{\rm in}^{\rm s}\right)^3 \hat{Q}_{\rm out} + W_{\rm in}^{\rm s}\Delta\hat{c}_{\rm in}^{\rm s}, \tag{48}$$

$$\hat{\Psi}_3 = \hat{\Psi}_2 - \left(\lambda_{\rm out}^{\rm s}\right)^3 \hat{A}_{\rm out}^{-1}\hat{Q}_{\rm out}. \tag{49}$$

For the concentrations in *Cucumis melo* and a bundle-sheath pressure of 1 bar, the resulting values in the phloem are $\hat{\Psi}_2 = -0.83$ and $\hat{\Psi}_3 = -0.97$ corresponding to dimensional values $\Psi_2 = -4.2$ bar and $\Psi_3 = -4.9$ bar for the potentials and $p_2 = 8.3$ bar and $p_3 = 7.6$ bar for the hydrostatic pressures.

C. The loading unit as a part of the phloem

So far our modeling has not taken into account that the sieve elements are part of the phloem vascular system, and that sap is therefore transported from one sieve element to the next along the phloem vasculature. The pressure drop between the sieve elements needed for this flow is very small compared to the pressure drops across the PDs, which we have been considering so far, since the sieve elements and even the pores in the sieve plates are several orders of magnitude wider. Thus the sieve elements all probably have roughly the same pressures and concentrations. If we also suppose that there is no direct water exchange between the sieve elements and the apoplast, the sugar and water, which is loaded into the sieve elements, should have those same concentrations. The simplified flow in the last subsection, where we assumed equal sugar concentrations in the IC and SE and thus pure bulk advection through the IC-SE interface, would then be impossible, since it would result in the *dilution* of the phloem sap due to the different hindrances of the sugars and the water in the plasmodesmata. To find an appropriate condition, we denote the sugar flow rate from along the sieve tube (i.e., from one sieve element to the next) by $\Phi_{\rm SE}$ and the amount provided by each IC as $\Delta\Phi_{\rm SE}$. If the concentration in the sieve element (of some solute) is c, the sugar flow is related to the water flow rate Q simply by $\Phi_{\rm SE} = Q$ and the condition described above would then amount to $\Delta\Phi_{\rm SE} = c\Delta Q = \Phi_{\rm out}$, where $\Phi_{\rm out}$ is the flow rate of this particular solute across the IC-SE interface.

With no direct water exchange between the sieve element and the xylem, $\Delta Q = Q_{\rm out}$. Thus the conservation laws (23) and (22) result in the following equations, where at the IC-SE interface the sucrose and oligomer flux rates are both conserved and can therefore be treated separately, i.e.,

$$\begin{aligned}
\hat{\Phi}_{\rm out}^{\rm s(o)} &= \hat{Q}_{\rm out}\hat{c}_3^{\rm s(o)} \\
&\Rightarrow W_{\rm out}^{\rm s}\hat{Q}_{\rm out}\hat{c}_2^{\rm s} + \hat{A}_{\rm out}\hat{D}_{\rm out}^{\rm s}\left[\hat{c}_2^{\rm s} - \hat{c}_3^{\rm s}\right] = \hat{Q}_{\rm out}\hat{c}_3^{\rm s} \qquad (50)\\
&\Rightarrow W_{\rm out}^{\rm o}\hat{Q}_{\rm out}\hat{c}_2^{\rm o} + \hat{A}_{\rm out}\hat{D}_{\rm out}^{\rm o}\left[\hat{c}_2^{\rm o} - \hat{c}_3^{\rm o}\right] = \hat{Q}_{\rm out}\hat{c}_3^{\rm o} \qquad (51)\\
\hat{\Phi}_{\rm in} &= (x^{\rm s} + 2x^{\rm o})\left(\hat{\Phi}_{\rm out}^{\rm s} + \hat{\Phi}_{\rm out}^{\rm o}\right) \\
&\Rightarrow W_{\rm in}^{\rm s}(\hat{Q}_{\rm out} - \hat{Q}_2) + \hat{D}_{\rm in}^{\rm s}\Delta\hat{c}_{\rm in}^{\rm s} \\
&= (x^{\rm s} + 2x^{\rm o})\hat{Q}_{\rm out}\left(\hat{c}_3^{\rm s} + \hat{c}_3^{\rm o}\right). \qquad (52)
\end{aligned}$$

Here the dimensionless forms of (3) and (4) of the sugar in and out flow rates are used with $\hat{\Phi}_{\rm out} = \hat{\Phi}_{\rm out}^{\rm s} + \hat{\Phi}_{\rm out}^{\rm o}$. The average equation (21) with $\bar{W}_{\rm out}$ and $\bar{D}_{\rm out}$ cannot be employed here, since the sugar ratios $c_3^{\rm s(o)}/c_3$ in the SE are in general not equal to $c_2^{\rm s(o)}/c_2 = x^{\rm s(o)}$ in the IC. From these equations the SE

concentrations $\hat{c}_3^{\mathrm{s}}$ and $\hat{c}_3^{\mathrm{o}}$ can be expressed as

$$\hat{c}_3^{\mathrm{s(o)}} = \hat{c}_2^{\mathrm{s(o)}} \frac{W_{\mathrm{out}}^{\mathrm{s(o)}} \hat{Q}_{\mathrm{out}} + \hat{A}_{\mathrm{out}} \hat{D}_{\mathrm{out}}^{\mathrm{s(o)}}}{\hat{Q}_{\mathrm{out}} + \hat{A}_{\mathrm{out}} \hat{D}_{\mathrm{out}}^{\mathrm{s(o)}}}. \tag{53}$$

Depending on $\hat{Q}_{\mathrm{out}}$ the SE concentration $\hat{c}_3 = \hat{c}_3^{\mathrm{s}} + \hat{c}_3^{\mathrm{o}}$ will take a value between $\hat{c}_2^{\mathrm{s}} W_{\mathrm{out}}^{\mathrm{s}} + \hat{c}_2^{\mathrm{o}} W_{\mathrm{out}}^{\mathrm{o}}$ in the case of a very high advective contribution at the IC-SE interface, and $\hat{c}_2$ for a very high diffusive contribution. The bulk flow $\hat{Q}_{\mathrm{out}}$ can be determined from (50), (51), and (52) with $\hat{Q}_2 = 0$. Using the specific values from Table I, the resulting SE concentrations in *Cucumis melo* would then be $\hat{c}_3^{\mathrm{s}} = 0.7$ and $\hat{c}_3^{\mathrm{o}} = 1.4$ so that the total SE concentration $\hat{c}_3 = 2.1$ lies as expected between $\hat{c}_2^{\mathrm{s}} W_{\mathrm{out}}^{\mathrm{s}} + \hat{c}_2^{\mathrm{o}} W_{\mathrm{out}}^{\mathrm{o}} = 1.3$ and $\hat{c}_2 = 2.5$. The bulk contributions to the sugar flow rate at the different interfaces are then calculated with

$$\frac{\hat{\Phi}_{\mathrm{in}}^{\mathrm{bulk}}}{\hat{\Phi}_{\mathrm{in}}} = \frac{W_{\mathrm{in}}^{\mathrm{s}}}{(x^{\mathrm{s}} + 2x^{\mathrm{o}})\left(\hat{c}_3^{\mathrm{s}} + \hat{c}_3^{\mathrm{o}}\right)} = 0.14, \tag{54}$$

$$\frac{\hat{\Phi}_{\mathrm{out}}^{\mathrm{bulk}}}{\hat{\Phi}_{\mathrm{out}}} = \frac{W_{\mathrm{out}}^{\mathrm{s}} \hat{c}_2^{\mathrm{s}} + W_{\mathrm{out}}^{\mathrm{o}} \hat{c}_2^{\mathrm{o}}}{\hat{c}_3^{\mathrm{s}} + \hat{c}_3^{\mathrm{o}}} = 0.62. \tag{55}$$

Thus the advective flow from the intermediary cell into the sieve element in this case contributes about 62% to the overall sugar outflow while at the BSC-IC interface the bulk contribution would merely be 14%. Furthermore the water potentials become $\Psi_2 = -3.9$ bar (IC) and $\Psi_3 = -3.3$ bar (SE) [using Eqs. (35) and (36)], and the pressures are $p_2 = 8.6$ bar and $p_3 = 7.3$ bar. So we believe that we have a consistent picture, where all the water necessary for the sap translocation in the phloem is provided together with the sugar through the plasmodesmata with no further need of osmotic water uptake.

D. Diffusion of raffinose

Up to this point, we have treated the oligosaccharides as one species with properties largely determined by stachyose, the one present in largest concentrations. This treatment presumably gives good estimates for the transport rates and water flux, but we still have to account for the fact that raffinose, which is smaller than stachyose, does not diffuse back into the bundle sheath. The transport of raffinose would be given as

$$\hat{\Phi}_{\mathrm{in}}^{\mathrm{r}} = \frac{1}{2} W^{\mathrm{r}} \hat{Q}_{\mathrm{in}} \hat{c}^{\mathrm{r}} - \frac{H_{\mathrm{in}}^{\mathrm{r}} f^{\mathrm{r}}}{\left(\lambda_{\mathrm{in}}^{\mathrm{s}}\right)^3 N_{\mathrm{in}}^{\mathrm{r}}} \hat{c}^{\mathrm{r}}, \tag{56}$$

where we have used the average raffinose concentration $\hat{c}^{\mathrm{r}}/2$ between BSC and IC in the advection term. Here we assume that the bulk water flow $\hat{Q}_{\mathrm{in}}$ is still given by Eq. (28) used above, i.e.,

$$\hat{Q}_{\mathrm{in}} = \left(\lambda_{\mathrm{in}}^{\mathrm{s}}\right)^{-3} \left[\hat{\Psi}_1 - \hat{\Psi}_2 + W_{\mathrm{in}}^{\mathrm{s}} \Delta \hat{c}_{\mathrm{in}}^{\mathrm{s}}\right], \tag{57}$$

and we investigate whether the bulk flow is sufficient to block the diffusion of raffinose which would mean that $\hat{\Phi}_{\mathrm{in}}^{\mathrm{r}}$ is actually positive. With the coefficients characterizing the movement of raffinose denoted by the superscript r, we get

$$\hat{\Phi}_{\mathrm{in}}^{\mathrm{r}} \approx \left[\frac{W_{\mathrm{in}}^{\mathrm{r}} W_{\mathrm{in}}^{\mathrm{s}}}{2} \Delta \hat{c}_{\mathrm{in}}^{\mathrm{s}} - \frac{H_{\mathrm{in}}^{\mathrm{r}} f^{\mathrm{r}}}{N_{\mathrm{in}}^{\mathrm{r}}}\right] \frac{\hat{c}^{\mathrm{r}}}{\left(\lambda_{\mathrm{in}}^{\mathrm{s}}\right)^3}, \tag{58}$$

where we have neglected $\hat{\Psi}_1 - \hat{\Psi}_2$ which is typically less than or equal to 0. Using the raffinose radius $r^{\mathrm{r}} = 0.52$ nm from a 3D-structure model [5], the half-slit width $h_{\mathrm{in}} = 0.6$ nm as above and the measured free diffusion coefficient $D^{\mathrm{r}} = 2.15\ \mathrm{m^2\,s^{-1}}$ [21] in cytosol (half of the value in water) with $\Delta \hat{c}_{\mathrm{in}}^{\mathrm{s}} = 0.3$ we find $\frac{1}{2} W_{\mathrm{in}}^{\mathrm{r}} W_{\mathrm{in}}^{\mathrm{s}} \Delta \hat{c}_{\mathrm{in}}^{\mathrm{s}} - \frac{H_{\mathrm{in}}^{\mathrm{r}} f^{\mathrm{r}}}{N_{\mathrm{in}}^{\mathrm{r}}} \approx -0.26$ and thus $\hat{\Phi}_{\mathrm{in}}^{\mathrm{r}} < 0$ meaning that the bulk flow *cannot* block the back diffusion of the intermediate sized raffinose molecules.

Thus, to avoid the diffusion of raffinose back into the bundle sheath we need a half-slit width which is very close to the radius of the raffinose molecules, denoted by r^{r} above. Since these molecules are not spherical, the relevant size depends strongly on how it is defined and/or measured, and thus the hydrodynamic radius of raffinose can vary between values 10% and 20% above that of the sucrose molecules. In addition the corresponding value of $\lambda_{\mathrm{in}}^{\mathrm{s}} \geqslant 0.8$ is at the limit (or above) of the range of validity of the hindrance factors, so all in all our results will be somewhat uncertain. Using the value $h_{\mathrm{in}} = r^{\mathrm{r}} = 0.52$ nm from 3D modeling [5] gives $\lambda_{\mathrm{in}}^{\mathrm{s}} \approx 0.8$ for the sucrose molecules. Using this value in our equations does not change the qualitative features of the solutions obtained above (see Fig. 4). In this case, using Eq. (38), the sugar current would still be larger than the measured value (14 times larger instead of 30 times larger with the half-slit width $h_{\mathrm{in}} = 0.6$ nm). Taking the values $r^{\mathrm{s}} = 0.52$ nm for the sucrose radius and $r^{\mathrm{r}} = 0.57$ nm as half-slit width directly from the Einstein relation [5] gives us $\lambda_{\mathrm{in}}^{\mathrm{s}} \approx 0.9$, and in this case we are above the stated range of validity of $H(\lambda)$. If we use the expressions (10) and (11) we get $H = 0.03$ and $W = 0.09$. Using again Eq. (38) with $f^{\mathrm{s}} = 1$, we obtain

$$\hat{\Phi}_{\mathrm{in}} = \frac{H(\lambda = 0.9)}{2\pi N_{\mathrm{A}} c_1 (r^{\mathrm{s}})^3 0.9} \Delta \hat{c}_{\mathrm{in}}^{\mathrm{s}} = 0.079, \tag{59}$$

which is still about three times the measured value 0.025. To get down to the experimental value we have to decrease the half-slit width below r^{r} to $h_{\mathrm{in}} = 0.54$ nm, i.e., $\lambda_{\mathrm{in}}^{\mathrm{s}} = 0.96$.

VI. CONCLUSION

We have analyzed the feasibility of the polymer trap loading mechanism (active symplasmic loading) in terms of the coupled water and sugar movement through the plasmodesmata in the cellular interfaces leading from the bundle sheath to the phloem. We used the Kedem-Katchalsky equations and model the pores in the cell interfaces as narrow slits. This allowed us to compute the membrane coefficients using results on hindered diffusion and convection, and to check whether they can act as efficient filters, allowing sucrose to pass, but not raffinose and stachyose, synthesized in the intermediary cells. Based on the very limited available data for plasmodesmata geometry, sugar concentrations, and flux rates, we conclude that this mechanism can in principle function, but, since the difference in size between raffinose and sucrose is only 10%–20%, we are pressing the theories for hindered transport to the limit of (or beyond) their validity. We find that sugar loading is predominantly diffusive across the interface separating the bundle sheath from the phloem. However, the sugar translocation into the sieve tube, where the vascular sugar transport takes place, can be dominated by advection

(bulk flow). This allows the plant to build up both the large hydrostatic pressure needed for the vascular sugar transport and the high concentration needed to make this transport efficient. This is possible because the water uptake to the sieve tubes happens directly through the plasmodesmata instead of through aquaporins in the cell membranes of the phloem. Thus, the water in the phloem has to be taken up across the plasma membranes of the pre-phloem pathway, e.g., the bundle sheath cells. As mentioned earlier, the experimental data available for these plants are very limited. It would be of great importance to have more information on the concentrations and pressures in the cells as well as the diffusivities across the important interfaces. It would also be of importance to extend the analysis of the sugar translocation all the way back to the mesophyll cells, where it is produced.

ACKNOWLEDGMENTS

We are grateful to the Danish Research Council *Natur og Univers* for support under Grant No. 12-126055.

[1] P. F. Scholander, E. D. Bradstreet, E. A. Hemmingsen, and H. T. Hammel, Science **148**, 339 (1965).
[2] L. Taiz and E. Zeiger, *Plant Physiology*, 3rd ed. (Sinauer Associates, Sunderland, MA, 2002).
[3] E. Münch, *Die Stoffbewegungen in der Pflanze* (Fischer, Jena, 1930).
[4] E. A. Rennie and R. Turgeon, Pub. Natl. Acad. Sci. USA **106**, 14162 (2009).
[5] J. Liesche and A. Schulz, Front. Plant Sci. **4**, 207 (2013).
[6] E. Haritatos, F. Keller, and R. Turgeon, Planta (Heidelberg) **198**, 614 (1996).
[7] G. Volk, R. Turgeon, and D. Beebe, Planta (Heidelberg) **199**, 425 (1996).
[8] K. Schmitz, B. Cuypers, and M. Moll, Planta (Heidelberg) **171**, 19 (1987).
[9] G. D. Fisher, Planta (Heidelberg) **169**, 141 (1986).
[10] M. T. Tyree and M. H. Zimmermann, *Xylem Structure and the Ascent of Sap* (Springer, Heidelberg, 2002).
[11] U. Zimmermann, D. Huesken, and E.-D. Schulze, Planta (Heidelberg) **149**, 445 (1980).
[12] P. Nobel, *Plant Physiology*, 2nd ed. (Academic Press, San Diego, 1999).
[13] O. Kedem and A. Katchalsky, Biochim. Biophys. Acta **27**, 229 (1958).
[14] P. Henrion, Trans. Faraday Soc. **60**, 72 (1964).
[15] L. Craig and A. Pulley, Biochem. **1**, 89 (1962).
[16] A. G. Roberts and K. J. Oparka, Plant Cell Environ. **26**, 103 (2003).
[17] E. Waigmann, A. Turner, J. Peart, K. Roberts, and P. Zambryski, Planta (Heidelberg) **203**, 75 (1997).
[18] P. Dechadilok and W. M. Deen, Ind. Eng. Chem. Res. **45**, 6953 (2006).
[19] C. E. J. Botha, B. J. Hartley, and R. H. M. Cross, Ann. Botany (London) **72**, 255 (1993).
[20] C. Maurel, Annu. Rev. Plant Biol. **48**, 399 (1997).
[21] P. Dunlop, J. Phys. Chem. **60**, 1464 (1956).

5.2 Diffusion and bulk flow in passive phloem loading

Manuscript under preparation.

Diffusion and bulk flow in passive phloem loading

Hanna Rademaker,[1] Katrine Engholm Villumsen,[1] Jean Comtet,[2] Tomas Bohr,[1] and Kaare Hartvig Jensen[1,*]

[1] *Department of Physics, Technical University of Denmark, DK 2800 Kgs. Lyngby, Denmark*
[2] *School of Chemical and Biomolecular Engineering, Cornell University, Ithaca, NY 14853*

(Dated: September 12, 2016)

Passive solute transport is often thought to be purely diffusive. However, in certain systems passive transport can be enhanced by an osmotically created bulk flow. This is of great importance in meso- and macroscopic biological systems, where diffusive transport speeds are much too slow. In particular, we study the uptake of photosynthesized sugars into the veins of plant leaves (sugar loading) in passively loading species, a group comprising many tree species. We argue, that passive loading inherently has an advective and a diffusive component, where the ratio of these depends on only a few key parameters. We demonstrate the advective transport mechanism in 3d-printed, biomimetic devices. Furthermore, we develop a theoretical model of passive loading to estimate the advective and diffusive transport contributions. We find that for parameter values typical for passively loading plants advection plays an important role, possibly even more important than diffusion. This prediction contradicts the common assumption of purely diffusive sugar loading in these plants and contributes to a detailed understanding of the passive loading mechanism.

INTRODUCTION

Like all vascular plants trees produce sugars in their leaves and distribute these sugars through the whole plant via the phloem tissue. In order to be exported from the leaf sugars are taken up into the phloem conduits, a process called phloem loading. Most herbaceous plants use active mechanisms to achieve this sugar uptake, with the help of enzymatic or membrane transporter proteins, while most trees load passively [1, 2]. Despite some seeming drawbacks, e.g. having to sustain a high sugar concentration in the mesophyll cells, these plants succeed in competing with species which predominantly use active loading. The average sugar concentration in their phloem sap still reaches about 3/4 of that in active loaders [3]. It has further been shown that some plants use passive loading as a fallback mechanism, when the usually dominant active loading is genetically switched off, e.g. in *Arabidopsis thaliana* [4].

Trees are of direct importance for the production of wood, fruits and to bind carbon dioxide [5, 6], and they also improve soil conditions of understorey plants in their vicinity [7]. They are interesting model plants to learn from, as they are robust, long-lived and grow to impressive heights. Not only will it be valuable to understand the details of how this vitally important group of plants distributes their photoassimilates throughout the plant, but the transport principle of passive loading might furthermore be transferable to other contexts, e.g. artificial transport systems (water treatment) or medical applications (drug delivery).

Sugars produced in the mesophyll cells of the leaf are loaded into the phloem conduits inside the veins, and the water necessary to drive the export is osmotically taken up from the xylem (Fig. 1). The prevailing understanding of passive loading is, that sugar moves symplastically – that is via plasmodesmal pores without crossing the plasma membrane – from the mesophyll into the phloem and purely by diffusion along the sucrose gradient. To quote one of the standard textbooks on plant physiology: "*Symplastic loading, in contrast, depends on the diffusion of sugars from the mesophyll to the sieve elements via the plasmodesmata.*"[8].

However, in the last years osmotically driven bulk flows enhancing the solute transport through plasmodesmata in symplastically loading plants have been proposed in several studies [9–12]. A careful analysis of the local water flows inside the leaf is necessary in order to understand whether and how a bulk flow assisting the sugar transport could be created.

While there are some studies of the active loading mechanisms [10, 12–15], a quantitative description of passive phloem loading has so far been neglected. For a physical understanding of the passive loading mechanism, we have to examine whether bulk flow plays a role in phloem loading in these plants and find the key parameters that determine the rates of sugar export. The solution of these tasks will be tied to the transport through plasmodesmata – small, intercellular pores connecting the sugar producing mesophyll with the export tissue in the phloem. Although their exact geometry, development and selectivity is subject to ongoing research [16–18], their ability to transport sucrose and other small solutes has been suspected [19] and known [20, 21] for many decades. Also the question of whether or not there can be bulk transport through plasmodesmata has been posed early on [22].

In this work, we present experiments with biomimetic devices, modeling the advective component of passive phloem loading. We further study the interplay between advection and diffusion in a theoretical model, describing sugar export from a system of three compartments, namely sugar reservoir (mesophyll), water reservoir (xylem) and export tissue (phloem). With the help

of this model, we identify relevant parameters determining the rate of sugar export in passive loading, and the proportions of advective and diffusive transport contributions.

We find that the size of the pores connecting sugar reservoir and export tissue, the interface areas, as well as the sugar concentration are the key parameters to determine sugar uptake into the export tissue. Comparing with typical values from plants, we find that this choice of parameter values indicates a significant contribution of advective transport to passive loading, as opposed to the common belief that passive phloem loading is purely diffusive. These findings contribute to a detailed understanding of the passive loading mechanism.

We organized this manuscript in the following manner: First, we present our findings from the experiments on biomimetic osmotic devices, implementing the advective transport component of passive loading. Next, we introduce a simple, functional model of the passive loading mechanism, allowing for the quantification of advective and diffusive contributions to the transport of solutes from a few key parameters like pore size, solute concentration and interface area ratios. The model also allows for the calculation of volume flow rates and sugar export rates. Finally, we argue that passively loading plants employ both, advection and diffusion, to take up sugars into their phloem transport system, and that the size of the plasmodesmal pores is the most critical parameter in determining the advective-diffusive transport ratio.

RESULTS

Advective flow component in passive phloem loading demonstrated in biomimetic devices

With the help of photosynthesis, plants produce sugars inside their leaves. These sugars, mostly sucrose, are then exported from the leaf via vascular conduits inside the phloem tissue and transported to regions of growth or storage at other locations inside the plant (Fig. 1).

As a first step of this transport, sugars have to get from the photosynthetically active mesophyll cells into the phloem conduits, a process called *phloem loading*. In contrast to active loading mechanisms, plants using passive symplastic loading have a higher concentration of sucrose inside the mesophyll than in the phloem. This concentration gradient leads to diffusion of sucrose from mesophyll to phloem cells through intercellular pores (*plasmodesmata*) connecting the cytoplasm of all cells along this path.

Plasmodesmata are small, membrane-lined channels and while they are 50 to 70 nm in diameter [23, 24], most of their volume is filled with endoplasmic reticulum, an organell reaching from the cytoplasm of one cell into the cytoplasm of the next cell. This leaves a cytoplasmic sleeve of a few nanometers for the transport of solutes, possibly even less, as the inner structure of this slit is assumed to consist of 9 nanopores of 2-4 nm width [24, 25]. This is similar to the pore diameter of a connexon, the unit structure of a gap junction, the animal cell equivalent of an aggregate of plasmodesmata [26]. For these gap junctions, a bulk flow enhancing diffusive solute transport has been postulated and shown experimentally in bovine eyes [27–29].

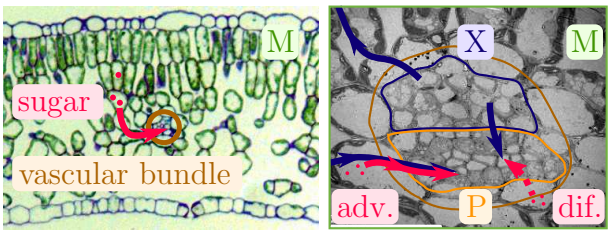

FIG. 1. Apple (*Malus sylvestris*) leaf cross sections. Inside plant leaves sugar is photosynthesized in the cells of the mesophyll (M) and loaded into the phloem cells (P) inside the vascular bundle. From there, sugar is exported from the leaf by the pressure gradient generated by the osmotic uptake of water from the xylem (X). *Left:* The cross section of a leaf shows the vascular bundle surrounded by mesophyll tissue. *Right:* Transmission electron micrograph of a cross section through the vascular bundle. Sugar loading is indicated by red arrows. Two loading configurations are indicated: sugar can diffuse into the phloem, while water enters directly from the xylem (diffusive, dif.) or a water bulk flow could enhance the sugar uptake (advective, adv.). Scale bar = 20 μm.

The export of sucrose from the phloem is then driven by the osmotic uptake of water from the xylem – either directly or via the mesophyll cells – and the resulting increase in turgor pressure. This is known as the Münch mechanism [30]. The xylem is in close proximity to the phloem, but is also connected to the mesophyll (see Fig. 1). While the pores between mesophyll and phloem are large enough to allow the passage of sucrose mostly unhindered (reflection coefficient $\sigma \leq 0.55$), the xylem is separated from the other compartments by plasma membrane. The plasma membrane allows for water exchange via aquaporins, but blocks sucrose completely.

While it is commonly assumed that sucrose merely diffuses from the mesophyll into the phloem, water from the xylem could assist in phloem loading by advecting sucrose over the mesophyll-phloem interface. We demonstrate this possible contribution to sugar loading with experiments in biomimetic devices. We model the function of this mechanism rather than mimicking the geometry of the plant structures, by using devices with three chambers, corresponding to a sugar reservoir (mesophyll), water reservoir (xylem) and export tissue (phloem) (Fig. 2). The membrane separating xylem and mesophyll chamber has a molecular weight cut-off (MWCO) of 100-500 Da,

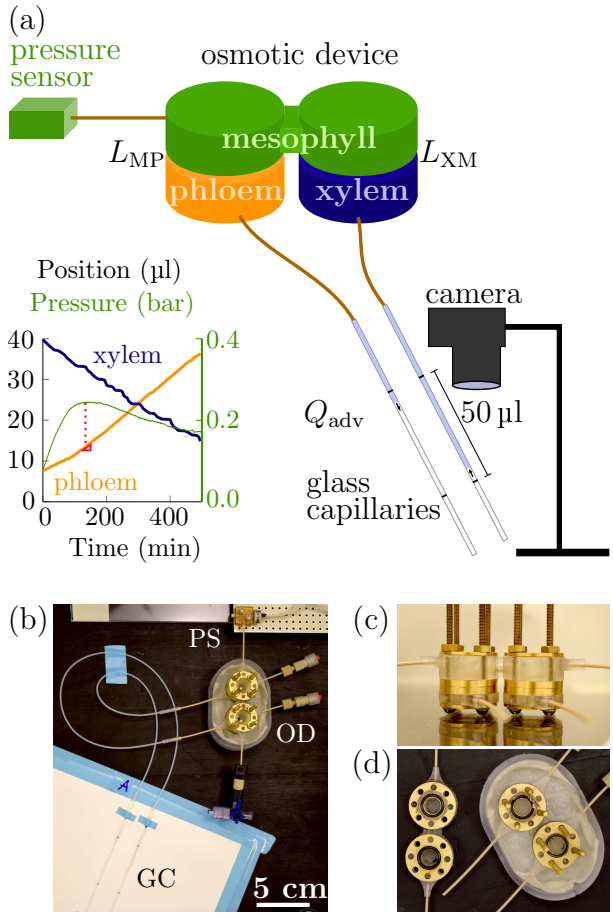

FIG. 2. We demonstrate the advective flow component of passive loading in biomimetic devices. a) The three compartments are separated by membranes with permeablities L_{XM} and L_{MP}. Pressure in the mesophyll compartment (sugar reservoir, green) builds up due to the osmotic uptake of water from the xylem compartment (water reservoir, blue) and sucrose solution is advected into the phloem compartment (export tissue, orange) We measure the flow rate out of the phloem by monitoring the position of the meniscus inside the glass capillary connected to the phloem and evaluate the flow rate Q_{adv} at the time when the maximum pressure is reached (red). The inset shows the time course of one experiment, displaying an example measurement for meniscus position in xylem and phloem, and the pressure in the mesophyll. b) Photograph of the setup, showing PS: pressure sensor, OD: osmotic device, GC: glass capillary. Assembled (c) and open (d) device.

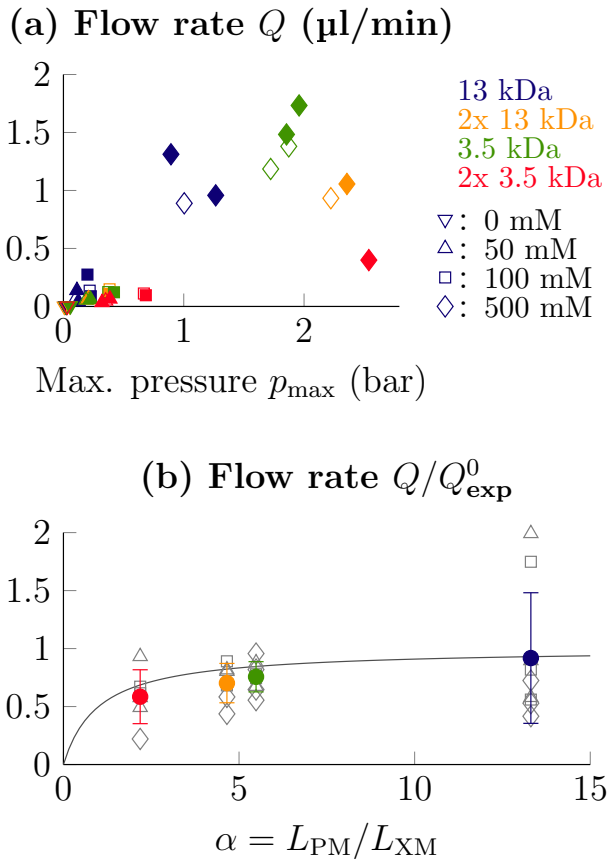

FIG. 3. Measuring the flow rates of sugar solution in advective, biomimetic devices. (a) The maximum pressure achieved p_{max} and the sugar sap export rate Q from the phloem compartment depend on the initial concentration of sucrose solution (circle: 0 mM, triangle: 50 mM, square: 100 mM and diamond: 500 mM) and the membrane type (blue: 13 kDa, yellow: 2x13 kDa, green: 3.5 kDa, red: 2x3.5 kDa). (b) The flow rate Q, normalized by the flow rate $Q^0_{exp} = L_{XM}ARTc_M$ for $L_{MP} \to \infty$, as a function of $\alpha = L_{MP}/L_{XM}$. The grey symbols in the background display single experiments, the colored circles represent the mean value for one membrane type, the error bars the standard deviation thereof.

which makes it almost impermeable to sucrose (342.3 Da, $\sigma_{XM} \approx 1$), while the membrane between mesophyll and phloem has a MWCO of at least 3.5 kDa, so that sucrose passes to good approximation unhindered ($\sigma_{MP} \approx 0.06$).

We start the experiment by flushing the mesophyll compartment with sucrose solution of known concentration c_M, while phloem and xylem are filled with pure water. Both phloem and xylem are connected to a water-filled glass capillary at atmospheric pressure. We then measure the pressure inside the mesophyll compartment and the resulting flow rate of fluid leaving the phloem during the next hours. The pressure inside the mesophyll p_M increases due to the osmotic uptake of water from the xylem, reaches a maximum and decreases again, as the incoming water dilutes the sucrose solution inside the mesophyll (inset in Fig. 2(a)).

At the time of the maximum pressure there is a short period where the system is in a steady state: the pressure is constant, and therefore also the flow rates in and out of the phloem are constant. The maximum pressure p_{max} and flow rate Q achieved in the course of one experiment increase with the initial concentration of sucrose, but also

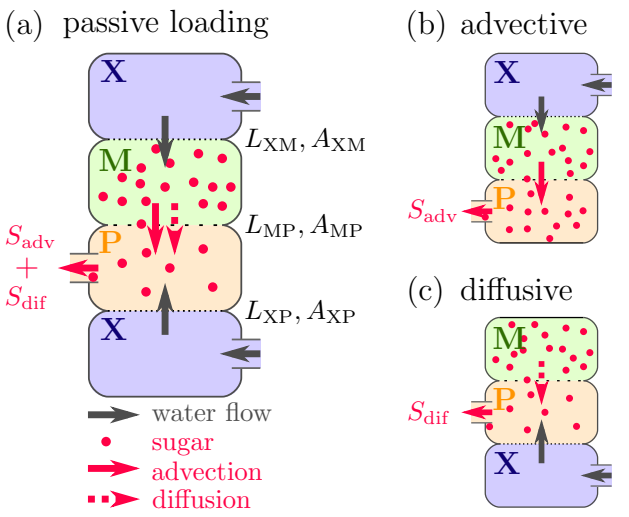

FIG. 4. Modeling advective and diffusive sugar transport contributions in passive phloem loading. We model the uptake of sugars from the mesophyll (M) into the phloem (P) with a system of compartments, separated by two types of membranes: fully osmotic membranes with permeability L_{XM} or L_{XP}, corresponding to cell membranes with aquaporins and leaky membranes with L_{MP}, corresponding to interfaces with plasmodesmal pores. In plant leaves, sugar can potentially be transported by both advection and diffusion, as mesophyll and phloem are in direct contact with the xylem (X), as shown in (a). To disentangle the contributions of advection and diffusion, we study a purely advective system (b), as used in the experiments on biomimetic devices, and a purely diffusive system (c). While the biomimetic devices are designed with equal interface areas A, the sizes of A_{XM}, A_{MP} and A_{XP} can be very different in plants (see section *Advective and diffusive transport in plants*).

depend on the permeabilities of the membranes between the compartments (Fig. 3(a)).

Scaling the measured flow rates Q with Q_0, corresponding to the measured initial flow rate for this concentration over a fully osmotic membrane, all data points fall onto a single line, when plotted over the ratio of membrane permeabilities $\alpha = L_{MP}/L_{XM}$ (Fig. 3(b)).

Modeling advective and diffusive contributions to passive solute transport

To describe and quantify advective and diffusive contributions to passive phloem loading we develop a mathematical model. Our model encompasses a stack of compartments, in different arrangements (see Fig. 4).

The interfaces are modeled as membranes, separating two compartments with different solute concentrations. The bulk flow Q of water over a membrane is

$$Q = LA(\sigma RT\Delta c - \Delta p) \tag{1}$$

where L is the permeability of the membrane in $\mathrm{m\,s^{-1}\,Pa^{-1}}$, A the area of the interface, R the gas constant, T the temperature, Δc the difference in concentration of solute and Δp the difference in hydrostatic pressure between the two compartments. The reflection coefficient σ takes a value between 0 and 1, 1 describing a fully osmotic membrane which cannot be crossed by solute, while 0 corresponds to a physical membrane, that solute can pass unhindered [31].

Due to the concentration gradient solute will diffuse across the membrane. If a bulk flow according to Eq. 1 is present, solute will additionally be dragged along, giving rise to an advective contribution to the solute transport

$$S = K_D\Delta c + (1-\sigma)Qc \tag{2}$$

where $K_D = \frac{\rho AD}{d}$ is the diffusive permeability of the solute in $\mathrm{m^3\,s^{-1}}$ with ρ the area fraction open for transport, A the membrane area, D the diffusion coefficient, d the thickness of the membrane and c the solute concentration in the compartment where the bulk flow originates. Note that the permeabilities K_D and L are in general not independent, as both increase with size and density of the pores of the membrane.

In the following paragraphs, we derive the equations for a system with three chambers corresponding to a sugar reservoir (mesophyll), a water reservoir (xylem) and export tissue (phloem). To disentangle the contributions from advective and diffusive sugar loading, we will distinguish two different arrangements. Sugar reservoir and export tissue are in both cases in direct contact. In the first case, the sugar reservoir is additionally in contact with the water reservoir, so that water is osmotically taken up into the sugar reservoir, advecting sugar into the phloem (Fig. 4(b)). In the second case, the water reservoir is in contact with the export tissue instead, in which case sugar can be transported into the export tissue by diffusion only (Fig. 4(c)).

The full model (Fig. 4(a)) can be found in the appendix.

Advective configuration (b)

The flow rate of water taken up into the sugar reservoir (M) according to Eq. 1 is $Q_{XM} = L_{XM}A_{XM}(RTc_M - p_M)$, where the water reservoir (X) is assumed to have a perfect osmotic membrane ($\sigma_{XM} = 1$), sugar concentration zero and to be at atmospheric pressure ($p_X = 0$). L_{XM} denotes the permeability of the membrane towards the water reservoir.

We assume a constant sugar concentration c_M in the sugar reservoir. As the membrane between sugar reservoir and export tissue (P) is a leaky membrane with $\sigma_{MP} = 0$, the steady-state concentration in the export tissue will be $c_P = c_M$. The bulk flow from sugar reser-

voir to export tissue has therefore no osmotic component, but is only driven by the hydrostatic pressure p_M as $Q_{MP} = L_{MP}A_{MP}p_M$, where we assume the export tissue to be at atmospheric pressure ($p_P = 0$).

Conservation of mass leads to equating the above relations $Q_{XM} = Q_{MP}$, and we find the pressure in the sugar reservoir to be $p_M = \frac{1}{1+\alpha}RTc_M$, introducing the dimensionless parameter $\alpha \equiv L_{MP}A_{MP}/L_{XM}A_{XM}$. With this result we can express the bulk flow in the advective configuration as

$$Q_{adv} = \frac{1}{1+\alpha}L_{MP}A_{MP}RTc_M = \frac{1}{1+\alpha}Q^0_{adv} \qquad (3)$$

with $Q^0_{adv} \equiv L_{MP}A_{MP}RTc_M$ the maximally achievable flow rate. For large values of α, $Q \approx Q^0_{adv}/\alpha$ and the flow rate is limited by L_{XM}, while for small α, the flow rate saturates at the maximal value $Q \approx Q^0_{adv}$, limited by L_{MP} (Fig. 5(a)).

Due to $c_P = c_M$ the sugar export has no diffusive component and can be calculated as $S = Q_{adv}c_M$, or

$$S_{adv} = \frac{1}{1+\alpha}c_M Q^0_{adv}. \qquad (4)$$

Diffusive configuration (c)

In the diffusive configuration water is taken up directly into the export tissue (P) as $Q_{XP} = L_{XP}A_{XP}RTc_P$ ($\sigma_{XP} = 1$). This means that sugar can merely diffuse into the export tissue from the sugar reservoir (M) and $S_{MP} = \frac{\rho A_{MP}D}{d}(c_M - c_P)$. Here the diffusion is assumed to be unhindered ($\sigma_{MP} = 0$). The steady state is reached, when the diffusive intake of sugars into the export tissue equals the export of sugars due to bulk flow caused by osmotic water uptake from the water reservoir (X), $S_{MP} = Q_{XP}c_P$, so that $\frac{\rho A_{MP}D}{d}(c_M - c_P) = L_{XP}A_{XP}RTc_P^2$. This quadratic equation for the sugar concentration in the export tissue,

$$c_P^2 + \beta c_M c_P - \beta c_M^2 = 0, \qquad (5)$$

is determined by the parameter $\beta \equiv \frac{\rho A_{MP}D}{dL_{XP}A_{XP}RTc_M}$. $1/\beta$ is a "mixed" Peclet number, i.e. a measure for advective versus diffusive transport. The flow rate can now be calculated in terms of this Peclet number:

$$Q_{dif} = \frac{\beta}{2}\left(\sqrt{1+4/\beta} - 1\right)Q^0_{dif} \qquad (6)$$

with $Q^0_{dif} \equiv L_{XP}A_{XP}RTc_M$. Comparing the flow at high and low Peclet numbers we find, that if advection dominates ($\beta \ll 1$), $Q = \sqrt{\beta}Q^0_{dif}$, while if diffusion dominates ($\beta \gg 1$), $Q = Q^0_{dif}$ (Fig. 5(b)). The sugar export rate $S_{dif} = c_P Q_{dif}$ is calculated as

$$S_{dif} = \frac{\beta^2}{4}\left(\sqrt{1+4/\beta} - 1\right)^2 c_M Q^0_{dif}. \qquad (7)$$

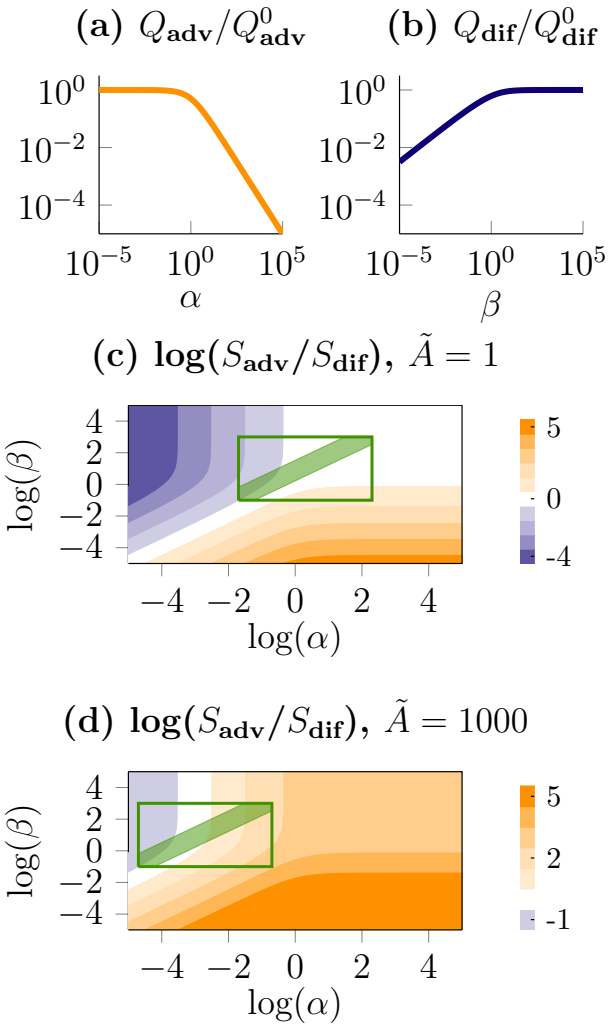

FIG. 5. Comparing advective and diffusive solute transport contribution. From our theoretical model we calculate the bulk flow Q for the advective (a) and the diffusive configuration (b), depending on the respective parameters $\alpha = L_{MP}A_{MP}/L_{XM}A_{XM}$ and $\beta = \frac{\rho A_{MP}D}{dL_{XP}A_{XP}RTc_M}$, and normalized by the respective maximally achievable flow rates Q^0_{adv} and Q^0_{dif}. (c,d) The ratio of the advective and diffusive sugar flux S_{adv}/S_{dif} can be larger than 1 (orange) or smaller (blue), depending on the choice of α, β and $\tilde{A} = A_{XM}/A_{PX} \approx A_{XM}/A_{MP}$. The physiologically relevant range of α and β (green line) can be narrowed down further (shaded region), by introducing $K \equiv \alpha/\beta$. K can be directly estimated from the plasmodesmal pore size and sucrose concentration in the mesophyll, assuming cylindrical pores: $K = \frac{r^2 RTc_M}{8\eta D\tilde{A}}$. In the biomimetic devices, all interface areas are equal ($\tilde{A} = 1$, (c)), while in plant leaves the surface area of the mesophyll cells is much larger than that of the phloem ($\tilde{A} \gg 1$, (d)).

Advective and diffusive transport in plants

The ratio of advectively and diffusively transported sucrose can be calculated from Eqs. 4 and 7 as

$$\frac{S_{\mathrm{adv}}}{S_{\mathrm{dif}}} = \frac{\frac{L_{\mathrm{MP}}A_{\mathrm{MP}}}{L_{\mathrm{XP}}A_{\mathrm{XP}}}}{(1+\alpha)\,\frac{\beta^2}{4}\left(\sqrt{1+\frac{4}{\beta}}-1\right)^2} \tag{8}$$

$$= \frac{\tilde{A}\alpha}{(1+\alpha)\,\frac{\beta^2}{4}\left(\sqrt{1+\frac{4}{\beta}}-1\right)^2} \tag{9}$$

which in addition to α and β also depends on the ratio of interface areas $\tilde{A} \equiv A_{\mathrm{XM}}/A_{\mathrm{XP}}$, and assumes equal membrane permeabilities towards the xylem $L_{\mathrm{XP}} = L_{\mathrm{XM}}$. In the experiments on biomimetic devices the interfaces have equal areas and $\tilde{A} = 1$. In plant leaves, the surface over which water can enter the mesophyll cells A_{XM} is much larger than the interface between phloem and xylem (A_{XP}) or mesophyll and phloem (A_{MP}). We estimate $\tilde{A}$ to be approximately 1000 (see Materials and Methods). Compared to A_{XM} the latter two are approximately equal, as they correspond to the cell membrane of the phloem cells, over which water and sugar can enter the phloem, so that $\tilde{A} = A_{\mathrm{XM}}/A_{\mathrm{XP}} \approx A_{\mathrm{XM}}/A_{\mathrm{MP}}$.

Fig. 5 shows the proportions of advectively and diffusively exported sugar $S_{\mathrm{adv}}/S_{\mathrm{dif}}$ depending on α and β, calculated from Eq. 9, assuming equal interface areas ($\tilde{A} = 1$, Fig. 5(c)) as in the biomimetic devices, or a relatively large xylem-mesophyll interface ($\tilde{A} \gg 1$, Fig. 5(d)), as expected in plant leaves.

We estimate the relevant ranges of α and β in plant leaves from literature values (Table I). If we assume cylindrical plasmodesmal pores of radius r, length d and area covering fraction $\rho = \pi r^2 n n_0$, and Poiseuille flow with resistance $\frac{8\eta d}{\pi r^4}$ through these pores, we can write $L_{\mathrm{MP}} = \frac{\rho r^2}{8\eta d}$ and $K_D = \frac{\rho A_{\mathrm{MP}} D}{d}$. Assuming a large mesophyll surface area ($\tilde{A} = 1000$), we find $\alpha = 2{\cdot}10^{-5}..2{\cdot}10^{-1}$ and $\beta = 1\cdot10^{-1}..1\cdot10^{3}$, indicated by the green frame in Fig. 5(d).

However, the parameters α and β are interdependent, as they both depend on the size of the plasmodesmal pores. We can thereby confine the possible range further, if we introduce the parameter K as

$$K \equiv \frac{dL_{\mathrm{MP}}RTc_{\mathrm{M}}}{\rho D\tilde{A}} = \frac{\alpha}{\beta} \tag{10}$$

which is a Peclet number for the transport over the membrane between sugar reservoir and export tissue. K can be expressed in terms of the pore radius r, area ratio $\tilde{A}$ and sugar concentration c_{M} as

$$K = \frac{r^2RTc_{\mathrm{M}}}{8\eta D\tilde{A}}. \tag{11}$$

The range of K is approximately $3\cdot10^{-5}$ to $6\cdot10^{-4}$, using the parameters in Table I (shaded region inside the green frame in Fig. 5(d)). In this range, $S_{\mathrm{adv}}/S_{\mathrm{dif}}$ is between 10^{-1} and 10^{2}, meaning that at least 10% of the sugar is transported advectively, or that diffusion might actually be negligible. Even assuming equal areas ($\tilde{A} = 1$), gives a range of 45% to 50% advectively transported sugar (shaded green area in Fig. 5(c)).

Importance of the three key parameters

The model presented in the above paragraphs allows us to identify three key traits which determine the proportions of advective and diffusive transport in plants: the sugar concentration in the mesophyll c_{M}, the ratio of surface area of the entity of mesophyll cells to the surface area of phloem cells $\tilde{A}$ and the radius of the plasmodesmal pores r. The sensitivity to changes in these parameters is however quite different, as can be seen from Eq. 9.

While the sugar concentration c_{M} certainly determines the total sugar flux $S_{\mathrm{adv}} + S_{\mathrm{dif}}$, it is of less importance for the ratio of advective to diffusive transport. c_{M} only enters in β, and β is proportional to $1/c_{\mathrm{M}}$, which means that if β is close to or larger than 1 – as would be expected from the literature values – $S_{\mathrm{adv}}/S_{\mathrm{dif}}$ is almost constant in c_{M}.

$\tilde{A}$ enters Eq. 9 directly, but also enters in α. $S_{\mathrm{adv}}/S_{\mathrm{dif}}$ is therefore proportional to $\tilde{A}/(1 + \tilde{A}L_X/L_{\mathrm{MP}})$, and the area ratio $\tilde{A}$ is only important when it is of similar size as L_{MP}/L_X. The literature values indicate that $L_{\mathrm{MP}} \approx L_X$, so $\tilde{A}$ becomes important when close to 1. As discussed in the section *Advective and diffusive transport in plants* it seems more likely, that $\tilde{A}$ is much larger than 1, in which case $S_{\mathrm{adv}}/S_{\mathrm{dif}}$ is independent of $\tilde{A}$.

Finally, the parameter with the strongest and highly non-linear influence, is the pore radius r. It enters in $\alpha \propto L_{\mathrm{MP}} \propto \rho r^2 \propto r^4$ and in $\beta \propto \rho \propto r^2$. Interestingly, r becomes especially influential for large values of $\tilde{A}$.

DISCUSSION AND CONCLUSION

In contrast to the classical view on passive phloem loading our study indicates the importance of advection in sugar loading. Depending on the actual value of the key parameters sugar concentration, interface area ratio and size of the plasmodesmal pores between mesophyll and phloem, the transport can be dominated by either diffusion or advection.

As discussed in the section *Importance of the three key parameters*, we find that the plasmodesmal pore radius has the strongest influence on the ratio of advective to diffusive transport. To narrow down the possible range of this ratio in general, or to assign a ratio to a certain species, it is crucial to measure this pore radius precisely.

Plants might even use this strong dependency and modify the size of the plasmodesmal pores by e.g. de-

Quantity		Value	Unit	Ref.
Membrane permeability	$L_{\mathrm{XM}}, L_{\mathrm{XP}}$	$5 \cdot 10^{-14}..10^{-12}$	$\mathrm{m\,s^{-1}\,Pa^{-1}}$	[32]
PD density	n	1..30	$\mu\mathrm{m}^{-2}$	[9]
# nanopores per PD	n_0	9		[25]
PD pore radius	r	1..2	nm	[24, 25]
PD length	d	0.1	µm	[33]
Diffusion coefficient	D_{suc}	$5 \cdot 10^{-10}$	$\mathrm{m^2\,s^{-1}}$	[34]
Viscosity	η	$2 \cdot 10^{-3}$	Pa s	[35]
Sucrose concentration	c_{M}	100..500	mM	[36]
Area ratio $A_{\mathrm{XM}}/A_{\mathrm{XP}}$	$\tilde{A}$	1000		[33]

TABLE I. Literature values for parameters in leaves of passively loading plants used to estimate ranges of α and β.

position of callose at the entrance of the plasmodesma. Since plasmodesmata also transport signaling molecules like hormones, it might be beneficial for the plant to be able to "switch off" the bulk flow, in a situation where bidirectional transport is necessary.

Furthermore, to narrow down the range of α, we need direct measurements of L_{XM} and L_{XP}, the water permeabilities of the plasma membrane in both mesophyll and phloem cells, or a method to infer the permeability from the area density of aquaporins and measurements thereof.

As for direct, time resolved measurements of the transport of solutes from cell to cell, there have been efforts to measure effective diffusion coefficients with microscopy techniques like photoactivation [37]. The time resolution is however limited, especially for measurements in 3 dimensions.

MATERIALS AND METHODS

Biomimetic devices

Biomimetic devices are 3d-printed on a Formlabs Form 1+ printer, using the "clear" resin (version 2) at a resolution of 0.1 mm. The respective volumes of sugar reservoir, water reservoir and export chamber are 1725/425/425 µl, the interface areas are $1.075 \cdot 10^{-4}\,\mathrm{m}^2$. O-ring holders are made from brass and glued to the 3d-printed part using cyanoacrylate glue. We use Spectra por dialysis tubes with molecular weight cut-offs $100 - 500$ Da, 3.5 kDa and $12 - 14$ kDa as membranes between the compartments. A 5 cm long piece of PEEK (polyether ether ketone) tubing is glued to every inlet and outlet of all compartments with cyanoacrylate glue. The inlet of the water reservoir and the outlet of the exporting compartment are each connected to a glass capillary tube with PTFE (polytetrafluoroethylene) tubing. Glass capillary tubes are micro pipettes (BLAUBRAND®, intraMark, $50 - 100$ µl), and the volume between the two black marks on the tube is 50 µm.

Time course of an experiment

In preparation of an experiment, the device is assembled with pieces of membrane – one 100-500 Da membrane (osmotic) between water reservoir and sugar reservoir and one or two layers of leaky membrane between sugar reservoir and export compartment. Each membrane is held in place and sealed with the help of two rubber o-rings and the device is closed by tightening the screws. All compartments are filled with DI (deionized) water and the meniscus positions inside the glass capillaries adjusted between the two black marks. To start an experiment, the sugar reservoir of the device is flushed with 6 ml of sugar solution of concentration 0 mM, 50 mM, 100 mM or 500 mM from a syringe. The outlet of the sugar reservoir is then connected to a pressure sensor (LabSmith, uProcess™, 250 kPa or 800 kPa) with PEEK tubing. All other inlets are closed with Luer-Tight™ fittings. The device is placed in a 3d-printed humidity chamber with wet tissues to minimize evaporative water losses from the device. Within 20 s after closing the inlets, we start monitoring the meniscus position with a digital camera (1 frame per minute or 1 frame per 5 minutes) and taking pressure data (1 measurement per second). For some of the 100 mM and 500 mM experiments it is necessary to re-adjust the meniscus position during the experiment. This causes small bumps or spikes in the pressure measurements, but does not significantly effect the maximally reached pressure or flow rate of the experiment. All experiments are carried out at room temperature ($22 - 27.5$°C).

Pressure tightness of the devices

As a control experiment, the devices are filled with DI water and pressurized with a syringe to 2 bar, all inlets and outlets are closed and the decay of pressure over time is measured. The pressure decays to about $1/e$ of the starting value in approximately 700 minutes. The time until the maximum pressure is reached in the

experiments is between 60 minutes for the experiments with 500 mM concentration of sucrose and 700 minutes for the experiments with 50 mM. The loss is mainly due to lateral movement of water through the membranes, although there are also losses through the 3d-print resin or possibly expansion of the reservoir volume under pressure.

Measurement of membrane permeability L_p

The permeability of the membranes is measured by connecting the sugar reservoir to a syringe pump and slowly pressing water through the membranes while directly measuring the pressure with the pressure sensor and monitoring the flow rate with help of the glass capillaries.

Resolution of pressure and flow rate

The accuracy of the pressure sensors is specified as 1% of the maximum pressure (250 kPa or 800 kPa). We use two parallel setups ('A' and 'B'). Setup A is always used with the 800 kPa pressure sensor and a Nikon D5300 camera with resolution 6000x4000 pixel, resulting in a resolution of 0.033 µl in measuring the position of the meniscus inside the glass capillary. Setup B is used with the 250 kPa pressure sensor and a Nikon D70s camera with resolution 3008x2000 pixel (0.04 µl). The position of the meniscus is evaluated from the images with Matlab, determining the steepest slope in light intensity between the two black marks on the glass capillary.

Estimation of the area ratio $\tilde{A}$

We find a rough estimate for $\tilde{A} = A_{\mathrm{XM}}/A_{\mathrm{XP}}$ from geometrical leaf parameters. We assume a minor vein density of 50 cm/cm^2 [38], which for parallel venation corresponds to a distance of 200 µm between two veins. Now looking at the cross section of a leaf (electron microscopy image of a poplar leaf [33]), we assume a leaf thickness of 200 µm. In a cross section of $200 \times 200\,\mu\mathrm{m}^2$ will then be one minor vein. Approximating a mesophyll cell as a sphere which is 20 µm in diameter, there will be space for 100 mesophyll cells in a slab of thickness 20 µm thickness of this cross section, if the palisade mesophyll takes up half of the cross section and is densely packed, while the spongy mesophyll takes up the other half of the cross section with a packing ratio of 2/3:

$$n_{\mathrm{M}} = \frac{200\,\mu\mathrm{m}\times 100\,\mu\mathrm{m}}{\pi(10\,\mu\mathrm{m})^2} + \frac{2\times 200\,\mu\mathrm{m}\times 100\,\mu\mathrm{m}}{3\pi(10\,\mu\mathrm{m})^2} \approx 100$$

The surface of one mesophyll cell is $4\pi r^2 \approx 1250\,\mu\mathrm{m}^2$ and the total surface area of the mesophyll cells in this slab is therefore $A_{\mathrm{XM}} = 125,000\,\mu\mathrm{m}^2$.

Assuming 3 sieve elements per minor vein with sieve element radius 1 µm, the phloem surface area in the 20 µm slab is $A_{\mathrm{XP}} = 2\pi \times 1\,\mu\mathrm{m} \times 20\,\mu\mathrm{m} = 125\,\mu\mathrm{m}^2$.

Our estimate for the area ratio is thus $\tilde{A} \approx 1000$.

H.R. was supported by the Danish Council for Independent Research | Natural Sciences (Grant No. 12-126055). K.H.J. was supported by a research grant (13166) from Villum Fonden.

* khjensen@fysik.dtu.dk

[1] E. A. Rennie and R. Turgeon, Proceedings of the National Academy of Sciences **106**, 14162 (2009).
[2] C. Zhang, L. Han, T. L. Slewinski, J. Sun, J. Zhang, Z.-Y. Wang, and R. Turgeon, Plant physiology **166**, 306 (2014).
[3] K. H. Jensen, J. A. Savage, and N. M. Holbrook, Journal of The Royal Society Interface **10**, 20130055 (2013).
[4] A. C. Srivastava, K. Dasgupta, E. Ajieren, G. Costilla, R. C. McGarry, and B. G. Ayre, Annals of Botany **104**, 1121 (2009).
[5] G. B. Bonan, Science **320**, 1444 (2008).
[6] Y. Pan, R. A. Birdsey, J. Fang, R. Houghton, P. E. Kauppi, W. A. Kurz, O. L. Phillips, A. Shvidenko, S. L. Lewis, J. G. Canadell, *et al.*, Science **333**, 988 (2011).
[7] F. Abdallah, R. Michalet, J.-P. Maalouf, S. Ouled-Dhaou, B. Touzard, Z. Noumi, and M. Chaieb, Journal of Vegetation Science (2016), 10.1111/jvs.12402.
[8] L. Taiz, E. Zeiger, I. M. Møller, and A. S. Murphy, *Plant physiology and development*, 6th ed. (Sinauer, 2015).
[9] O. V. Voitsekhovskaja, O. A. Koroleva, D. R. Batashev, C. Knop, A. D. Tomos, Y. V. Gamalei, H.-W. Heldt, and G. Lohaus, Plant Physiology **140**, 383 (2006).
[10] J. Dölger, H. Rademaker, J. Liesche, A. Schulz, and T. Bohr, Physical Review E **90**, 042704 (2014).
[11] A. Schulz, Journal of plant research **128**, 49 (2015).
[12] J. Comtet, R. Turgeon, and A. D. Stroock, arXiv preprint arXiv:1603.04058 (2016).
[13] E. Truernit and N. Sauer, Planta **196**, 564 (1995).
[14] T.-k. J. Sze, P. Dutta, and J. Liu, Journal of Nanotechnology in Engineering and Medicine **4**, 031005 (2013).
[15] T.-k. J. Sze, J. Liu, and P. Dutta, Journal of Fluids Engineering **136**, 021206 (2014).
[16] T. M. Burch-Smith and P. C. Zambryski, Annual review of plant biology **63**, 239 (2012).
[17] K. Knox, P. Wang, V. Kriechbaumer, J. Tilsner, L. Frigerio, I. Sparkes, C. Hawes, and K. Oparka, Plant physiology **168**, 1563 (2015).
[18] C. Faulkner, E. Petutschnig, Y. Benitez-Alfonso, M. Beck, S. Robatzek, V. Lipka, and A. J. Maule, Proceedings of the National Academy of Sciences **110**, 9166 (2013).
[19] A. D. Meeuse, The Botanical Review **7**, 249 (1941).
[20] M. Tyree, Journal of Theoretical Biology **26**, 181 (1970).
[21] A. Robards, Annual Review of Plant Physiology **26**, 13 (1975).
[22] B. Gunning and R. Overall, Bioscience **33**, 260 (1983).
[23] D. Fisher, Planta **169**, 141 (1986).

[24] K. Robinson-Beers and R. F. Evert, Planta **184**, 307 (1991).
[25] B. Ding, R. Turgeon, and M. Parthasarathy, Protoplasma **169**, 28 (1992).
[26] P. Unwin and G. Zampighi, Nature **283**, 545 (1980).
[27] R. Mathias, J. Rae, and G. Baldo, Physiological reviews **77**, 21 (1997).
[28] R. T. Mathias, J. Kistler, and P. Donaldson, Journal of Membrane Biology **216**, 1 (2007).
[29] O. A. Candia, R. Mathias, and R. Gerometta, Investigative ophthalmology & visual science **53**, 7087 (2012).
[30] E. Münch, *Stoffbewegungen in der Pflanze* (G. Fischer, Jena, 1930).
[31] O. Kedem and A. Katchalsky, Biochimica et biophysica Acta **27**, 229 (1958).
[32] P. J. Kramer and J. S. Boyer, *Water relations of plants and soils* (Academic press, 1995).
[33] W. A. Russin and R. F. Evert, American Journal of Botany , 1232 (1985).
[34] P. N. Henrion, Transactions of the Faraday Society **60**, 75 (1964).
[35] J. Liesche and A. Schulz, Frontiers in plant science **4**, 207 (2013).
[36] Q. Fu, L. Cheng, Y. Guo, and R. Turgeon, Plant Physiology **157**, 1518 (2011).
[37] J. Liesche and A. Schulz, Plant physiology **159**, 355 (2012).
[38] L. Sack, C. Scoffoni, A. D. McKown, K. Frole, M. Rawls, J. C. Havran, H. Tran, and T. Tran, Nature Communications **3**, 837 (2012).

S1 Calculation of the full model (XMPX)

We study the full model of the four layer system as shown in Fig. 4(a). Additionally, we include a non-zero pressure in the xylem p_{X} and the phloem p_{P}. We use the same definitions for α, β and $\tilde{A}$ as above:

$$\alpha \equiv \frac{L_{\mathrm{MP}} A_{\mathrm{MP}}}{L_{\mathrm{XM}} A_{\mathrm{XM}}} \tag{12}$$

$$\beta \equiv \frac{\rho A_{\mathrm{MP}} D}{d L_{\mathrm{XP}} A_{\mathrm{XP}} R T c_{\mathrm{M}}} \tag{13}$$

$$\tilde{A} \equiv \frac{A_{\mathrm{XM}}}{A_{\mathrm{XP}}} \approx \frac{A_{\mathrm{XM}}}{A_{\mathrm{MP}}} \tag{14}$$

The bulk flows over the three interfaces are described by

$$Q_{\mathrm{XM}} = L_{\mathrm{XM}} A_{\mathrm{XM}} (R T c_{\mathrm{M}} - (p_{\mathrm{M}} - p_{\mathrm{X}})) \tag{15}$$

$$Q_{\mathrm{MP}} = L_{\mathrm{MP}} A_{\mathrm{MP}} (R T (c_{\mathrm{P}} - c_{\mathrm{M}}) - (p_{\mathrm{P}} - p_{\mathrm{M}})) \tag{16}$$

$$Q_{\mathrm{XP}} = L_{\mathrm{XP}} A_{\mathrm{XP}} (R T c_{\mathrm{P}} - (p_{\mathrm{P}} - p_{\mathrm{X}})). \tag{17}$$

The sugar loading into the phloem is

$$S = \frac{\rho A_{\mathrm{MP}} D}{d} (c_{\mathrm{M}} - c_{\mathrm{P}}) + Q_{\mathrm{MP}} c_{\mathrm{M}}. \tag{18}$$

Furthermore, we have the following conservation laws

$$(Q_{\mathrm{MP}} + Q_{\mathrm{XP}}) c_{\mathrm{P}} = S \tag{19}$$

$$Q_{\mathrm{XM}} = Q_{\mathrm{MP}}. \tag{20}$$

These six equations allow to solve for the six unknowns $Q_{\mathrm{XM}}, Q_{\mathrm{MP}}, Q_{\mathrm{XP}}, S, c_{\mathrm{P}}, p_{\mathrm{M}}$. Inserting Eq. 15 and Eq. 16 into Eq. 20 we find the mesophyll pressure

$$p_{\mathrm{M}} = R T c_{\mathrm{M}} - \frac{\alpha}{\alpha + 1} (R T c_{\mathrm{P}} - p_{\mathrm{P}}) + \frac{p_{\mathrm{X}}}{1 + \alpha}, \tag{21}$$

and with this and Eq. 16 the bulk flow component

$$Q_{\mathrm{adv}} = Q_{\mathrm{MP}} = \frac{1}{1 + \alpha} L_{\mathrm{MP}} A_{\mathrm{MP}} (R T c_{\mathrm{P}} - (p_{\mathrm{P}} - p_{\mathrm{X}})). \tag{22}$$

Inserting this, as well as Eqs. 17 and 18 into 19 gives a quadratic equation for the concentration in the phloem:

$$\frac{1}{1+\alpha}L_{\mathrm{MP}}A_{\mathrm{MP}}(RTc_{\mathrm{P}}-(p_{\mathrm{P}}-p_{\mathrm{X}}))c_{\mathrm{P}}+L_{\mathrm{XP}}A_{\mathrm{XP}}(RTc_{\mathrm{P}}-(p_{\mathrm{P}}-p_{\mathrm{X}}))c_{\mathrm{P}}$$
$$=\frac{\rho A_{\mathrm{MP}}D}{d}(c_{\mathrm{M}}-c_{\mathrm{P}})+c_{\mathrm{M}}\frac{1}{1+\alpha}L_{\mathrm{MP}}A_{\mathrm{MP}}(RTc_{\mathrm{P}}-(p_{\mathrm{P}}-p_{\mathrm{X}})) \quad (23)$$

$$\frac{1}{1+\alpha}\frac{L_{\mathrm{MP}}A_{\mathrm{MP}}}{L_{\mathrm{XP}}A_{\mathrm{XP}}RT}(RTc_{\mathrm{P}}-(p_{\mathrm{P}}-p_{\mathrm{X}}))c_{\mathrm{P}}+\frac{L_{\mathrm{XP}}A_{\mathrm{XP}}}{L_{\mathrm{XP}}A_{\mathrm{XP}}RT}(RTc_{\mathrm{P}}-(p_{\mathrm{P}}-p_{\mathrm{X}}))c_{\mathrm{P}}$$
$$=\frac{\rho A_{\mathrm{MP}}D}{dL_{\mathrm{XP}}A_{\mathrm{XP}}RTc_{\mathrm{M}}}c_{\mathrm{M}}(c_{\mathrm{M}}-c_{\mathrm{P}})+c_{\mathrm{M}}\frac{1}{1+\alpha}\frac{L_{\mathrm{MP}}A_{\mathrm{MP}}}{L_{\mathrm{XP}}A_{\mathrm{XP}}RT}(RTc_{\mathrm{P}}-(p_{\mathrm{P}}-p_{\mathrm{X}})) \quad (24)$$

$$\frac{\tilde{A}\alpha}{1+\alpha}\frac{1}{RT}(RTc_{\mathrm{P}}-(p_{\mathrm{P}}-p_{\mathrm{X}}))c_{\mathrm{P}}+\frac{1}{RT}(RTc_{\mathrm{P}}-(p_{\mathrm{P}}-p_{\mathrm{X}}))c_{\mathrm{P}}$$
$$=\beta c_{\mathrm{M}}(c_{\mathrm{M}}-c_{\mathrm{P}})+c_{\mathrm{M}}\frac{\tilde{A}\alpha}{1+\alpha}\frac{1}{RT}(RTc_{\mathrm{P}}-(p_{\mathrm{P}}-p_{\mathrm{X}})) \quad (25)$$

$$\frac{\tilde{A}\alpha}{1+\alpha}\left(c_{\mathrm{P}}^2-\frac{p_{\mathrm{P}}-p_{\mathrm{X}}}{RTc_{\mathrm{M}}}c_{\mathrm{M}}c_{\mathrm{P}}\right)+c_{\mathrm{P}}^2-\frac{p_{\mathrm{P}}-p_{\mathrm{X}}}{RTc_{\mathrm{M}}}c_{\mathrm{M}}c_{\mathrm{P}}=\beta c_{\mathrm{M}}^2-\beta c_{\mathrm{M}}c_{\mathrm{P}}+\frac{\tilde{A}\alpha}{1+\alpha}\left(c_{\mathrm{M}}c_{\mathrm{P}}-\frac{p_{\mathrm{P}}-p_{\mathrm{X}}}{RTc_{\mathrm{M}}}c_{\mathrm{M}}^2\right) \quad (26)$$

$$\left(\frac{\tilde{A}\alpha}{\alpha+1}+1\right)c_{\mathrm{P}}^2+\left(\beta-\frac{\tilde{A}\alpha}{\alpha+1}-\left(\frac{\tilde{A}\alpha}{\alpha+1}+1\right)\left(\frac{p_{\mathrm{P}}-p_{\mathrm{X}}}{RTc_{\mathrm{M}}}\right)\right)c_{\mathrm{M}}c_{\mathrm{P}}-\left(\beta-\frac{\tilde{A}\alpha}{\alpha+1}\left(\frac{p_{\mathrm{P}}-p_{\mathrm{X}}}{RTc_{\mathrm{M}}}\right)\right)c_{\mathrm{M}}^2=0 \quad (27)$$

where we again used that $L_{\mathrm{XM}}=L_{\mathrm{XP}}$, when going from Eq. 24 to Eq. 25. The solution for c_{P} can then be inserted into Eq. 17 to find Q_{XP} and Eq. 19 to find the total sugar export S:

$$\tilde{S}=\frac{S}{\frac{\rho A_{\mathrm{MP}}Dc_{\mathrm{M}}}{d}}=\left(1-\frac{c_{\mathrm{P}}}{c_{\mathrm{M}}}\right)+\frac{\tilde{A}\alpha}{(1+\alpha)\beta}\left(\frac{c_{\mathrm{P}}}{c_{\mathrm{M}}}-\frac{p_{\mathrm{P}}-p_{\mathrm{X}}}{RTc_{\mathrm{M}}}\right). \quad (28)$$

The proportions of advectively versus diffusively transported sugar can be calculated from Eq. 18 as

$$\begin{aligned}\frac{S_{\mathrm{adv}}}{S_{\mathrm{dif}}}&=\frac{Q_{\mathrm{MP}}c_{\mathrm{M}}}{\frac{\rho A_{\mathrm{MP}}D}{d}(c_{\mathrm{M}}-c_{\mathrm{P}})}\\&=\frac{Q_{\mathrm{MP}}}{K_D(1-c_{\mathrm{P}}/c_{\mathrm{M}})}\\&=\frac{L_{\mathrm{MP}}A_{\mathrm{MP}}(RTc_{\mathrm{P}}-(p_{\mathrm{P}}-p_{\mathrm{X}}))}{(1+\alpha)\beta L_{\mathrm{XP}}A_{\mathrm{XP}}RTc_{\mathrm{M}}(1-c_{\mathrm{P}}/c_{\mathrm{M}})}\\&=\frac{\tilde{A}\alpha}{(1+\alpha)\beta}\left(\frac{c_{\mathrm{P}}/c_{\mathrm{M}}-\frac{p_{\mathrm{P}}-p_{\mathrm{X}}}{RTc_{\mathrm{M}}}}{1-c_{\mathrm{P}}/c_{\mathrm{M}}}\right).\end{aligned} \quad (29)$$

If $p_{\mathrm{P}}-p_{\mathrm{X}}=0$, Eq. 27 reduces to

$$\left(\frac{\tilde{A}\alpha}{\alpha+1}+1\right)c_{\mathrm{P}}^2+\left(\beta-\frac{\tilde{A}\alpha}{\alpha+1}\right)c_{\mathrm{M}}c_{\mathrm{P}}-\beta c_{\mathrm{M}}^2=0, \quad (30)$$

Eq. 29 to

$$\frac{S_{\mathrm{adv}}}{S_{\mathrm{dif}}}=\frac{\tilde{A}\alpha}{(1+\alpha)\beta}\left(\frac{c_{\mathrm{P}}/c_{\mathrm{M}}}{1-c_{\mathrm{P}}/c_{\mathrm{M}}}\right), \quad (31)$$

and Eq. 28 to

$$\begin{aligned}\tilde{S}&=\left(1-\frac{c_{\mathrm{P}}}{c_{\mathrm{M}}}\right)+\frac{\tilde{A}\alpha}{(1+\alpha)\beta}\frac{c_{\mathrm{P}}}{c_{\mathrm{M}}}\\&=1+\left(\frac{\tilde{A}\alpha}{(1+\alpha)\beta}-1\right)\frac{c_{\mathrm{P}}}{c_{\mathrm{M}}}.\end{aligned} \quad (32)$$

A special case is $p_{\mathrm{P}}-p_{\mathrm{X}}\to RTc_{\mathrm{M}}$. First we check the conditions for the existence of a real solution c_{P}^*. We find that

$$\frac{\tilde{A}\alpha}{\alpha+1}<\frac{\sqrt{2}-1}{2}\Rightarrow c_{\mathrm{P}}^*\in IR \quad (33)$$

$$\frac{\tilde{A}\alpha}{\alpha+1}<\frac{\sqrt{2}-1}{2}\wedge\beta>2\sqrt{2(a^2+a)}-2a-1\Rightarrow c_{\mathrm{P}}^*\in IR. \quad (34)$$

Next we check the conditions for c_P^* being in a physical range, namely $[0, 1]$:

$$\beta < 1 \Rightarrow \exists c_\mathrm{P}^* > 0 \tag{35}$$

$$\beta > 1 \wedge \beta > \frac{\tilde{A}\alpha}{\alpha+1} \Rightarrow \exists c_\mathrm{P}^* > 0 \tag{36}$$

$$\forall \alpha, \beta \ \Rightarrow c_\mathrm{P}^* < 1 \tag{37}$$

$$\frac{\tilde{A}\alpha}{\alpha+1} \to 0 \Rightarrow c_\mathrm{P}^* \to 1 \tag{38}$$

Boundary conditions

For any choice of parameters, the mesophyll has to be able to draw in water, e.g. for photosynthesis. This condition can be expressed as

$$\begin{aligned} & RTc_\mathrm{M} - (p_\mathrm{M} - p_\mathrm{X}) > 0 \\ \Leftrightarrow \quad & p_\mathrm{M} < RTc_\mathrm{M} + p_\mathrm{X}. \end{aligned} \tag{39}$$

Using the solution for the mesophyll pressure in Eq. 21, this is equivalent to

$$\begin{aligned} & RTc_\mathrm{M} - \tfrac{\alpha}{\alpha+1}(RTc_\mathrm{P} - p_\mathrm{P}) + \tfrac{p_\mathrm{X}}{1+\alpha} < RTc_\mathrm{M} + p_\mathrm{X} \\ \Leftrightarrow \quad & \tfrac{p_\mathrm{X}}{1+\alpha} - p_\mathrm{X} < \tfrac{\alpha}{\alpha+1}(RTc_\mathrm{P} - p_\mathrm{P}) \\ \Leftrightarrow \quad & p_\mathrm{P} - p_\mathrm{X} < RTc_\mathrm{P}. \end{aligned} \tag{40}$$

This effectively limits the choice of $\Delta p = p_\mathrm{P} - p_\mathrm{X}$. In the case where $p_\mathrm{P} - p_\mathrm{X} = RTc_\mathrm{P}$, Eq. 27 becomes

$$\begin{aligned} \left(\frac{\tilde{A}\alpha}{\alpha+1}+1\right) c_\mathrm{P}^2 + \left(\beta - \frac{\tilde{A}\alpha}{\alpha+1} - \left(\frac{\tilde{A}\alpha}{\alpha+1}+1\right)\left(\frac{RTc_\mathrm{P}}{RTc_\mathrm{M}}\right)\right) c_\mathrm{M} c_\mathrm{P} - \left(\beta - \frac{\tilde{A}\alpha}{\alpha+1}\left(\frac{RTc_\mathrm{P}}{RTc_\mathrm{M}}\right)\right) c_\mathrm{M}^2 &= 0 \\ \left(\frac{\tilde{A}\alpha}{\alpha+1}+1\right) \tilde{c}_\mathrm{P}^2 + \left(\beta - \frac{\tilde{A}\alpha}{\alpha+1} - \left(\frac{\tilde{A}\alpha}{\alpha+1}+1\right)\tilde{c}_\mathrm{P}\right) \tilde{c}_\mathrm{P} - \left(\beta - \frac{\tilde{A}\alpha}{\alpha+1}\tilde{c}_\mathrm{P}\right) &= 0 \\ \left(\beta - \frac{\tilde{A}\alpha}{\alpha+1}\right) \tilde{c}_\mathrm{P} - \left(\beta - \frac{\tilde{A}\alpha}{\alpha+1}\tilde{c}_\mathrm{P}\right) &= 0 \\ \beta\tilde{c}_\mathrm{P} &= \beta \\ \tilde{c}_\mathrm{P} &= 1. \end{aligned} \tag{41}$$

In this case diffusive transport stops, because $c_\mathrm{P} = c_\mathrm{M}$, but also advective transport stops, because water from the xylem can neither be drawn into the mesophyll nor the phloem (see conditions 39 and 40).

5.3 On the size of conifer needles

In revision. Target journal: PNAS.

On the size of conifer needles

Hanna Rademaker[a], **Maciej A. Zwieniecki**[b], **Tomas Bohr**[a], **and Kaare H. Jensen**[a,1]

[a]Department of Physics, Technical University of Denmark, DK 2800 Kgs. Lyngby, Denmark; [b]Department of Plant Sciences, University of California at Davis, Davis, CA 95616, USA

This manuscript was compiled on September 9, 2016

Plant leaf size varies by more than 3 orders of magnitude, from a few millimeters to over one meter. Conifer leaves, however, are relatively short and the majority of needles are no longer than 6 cm. The reason for the strong confinement of the trait-space is unknown. We show that sugars produced near the tip of long needles cannot be exported efficiently, because the pressure required to drive vascular flow would exceed the greatest available pressure (the osmotic pressure). This basic constraint leads to the formation of an inactive region of stagnant fluid near the needle tip, which does not contribute to sugar flow. Remarkably, we find that the size of the active part does not scale with needle length. We predict a single maximum needle size of 5 cm, in accord with data from 519 conifer species. This could help rationalize the recent observation that conifers have significantly smaller leaves than angiosperms, and provide a biophysical explanation for this intriguing difference between the two largest groups of plants.

plant leaf | conifer | sugar transport | osmotic pipe flow

Light capture and gas exchange associated with photosynthesis take place in plant leaves, organs strikingly adapted for these processes that are essential to life on Earth. A wide range of morphological and physiological traits are expressed in plant leaves. This has been appreciated since antiquity [1], but recent studies have revealed that only a remarkably small portion of the available trait-space is occupied by extant species [2, 3]. The physical mechanisms that impose constraints on the traits favored by evolution, however, remain poorly understood. A particularly intriguing case is that of needle or scale-bearing gymnosperms (conifers). Most species (75%) in this group have leaves that are shorter than 6 cm in length; only one genus (Pinus) has multiple species with needles longer than 25 cm. By contrast, leaves on broad-leaved angiosperms grow much larger. The mechanisms that limit the size of conifer needles are unknown.

Plant leaves are typically thin and flat, thereby maximizing the surface area exposed to light and promoting photosynthesis in which light energy is converted into chemical energy stored in sugar molecules. Leaves are generally arranged on the plant so as to expose their surfaces to light with little self-shading. Leaf size and shape is influenced by a number of factors, including light interception, gravity, wind, temperatures, herbivores, and vascular transport efficiency [4, 5]. The greatest diversity is found among broad-leaved angiosperm species, where leaf diameter spans 3 orders of magnitude, from 10^{-3} m to 1 m [2, 6]. By contrast, many gymnosperm species have slender needle- or scale-like leaves, which are significantly smaller. Although needles/scales are thought to be advantageous in dry or cold climates frequented by snow and frost, the mechanistic explanation why their size is constrained is missing [2].

The vascular architecture of leaves may hold clues to the reason for the difference in size between angiosperm and gymnosperm leaves. It is well established that a major innovation in angiosperms concerns xylem vessels, the vascular conduits that deliver water to leaves actively used in photosynthesis and passively lost to the atmosphere while obtaining CO_2. Angiosperm vessels are longer and larger-diameter conduits than gymnosperm tracheids, permitting higher hydraulic conductivities. This, together with a greater density of leaf veins, has made it possible for angiosperms to extend the range of leaf photosynthetic capacities to higher values and presumably also contributed to the evolution of large leaves in angiosperms [7].

However, the situation is remarkably different for the phloem vascular conduits, which transport sugars produced by photosynthesis between leaves and sites of growth or storage (e.g. roots, fruits, and shoots). In the stem, the cross sectional area A of phloem conduits is approximately equal in angiosperms and gymnosperms ($A_{\mathrm{stem}} \sim 500 - 1000\ \mu\mathrm{m}^2$, see [8]). In contrast, phloem conduits in conifer leaves are remarkably small, with areas in the range $A \sim 3 - 10\ \mu\mathrm{m}^2$ [9]. While the factors that limit phloem cell size to this range in conifer leaves are unknown, it is clear that the length and size of vascular conduits must impose constraints on sugar export rates. The pressure differential Δp required to drive flow over a length L scales inversely with the conduit area A, as $\Delta p \sim uL\eta/A$, where u is the flow speed and η is the sap viscosity. Thus a long and narrow tube requires a relatively large pressure Δp to sustain similar sugar export. However, because the sap flow is driven by osmosis, the available pressure is always limited by the cell's osmotic pressure, i.e. $\Delta p \leq RTc$, a fact which must reduce the efficiency of transport in relatively long needles.

Nevertheless, it should be noted that gymnosperms dom-

Significance Statement

Plant leaves photosynthesize sugars and release oxygen which are both essential to life on Earth. The diversity of plant leaves is astonishing, but while the sizes of broad leaves span from millimeters to meters, conifer needles are relatively short, typically less than 6 cm (data from 519 species). The reason for this strong confinement is unknown, despite the increasing interest in understanding the phenotypic trait-space of plants. Our study reveals that the efficiency of sugar export is compromised in long needles by the emergence of a stagnant zone near the needle tip, which does not contribute to export. Long needles are thus rarely observed, in part because the plant cannot generate sufficiently large pressures to drive transport.

H.R., M.Z., T.B. and K.H.J. designed research; H.R., M.Z., T.B. and K.H.J. performed research; H.R., M.Z., T.B. and K.H.J. analyzed data; and H.R., M.Z., T.B. and K.H.J. wrote the paper

The authors declare no conflict of interest.

[1]To whom correspondence should be addressed. E-mail: khjensen@fysik.dtu.dk

inated the Earth from around 300 million years ago (mya) until the evolution and diversification of angiosperms ($\sim$ 120 mya) and still have an advantage over angiosperms in extreme environments. Moreover, conifer trees hold the records for the world's tallest (112.7 m, *Sequoia sempervirens*) [10], widest (14.5 m, *Taxodium mucronatum*) [11], oldest ($\sim$ 4,900 yrs, *Pinus longaeva*) [12] and largest (1486 m^3, *Sequoiadendron giganteum*) [13] trees. These numbers suggest that although various factors may limit the absolute size of conifer leaves, the organisms are not suffering from small leaf size and we can expect photosynthesis and sugar export from conifer leaves to be highly efficient.

To explore the organization of flows within needles, and to rationalize the limits to their size, we proceed in the following way. First, we present data which demonstrate that conifer leaf lengths occupy a narrow range of sizes. Then we develop a mathematical model for sugar export from a slender leaf. Next, we explore the dependence of the sugar export rate on the geometric and material parameters. We show that a characteristic needle length exists, above which sugar export becomes inefficient due to the formation of a region of stagnant fluid near the needle tip. Finally, we conclude and discuss the implications for our understanding of observed leaf lengths in nature and related physiological transport problems.

Results

Conifer leaf size. A wide range of morphological and physiological traits are expressed in plants. To our knowledge, the diversity in leaf size and function was first discussed systematically by Theophrastus around 300 BC, who noted that *"To sum up, the differences between leaves are shewn in size, number, shape, hollowness, in breadth, roughness... These are all the differences in leaves stated somewhat generally, and this is a fairly complete list of examples."* ([1], p. 77). This classic and countless subsequent works have contributed to our understanding of the factors that influence leaf size and shape [4, 14]. Diaz *et al.*, however, recently reported that while diversity may appear almost unbounded, only a relatively small portion of the available trait-space is occupied by extant species [2]. Only particular ranges of traits – for instance, plant height, stem density, seed mass, and leaf size – are found in nature. The reason for this confinement remains elusive, and Diaz *et al.* state that: *"Our results are correlative and cannot prove rigorously why such a large share of the potential trait volume is not occupied. Still, from first principles many more combinations of traits than those observed seem feasible as far as biomechanics and evolutionary genetics are concerned."* ([2], p. 170).

The greatest diversity in leaf size is found among broad-leaved angiosperm woody species, where leaf diameter spans 3 orders of magnitude, from 1 mm to over 1 m [6]. The median leaf length from over 1900 species representing 95 families was 18 cm with 97% of species with leaves longer than 6 cm [6]. By contrast, we find that conifers – which have slender needle- or scale-like leaves – are significantly smaller (Fig. 1). Data presented here include 519 conifer species from 6 families (see supporting online material). The leaf length L has median value 2.3 cm, 75% of species have leaves shorter than 6 cm and 97.5% have leaves no longer than 23 cm. Moreover, leaf length follows an approximately exponential distribution characterized by a high density of species at short leaf lengths.

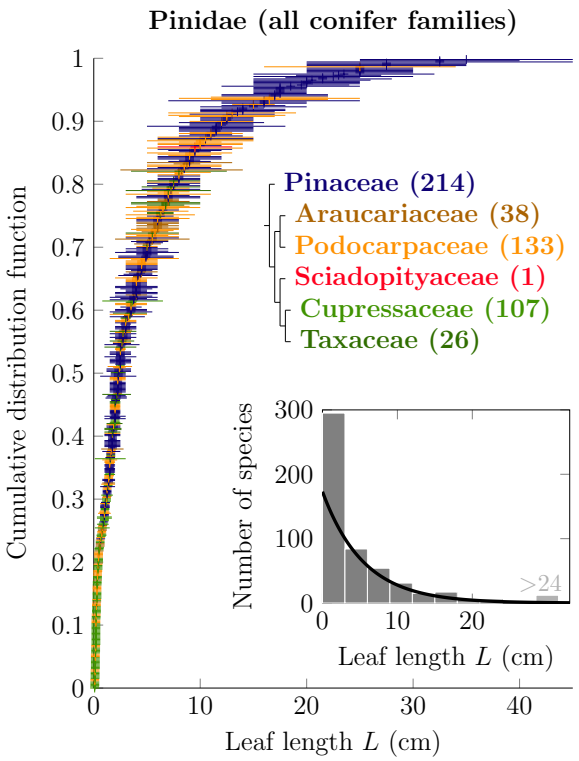

Fig. 1. Conifer leaf size follows a narrow distribution with a high density of short leaves. Cumulative distribution function (cdf) of leaf length is plotted as a function of the leaf length L for 519 species (6 families). Species are sorted according to their mean leaf length, and the horizontal lines indicate the observed range of leaf sizes for each species. The median leaf length is 2.3 cm, 75% of species have leaves shorter than 6 cm, while 97.5% have leaves no longer than 23 cm. Inset shows a histogram of the mean leaf length divided into bins of 3 cm. Note that leaf length is approximately exponentially distributed (solid line shows exponential fit as a guide to the eye). Data and source references are available in the supporting online material (Table S1).

As stated previously, the reason for the clustering of sizes in the range below 6 cm is unknown.

Efficiency of sugar export. To explore the biomechanics of sugar export from slender leaves, and to rationalize the limits to their size, we proceed by considering a mathematical model for sugar transport in conifer needles. Our approach follows models applied to describe aspects of long-distance sugar transport in plants (see e.g. Thompson and Holbrook [15] and Pickard and Abraham-Shrauner[16]), and to model transport in long narrow epithelia channels which absorb or secrete fluids in for instance the kidney, as discussed by Lin and Segel [17, 18].

Plant leaves capture energy from the sun and store it in the chemical bonds of sugars. These energy-rich molecules are distributed to distal parts of the plant and used in processes essential to cellular metabolism, organism growth, and reproduction. Sugar transport takes place in phloem cells which form a continuous microfluidic channel network from leaf to root. The current hypothesis for phloem transport dates to the 1920s when Ernst Münch proposed that gradients in cell turgor pressure drive the bulk flow of sugars and other solutes from sources to sinks [19]. Sources are regions of the plant where photosynthesis (or the breakdown of starch)

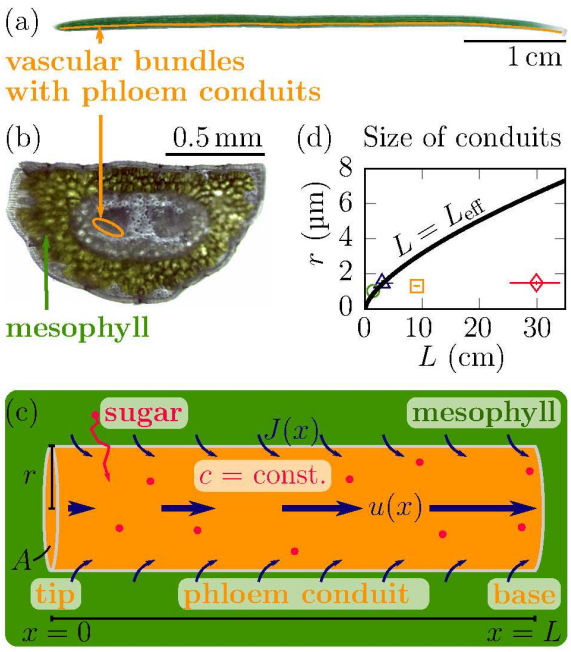

Fig. 2. Biomechanics of osmotic sugar export. (a),(b) Conifer needles are long and slender leaves which capture sunlight to photosynthesize sugars in the mesophyll cells (green tissue). Microfluidic phloem vascular conduits facilitate export of sugars to distal parts of the plant through a file of cellular tubes (sieve elements) located near the central axis of the needle (orange tissue). (c) We model a file of sieve elements as a single circular microchannel with radius r and length L. Sugars diffuse from the mesophyll into the phloem, and export is driven by osmotic uptake of water over the surface of the phloem at a flux $J = L_p(RTc - p)$, where c is the phloem sugar concentration, p is the phloem pressure, and L_p is the permeability of the cell membrane. The water potential outside the phloem is assumed to be zero ($RTc_{\text{ext}} - p_{\text{ext}} = 0$). The velocity inside the tube increases from $u(0) = 0$ to $u(L)$ according to Eq. (1). (d) Phloem tube radii are remarkably uniform among species with leaf length in the range $2 - 30$ cm. Plot shows mean individual conduit radius r as a function of needle length L for *Picea omorika* (green circle), *Abies nordmanniana* (blue triangle), *Pinus cembra* (orange square), and *Pinus palustris* (red diamond). Error bars indicate maximum error. Data reproduced from [9] (others). The black line indicates the predicted conduit radius from our model assuming $L = L_{\text{eff}}$ (Eq. (8)).

results in high concentrations of sugars and thus large turgor pressures due to osmosis. In contrast, sinks are regions of the plant where mitochondrial respiration and the incorporation of sugars into larger molecules reduces the concentration of osmotically active solutes and thus lowers turgor pressures. According to the Münch hypothesis, transport through the phloem results from these osmotically generated differences in pressure and occurs without any additional input of energy. In needles, phloem tubes are situated inside vascular bundles (Fig. 2(a-b)). Most of the $5 - 50$ bundled tubes that run in parallel span the entire length of the needle [*]. We therefore treat the dynamics of phloem transport in each conduit separately, assuming no interactions or exchange of material between adjacent channels. Our goal in the following is to quantify how quickly sugars can be removed (exported) from a needle, and how the efficiency of the process depends on the size of the needle and of the phloem conduits.

Sugar molecules are produced in the mesophyll by photosynthesis and subsequently diffuse into the phloem conduits. To quantify how quickly they can be exported, we consider a simple model of osmotic transport in a microchannel (Fig. 2(c)). The presence of sugar molecules in the phloem cells leads to an osmotic flux of water $J = L_p(RTc - p)$ across the cell membrane, where c is the concentration of sugar, R is the gas constant, T is temperature, p is cell turgor pressure, and L_p is the membrane permeability. Due to the uptake of water, the flow velocity $u(x)$ inside the conduit builds up along the x-axis from the tip of the needle at $x = 0$ (where $u(0) = 0$), as

$$\frac{\mathrm{d}u(x)}{\mathrm{d}x} = \frac{2L_p}{r}(RTc(x) - p(x)). \qquad [1]$$

where the parameter r is the conduit radius [†]. Sieve tubes in needles are relatively small, with conductive areas in the range $A = 3 - 10\ \mu\text{m}^2$ [9] (Fig. 2(d)). These export conduits are quite narrow when compared to tube sizes observed in leaves of flowering plants (e.g. $A = 16.2 - 89.5\ \mu\text{m}^2$ and $A = 12.9 - 29.9\ \mu\text{m}^2$ in maize and barley [20, 21]) and also in stems of both gymnosperms and angiosperms ($A \sim 500 - 1000\ \mu\text{m}^2$ [6]). Conservation of sugar mass leads to the continuity equation

$$\frac{\mathrm{d}}{\mathrm{d}x}(uc) = \gamma, \qquad [2]$$

where γ is the amount of sugar loaded from the mesophyll into the phloem per unit length and time. The sugar export flux from the needle – and its dependence on physical parameters – can be determined from a solution to Eq. (1) and Eq. (2) with appropriate boundary conditions. This will allow us to ascertain the efficiency of the process under various conditions. In the following, we therefore seek to compute the total sugar flux out of the needle $\Gamma = u(L)c(L)$, where the position $x = L$ corresponds to the needle base. We also determine the local loading rate $\gamma(x)$ which measures how much each part of the needle contributes to the production and export of energetic sugars. Finally, we determine the conduit pressure $p(x)$.

Before proceeding, however, we make two simplifying assumptions. First, we assume that the pressure variation and the flow velocity along the conduit are related by Darcy's law, $\mathrm{d}p/\,\mathrm{d}x = -8\eta u(x)/r^2$, with $\eta \simeq 4$ mPas the viscosity of the fluid [22]. This is reasonable because the channel aspect ratio $r/L \sim 10^{-4}$ is small and hence the lubrication approximation is valid. Second, we assume that the sugar concentration $c(x) = c$ is constant inside the conduit. Sugar molecules produced in the mesophyll are loaded into the phloem conduits by either protein pumps or by bulk flow and diffusion through plasmodesmata nanopores. Evidence suggests that plasmodesmata transport is the dominant mechanism in needles [23]. Our analysis, however, does not depend on details of the loading mechanism, as long as it is able to preserve a constant concentration inside the conduit. Presuming that diffusion is the slowest of the relevant transport processes, the assumption $c = \text{const}$ therefore at most requires that sugar molecules which are advected by the bulk flow along the needle can be quickly replenished by radial diffusion, i.e. that the Peclet number $Pe = ur/D < 1$. Using typical values ($u = 5 \times 10^{-5}$ m/s, $r = 10^{-6}$ m and $D = 5 \times 10^{-10}$ m^2/s) we find $Pe = 0.1$ in accord with the assumption $c(x) = \text{const}$.

With these simplifications, the governing equation Eq. (1) becomes

$$\frac{\mathrm{d}^2u(x)}{\mathrm{d}x^2} = 16\frac{L_p\eta}{r^3}u(x). \qquad [3]$$

[*] Ronellenfitsch *et al.* [9] found that 50% of conduits were longer than 75% of the needle length.

[†] This expression is valid for a cylindrical cell of radius r; in other geometries the factor $2/r$ should be replaced by the relevant cell surface-to-volume ratio.

The solution for the flow velocity $u(x)$ with boundary condition $u(0) = 0$

$$u(x) = \frac{1}{2}\sqrt{\frac{rL_p}{\eta}}\frac{\sinh\left(\sqrt{M}\frac{x}{L}\right)}{\cosh\sqrt{M}}\left(RTc - p(L)\right), \qquad [4]$$

where $p(L)$ is the pressure at the needle base and the non-dimensional Münch number $M = 16\eta L_p L^2/r^3$ characterizes the relative importance of viscous and membrane flow resistances. The outlet pressure $p(L)$ can be determined from the sink (e.g. root) pressure p_{sink} and the hydraulic resistance of the stem R_{stem}. This leads to $p(L) - p_{\text{sink}} = QR_{\text{stem}} = \pi r^2 u(L) R_{\text{stem}}$. An explicit expression for the pressure can be from obtained Eq. (4), which leads to

$$RTc - p(L) = \frac{RTc}{1 + \pi r^2 R_{\text{stem}} \frac{1}{2}\sqrt{\frac{rL_p}{\eta}}\tanh\sqrt{M}}, \qquad [5]$$

where we have assumed water potential equilibrium at the sink $p_{\text{sink}} = 0$. From the expression in Eq. (4) we can compute the loading rate $\gamma(x) = cu'$ and pressure $p(x)$ from Eq. (1)

$$\gamma(x) = \frac{2L_p}{r}c\frac{\cosh\left(\sqrt{M}\frac{x}{L}\right)}{\cosh\sqrt{M}}\left(RTc - p(L)\right), \qquad [6]$$

$$p(x) = RTc - \frac{\cosh\left(\sqrt{M}\frac{x}{L}\right)}{\cosh\sqrt{M}}\left(RTc - p(L)\right). \qquad [7]$$

For small values of M (corresponding to, say, a short and wide tube), the velocity u is a linear function of x, pressure decreases gradually, and the loading rate $\gamma = cu'$ is constant throughout the needle (Fig. 3). Each part of the needle thus contributes equally to the sugar export. In contrast, the situation is completely different when M is large, relevant for example in a long and narrow tube. In this case, the velocity profile is strongly non-linear and characterized by a stagnant zone at the needle tip. Near the base of the needle the speed u and loading rate γ both grow exponentially with position; $u, \gamma \propto \exp\left(\sqrt{M}(x/L - 1)\right)$, hence most material is collected from this region. Close to the tip the speed is relatively slow and almost no loading occurs (i.e. $\gamma(x)/\gamma(L) \ll 1$ and $u(x)/u(L) \ll 1$). Likewise, the pressure gradient is localized close to the needle base. In the limit of large M, the contribution from each part of the needle thus varies strongly, and the most significant contribution comes from a region closest to the needle base. The size of this region is the intrinsic length scale of the exponential, i.e.

$$L_{\text{eff}} = \frac{L}{\sqrt{M}} = \frac{r^{3/2}}{(16L_p\eta)^{1/2}}, \qquad [8]$$

where we used the definition of the Münch number. Remarkably, this effective needle length L_{eff} is independent of needle length L as well as the sugar concentration c. We note that related models have been analyzed in the context of long-distance sugar transport in plants [15, 16], and to model transport in epithelia channels [17, 18]. These systems, however, are characterized by a separation of scales, where material is added to the channel in a relatively short active portion of the channel of known length. In contrast, material is added along the entire channel in our system, and the size of the active region L_{eff} is an emergent property of the system. Moreover, we note that the active part of the channel is towards the needle

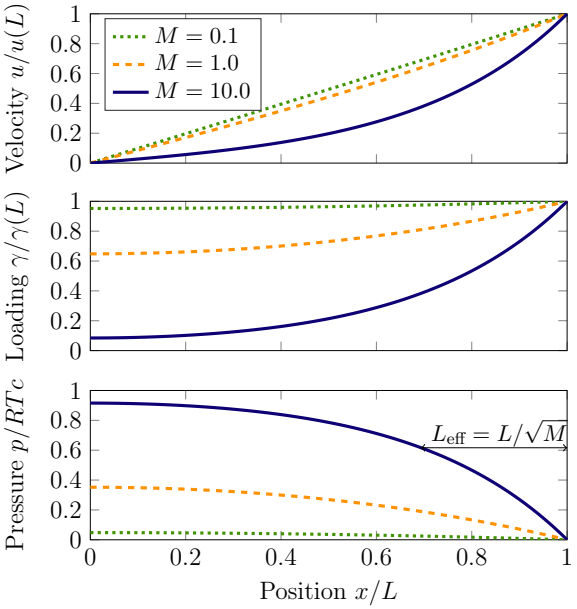

Fig. 3. Very long conduits are inefficient. Velocity u, loading γ, and pressure p plotted as a function of relative position x/L, as calculated from Eqs. 4 to 7, assuming $p(L) = 0$. For small Münch numbers M (e.g. short and wide conduits) the velocity u increases linearly along the tube and the loading function $\gamma = c\,\mathrm{d}u/\mathrm{d}x$ is approximately constant. For large M (e.g. long and narrow conduits) a stagnant zone forms near the tip ($x = 0$) and gradients in velocity, loading, and pressure are localized near the needle base. The main contribution to flow and sugar export comes from a region of length $L_{\text{eff}} = L/\sqrt{M}$ adjacent to the needle base (Eq. (8), indicated by an arrow for $M = 10$). Velocity and loading are normalized with respect to their terminal values ($u(L), \gamma(L)$) while pressure is plotted relative to the maximum value set by the osmotic pressure RTc. The Münch numbers corresponding to data from the four conifer species displayed in Fig. 2(d) are $M \approx 1$ (*A. nordmanniana* and *P. omorika*, $M \approx 10$ (*P. cembra*) and $M \approx 100$ (*P. palustris*).

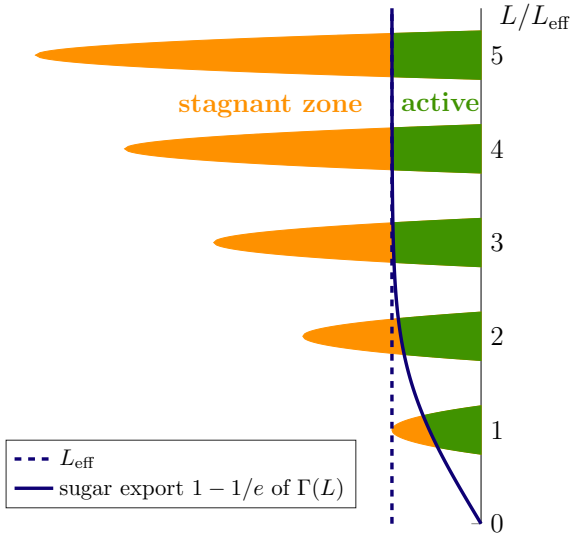

Fig. 4. Sugars exported from conifer needles originate predominantly from an active region of length $L_{\text{eff}} = r^{3/2}/(16\eta L_p)^{1/2}$ near the base (shaded green area, Eq. (8)). This region contributes 63% ($= 1 - 1/e$) to the total sugar export $\Gamma(L)$. The dashed vertical line indicates $L = L_{\text{eff}}$.

base (Fig. 4), and not towards the tip as assumed in Segel's standing gradient problem [17].

The total sugar flux leaving the needle $\Gamma = cu(L)$ allows us to gauge the relative performance of different needle designs as a function of the system parameters (using Eq. (4), Eq. (8) and the definition of the Münch number):

$$\Gamma = cu(L) = \frac{1}{2}\sqrt{\frac{rL_p}{\eta}}c\tanh\left(\frac{L}{L_{\text{eff}}}\right)(RTc - p(L)) \qquad [9]$$

From Eq. (9) we again find that the effective length L_{eff} is the characteristic size above which sugar export no longer scales linearly with needle length and very little can be gained by a further increase in length (Fig. 4). For instance, increasing needle size to $10 \cdot L_{\text{eff}}$ only increases sugar export by a factor 1.3.

The existence of a stagnant zone for lengths larger than L_{eff} is not restricted to the flow in a single tube with a constant concentration. In fact, one can show [24] that a system of coupled tubes will behave in essentially the same way, although the details depend on exactly how the tubes are distributed. Further, the case of constant concentration treated gives the maximal possible sugar export: If we assume that the plants can only generate concentrations up to some maximal value c_0, then the flow with $c(x) = c_0$ everywhere will have the largest velocity (see Materials and Methods section), and therefore the largest sugar export $\Gamma(L) = c(L)u(L)$.

We end our analysis of sugar export by briefly discussing the physical reason for the existence of the effective length (Eq. (8)) and its dependence on system parameters. First we note that the stagnant zone near the needle tip appears to be an intrinsic feature of the osmotic pumping process. While the pressure gradient is set by viscous Darcy friction $\mathrm{d}p/\,\mathrm{d}x \sim u\eta/r^2$, the maximum pressure attainable is the osmotic pressure RTc. This means that the pump can only sustain a flow speed u over a distance ℓ which obeys $RTc/\ell \sim u\eta/r^2$. The velocity itself, however, also depends on the factor RTc through Eq. (1), hence its maximum value scales as $u \sim L_p RTc\ell/r$. This sets an upper limit to the pipe length which can carry osmotic flow set by the scaling law $\ell \sim r^{3/2}/(\eta L_p)^{1/2}$, in accord with Eq. (8). It is quite surprising that the magnitude of the effective length does not depend on the available pressure differential $\Delta p = RTc$ (and hence sugar concentration c). This appears to be an intrinsic property of the osmotic flow process, where the Darcy pressure gradient is the result – and not cause – of the liquid flow.

In summary, we have shown that sugar export is influenced by a number of factors, including needle length. We have determined that a characteristic needle size exists which controls the efficiency of sugar export, and we have shown that if the needle length L exceeds L_{eff}, sugar output does not increase significantly. If these results are applicable to sugar export from conifer needles, we expect to find that L_{eff} provides an upper estimate of their length. This hypothesis is tested below.

Discussion

A relatively complete picture of the factors that influence sugar export from conifer needles and similar slender leaves has emerged. First and foremost, we have found that the osmotic flow mechanism used to export sugars imposes fundamental limitations on leaf size. For leaves longer than

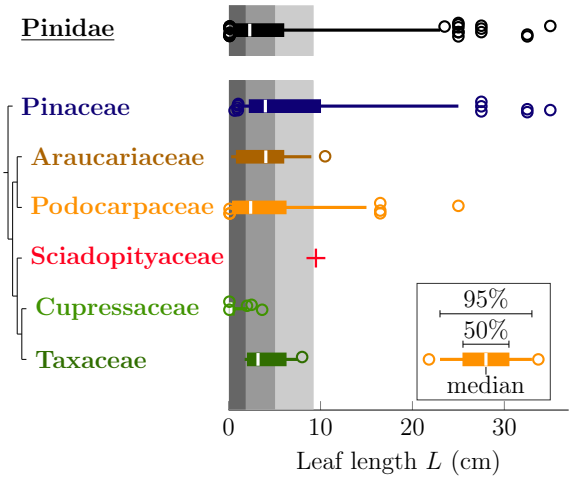

Fig. 5. Efficient leaves are found in multiple different conifer groups. Box and whisker graph of the phylogenetic distribution of leaf length L across extant conifers. Shaded gray regions indicate maximum leaf length predicted by Eq. (8) for phloem conduit radii $r = 1, 2, 3$ μm. The vertical line indicates the distribution median, while 50% of the data points are inside the box and 95% are inside the whiskers. Open circles indicate outliers. The Sciadopityaceae family, marked with a single '+', consists of only one species.

$L_{\text{eff}} = r^{3/2}/(16L_p\eta)^{1/2}$, transport efficiency is compromised by the formation of a region of stagnant fluid (Eq. (8), Fig. 4). The vascular conduits in the stagnant region cannot contribute to the export of sugars from the leaf, because the pressure required to do so would exceed the osmotic pressure. We note that the intrinsic active length scale L_{eff} is not expected to emerge from an analysis of the related standing gradient flow problem [17, 18], because that analysis assumes loading occurs in a known, relatively short, region of the channel.

The diversity of leaf sizes found in nature provides an ideal opportunity to test the generality of the results demonstrated by our analysis. When compared to the prediction that the effective leaf length L_{eff} provides an upper limit to leaf length (see Eq. (8)), our theory gives an upper bound $L_{\text{eff}} = 5.0$ cm, obtained with $r = 2$ μm, $L_p \sim 5 \times 10^{-14}$ m/s/Pa, and $\eta = 4$ mPas [8, 15]. We note that the effective length $L_{\text{eff}} \sim r^{3/2}$ is sensitive to variation in conduit radius r. The range of observed values is $r = 1$ μm to 3 μm corresponding to effective lengths between $L_{\text{eff}} = 1.8$ cm and $L_{\text{eff}} = 9.2$ cm. The predicted L_{eff} correlates with the median length of conifer needles (Fig. 5). From an evolutionary perspective, we note that conifer leaves most likely evolved once and are homologous in different conifer families (Fig. 5). Thus it might not be surprising that despite conifers covering a wide range of geographic and environmental conditions [25], their leaves remain highly constrained in length, presumably due to the small radius of phloem tubes. Such a constraint results in an effective limit on sugar export rate from a single leaf and if high productivity and competitive growth rates of trees have to be achieved, it can only be realized by an increased leaf number per stem length, as observed in conifers [26–28].

Our results could thus help rationalize the recent observation that conifers have significantly smaller leaves than angiosperms [2], and provide a biophysical explanation for this intriguing difference between the two largest groups of plants. An exception might be the genus *Pinus* that surprisingly has a

number of species with needle lengths exceeding L_{eff}, suggesting the presence of a stagnant zone. This particular inefficiency might be an adaptive trait related to the evolutionary history of the genus. Although the genus *Pinus* evolved in Cretaceous, major species radiation occurred with the evolution of grasses and grassland ecosystems in Miocene [25, 29]. Thus this radiation could be interpreted as a response to newly emerged competition. In the juvenile phase fast growing, long needles would be best suited to compete with long leaf grasses, where the tip is the most productive part of the leaf. Once off the grass layer, needle length is reduced by a significant fraction, in the case of *Pinus palustris* by 1/2 from 45 cm to 20cm. Though still representing significant deviation from L_{eff}, such reduction suggests developmentally limited but significant improvement of the needle's efficiency. We note that angiosperm leaf lengths in maize and barley (which are approximately linear in architecture) are consistent with predictions from Eq. (8), although the limited data set on phloem radius sizes does not allow us to draw definite conclusions [20, 21], this suggests that the inefficiency of *Pinus* is only limited to this genus and not related to leaf shape.

We end by emphasizing that efficient sugar export from leaves is one among many factors that allows the organisms to survive natural selection, physiological challenges and competitive exclusions. Several environmental effects (e.g. wind, snow load, drought, light level) were previously used to explain limits to leaf sizes, their morphology and the relative performance of species in particular environments [4, 30]. Trade-offs are associated with each trait, and no single globally optimum strategy exists. Hence needles longer than 5 cm can exist, although we expect them to be rare. However, the intrinsic physiological properties role of transport has not previously been considered. We also note that our simplified model of sugar transport does not include details of several potentially important factors, including photosynthesis, sugar loading [23, 31], and interactions between adjacent phloem conduits [9]. Consideration of these factors could improve prediction of size limits for particular species, nevertheless, the presented mechanistic model explaining upper bound to leaf size in conifers offers first insight into the role of phloem physiology on morphology in conifers, and to our knowledge such approach has not been found prior to this work.

Materials and Methods

Anatomical data of conifer leaves. Conifer leaf lengths for 519 species in 6 families were obtained from The Gymnosperm Database [32]. All values and source references are available in the supporting online material (Table S1). With few exceptions, a typical maximal and minimal value of leaf length is given in The Gymnosperm Database. In Fig. 1 we plotted the mean of these two values, with the error bars indicating the full range. For the box plot in Fig. 5, only the mean value was used. For 37 species only one typical value was given in the database, in which case we used this value instead of the mean.

Constant concentration gives maximal flow rate. We show in the following, that the constant concentration profile $c(x) = c_0$ does indeed lead to the highest flow velocity at the end of the conduit $u(L)$, if c_0 is the maximum concentration the plant can generate. If we start again from Eq. (1) and assume any concentration profile $c(x)$, the governing equation is

$$\begin{aligned}\frac{\mathrm{d}^2u(x)}{\mathrm{d}x^2} &= \frac{2L_p}{r}\left(RT\frac{\mathrm{d}c(x)}{\mathrm{d}x}+\frac{\mathrm{d}p}{\mathrm{d}x}\right)\\ &= \frac{2L_pRT}{r}\frac{\mathrm{d}c(x)}{\mathrm{d}x}+\frac{M}{L^2}u(x),\end{aligned} \qquad [10]$$

where we used Darcy's law and the definition of the Münch number. This equation is solved by the following expression for the velocity:

$$\begin{aligned}u(x) =&\frac{2L_p}{r}\left[\frac{L}{\sqrt{M}}\frac{\sinh\left(\sqrt{M}\frac{x}{L}\right)}{\cosh\sqrt{M}}(RTc_0-p(L))\right.\\ &+\cosh\left(\sqrt{M}\frac{x}{L}\right)\int_0^x\cosh\left(\sqrt{M}\frac{x'}{L}\right)RT\left(c(x')-c_0\right)\,\mathrm{d}x'\\ &+\sinh\left(\sqrt{M}\frac{x}{L}\right)\int_x^L\sinh\left(\sqrt{M}\frac{x'}{L}\right)RT\left(c(x')-c_0\right)\,\mathrm{d}x'\\ &\left.-\tanh\sqrt{M}\sinh\left(\sqrt{M}\frac{x}{L}\right)\int_0^L\cosh\left(\sqrt{M}\frac{x'}{L}\right)RT\left(c(x')-c_0\right)\,\mathrm{d}x'\right]\end{aligned} \qquad [11]$$

as can be verified by differentiating the solution twice and inserting into Eq. (10). Thus, the velocity at the end of the conduit is

$$\begin{aligned}u(L) =&\frac{2L_p}{r}\left[\frac{L}{\sqrt{M}}(RTc_0-p(L))\tanh\sqrt{M}\right.\\ &\left.+\frac{1}{\cosh\sqrt{M}}\int_0^L\cosh\left(\sqrt{M}\frac{x'}{L}\right)RT(c(x')-c_0)\,\mathrm{d}x'\right]\\ =&u(L)_{c=c_0}+\frac{2L_p}{r\cosh\sqrt{M}}\int_0^L\cosh\left(\sqrt{M}\frac{x'}{L}\right)RT(c(x')-c_0)\,\mathrm{d}x'\end{aligned} \qquad [12]$$

If $c(x')$ can never exceed c_0, the integral in Eq. (12) can never give a positive contribution to the output velocity. The maximally achievable velocity is therefore the one found for the constant concentration case, $u(L)_{c=c_0}$ (see Eq. (9)).

ACKNOWLEDGMENTS. H.R. was supported by the Danish Council for Independent Research | Natural Sciences (Grant No. 12-126055). K.H.J. was supported by a research grant (13166) from VILLUM FONDEN.

1. Theophrastus (1916) *Enquiry into Plants* ed. Hort AF. (Harvard University Press).
2. Díaz S et al. (2016) The global spectrum of plant form and function. *Nature* 529(7585):167–171.
3. Kunstler G et al. (2016) Plant functional traits have globally consistent effects on competition. *Nature* 529(7585):204–207.
4. Onoda Y et al. (2011) Global patterns of leaf mechanical properties. *Ecology letters* 14(3):301–312.
5. Niklas KJ (1992) *Plant biomechanics.* (University of Chicago Press).
6. Jensen KH, Zwieniecki MA (2013) Physical limits to leaf size in tall trees. *Physical Review Letters* 110(1).
7. Zwieniecki MA, Boyce CK (2014) Evolution of a unique anatomical precision in angiosperm leaf venation lifts constraints on vascular plant ecology. *Proceedings of the Royal Society of London B: Biological Sciences* 281(1779).
8. Jensen KH, Liesche J, Bohr T, Schulz A (2012) Universality of phloem transport in seed plants. *Plant, Cell and Environment* 35:1065–1076.
9. Ronellenfitsch H et al. (2015) Scaling of phloem structure and optimality of photoassimilate transport in conifer needles. *Proceedings of the Royal Society of London B: Biological Sciences* 282(1801).
10. Koch GW, Sillett SC, Jennings GM, Davis SD (2004) The limits to tree height. *Nature* 428(6985):851–854.
11. Dorado O et al. (1996) The arbol del tule (taxodium mucronatum ten.) is a single genetic individual. *Madroño* pp. 445–452.
12. Currey DR (1965) An ancient bristlecone pine stand in eastern nevada. *Ecology* pp. 564–566.
13. Burns RM, Honkala BH, et al. (1990) *Silvics of North America. Conifers.* (Washington) Vol. 1, pp. 552–562.
14. Taiz L, Zeiger E (2010) *Plant Physiology.* (Sinauer Associates, Inc., Sunderland, MA), Fifth edition edition.
15. Thompson MV, Holbrook NM (2003) Application of a single-solute non-steady-state phloem model to the study of long-distance assimilate transport. *Journal of Theoretical Biology* 220(4):419–455.
16. Pickard WF, Abraham-Shrauner B (2009) A simplest steady-state Münch-like model of phloem translocation, with source and pathway and sink. *Functional Plant Biology* 36(7):629.

17. Segel LA (1970) Standing-gradient flows driven by active solute transport. *Journal of theoretical biology* 29(2):233–250.
18. Lin C, Segel LA (1974) *Mathematics Applied to Deterministic Problems*. (SIAM).
19. Münch E (1930) *Die Stoffbewegungen in der Pflanze*. (Gustav Fischer, Jena).
20. Dannenhoffer JM, Ebert Jr. W, Evert RF (1990) Leaf Vasculature in Barley, Hordeum vulgare (Poaceae). *American Journal of Botany* 77(5):636–652.
21. Russell S, Evert RF (1985) Leaf vasculature in Zea mays L. *Planta* 164:448–458.
22. Jensen KH et al. (2012) Modeling the Hydrodynamics of Phloem Sieve Plates. *Frontiers in Plant Science* 3.
23. Liesche J, Martens HJ, Schulz A (2011) Symplasmic transport and phloem loading in gymnosperm leaves. *Protoplasma* 248(1):181–190.
24. Rademaker H, Jensen KH, Bohr T (2016) (unpublished).
25. Leslie AB et al. (2012) Hemisphere-scale differences in conifer evolutionary dynamics. *Proceedings of the National Academy of Sciences* 109(40):16217–16221.
26. Gower ST, Norman JM (1991) Rapid estimation of leaf area index in conifer and broad-leaf plantations. *Ecology* 72(5):1896–1900.
27. Poorter H et al. (2012) Biomass allocation to leaves, stems and roots: meta-analyses of interspecific variation and environmental control. *New Phytologist* 193(1):30–50.
28. Brouat C, Gibernau M, Amsellem L, McKey D (1998) Corner's rules revisited: ontogenetic and interspecific patterns in leaf–stem allometry. *New Phytologist* 139(3):459–470.
29. Stromberg C (2011) Evolution of grasses and grassland ecosystems. *Annu. Rev. Earth Planet. Sci.* 39:517–544.
30. Niklas KJ (1994) *Plant allometry: the Scaling of Plant Form and Process*. (University of Chicago Press).
31. Turgeon R (2010) The role of phloem loading reconsidered. *Plant Physiology* 152(4):1817–1823.
32. Earle CJ (2015) The Gymnosperm Database. Pinidae. (http://www.conifers.org/zz/pinales.htm). Accessed 2016.02.13.

5.4 Osmotically driven flows and maximal transport rates in systems of long, linear porous pipes

Manuscript under preparation. Target journal: Journal of Fluid Mechanics.

Osmotically driven flows and maximal transport rates in systems of long, linear porous pipes

Hanna Rademaker, Kaare Hartvig Jensen and Tomas Bohr†,

Department of Physics, Technical University of Denmark 2800 Kgs. Lyngby, Denmark

(Version: 14 September 2016)

We study the flow of water and solutes in linear cylindrical pipes with semipermeable walls (membranes), driven by concentration differences across the membranes, inspired by the sieve tubes in conifer needles. The aim is to determine the efficiency of such systems. For single pipes, we assume that the velocity at the entrance (the tip of the needle) is zero, and we determine the velocity profile throughout the pipe and the outflow at the end of the pipe, where the pressure is specified. This is done for the particular case where the concentration of the solute is constant inside the pipe, and it is shown that the system has a characteristic length scale $L_{\rm eff} \sim r_0^{3/2}(L_p\eta)^{-1/2}$, where r_0 is the pipe radius, L_p is the permeability of the wall and η is the viscosity of the fluid. Osmotic flows in pipes with lengths $L \gg L_{\rm eff}$ will contain a stagnant zone from the entrance, where the velocity is very small. The outflow comes from a region of length $L_{\rm eff}$ near the end, and the increase of velocity, if the pipe is made longer, is marginal. We show that relaxing the assumption of constant solute concentration c_0 cannot lead to larger outflows, as long as the local concentration never exceeds c_0. We determine the viscous dissipation for a single pipe and the result for the total dissipation, including bulk dissipation in the pipe and the flow through the pores of the membrane (modelled as a systems of cylindrical pipes), is $\dot{W}_{\rm tot} = -\int_0^L RTc'(x)Q(x)dx + (RTc(L) - p(L))\,Q(L) - (RTc(0) - p(0))\,Q(0)$ where $Q(x)$ is the flow rate, $p(x)$ is the pressure and L is the length of the pipe. We finally generalise these results to systems of interacting parallel, cylindrical pipes with a power law distribution of lengths (as in the sieve tubes of conifer needles). For constant concentration we give an analytical solution for the velocity profile in terms of modified Bessel functions and show that the results are surprisingly similar to the single pipe results regarding the stagnant zone and value of $L_{\rm eff}$. We evaluate the dissipation for the pipe system, but in contrast to earlier work, we find that the dissipation grows monotonically with the power law exponent. The biological context and some of the mathematical results have been described in Rademaker *et al.* (2016).

Key words: Osmotic flow. Stagnant zone. Flows in pine needles. Dissipation in porous pipe.

1. Introduction

In this paper we present analytical results for stationary flows in systems of straight pipes with porous, semipermeable walls, driven by osmotic water uptake. Such systems

† Email address for correspondence: tbohr@fysik.dtu.dk

are found in the sieve tubes of the phloem in plant leaves, which are responsible for the sugar export (see e.g., Jensen *et al.* (2016)), and our results pertain in particular to leaves with a linear vein-architecture, such as conifer needles and grass leaves. A central aim is to determine the maximal flow rates, and thus solute transport rates, such systems can carry. The biological context has been described in Rademaker *et al.* (2016), where also many of the results for single tubes have been given. For definiteness, we shall call the solute "sugar", although it could be basically anything soluble, which cannot pass the pipe walls.

We shall first discuss the flow in a single tube, closed in one end (or with the velocity specified), representing the interior of the leaf or needle, and open in the other end, representing the outlet to the petiole, where we specify pressure or resistance. Sugar is assumed to be loaded into the tube by some mechanism (see e.g., Jensen *et al.* (2016)), and we study in particular the case where this loading mechanism is able to keep the sugar concentration constant throughout the pipe, since we shall show that this is the configuration carrying the largest flow. We shall derive both flow rates and energy dissipation, including also the dissipation of the flow through the membrane wall.

We shall continue with flows in systems of coupled linear pipes, using the methods developed in Zwieniecki *et al.* (2006), and present analytical solutions for flow rates and dissipation, again in the constant concentration case.

2. The Münch-Horwitz equations for a single pipe

We consider a system as shown in Fig. 1 with an open permeable pipe or tube inside a medium. In plants the sieve tubes of the phloem are roughly of this form, and in the leaves their radii (r_0) are in the µm regime while their length (L) is centimetric. The slender (lubrication) approximation used by Aldis (1988) to describe such flows is thus extremely well-suited. He showed that in the lubrication approximation, the stationary flow field has the form

$$v_r(r,x) = f(r)v_0(x) \tag{2.1}$$

$$v_x(r,x) = g(r)V_0(x) \tag{2.2}$$

where

$$f(r) = \frac{r^3}{r_0^3} - 2\frac{r}{r_0} \tag{2.3}$$

$$g(r) = \left[1 - \frac{r^2}{r_0^2}\right]\frac{4}{r_0} \tag{2.4}$$

and where $v_0(x)$ is the radial osmotic inflow given by

$$v_0(r,x) = v_r(r_0,r) = L_p\big[RTc(r_0,x) - p(r_0,x)\big] \tag{2.5}$$

and

$$V_0(r,x) = \left[1 - \frac{r^2}{r_0^2}\right]\frac{4}{r_0}\int_0^x v_0(x')dx'. \tag{2.6}$$

In the lubrication approximation the pressure does not vary over the pipe cross-section. If the solute is also "well-stirred", we can drop the r-dependence also for the concentration and replace the boundary condition (2.6) by a mean value expressed in terms of the average fields $u(x) = \bar{v}_x(r,x) = (2/r_0)V_0(x)$, $c(x) = \bar{c}(r,x)$ and $p(x) = \bar{p}(r,x)$, averaged over the cross-section. This can be done if the radial Péclet number Pé $= v_0L/D$, where D is the molecular diffusion, is small enough (see Jensen *et al.* (2016) for more details),

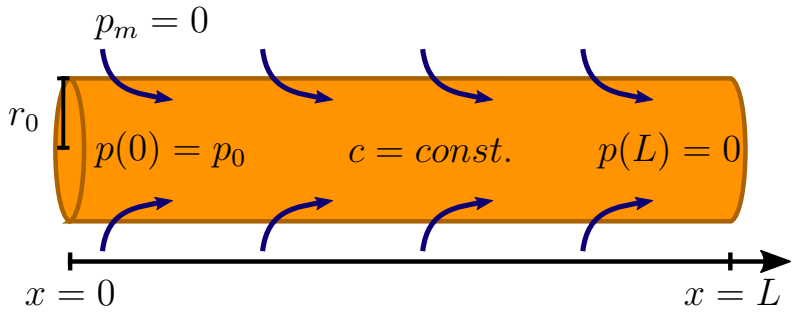

FIGURE 1. A single tube of length L and and circular cross-section of radius r_0, closed on one side, is filled with solute of constant concentration c. Water is osmotically dragged in from the surrounding medium and creates a bulk flow along the tube in positive x-direction.

and one finds for the average fields:

$$\frac{du}{dx} = \frac{2L_p}{r_0}(RTc(x) - p(x)) \tag{2.7}$$

and similarly for the flow rate $Q(x)$

$$\frac{dQ}{dx} = \pi r_0^2 \frac{du}{dx} = 2\pi r_0 L_p (RTc(x) - p(x)). \tag{2.8}$$

The pressure varies along the tube following Darcy's law:

$$\frac{dp}{dx} = -\frac{8\eta}{r_0^2} u(x). \tag{2.9}$$

These equations (called the Münch-Horwitz equations) should be supplemented by an equation for the sugar loading, the reaction-diffusion equation

$$\frac{d(uc)}{dx} = D\frac{d^2\, c}{dx^2} + \Upsilon(x), \tag{2.10}$$

defining the loading function $\Upsilon(x)$. In the following, we shall assume that this loading function is able to keep the concentration $c(x)$ constant $= c$ throughout the tube. This does not seem far from the situation in many plants and it is close to the situation obtained from "target concentration" models (Jensen *et al.* 2012). We shall later show that this situation is actually optimal, in the sense that no concentration profile, limited everywhere by the value c, can generate larger flows than the constant one where $c(x) = c$ everywhere. Thus dropping the x-dependence on c, we can differentiate (2.7) and insert (2.9) to obtain

$$\frac{d^2u}{dx^2} = -\frac{2L_p}{r_0}\frac{dp}{dx} = \frac{16\eta L_p}{r_0^3} u(x) \tag{2.11}$$

With the Münch number

$$M = \frac{16\eta L_p L^2}{r_0^3}, \tag{2.12}$$

using the characteristic velocity and pressure scales as

$$u^* = \frac{2LL_pRTc}{r_0} \tag{2.13}$$

$$p^* = RTc \tag{2.14}$$

and thus dimensionless variables

$$s = x/L \tag{2.15}$$
$$U(x) = u/u^* \tag{2.16}$$
$$P(x) = p/p^* \tag{2.17}$$

we can rewrite the equations as

$$\frac{dU}{ds} = c(s) - P(s) \tag{2.18}$$
$$\frac{dP}{ds} = -M\,U(s) \tag{2.19}$$

showing that the Münch number M is actually the only coefficient left. The square root of the Münch number will recur frequently, so we shall give it its own symbol m. If we introduce the "wall length"

$$l_0 = \eta L_p \tag{2.20}$$

which is a a material parameter describing the porosity of the pipe (actually more the ratio of the area of the pores in the porous wall to their length, see later) and typically has values around 10^{-17} m in plants, we can write m in terms of two important aspect ratios

$$\alpha = \frac{r_0}{L} \tag{2.21}$$

which is the aspect ratio of the system, typically around 10^{-3} in conifer leaf veins, and

$$\beta = \frac{l_0}{r_0} \tag{2.22}$$

with typical values around 10^{-11}. Then

$$m = \sqrt{M} = 4\frac{\sqrt{\beta}}{\alpha} \tag{2.23}$$

which is *independent* of L. When L (or m) becomes large, the velocity scale u^* defined in (2.13) becomes much larger that the typical velocities. As we shall see in the following, we would get a better value for the characteristic velocity by replacing L in (2.13) by the value

$$L_{\text{eff}} = \frac{L}{m} = \frac{r_0^{3/2}}{(16 L_p \eta)^{1/2}}, \tag{2.24}$$

2.1. *Solution with constant concentration*

We now solve (2.11) in the form

$$\frac{d^2U}{ds^2} = m^2 U(s). \tag{2.25}$$

with the general solution

$$U(s) = A\sinh(ms) + B\cosh(ms) \tag{2.26}$$

with the constants A and B to be determined. As a boundary condition, we assume that the velocity at the beginning of the tube is known

$$u(0) = U_0 \tag{2.27}$$

which determines

$$B = U_0. \tag{2.28}$$

Together (2.7) and the first derivative of (2.26) give A in terms of the pressure at the beginning of the tube $P(0) = P_0$, as:

$$A = m^{-1}\,(1 - P_0) \tag{2.29}$$

To determine P_0, we integrate (2.19):

$$P(L) = P_0 - m^2 \int_0^1 U(s)ds = P_0 + (1 - P_0)\,(1 - \cosh m) - m\,u_0 \sinh m \tag{2.30}$$

or

$$1 - P_0 = \frac{1 - P(1)}{\cosh m} - mU_0 \tanh m \tag{2.31}$$

Using this result in (2.29) we get the final expression for U:

$$U(s) = \frac{1}{m}\,(1 - P(L))\frac{\sinh(ms)}{\cosh m} + \frac{U_0}{\cosh m}\,(\cosh m \cosh(ms) - \sinh m \sinh(ms)) \tag{2.32}$$

$$= \frac{1}{m}\,(1 - P(L))\frac{\sinh(ms)}{\cosh m} + \frac{U_0}{\cosh m}\cosh(m(1 - s)) \tag{2.33}$$

The velocity reached at the end of the tube is then

$$U(1) = \frac{1}{m}\,(1 - P(L))\tanh m + \frac{U_0}{\cosh m}. \tag{2.34}$$

For the special case

$$U_0 = 0 \tag{2.35}$$

$$P(L) = 0 \tag{2.36}$$

we get the simple results

$$U(s) = \frac{1}{m}\,(1 - P(L))\frac{\sinh(ms)}{\cosh m} \tag{2.37}$$

$$U(1) = \frac{1}{m}\,(1 - P(L))\tanh m \tag{2.38}$$

$$1 - P_0 = \frac{1 - P(1)}{\cosh m} \tag{2.39}$$

Returning to dimensional variables, the solutions (for $u_0 = 0$) are

$$u(x) = \frac{2L_pL}{r_0 m}\,(RTc - p(L))\frac{\sinh\left(m\frac{x}{L}\right)}{\cosh m} \tag{2.40}$$

$$Q(x) = \frac{2\pi r_0 L_p L}{m}\,(RTc - p(L))\frac{\sinh\left(m\frac{x}{L}\right)}{\cosh m} \tag{2.41}$$

$$RTc - p_0 = \frac{RTc - p(L)}{\cosh m} \tag{2.42}$$

2.2. *The stagnant zone*

As one can see in Fig. 2, the velocity field (2.37) has a scale set by $m = \sqrt{M}$, corresponding to a length

$$L_{\text{eff}} = \frac{L}{m} = \frac{r_0^{3/2}}{(16L_p\eta)^{1/2}}, \tag{2.43}$$

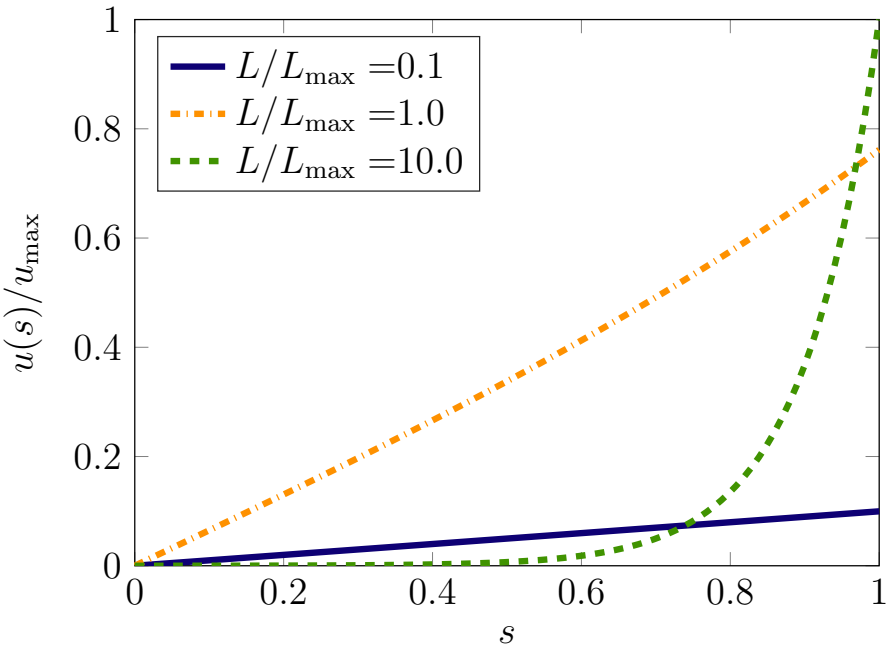

FIGURE 2. Velocity along a single pipe for different L/L_{eff} as given by Eq. 2.44, normalized by $u_{\max}$ given by (2.45).

Pipes that are substantially larger than this length will carry very little additional current, and the reason is that the velocity remains very small until a distance of approximately L_{eff} from the tip. To make this more clear we can rewrite (2.40) as

$$u(s) = u_{\max} \frac{\sinh\left(\frac{L}{L_{\text{eff}}} s\right)}{\cosh \frac{L}{L_{\text{eff}}}} \tag{2.44}$$

with

$$u_{\max} = \frac{2L_p L_{\text{eff}}}{r_0} \left(RTc - p(L)\right) \tag{2.45}$$

If we fix $u_{\max}$, u will vary along the tube as shown in Fig. 2, for different L. Note that the slope of the curves at small s (i.e., $m \cosh^{-1} m$) is a non-monotonic function of m with a maximum at $m = L/L_{\text{eff}} \approx 1.2$. Fig. 3 shows the velocity at the end of the pipe

$$u(1) = u_{\max} \tanh \frac{L}{L_{\text{eff}}} \tag{2.46}$$

which approaches $u_{\max}$ for large L/L_{eff}. In that regime, very little is gained by making the pipe longer: the sugar is only transported within the last segment of length of the order L_{eff}, and the output flux remains fixed at $u_{\max}$. Thus the entire region from the tip to a distance L_{eff} from the base will be basically stagnant.

3. Solution for non-constant concentration

For non-constant concentration $c(x)$ it is advantageous to rewrite the Münch-Horwitz equations slightly. Differentiating (2.19) and inserting into (2.18) gives

$$\frac{d^2P}{ds^2} - m^2 P = -m^2 C(s) \tag{3.1}$$

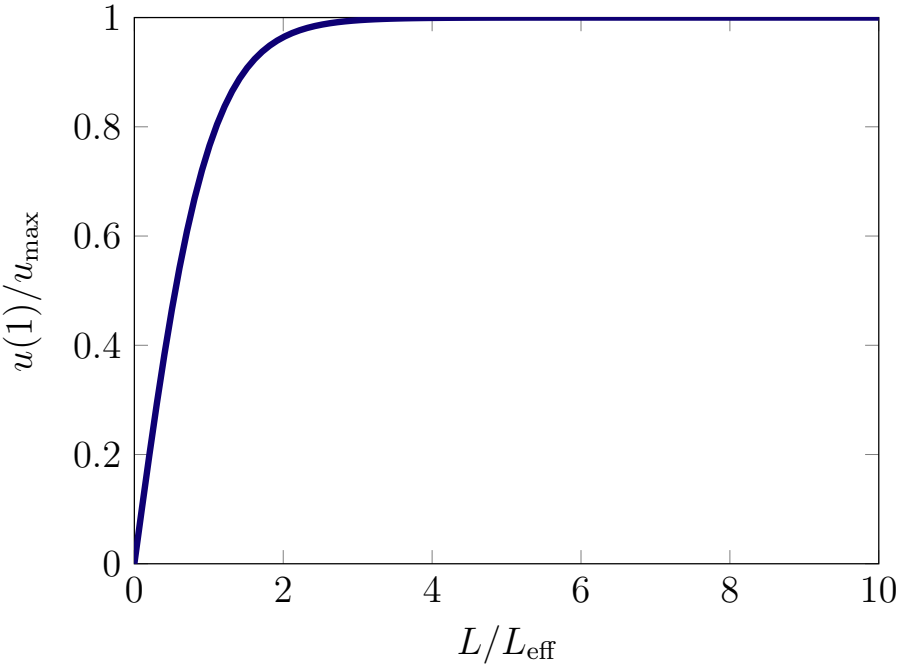

FIGURE 3. Velocity at the end of a single tube as given by Eq. 2.46, normalized by $u_{\max}$ given by (2.45).

where P and C have been scaled with the maximal concentration c_0 in the pipe: $C(s) = c(x)/c_0$ and $P(s) = p(x)/(RTc_0)$ and we want to solve the boundary value problem

$$P'(0) = -m^2 U(0) = 0 \tag{3.2}$$

$$P(1) = P_1 \tag{3.3}$$

For constant concentration $c(s) = c_0$ we get the solution

$$c_0 - P(s) = \frac{c_0 - P_1}{\cosh m} \cosh(ms) \tag{3.4}$$

and

$$U(s) = -\frac{1}{m^2} P'(s) = \frac{c_0 - P_1}{m \cosh m} \sinh(ms) \tag{3.5}$$

corresponding to Eq. (2.38) above. Using the variable $y(s) = c_0 - P(s)$, we (3.1) becomes

$$\frac{d^2 y}{ds^2} - m^2 y = m^2 (c(s) - c_0) \tag{3.6}$$

where the boundary conditions now are:

$$y'(0) = -p'(0) = m^2 u(0) = 0 \tag{3.7}$$

$$y(1) = c_0 - p_1 = y_1. \tag{3.8}$$

We divide this into a inhomogeneous differential equation with homogeneous boundary conditions

$$\frac{d^2 y}{ds^2} - m^2 y = f(s) \tag{3.9}$$

with

$$y'(0) = y(1) = 0 \tag{3.10}$$

and a homogeneous differential equation with inhomogeneous boundary conditions:

$$\frac{d^2y}{ds^2} - m^2 y = 0 \tag{3.11}$$

with

$$y'(0) = 0 \tag{3.12}$$

and

$$y(1) = y_1. \tag{3.13}$$

The latter *homogeneous* equation has the solution

$$\frac{d^2y_h}{ds^2} - m^2 y_h = 0 \tag{3.14}$$

with the *inhomogeneous* boundary conditions

$$y_h'(0) = 0 \tag{3.15}$$

and

$$y_h(1) = y_1. \tag{3.16}$$

Choosing

$$y_h(s) = A\sinh ms + B\cosh ms \tag{3.17}$$

we get $y_h'(0) = Av\cosh vs = 0$ implying that $A = 0$. Further $y_h(1) = B\cosh v = y_1$ implies that

$$B = \frac{y_1}{\cosh m} \tag{3.18}$$

so

$$y_h(s) = \frac{y_1}{\cosh m}\cosh ms. \tag{3.19}$$

3.1. *Green's function for the inhomogenous problem*

The Green's function satisfies

$$\frac{d^2G(s,\xi)}{ds^2} - m^2 G(s,\xi) = \delta(s-\xi) \tag{3.20}$$

or, denoting derivatives by subscripts,

$$G_{ss}(s,\xi) - m^2 G(s,\xi) = 0 \quad \text{for} \quad s \neq \xi \tag{3.21}$$

with

$$G_s(0,\xi) = 0 \tag{3.22}$$

$$G(1,\xi) = 0 \tag{3.23}$$

$$G(s = \xi^+, \xi) = G(s = \xi^-, \xi) \tag{3.24}$$

(continuity of G at $s = \xi$)

$$G_s(s = \xi^+, \xi) = G_s(s = \xi^-, \xi) + 1 \tag{3.25}$$

(discontinuity of G_s at $s = \xi$). The general solution of (3.21) is

$$G(s,\xi) = A_1(\xi)\sinh ms + B_1(\xi)\cosh ms \quad \text{for} \quad s < \xi \tag{3.26}$$

$$G(s,\xi) = A_2(\xi)\sinh ms + B_2(\xi)\cosh ms \quad \text{for} \quad s > \xi \tag{3.27}$$

and applying the additional conditions at the boundary and in the enterior ($s = \xi$) we get

$$G(s,\xi) = G_<(s,\xi) = \frac{\sinh m\xi \cosh ms}{m} - \frac{\cosh m\xi \cosh ms}{v} \tanh m \text{ for } s < \xi \quad (3.28)$$

$$G(s,\xi) = G_>(s,\xi) = \frac{\cosh m\xi \sinh ms}{m} - \frac{\cosh m\xi \cosh ms}{v} \tanh m \text{ for } s > \xi. \quad (3.29)$$

3.2. *The complete solution*

The complete solution can now be written in terms of the the inhomogeneity: $f(s)$ as

$$\begin{aligned} y(s) &= y_h(s) + \int_0^1 G(s,\xi) f(\xi) d\xi \\ &= y_h(s) + \int_0^s G_>(s,\xi) f(\xi) d\xi + \int_s^1 G_<(s,\xi) f(\xi) d\xi \\ &= \frac{y_1}{\cosh m} \cosh ms + \int_0^s \left(\frac{\cosh m\xi \sinh ms}{m} - \frac{\cosh m\xi \cosh ms}{m} \tanh m \right) f(\xi) d\xi \\ &\quad + \int_s^1 \left(\frac{\sinh m\xi \cosh ms}{m} - \frac{\cosh m\xi \cosh ms}{m} \tanh m \right) f(\xi) d\xi \\ &= \frac{y_1}{\cosh m} \cosh ms - \frac{\tanh m \cosh ms}{m} \int_0^1 \cosh m\xi \, f(\xi) d\xi + \frac{\sinh ms}{m} \int_0^s \cosh m\xi \, f(\xi) d\xi \\ &\quad + \frac{\cosh ms}{m} \int_s^1 \sinh m\xi \, f(\xi) d\xi \end{aligned} \quad (3.30)$$

Returning to the original variables $f(s) = m^2(c(s) - c_0)$, $P(s) = c_0 - y(s)$ and

$$U(s) = -\frac{1}{m^2} P'(s) = \frac{1}{m^2} y'(s) = \frac{1}{m^2} y'(s) \quad (3.31)$$

we find

$$\begin{aligned} U(s) &= \frac{c_0 - P_1}{m \cosh m} \sinh ms - \frac{\tanh m \sinh ms}{v^2} \int_0^1 \cosh m\xi \, f(\xi) d\xi \\ &\quad + \frac{\cosh ms}{m^2} \int_0^s \cosh v\xi \, f(\xi) d\xi + \frac{\sinh ms}{m^2} \int_s^1 \sinh m\xi \, f(\xi) d\xi \end{aligned} \quad (3.32)$$

or

$$\begin{aligned} U(s) &= \frac{c_0 - p_1}{v \cosh v} \sinh vs - \tanh v \sinh vs \int_0^1 \cosh m\xi \, (c(\xi) - c_0) \, d\xi \\ &\quad + \cosh vs \int_0^s \cosh v\xi \, (c(\xi) - c_0) \, d\xi + \sinh ms \int_s^1 \sinh m\xi \, (c(\xi) - c_0) \, d\xi. \end{aligned} \quad (3.33)$$

For the output, we get

$$\begin{aligned} U(1) &= \frac{c_0 - P_1}{m} \tanh m - \frac{\sinh^2 m}{\cosh m} \int_0^1 \cosh m\xi \, (c(\xi) - c_0) d\xi \\ &\quad + \cosh m \int_0^1 \cosh m\xi \, (c(\xi) - c_0) d\xi \\ &= \frac{c_0 - P_1}{m} \tanh m + \frac{1}{\cosh m} \int_0^1 \cosh m\xi \, (c(\xi) - c_0) d\xi \end{aligned} \quad (3.34)$$

and the sugar-output is $Q(1) = U(1)c(1)$. In other words

$$U(1) = U_0(1) + \frac{1}{\cosh m} \int_0^1 \cosh m\xi \, (c(\xi) - c_0) d\xi \tag{3.35}$$

where $U_0(1)$ is the output flow velocity (3.5) for constant concentration $c = c_0$. If $c(s)$ never exceeds c_0, the integral in (3.35) cannot be positive, and the maximal velocity achievable is therefore the one found for the constant concentration case.

4. Viscous dissipation

We shall determine the viscous dissipation in the flows studied in Sec. 2, by looking firstly at the dissipation in the bulk flow, and secondly at the flow through the porous semipermeable walls.

4.1. *Dissipation in the bulk flow*

The viscous dissipation for an axially symmetric flow, such as the Aldis flow field given by Eq. (2.1)-(2.2), can be written as

$$\dot{W} = 2\eta \int dV \left[\left(\frac{\partial v_r}{\partial r} \right)^2 + \left(\frac{v_r}{r} \right)^2 + \left(\frac{\partial v_x}{\partial x} \right)^2 + \frac{1}{2} \left(\frac{\partial v_r}{\partial x} + \frac{\partial v_x}{\partial r} \right)^2 \right]. \tag{4.1}$$

For the Aldis flow we can further write the velocity components in the separated form

$$v_r = f(r) v_0(x) \tag{4.2}$$

$$v_x = g(r) V_0(x) \tag{4.3}$$

with

$$V_0'(x) = v_0(x) \tag{4.4}$$

and the flow rate is

$$Q(x) = 2\pi r_0 V_0(x). \tag{4.5}$$

To obtain the Aldis solution, we made the assumption that $v_r \ll v_x$ and $\partial/\partial x \ll \partial r$, so the dominant term in the dissipation is

$$\dot{W}_{\text{lub}} = \eta \int dV \left(\frac{\partial v_x}{\partial r} \right)^2 = \eta \int dV \left(g'(r) \right)^2 V_0^2(x) = \frac{8\eta}{r_0^4} \int_0^L Q^2(x) dx \tag{4.6}$$

where we have used that $g'(r) = -8r/r_0^3$. Using the Darcy relation (2.9) this can be written

$$\dot{W}_{\text{lub}} = -\int_0^L p'(x) Q(x) dx \tag{4.7}$$

and for a normal Poiseuille flow in a cylindrical pipe with solid walls this becomes $Q\delta p$ as it should. The additional terms in (4.1) can be written in ascending orders of $1/r_0^2$ as

$$\begin{aligned} \Delta\dot{W}_{\text{add}} = & \frac{11}{48\pi} \int_0^L \left(Q'' \right)^2 dx \\ & + \frac{1}{3\pi} \frac{\eta}{r_0^2} \left(5 \int_0^L \left(Q' \right)^2 dx + 8 \left(Q'(L) Q(L) - Q'(0) Q(0) \right) \right). \end{aligned} \tag{4.8}$$

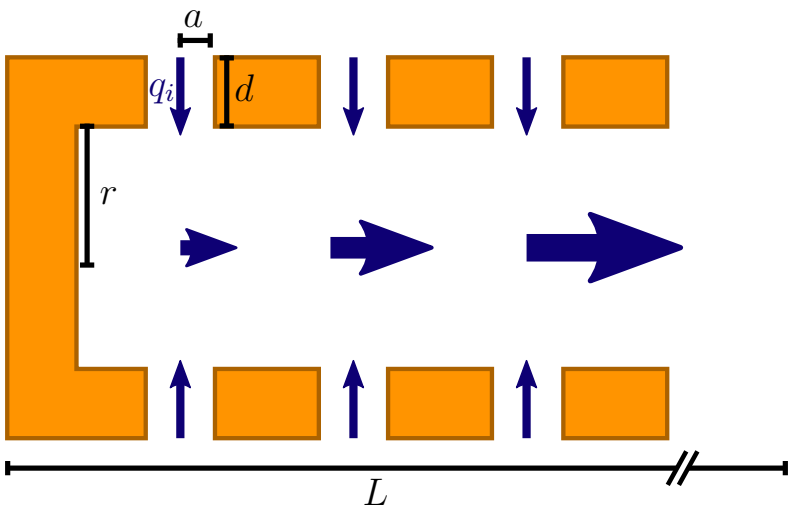

FIGURE 4. A membrane tube with pores of radius a and length d.

and in order of magnitude they correspond to replacing 2 or 4 factors of r_0 by factors of L and it would thus not be justified to keep them in the lubrication limit used to obtain Eq. (2.1)-(2.2).

4.2. *Dissipation of the flow through the pores of the wall*

We make the assumption that the surface of the tube is a semipermeable membrane with N same-sized, cylindrical pores of radius a and length d, where d is the thickness of the membrane (see Fig. 4). We expect this model to be useful, even though, in the context of plant leaves the pores (aquaporins) are of nanometric size, which implies that neither the approximation of cylindrical pores nor the validity of the Navier-Stokes equation is well-founded. The density n of pores, per length, is assumed constant, so $n = N/L$. Through each of the pores we assume a Poiseuille flow with resistance

$$R_i = \frac{\Delta\Pi_i}{q_i} = \frac{8\eta d}{a^4}. \tag{4.9}$$

The total resistance R of all pores in parallel is related to the permeability L_p:

$$\frac{1}{R} = \frac{N}{R_i} = \frac{N(L)a^4}{8\eta d} \equiv 2\pi r_0 L L_p \tag{4.10}$$

giving the relation

$$L_p = \frac{na^4}{16\pi\eta d}. \tag{4.11}$$

The dissipation inside the pore is dependent on the choice of pore radius a and covering fraction ϕ, since this determines the actual inflow velocity $v_i(x)$. With the covering fraction

$$\phi = \frac{n\pi a^2}{2\pi r_0}, \tag{4.12}$$

they are connected as

$$v_0(x)2\pi r_0 dx = v_i(x)n\pi a^2 dx \tag{4.13}$$

or

$$v_0(x) = \phi\, v_i(x). \tag{4.14}$$

The viscous dissipation through all pores in the membrane is

$$\begin{aligned}\dot{W}_{\text{mem}} &= \frac{8\eta d}{a^4} n \int_0^L q_i^2(x)dx \\ &= \frac{8\eta d}{a^4} n\pi^2 a^4 \int_0^L v_i^2(x)dx \\ &= \frac{8\eta d}{a^4} \frac{n\pi^2 a^4}{\phi^2} \int_0^L v_0^2(x)dx \\ &= \frac{2\pi r_0}{L_p} \int_0^L v_0^2(x)dx \qquad (4.15) \\ &= \frac{1}{2\pi r_0 L_p} \int_0^L \left(Q'(x)\right)^2 dx \qquad (4.16)\end{aligned}$$

We might wonder, whether it is valid to retain this term compared to the terms in Eq. (4.8), which we discarded. In particular, the last term in (4.8) part of which has precisely the same form as (4.16). The ratio of the coefficients is roughly $(\eta/r_0^2)r_0 L_p = \eta L_p/r_0 = l_0/r_0 = \beta$, which was indeed assumed to be small. Using the governing equation (2.7), we can rewrite (4.16) as

$$\dot{W}_{\text{mem}} = \int_0^L (RTc(x) - p(x))Q'(x)dx \qquad (4.17)$$

and it can thereby be combined elegantly with the resistance in the pipe (4.7). The total dissipation is

$$\begin{aligned}\dot{W}_{\text{tot}} &= \dot{W}_{\text{mem}} + \dot{W}_{\text{lub}} \\ &= \int_0^L \left(RTc(x) - p(x)\right) Q'(x)dx - \int_0^L Q(x)p'(x) \\ &= \int_0^L RTc(x)Q'(x)dx - \int_0^L \frac{d}{dx}(pQ)dx \\ &= \int_0^L RTc(x)Q'(x)dx - [pQ]_0^L \\ &= \int_0^L RTc(x)Q'(x)dx + p(0)Q(0) - p(L)Q(L) \\ &= -\int_0^L RTc'(x)Q(x)dx + \left(RTc(L) - p(L)\right) Q(L) - \left(RTc(0) - p(0)\right) Q(0) \qquad (4.18)\end{aligned}$$

In particular, if the concentration is constant, this can be written

$$\dot{W}_{\text{tot}} = \left(RTc - p(L)\right) Q(L) - \left(RTc - p(0)\right) Q(0). \qquad (4.19)$$

This shows clearly that the driving force in this case is not just the pressure (as in the normal Poiseuille flow), but the "water potential" $p - RTc$. If the velocity is zero at $x = 0$ (as in the analytical solution (2.41) in Sec. 2) we get the simple form

$$\dot{W}_{\text{tot}} = \left(RTc - p(L)\right) Q(L) = 2\pi r_0 L L_p (RTc - p(L))^2 \frac{\tanh m}{m} \qquad (4.20)$$

The individual contributions are similarly

$$\dot{W}_{\text{lub}} = \pi r_0 L L_p (RTc - p(L))^2 \left(-\frac{1}{\cosh^2 m} + \frac{\tanh m}{m}\right), \qquad (4.21)$$

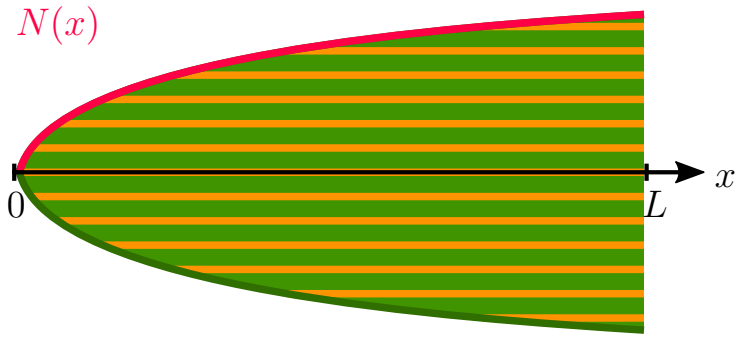

FIGURE 5. A system of parallel pipes as in a conifer needle

and

$$\dot{W}_{\text{mem}} = \pi r_0 L L_p (RTc - p(L))^2 \left(\frac{1}{\cosh^2 m} + \frac{\tanh m}{m} \right) \tag{4.22}$$

so when we add these contributions the $\cosh^{-2} m$ terms cancel.

5. Systems of Parallel Pipes with power law distribution

We now consider a system of parallel, cylindrical pipes as shown in Fig. 5, as it is found in a conifer needle (Zwieniecki *et al.* 2006; Ronellenfitsch *et al.* 2015; Rademaker *et al.* 2016). We follow a stationary flow in one direction x - say, along the central axis of a needle, from $x = 0$ at the tip to $x = L$ at the base. Let $N(x)$ be the number of (cylindrical) tubes at a given x, each of them having a radius $r(x)$. We shall assume that they *interact*, i.e., that the system has a unique velocity $u(x)$ and pressure $p(x)$ shared by the pipes, using the method developed by Zwieniecki *et al.* (2006). The flow rate in each tube is $q(x) = \pi r(x)^2 u(x)$ and the total flow rate is $Q(x) = N(x)q(x)$. In the present work, we shall assume that the pipe-radius is constant, i.e., that $r(x) = r_0$, since this seems to be the case for phloem tubes in conifer needles (Ronellenfitsch *et al.* 2015).

The equation for the osmotic water uptake (the "Münch" equation) is then

$$\frac{dQ}{dx} = \pi r_0^2 \frac{dN(x)u(x)}{dx} = 2\pi r_0 N(x) L_p (RTc(x) - p(x)) \tag{5.1}$$

and Darcy's law (or Poiseuille's law)

$$\frac{dp}{dx} = -\frac{8\pi\eta}{\pi r_0^2} u(x). \tag{5.2}$$

Assuming again that $c(x)$ is a constant, we can divide (5.1) by $N(x)$ and use (5.2) to get

$$Q''(x) - \frac{d\log(N(x))}{dx} Q'(x) = 16\eta L_p \frac{1}{r_0^3} Q(x) \tag{5.3}$$

where the pressure has been eliminated. The constancy of c implies that the loading function is given as

$$\Gamma = \frac{d}{dx}\left(Q(x)c(x)\right) = c\frac{dQ}{dx} \tag{5.4}$$

and will not in general be constant. Using again the dimensionless variable $s = x/L$ we can write this as

$$Q''(s) - \frac{d\log(N(s))}{ds} Q'(s) - MQ(s) = 0 \tag{5.5}$$

where M is the Münch number (2.12). If the number of pipes is distributed as a power law

$$N(x) = N_0 \left(\frac{x}{L}\right)^a = N_0 s^a \tag{5.6}$$

where $N_0 = N(x = L)$ we get

$$Q''(s) - as^{-1}Q'(s) - MQ(s) = 0. \tag{5.7}$$

To understand the boundary conditions for this equation, we need to go back and look at the pressure through the osmotic intake (5.1). At $x \to 0$ this gives

$$\frac{dQ}{dx} = \frac{1}{L}\frac{dQ}{ds} \to 2\pi r_0 N(s \to 0) L_p (RTc - p_0) \tag{5.8}$$

in which we need to determine p_0, which we assume is going to a constant. This can be done via the Darcy relation (5.2)

$$p_0 - p(L) = \frac{8\pi\eta}{\pi^2 r_0^4} \int_0^L \frac{Q(x)}{N(x)}\, dx \tag{5.9}$$

and if we would e.g. assume that the pipes are open to the outside or a medium with the same pressure as *outside* of the pipes at $x = 0$, we could set $p(L) = 0$ giving

$$p_0 = \frac{8\pi\eta}{\pi^2 r_0^4} \int_0^L \frac{Q(x)}{N(x)}\, dx. \tag{5.10}$$

We will, however, keep $p(L)$ as a parameter for the rest of this calculation. The substitution $z = ms$ transforms (5.7) to the universal equation

$$Q''(z) - az^{-1}Q'(z) - Q(z) = 0 \tag{5.11}$$

which has a singular point at $z = 0$. The ansatz

$$Q(z) = z^b v(z) \tag{5.12}$$

leads to the equation

$$z^{b-2}\left(z^2 v'' + (2b - a)zv' - (z^2 - b(b - 1 - a))v\right) = 0. \tag{5.13}$$

If we set $2b - a = 1$ or $a = 2b - 1$, we get $b(b - 1 - a) = -b^2$ and

$$z^2 v'' + zv' - (z^2 + b^2)v = 0 \tag{5.14}$$

which is the modified Bessel equation of order b with solutions

$$v(z) = AI_b(z) + BK_b(z) \tag{5.15}$$

where $I_b(z) \sim z^b$ and $K_b(z) \sim z^{-b}$ for small z. These two solutions correspond to two solutions for Q behaving as x^{2b} and being regular when $x \to 0$. If we assume that $p_0 \neq RTc$ or at least that p_0 does not diverge at $x = 0$ we conclude that $Q'(x)$ vanishes at $x = 0$ at least like $N(x) \sim x^a$ which means that Q cannot be regular at $x = 0$. On the other hand, the solution going like z^{2b} gives $Q'(z) \sim z^{2b-1} \sim z^a \sim N(z)$ correctly. We finally conclude that $v(z) = AI_b(z)$ or

$$Q(s) = (sm)^b v(sm) = Am^b s^b I_b(ms). \tag{5.16}$$

From this we get

$$u(s) = \frac{Q(s)}{\pi r_0^2 N(s)} = \frac{A}{\pi r_0^2 N_0} m^b s^{b-a} I_b(ms) = \frac{A}{\pi r_0^2 N_0} m^b s^{1-b} I_b(ms). \tag{5.17}$$

For small z

$$I_b(z) \approx k_b z^b \tag{5.18}$$

where

$$k_b = \frac{1}{2^b \Gamma(1+b)}. \tag{5.19}$$

To fix A we need to integrate u from (5.17) according to (5.10)

$$\begin{aligned} p_0 - p(L) &= RTc - p(L) - (RTc - p_0) \\ &= \frac{8\eta}{r_0^2}\int_0^L u(x)\,dx = \frac{8\eta L}{r_0^2}\int_0^1 u(s)\,ds = \frac{8\eta L A}{\pi r_0^4 N_0} G_b(m) \end{aligned} \tag{5.20}$$

where

$$G_b(m) = m^b \int_0^1 s^{1-b} I_b(ms)\,ds \tag{5.21}$$

Further, for small s

$$Q(s) = A m^b s^b I_b(ms) \approx A k_b m^{2b} s^{2b} \tag{5.22}$$

and

$$LQ'(x) = Q'(s) \approx 2Abk_b m^{2b} s^{2b-1} \approx 2\pi r_0 L N_0 s^a L_p (RTc - p_0) \tag{5.23}$$

and, again using $2b - 1 = a$ the s-dependence cancels and we get

$$A = \frac{\pi r_0 L N_0 L_p}{b k_b m^{2b}} (RTc - p_0). \tag{5.24}$$

Using the two equations (5.20) and (5.24), we can compute p_0 and A:

$$A = \frac{2\pi r_0 L N_0 L_p}{2bk_b m^{2b} + m^2 G_b(m)} \left(RTc - p(L)\right) \tag{5.25}$$

and for p_0 by

$$RTc - p_0 = \frac{2bk_b m^{2b}}{2bk_b m^{2b} + m^2 G_b(m)} \left(RTc - p(L)\right) = \frac{RTc - p(L)}{1 + (2bk_b)^{-1} m^{2(1-b)} G_b(m)}. \tag{5.26}$$

As $m \to 0$, $G(m) \sim m^{2b}$ and the RHS approaches 0 and $p_0 \to 0$ as it should.

To do the integral for $G_b(m)$ we use (see e.g. Gradshteyn and Ryzhik, p. 684)

$$\int_0^1 s^{1-b} I_b(as)\,ds = a^{-1} I_{b-1}(a) - \frac{a^{b-2}}{2^{b-1}\Gamma(b)} \tag{5.27}$$

so

$$G_b(m) = m^b \int_0^1 s^{1-b} I_b(ms)\,ds = m^{b-1} I_{b-1}(m) - \frac{m^{2(b-1)}}{2^{b-1}\Gamma(b)} \tag{5.28}$$

so that

$$m^2 G_b(m) = m^{b+1} I_{b-1}(m) - m^{2b} k_{b-1} \tag{5.29}$$

and we are now in a position to evaluate the flux $Q(s)$ from (5.22):

$$Q(s) = A m^b s^b I_b(ms) \tag{5.30}$$

$$= \frac{2\pi r_0 L N_0 L_p \left(RTc - p(L)\right)}{2bk_b m^{2b} + m^2 G_b(m)} m^b s^b I_b(ms). \tag{5.31}$$

The denominator can be written as

$$2bk_b m^{2b} + m^2 G_b(m) = (2bk_b - k_{b-1}) m^{2b} + m^{b+1} I_{b-1}(m) = m^{b+1} I_{b-1}(m) \tag{5.32}$$

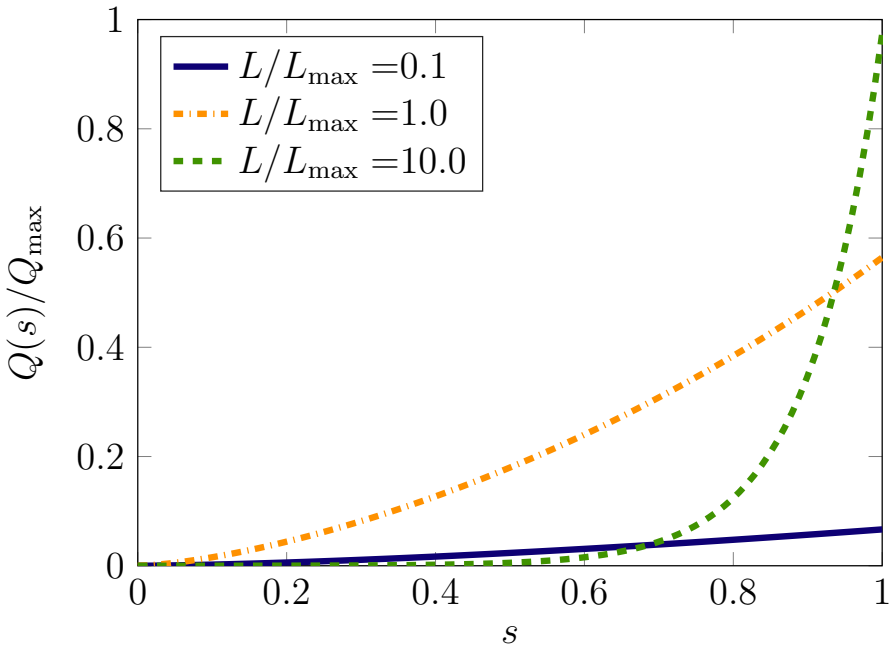

FIGURE 6. The function $Q(s)$ given by (5.34) for $b = 3/4$, scaled by $Q_{\max}$ (5.35).

where the last equality comes from the fact that

$$k_b = \frac{1}{2^b \Gamma(b+1)} = \frac{1}{2^{b-1} 2b \Gamma(b)} = \frac{k_{b-1}}{2b} \tag{5.33}$$

so $2bk_b - k_{b-1} = 0$. We can then write

$$Q(s) = 2\pi r_0 L N_0 L_p \left(RTc - p(L)\right) \frac{s^b I_b(ms)}{m I_{b-1}(m)} = Q_{\max} \frac{s^b I_b(ms)}{I_{b-1}(m)} \tag{5.34}$$

where

$$Q_{\max} = 2\pi r_0 L_{\text{eff}} N_0 L_p \left(RTc - p(L)\right) \tag{5.35}$$

and the behaviour of $Q(s)$ is shown in Fig. 6, where we have chosen $a = 1/2$ and $b = (a+1)/2 = 3/4$. Note the strong similarity with Fig. 2. In particular the output at $x = L$ is

$$Q(x = L) = Q(s = 1) = Q_{\max} \frac{I_b(m)}{I_{b-1}(m)}. \tag{5.36}$$

Similarly, we can write the expression for the pressure (5.26) as

$$\frac{RTc - p_0}{RTc - p(L)} = \frac{2bk_b}{m^{1-b} I_{b-1}(m)}. \tag{5.37}$$

For small m we find

$$Q(x = L) \to \frac{1}{2b} 2\pi r_0 L N_0 L_p RTc. \tag{5.38}$$

For large m we can use the asymptotic behaviour:

$$I_n(x) \approx \frac{e^x}{\sqrt{2\pi x}} \tag{5.39}$$

together with (5.36) to get

$$Q(x = L) = Q_{\max} \frac{I_b(m)}{I_{b-1}(m)} \to Q_{\max} \tag{5.40}$$

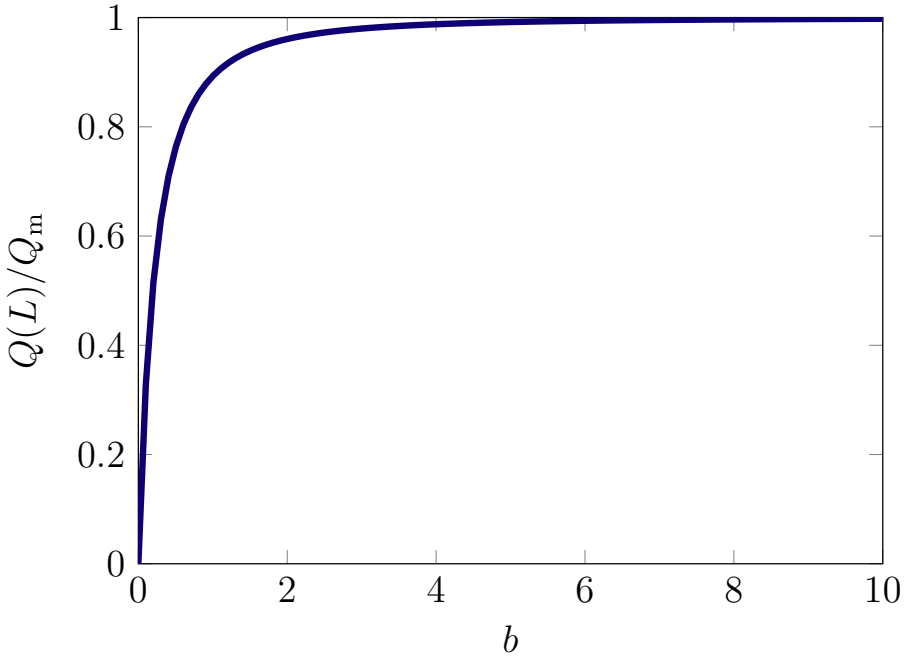

FIGURE 7. The function $Q(L, b, m)$ from (5.43) for $m = 1$, scaled by the value Q_{m}, given by (5.44).

which means that the output becomes *independent* of L in this limit (for fixed pressure $p(L)$ at the outlet). Similarity, the pressure p_0 becomes, for large m:

$$\frac{RTc - p_0}{RTc - p(L)} \to 2bk_b(2\pi)^{1/2}m^b e^{-m} \tag{5.41}$$

so p_0 approaches RTc exponentially. To compare results at different exponents a (and $b = (a + 1)/2$) we might constrain the system by demanding that the total length of tubes should be fixed. Returning to the density of starting tubes $\rho(x) = N'(x)$, we can express the total "volume" of tubes as

$$\begin{aligned}\frac{V_0}{\pi r_0^2} &= \int_0^L \rho(x)(L - x)dx = \int_0^L N'(x)(L - x)dx = LN(L) - \int_0^L N'(x)xdx \\ &= \int_0^L N(x)dx = L\int_0^1 N(s)ds = \frac{LN_0}{a + 1} = \frac{LN_0}{2b}\end{aligned} \tag{5.42}$$

Using this expression to eliminate $N_0 = 2bV_0/(\pi r_0^2 L)$ in (5.36) gives the output

$$Q(L) = \frac{4bV_0L_p\,(RTc - p(L))}{r_0}\frac{I_b(m)}{mI_{b-1}(m)} = 2Q_{\mathrm{m}}\frac{bI_b(m)}{I_{b-1}(m)} \tag{5.43}$$

where

$$Q_{\mathrm{m}} = \frac{2V_0L_{\mathrm{eff}}L_p}{r_0L}\,(RTc - p(L)) \tag{5.44}$$

and we have (again) used (2.24)

$$m = \frac{L}{L_{\mathrm{eff}}} = 4\left(\frac{\eta L_p}{r_0}\right)^{1/2}\frac{L}{r_0} \tag{5.45}$$

The dependence on b with fixed m is shown in Fig. 7. For a single pipe, we have computed the viscous dissipation above and the result is

$$\dot{W}_{\mathrm{tot}} = \left[(RTc - p)\,Q\right]_0^L = (RTc - p(L))\;Q(L) \tag{5.46}$$

since $Q(0) = 0$ and the concentration is constant. In the present model of parallel pipes the dissipation would similarly be (with $N'(x)$ pipes starting per length)

$$\dot{W}_{\text{tot}} = \int_0^L \left[(RTc - p)\, Q\right]_x^L N'(x)dx \tag{5.47}$$

$$= (RTc - p(L))\, Q(L) \int_0^L N'(x)dx - \int_0^L (RTc - p(x))Q(x)N'(x)dx \tag{5.48}$$

$$= N_0\, (RTc - p(L))\, Q(L) - \int_0^L (RTc - p(x))Q(x)N'(x)dx \tag{5.49}$$

$$= \int_0^L N(x)\frac{d}{dx}\left[(RTc - p(x))Q(x)\right] dx. \tag{5.50}$$

Using

$$Q'(x) = 2\pi r_0 L_p N(x)(RTc - p(x)) \tag{5.51}$$

we can rewrite $\dot{W}$ as

$$\begin{aligned}
\dot{W}_{\text{tot}} &= \frac{1}{2\pi r_0 L_p}\int_0^L N(x)\frac{d}{dx}\left(\frac{Q(x)Q'(x)}{N(x)}\right)dx \\
&= \frac{1}{2\pi r_0 L L_p}\int_0^1 N(s)\frac{d}{ds}\left(\frac{Q(s)Q'(s)}{N(s)}\right)ds \\
&= \frac{1}{4\pi r_0 L L_p}\int_0^1 \left(\frac{d^2}{ds^2}Q^2(s) - \frac{N'(s)}{N(s)}\frac{d}{ds}Q^2(s)\right)ds \\
&= \frac{1}{4\pi r_0 L L_p}\left(\big(Q^2(s)\big)'(1) - \big(Q^2(s)\big)'(0)\big) - \int_0^1 \frac{d\log N(s)}{ds}\frac{d}{ds}Q^2(s)ds\right) \\
&= \frac{1}{4\pi r_0 L L_p}\left(\big(Q^2(s)\big)'(1) - \big(Q^2(s)\big)'(0)\big) - a\int_0^1 \frac{1}{s}\frac{d}{ds}Q^2(s)ds\right) \\
&= \frac{1}{4\pi r_0 L L_p}\left(\big(Q^2(s)\big)'(1) - \big(Q^2(s)\big)'(0)\big) - a\int_0^1 \frac{1}{s^2}Q^2(s)ds - aQ^2(1)\right)
\end{aligned} \tag{5.52}$$

where we have used that $N'(s)/N(s) = a/s$ and that $Q(s) \sim s^b$ for small s, so $Q^2(s)s^{-1} \sim s^{2b-1} = s^a \to 0$ for $s \to 0$. Using (5.34), we have

$$Q(s) = 2\pi r_0 L N_0 L_p RTc\frac{s^b I_b(ms)}{mI_{b-1}(m)} \tag{5.53}$$

and, inserting $N_0 = 2bV_0/(\pi r_0^2 L)$

$$Q(s) = \frac{4bV_0 L_p RTc}{r_0}\frac{s^b I_b(ms)}{mI_{b-1}(m)}. \tag{5.54}$$

which should be inserted into (5.52) to get the final expression.

In (Ronellenfitsch *et al.* 2015) the dissipation is given as $\dot{W} = Q(L)\Delta p$, where Δp is the pressure drop along the pipes, i.e., $\Delta p = p_0 - p(L)$. This clearly differs from our value (4.18) for a single pipe with general concentration field and (5.46) for a single pipe with constant concentration as well as (5.47) for a system of pipes with constant concentration. In their work they assume that the loading is constant, but they show that the concentration is in fact nearly constant in the situations they study. Indeed, we would argue that when the constant loading results differ strongly from the constant concentration ones, the former are rather unphysical. Constant loading together with

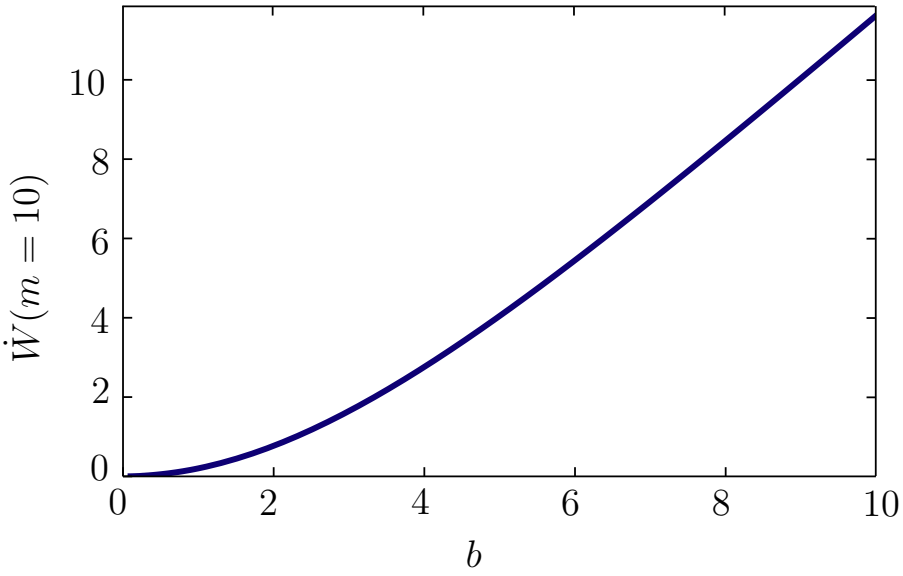

FIGURE 8. The function $\dot{W}(b)$ from (5.52) for $m = 10$.

large M would imply the building up of very large pressures, much larger than any physically possible RTc, which in our analysis sets the limiting pressure. On the basis of their value for the dissipation rate, it is shown in (Ronellenfitsch *et al.* 2015) that there is a value $a = 1/2$ of the exponent for the pipe length distribution, $N = N_0(x/L)^a$, which minimizes the dissipation - independent of m. With our dissipation function (5.52), no extremum seems to exist. As an example, Fig. 8 show the dissipation rate for $m = 10$ as function of $b = (a + 1)/2$, and it is monotonically growing with b.

REFERENCES

ALDIS, GEOFFREY K. 1988 The unstirred layer during osmotic flow into a tubule. *Bulletin of Mathematical Biology* **50**, 531–545.

JENSEN, K. H., BERG-SØRENSEN, K., BRUUS, H., HOLBROOK, N. M., LIESCHE, J., SCHULZ, A., A., ZWIENIECKI M. & BOHR, T. 2016 Sap flow and sugar transport in plants. *Reviews of Modern Physics* **XXX**, XX–YY.

JENSEN, KAARE H., BERG-SØRENSEN, KIRSTINE, FRIIS, SØREN M.M. & BOHR, TOMAS 2012 Analytic solutions and universal properties of sugar loading models in münch phloem flow. *Journal of Theoretical Biology* **304**, 286–296.

RADEMAKER, H., ZWIENIECKI, M. A., BOHR, T. & JENSEN, K. H. 2016 On the size of conifer needles. *Preprint 2016* **XXX**, XX–YY.

RONELLENFITSCH, HENRIK, LIESCHE, JOHANNES, JENSEN, KAARE H., HOLBROOK, N. MICHELE, SCHULZ, ALEXANDER & KATIFORI, ELENI 2015 Scaling of phloem structure and optimality of photoassimilate transport in conifer needles. *Proceedings of the Royal Society of London B: Biological Sciences* **282** (1801).

ZWIENIECKI, MACIEJ A., STONE, HOWARD A., LEIGH, ANDREA, BOYCE, C. KEVIN & HOLBROOK, N. MICHELE 2006 Hydraulic design of pine needles: one-dimensional optimization for single-vein leaves. *Plant, Cell and Environment* **29** (5), 803–809.

6 Additions to the papers / Work in progress

This chapter contains additional information, figures and experiments to the four papers included in Chapter 5. Some of the experiments presented in this chapter were not completed to a sufficient degree to be part of a publication, others are in an early stage of preparation to be published (Sec. 6.5.3).

6.1 Additions to the polymer trap paper

6.1.1 Further remarks on the polymer trap

In this section I review a very recent model of the polymer trap mechanism [Comtet et al., 2016], which is taking our work [Dölger et al., 2014] one step further. The scope of the model by Comtet et al. is not only the polymer trap, but also passive symplasmic loading. In their model, polymer trapping turns into passive loading simply by decreasing the rate of enzymatic oligomerization to zero.

While the models use very similar governing equations, they differ in the following details. Firstly, Comtet et al. model the enzymatic polymerization with an explicit parameter depending on the Michaelis-Menten constant of the process, while we set the polymerization rate implicitly by using a fixed concentration ratio of oligomers to sucrose in the CC-SE complex.

Secondly, Comtet et al. include the global transport to the sugar sinks (roots) with a resistor model, while we focus on local transport inside the leaf, and only in one "special" case consider influence of the export from the leaf. Bringing these two differences together, Comtet et al. call their model an *integrated* model.

Thirdly, Comtet et al. allow for a variable Peclet number Pe of the PDs and thus the flux of sucrose from mesophyll to phloem Φ_{in} depends on Pe as in Eq. (6.2). In our model, we assume a small Peclet number, resulting in a linear concentration profile of sucrose inside the PDs, and decoupled advective and diffusive components of sugar transport as in Eq. (6.5). The difference in calculating the bulk flow (Eq. (6.1) and Eq. (6.4)) is due to our assumption of complete blockage of the oligomer ($W_{\text{in}}^{\text{o}} = 0$ and $c_1^{\text{o}} = 0$), while Comtet et al. allow the back diffusion of oligomers. The relevant equations are compared below (Eqs. (6.1)-(6.5)), using the notation of Dölger et al. to simplify the comparison.

Note that Comtet et al. give the sugar transport in $\text{mol}\,\text{m}^{-2}\,\text{s}^{-1}$ and water flux in $\text{m}\,\text{s}^{-1}$, where we use $\text{mol}\,\text{s}^{-1}$ and $\text{m}^3\,\text{s}^{-1}$, and that I introduced A_{PD}, which is the area

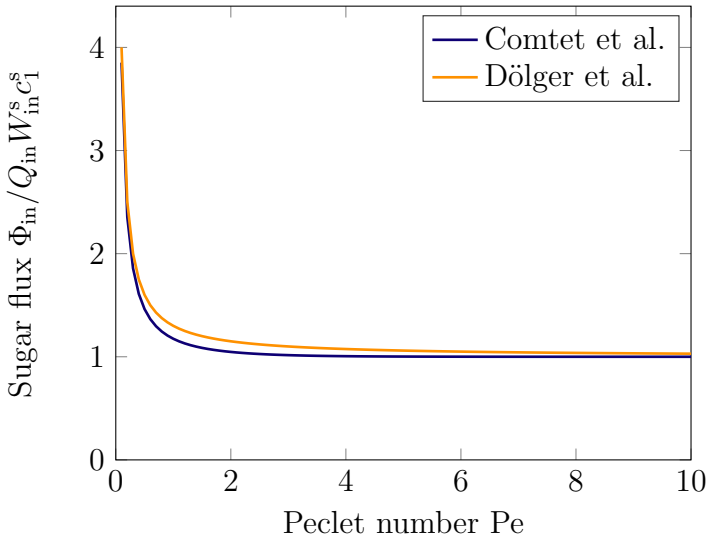

Figure 6.1: Comparison of sugar fluxes calculated as in Comtet et al. [2016] (blue, $\frac{\Phi^s_{in}}{Q_{in}W^s_{in}c^s_1} = 1 + \frac{\Delta c^s_{in}}{c^s_1}\frac{1}{e^{Pe}-1}$) and Dölger et al. [2014] (orange, $\frac{\Phi_{in}}{Q_{in}W^s_{in}c^s_1} = 1 + \frac{\Delta c^s_{in}}{c^s_1}\frac{1}{Pe}$). For the plot, $\frac{\Delta c^s_{in}}{c^s_1} = 0.3$, as it is in *Cucumis melo*.

available for transport per one PD. A_{PD} differs for the two models, due to the slightly different geometries assumed in the two papers: $A^{Comtet}_{PD} = 9\pi r^2_{pore}$ (9 cylindrical pores per PD) and $A^{Dölger}_{PD} = 4\pi r_{PD} h$ (one slit pore with half slit-width h per PD).

$$\text{Comtet et al.:} \quad Q_{in} = \frac{\xi_{in}}{A_{in}}\left(\Delta P_{in} - RT\left[(1 - W^s_{in}(\lambda_s))\Delta c^s_{in} + (1 - W^o_{in}(\lambda_o))\Delta c^o_{in}\right]\right) \tag{6.1}$$

$$\Phi^s_{in} = Q_{in}\, W^s_{in}(\lambda_s)\left[c^s_1 + \frac{\Delta c^s_{in}}{e^{Pe_s} - 1}\right] \tag{6.2}$$

$$\text{with} \quad Pe^s_{in} = \frac{Q_{in}\, W^s_{in}(\lambda_s)\, d}{H(\lambda_s)\, n_{PD}\, A_{PD}\, D^s} \tag{6.3}$$

$$\text{Dölger et al.:} \quad Q_{in} = \xi_{in}\left(\Delta P_{in} - RT\left[(1 - W^s_{in}(\lambda_s))\Delta c^s_{in} - c^o_2\right]\right) \tag{6.4}$$

$$\Phi_{in} = Q_{in}\, c^s_1\, W^s_{in}(\lambda_s) + \frac{A_{in}}{d}\, H(\lambda_s)\, n_{PD}\, A_{PD}\, D^s\, \Delta c^s_{in}. \tag{6.5}$$

Eq. (6.2) can be approximated for large and small Peclet numbers as

$$\text{for } Pe \gg 1 \Rightarrow \qquad \Phi^s_{in} = Q_{in}\, W^s_{in}(\lambda_s)\left[c^s_1 + e^{-Pe}\Delta c^s_{in}\right] \tag{6.6}$$

$$\text{for } Pe \ll 1 \Rightarrow \qquad \Phi^s_{in} = Q_{in}\, W^s_{in}(\lambda_s)\left[c^s_1 + \frac{\Delta c^s_{in}}{Pe_s}\right] \tag{6.7}$$

Note that Eq. (6.7) is equivalent to Eq. (6.5).

Fig. 6.1 displays the sugar flux Φ_{in} for both models as a function of the Peclet number. The plot shows, that the approximation of small Peclet number as used in Dölger et al. gives a good estimate both for small and large Peclet numbers, and that the deviation in the intermediate range is at most 10%. In this plot the relative

concentration difference is $\frac{\Delta c^s_{\text{in}}}{c^s_1} = 0.3$ as in Dölger et al. (using literature values for *Cucumis melo*). We estimated the Peclet number for sucrose transport through the PDs in our paper to be Pe ≈ 0.14.

Comparing the numerical factors entering Eqs. (6.2) and (6.5) which differ due to the assumptions of PD geometry, we see that this difference is negligible:

$$\text{Comtet et al.:} \quad \frac{d}{n_{\text{PD}} A_{\text{PD}}} = \frac{d}{n_{\text{PD}} 9\pi r^2_{\text{pore}}} \tag{6.8}$$

$$= \frac{1.4 \cdot 10^{-7}\,\text{m}}{5 \cdot 10^{13}\,\text{m}^{-2} \cdot 9\pi (1.1 \cdot 10^{-9}\,\text{m})^2} \tag{6.9}$$

$$\approx 8.2 \cdot 10^{-5}\,\text{m} \tag{6.10}$$

$$\text{Dölger et al.:} \quad \frac{d}{n_{\text{PD}} A_{\text{PD}}} = \frac{d}{n_{\text{PD}} 4\pi r_{\text{PD}} h} \tag{6.11}$$

$$= \frac{10^{-7}\,\text{m}}{10^{13}\,\text{m}^{-2} \cdot 4\pi \cdot 2.5 \cdot 10^{-8}\,\text{m} \cdot 6 \cdot 10^{-10}\,\text{m}} \tag{6.12}$$

$$\approx 5.3 \cdot 10^{-5}\,\text{m}. \tag{6.13}$$

In the following I will compare the conclusions that can be drawn from the two modeling approaches. We use a set of literature values of sugar concentrations and morphological features for a certain polymer trap species (*Cucumis melo*), whenever we calculate a numeric value for a flux, while Comtet et al. stay in a more general view, indicating typical ranges found in plants. They draw a couple of more general conclusions.

Both models agree, that the polymer trap mechanism is physically feasible, in the sense that by oligomerizing sucrose to raffinose and stachyose, the overall sugar concentration in the phloem can be elevated, and a sufficiently high sucrose flux into the phloem is possible.

Both models further agree, that the advective contribution to sugar loading can in general not be neglected. We show this for the example of *C. melo*, where the advective contribution is estimated to be 10 to 20 % of the total sugar loading.

Comtet et al. explore the effect of oligomerization on the sugar export and find that oligomerization always accelerates sugar export for a given sucrose concentration in the mesophyll, and also that oligomerization enables lower sucrose concentration in the mesophyll for a given export rate. This indicates an advantage for plants using the oligomerization strategy, in terms of higher sugar export rate as well as lower risk of herbivory for plants with reduced concentration of sugars in the mesophyll.

I am slightly confused about one conclusion of Comtet et al. In our work, we estimated that for typical concentrations and flow rates in *C. melo*, the convection through the PDs is not strong enough to block the back diffusion of oligomers into the bundle sheath/mesophyll, if the slit-width of the PDs is slightly larger than the oligomer diameter. We therefore conclude, that the slit-width of the PDs must actually be smaller than the oligomers, if the experimental observation of basically no oligomers in the mesophyll is true. Opposed to that, Comtet et al. state that segregation of oligomers can be achieved in a physiologically reasonable range, even for pores larger than the oligomers.

Beyond this, Comtet et al. found that even higher export rates can be achieved, if one allows the back diffusion of oligomers. We did not study this case for two reasons. Firstly, our model predicts sugar export rates well above the measured value found by Schmitz et al. [1987], even for slit-widths equal to the diameter of the raffinose molecules. Secondly, to our knowledge, the concentrations of oligomers measured in the mesophyll are very low. There is speculation about a possible degradation of oligomers in the mesophyll by alpha-galactosidase [Liesche and Schulz, 2013]. Further studies would be necessary to validate or reject this argument.

6.1.2 Measurements of cell coupling – photoactivation experiments

Introduction These experiments were an attempt to study active symplasmic phloem loading directly, namely monitoring the uptake of molecules from the mesophyll into the phloem of a polymer trap species. I would like to thank Johannes Liesche and Alexander Schulz (University of Copenhagen) for introducing me to the method of photoactivation and for support during this study.

The idea is to use a fluorescent dye (6(5)carboxyfluorescein) which is of similar size as sucrose and can be used as a tracer of phloem sap movement when introduced into the plant [Grignon et al., 1989], and to measure the transport rate of this dye over the bundle sheath-intermediary cell interface. This can be done by using the method of photoactivation (also "uncaging"), where a dye is used, which only fluoresces after prior activation with ultraviolet (UV) laser light. The dye can thus be conveniently introduced into the leaf, and then be activated in a certain region of interest (ROI), like a specific cell.

Materials and Methods We used musk melon (*Cucumis melo*) plants, grown in the green house at the University of Copenhagen. Musk melon is known to use the polymer trap loading mechanism (see Sec. 2.3.2), which entails that companion cells are referred to as intermediary cells, which have symplasmic connectivity with the bundle sheath cells via plasmodesmata.

The experiments were done on mature leaves, which were detached from the plant right before the experiment and glued upside down onto a glass slide using medical adhesive. The epidermis was peeled off from a small area (about 0.5 to 1 cm^2) on the lower side of the leaf, while covered with a drop of buffer solution (phosphate buffered saline, 10 mM, pH 7.4). A drop (50 to 70 µl) of solution of caged fluorescein (fluorescein bis-(5-carboxymethoxy-2-nitrobenzyl) ether, 20 µg/ml) in buffer solution was applied to the peeled area and incubated under a cover slip and aluminium foil for 20 min. The peeled area was then washed by replacing the drop with buffer solution three times. Finally, the drop was replaced with a water drop for imaging.

Experiments were done on a confocal laser scanning microscope (CLSM, Leica SP5-X) acquiring 3d-stacks of images using the resonant scanner for fastest imaging, a UV laser (355 nm) for uncaging and an argon laser (488 nm) for fluorescence excitation.

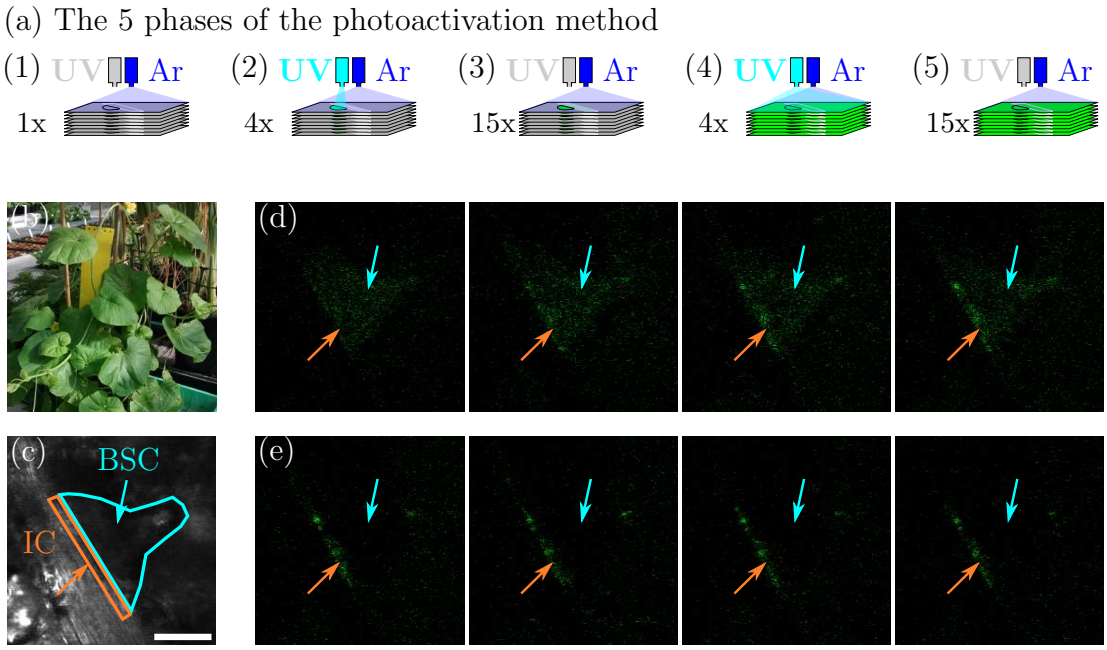

Figure 6.2: Photoactivation experiments on an active symplasmic (polymertrap) loading species.(a) The five phases of the photoactivation method: (1) prebleaching, (2) ROI uncaging, (3) post-photoactivation I, (4) field-of-view uncaging, (5) post-photoactivation II. For a detailed description see text. (b) *Cucumis melo* plant. The largest leaves are about 25 cm in diameter. (c) Bright field, grayscale microscopy image of the bundle sheath cell (BSC, turquoise) and intermediary cell (IC, red) inside the *C. melo* leaf used in this experiment. Scale bar: 20 µm. (d) Time series of phase (2) of the photoactivation experiment, where the UV laser illuminates only the BSC. Arrows pointing to the same locations in the BSC and IC as in (c) as a guide to the eye. Fluorescein from the BSC is transported into the IC already from the first frame. The images are taken at the same height of the z-stack. The time between two frames is 2 s. (e) Time series of phase (3), where the UV laser is switched off. Comparing the last frame of (d) and the first frame of (e), the uncaged fluorescein disappears in the BSC. The transport seems to happen very fast, too fast to capture it in this experiment. Fluorescein has accumulated inside the IC, probably inside the vacuoles and is slowly fainting.

Emission light was measured in the range 495 nm to 550 nm. A dip-in type objective was used with 40-fold magnification.

After selecting an appropriate location on the sample with a unobstructed view on a bundle sheath cell and the neighboring intermediary cell, the xy-region of interest (ROI) and the z-range were defined, so that the whole bundle sheath cell volume was covered, but ideally not more than that. The experiment consisted of 5 phases: (1) pre-bleaching, (2) ROI uncaging, (3) post-photoactivation I, (4) field-of-view uncaging, (5) post-photoactivation II (see Fig. 6.2).

The pre-photoactivation images were a control measurement, where the z-stack was imaged for one frame while illuminating with the argon laser, which shows the background fluorescence. In the ROI uncaging phase the UV laser and the argon laser were on, where the UV laser illuminated only the ROI. The z-stack was imaged for 4 frames. In post-photoactivation I, the UV laser was switched off, the sample was imaged for 11 frames. This phase was the actual measurement, where two frames could be compared to describe the movement of uncaged fluorescein. Then, in the field-of-view uncaging, the argon laser and the UV laser illuminated the whole field of view for another 4 frames. Finally, in the post-photoactivation II phase the UV laser was switched off again and the stack was imaged for 11 frames. The post-photoactivation II images were used for determining the volume which was accessible to the tracer for each cell.

The method of photoactivation for studying cell coupling is described in detail in [Liesche and Schulz, 2015].

Results We tried to determine the effective diffusion coefficient for the hindered diffusion from the bundle sheath cell (BSC) into the neighboring intermediary cell (IC) of the phloem, via plasmodesmata (PDs):

$$D_{\text{eff}} = \gamma H D_{\text{free}} \tag{6.14}$$

where D_{free} is the unhindered diffusion coefficient of fluorescein in cytosol, γ the pore density and H is the hindrance factor. Experimentally, D_{eff} can be determined assuming Fick's law:

$$D_{\text{eff}} = \frac{Jd}{\Delta c}. \tag{6.15}$$

While d is just the thickness of the cell wall, or in other words the length of the PDs, the concentration difference Δc and the solute flux J are both proportional to the measured intensity I of fluorescence (in arbitrary units), by some unknown factor ξ:

$$\Delta c = \xi \left(I_{\text{BSC}}(t_1) - I_{\text{IC}}(t_1) \right), \tag{6.16}$$

where t_1 is the time of the first observation, or frame, and

$$J_{\text{BSC}\,\rightarrow\,\text{IC}} = \frac{\xi \left(I_{\text{IC}}(t_2) - I_{\text{IC}}(t_1) \right)}{A_{\text{BSC/IC}}\, \Delta t} \tag{6.17}$$

where $\Delta t = t_2 - t_1$ is the time between two observations and A is the interface area, so that

$$D_{\text{eff}} = \frac{d \left(I_{\text{IC}}(t_2) - I_{\text{IC}}(t_1) \right)}{A_{\text{BSC/IC}}\, \Delta t \left(I_{\text{BSC}}(t_1) - I_{\text{IC}}(t_1) \right)}, \tag{6.18}$$

which does not depend on ξ. To evaluate the data, we assumed $d = 0.1\,\mu m$, while all other quantities are determined from the microscopy images: Δt is simply the time between two frames, that is, the time between taking two full z-stacks. In our experiments Δt is about 1.5 to 3 s for a z-range of approximately 20 to 40 µm.

Discussion There were several issues when conducting and evaluating the experiments:

Firstly, the transport of fluorescein from bundle sheath cell (BSC) into intermediary cell (IC) was often not observable. After uncaging fluorescein in a bundle sheath cell (BSC), we expected most of the dye to leave the cell towards the phloem, that is into the intermediary cell (IC). Often the dye moved towards a neighboring mesophyll cell instead or "disappeared", probably to a cell above or below, which was not monitored in the experiment.

Secondly, fluorescein had a tendency to accumulate in the IC (like in the example in Fig. 6.2). Fluorescein which accumulates in the IC, is probably taken up into the vacuole or another organelle of the cell, and does not contribute to the concentration in the cytosol. It should therefore be disregarded when calculating the concentration potential in Eq. (6.18), which is difficult to do in practice.

Thirdly, the time scale of sugar transport might have been too small to observe with this technique. There were a couple of cases, where a relatively large concentration of dye disappeared from one frame to the next, indicating a very rapid transport away from the cell were the uncaging took place. Comparing the time scale of the experiment ($\Delta t \approx 2\,s$) with the translocation speed in the phloem ($u_{\text{phloem}} \approx 100\,\mu m/s$) and the size of the image (193 µm x 193 µm), it seems likely that a lot of the fluorescein in the cytosol of the phloem cells is already flushed away after one frame. This is of course assuming that the phloem is still running, after detaching the leaf from the plant, peeling off part of the epidermis and keeping the leaf in the dark for about half an hour. It might explain the disappearance of fluorescein in some cases though.

We discontinued the experiments at this point, because they were quite time-taking and we were not sure whether we could achieve reliable and reproducible results.

6.2 Additions to the passive loading paper

Introduction 3d-printed, biomimetic devices were developed as part of the passive loading study (Sec. 5.2). This section describes the design process of the devices in greater detail than done in the paper, and discusses advantages and disadvantages of this design.

Materials and methods The design for the 3d-printed chambers was done with OpenSCAD [OpenSCAD, 2016] and exported to an STL file. Fig. 6.3 shows the design used in the experiment (a,f) and some alternative designs (d,e). The chambers were then printed on a formlabs Form1+ printer with clear resin (version 02),

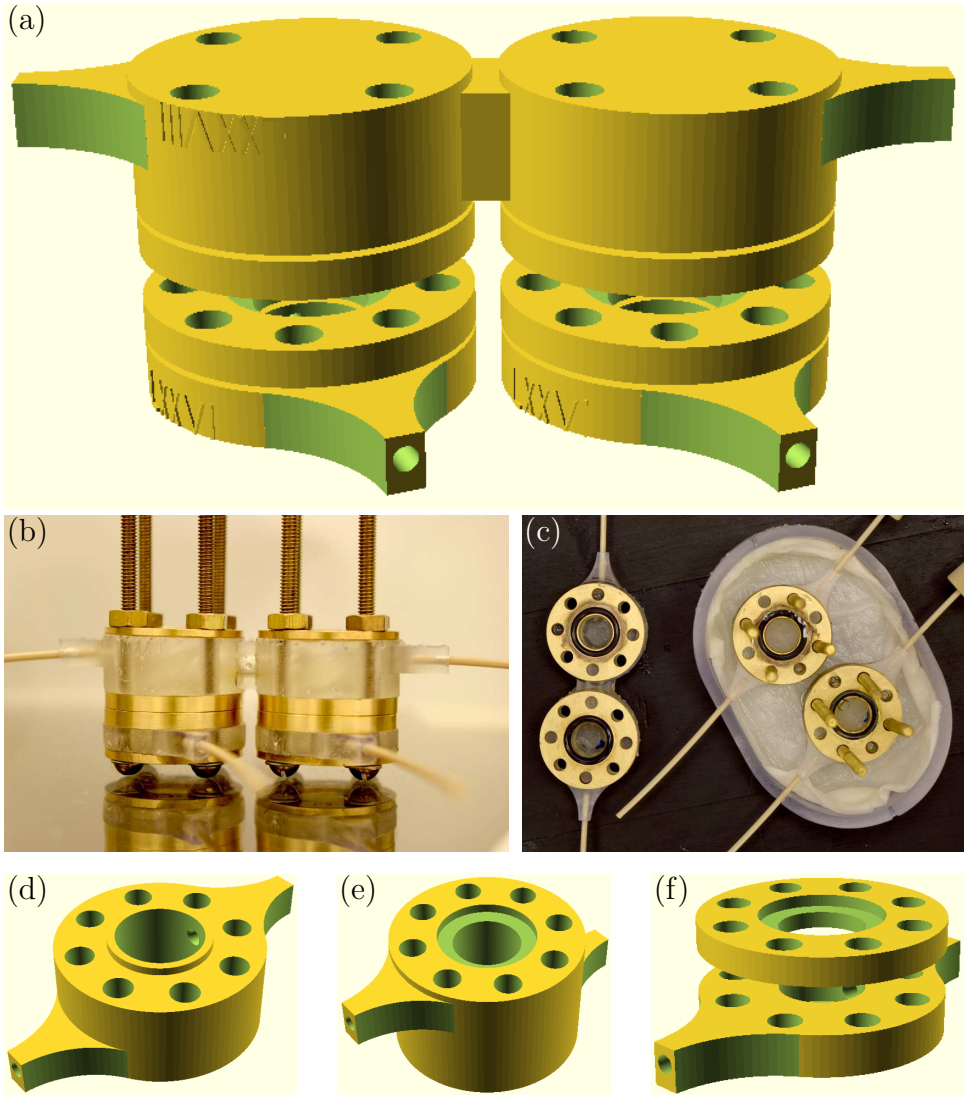

Figure 6.3: Designs of biomimetic devices. (a) Rendered image of the design used for the experiments. There is one large compartment on top and two smaller ones on the bottom. Between the compartments are two metal disks holding the o-rings. (b,c) Photographs of the device used in the experiments. The white-transparent part is 3-d printed, the metal disks were fabricated by the workshop. (d) Single compartment of an alternative design where the membrane is squeezed between two rims. (e) Single compartment of an alternative design where the o-ring cavity is part of the 3d-printed part. (f) Single compartment of the device finally used in the experiments. A single compartment is 2.6 cm in diameter, the fluid filled chamber within is 0.9 cm in diameter.

at medium resolution (0.1 mm). After printing, the chambers were washed with isopropanol two times to remove remaining liquid resin, first for 5 min while shaking the bath, then for 20 min while stirring with a magnetic stirrer bar. Inbetween the two washing steps, all inlets were flushed with isopropanol with the help of a syringe and needle tip. After washing with isopropanol, the chambers were left to dry under the fumehood for about 10 min, then rinsed with de-ionised water for about 5 min and finally the support structures were cut off and the chambers were blow-dried with pressurized air. The chambers were not used before the next day, and were stored in closed petri dishes sealed with parafilm.

Several ways to assemble the devices were used (Fig. 6.3):

1. all 3d-print device, membrane pressed between two rims,
2. all 3d-print device, membrane glued between two rims,
3. all 3d-print device, membrane between two o-rings,
4. layered 3d-print and brass device, membrane between two o-rings.

In the end, device type 4 was used (layered, o-rings) and the following description will focus on this device type. The chambers were combined to a device by glueing each chamber to a brass support layer with shear-hardening cyanoacrylate glue (CA glue, also "super glue"). Then a 5 cm long piece of PEEK tubing (outer diameter: 1/16 inches, inner diameter: 0.3 inches) was glued to each inlet of the chamber using CA glue. CA glue hardens very quickly, so the devices could be assembled right after glueing, or be stored until they were needed.

The brass support layer has a cavity for an o-ring. Right before assembling the devices, a rubber o-ring was inserted into each cavity. The screws were inserted into the lower half of the device, and the lower half was filled with water until a bulge formed on top of the o-ring. Then a piece of membrane was put onto the water drop and a little bit of the water was sucked back into the syringe. This way the membrane was held in place on the o-rings quite well and did not slip to the side, when the upper half of the device was lowered onto the other half.

The screws were tightened by hand and with the help of a wrench, basically as tight as possible. Now also the upper chamber was filled with water. These steps were carried out rather fast, as the membranes should never be allowed to dry out.

Results The devices using o-rings and brass support layers (type 4) achieved good results regarding pressure tightness (Fig. 6.4). Devices with glued membranes (type 2) were similarly pressure tight, but had of course the disadvantage that the membranes could not simply be exchanged. Devices with the membranes pressed together between two 3d-print rims (type 1) and devices with o-rings, but without the brass support layers (type 3) could never hold any significant pressure at all.

One problem with the design of the devices was that the membranes deformed plastically under pressure, changing the relative volume of the chambers and also the

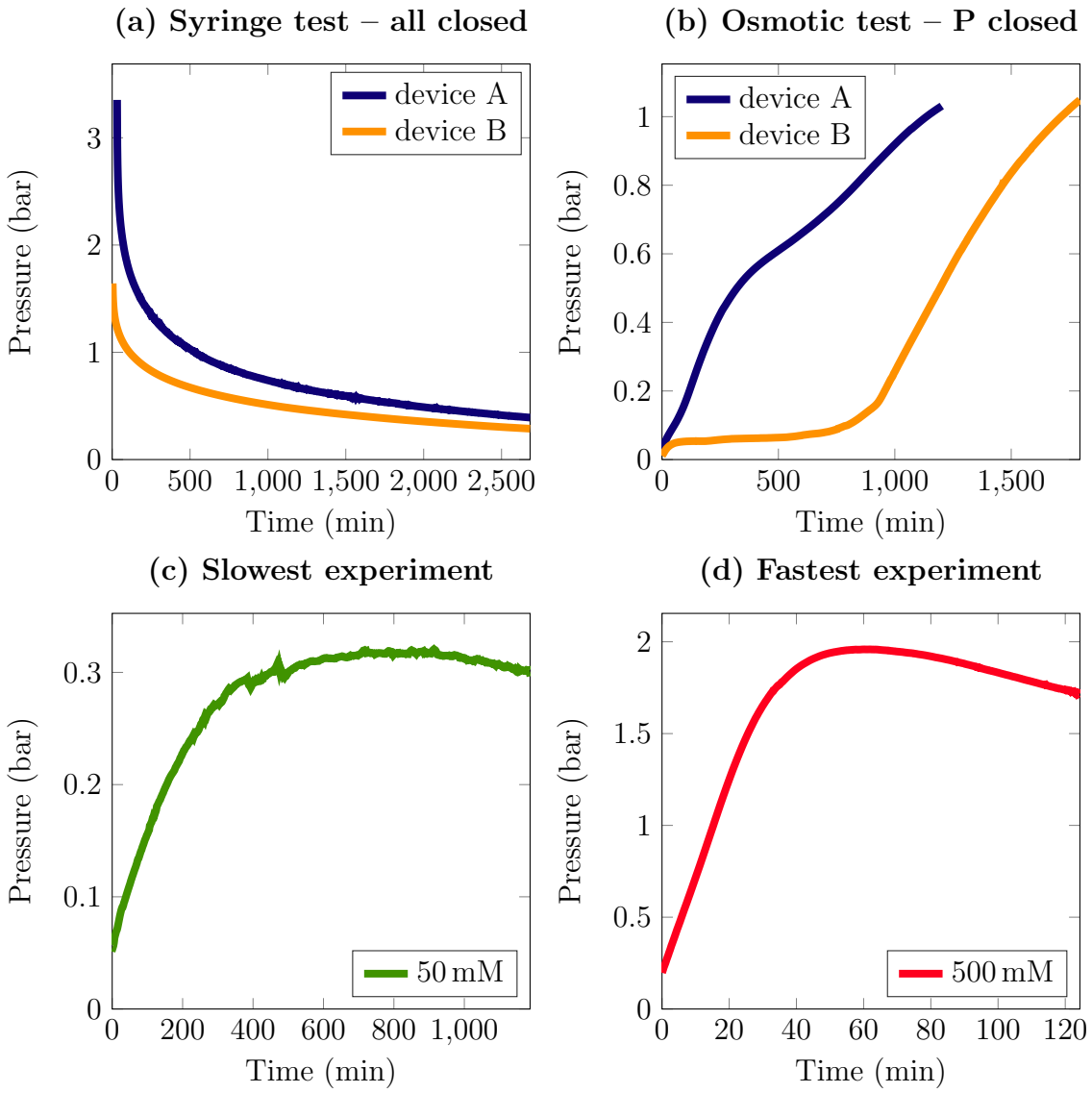

Figure 6.4: Pressure tests of biomimetic devices. (a) The water-filled devices were pressurized with a syringe. All outlets were closed and the decay of pressure was measured over time. (b) The devices were filled with water in the phloem and xylem compartment, and with sucrose solution (100 mM) in the mesophyll compartment. The phloem and mesophyll outlets were closed, while the xylem was open and connected to a water reservoir. The examples show, that the time course of pressure build-up depends on the initial conditions of the membranes. (c,d) Pressure measurements of experiments with the longest/shortest time scale (50 mM, 500 mM). The phloem is open and the xylem is connected to a water reservoir. The maximum pressure is reached after approximately 700 min/60 min.

membrane permeability (which got larger after the membrane had been subjected to high pressures). This could be improved by making the interface area between the chambers smaller, which would in turn slow down the experiment.

Discussion Developing a functional, pressure tight design of the devices took longer than anticipated. We originally also wanted to develop a diffusive device (MPX) and a full device (XMPX) (Fig. 4.2), these designs could not be finished during this Ph.d. study though.

As a next step, an controlled evaporating surface could be part of the device, simulating the evaporation through stomata in a leaf. This might be possible to implement in the form of a hydrogel surface on the outer sides of the xylem compartments.

Further experiments could include the construction of a network of sugar sources and sinks, using several connected devices. These more complicated device designs could give rise to interesting and possibly unexpected results.

6.3 Additions to the conifer needle paper

As an addition to Fig. 2(d) of the conifer needle paper, we looked at the relation of sieve element radius and leaf length in other gymnosperm and angiosperm species. The data was taken from the paper by Jensen et al. [2012b] and states the sieve element cross sections in the stem, as there is very few data available for measurements on leaves. We expect the sieve element radius in the stem to be larger than in the leaf. The line where $L = L_{\text{eff}}$ gives a good estimate of the lower limit for sieve element size in most species (Fig. 6.5).

6.4 Additions to the osmotic flows in porous pipes paper

We looked at the total sugar export $\Gamma = cu(L)$ of the linear leaf as a function of radius and length to see whether there is an optimal value for these parameters. Fig. 6.6 shows Γ as a function of conduit radius and length, as given by

$$\Gamma(r, L) = \frac{1}{2}\sqrt{\frac{r}{\eta L_p}} L_p R T c^2 \tanh\left(4\sqrt{\frac{\eta L_p}{r}}\frac{L}{r}\right) \tag{6.19}$$

assuming that the pressure at the base is $p(L) = 0$. For a given length there is an optimal radius where the sugar export is maximal (Fig. 6.6(a)), while for a fixed radius the sugar export increases monotonically with length (Fig. 6.6(b)). One can calculate the effective length $L_{\text{eff}} = r^{3/2}/\sqrt{16\eta L_p}$, at which the Münch number is 1. Increasing the length further is not efficient, since the gain in sugar export is relatively small due to the formation of the stagnant zone described in our paper. These points are marked with a red $\times$ for each curve in Fig. 6.6(b).

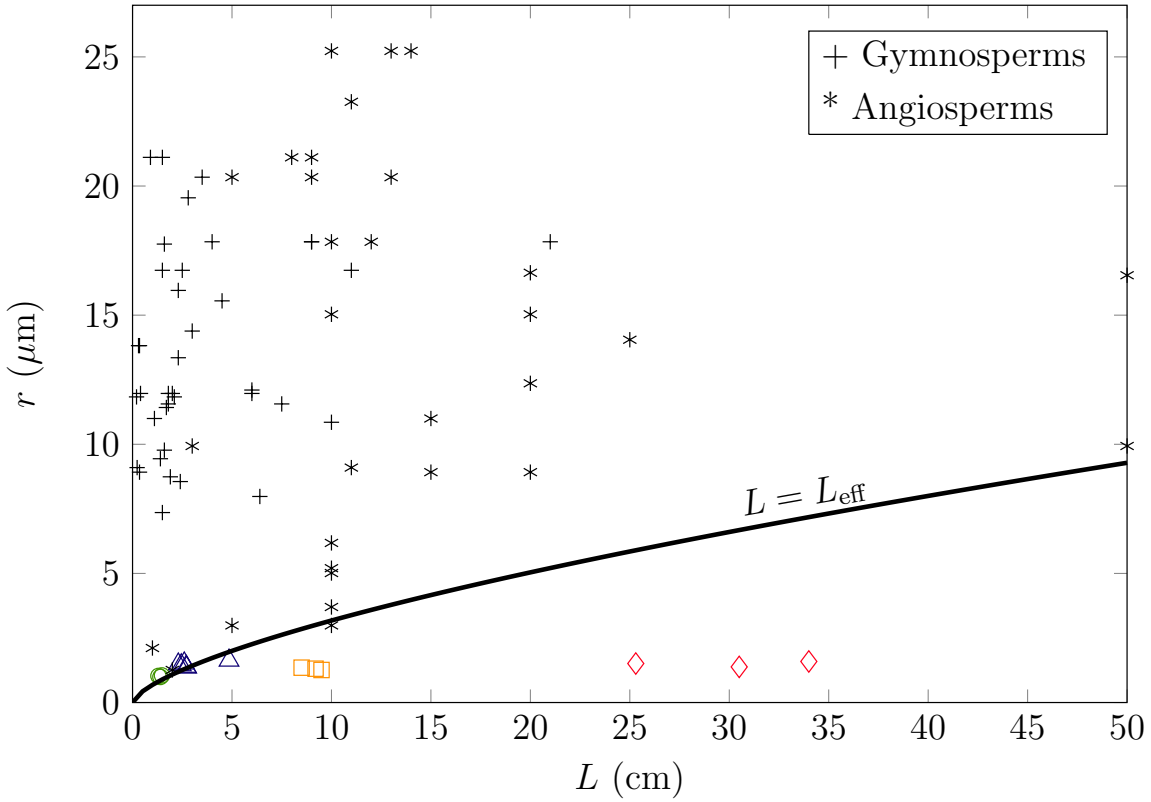

Figure 6.5: Additional data for Fig. 2(d) in paper III (Sec. 5.3). The colored symbols are the data used in the paper which represent leaves of four conifer species and the sieve element radii within. The black symbols are measurements on gymnosperms and angiosperms, where the sieve element radius is measured in the stem. We expect these sieve elements to be larger than in the leaf. The line where $L = L_{\text{eff}}$ predicts a lower limit for sieve element size in most species. Conifer needle data is taken from [Ronellenfitsch et al., 2015b], the additional data points are from [Jensen et al., 2012b]. For this plot, we calculated the conduit radius from the measured cross sectional area assuming cylindrical conduits.

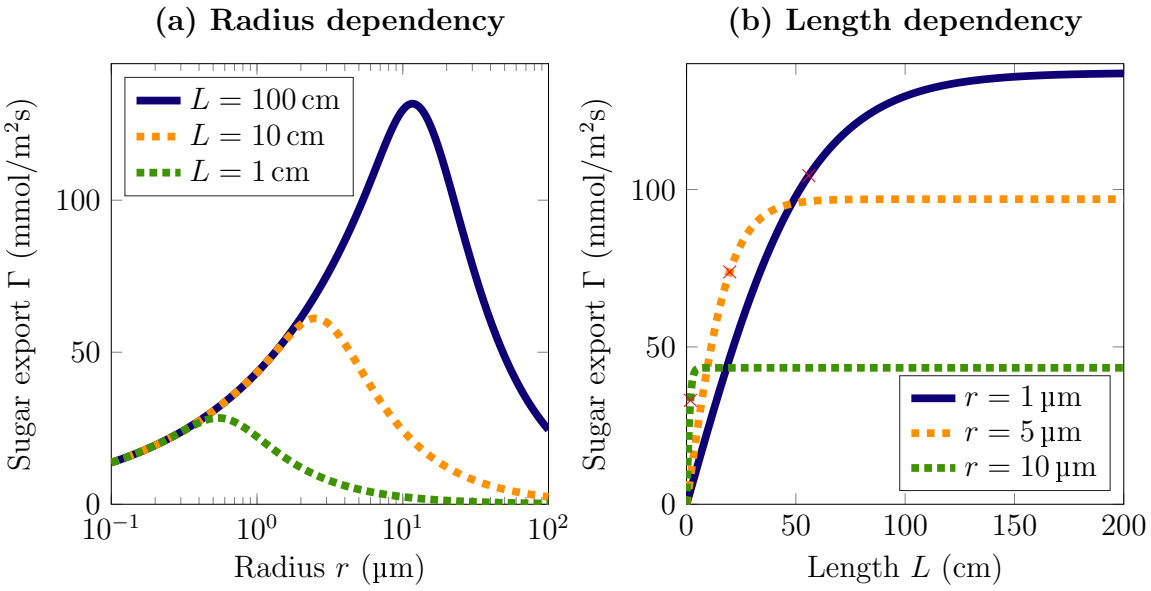

Figure 6.6: The total sugar export from a tube of radius r and length L, assuming sugar concentration $c = 100\,\mathrm{mM}$, permeability $L_p = 5 \cdot 10^{-14}\,\mathrm{m/s\,Pa}$, and viscosity $\eta = 4 \cdot 10^{-3}\,\mathrm{Pa\,s}$. (a) For a given leaf length the sugar export is maximal at an optimal radius. (b) For a given radius the sugar export grows monotonically with leaf length. Making the tube longer than the effective length $L_{\mathrm{eff}} = r^{3/2}/\sqrt{16\eta L_p}$ is inefficient though, as the gain in exported sugar is relatively small. L_{eff} is marked with a red $\times$ for each curve.

6.5 Microscopy studies of internal structure of leaf venation

In order to accurately describe fluid flows inside the leaf, we have to explore the detailed internal structure of veins. Geometry and morphology of venation features like vein diameter and vein length per leaf area have been studied extensively [Sack et al., 2012], and recently also the interest in topological traits of venation has increased [Ronellenfitsch et al., 2015a]. However, surprisingly little systematic work has been done on the internal geometry, e.g. sizes and numbers of sieve elements and xylem vessels inside a vein, especially for reticulated leaf venation. The few studies that exist concern species with parallel venation as found in grasses [Russell and Evert, 1985; Dannenhoffer et al., 1990] and conifer needles [Ronellenfitsch et al., 2015b].

6.5.1 Mapping petiole sieve elements to regions on the leaf blade

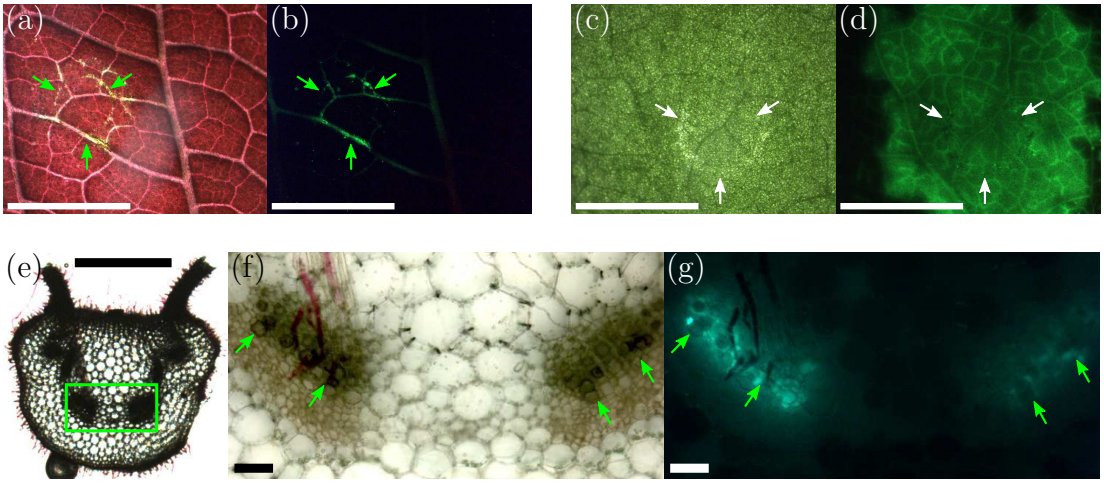

Figure 6.7: Infiltration of leaves of *Coleus blumei* (a,b,e-g) and *Nicotiana benthamiana* (c,d) with fluorescein. Comparing of the bright field images in (a) and (c) with their corresponding fluorescence images (b) and (d), one can see the uptake of fluorescein into the veins around the site of infiltration marked by the arrows. About 3 to 5 hours later fluorescein was found in the midvein close to the base of the leaf, however not in the phloem tissue (e-g). The green frame in the bright field image in (e) indicates the location of the vascular bundles in (f,g). The arrows point to the boundary between xylem (above arrows) and phloem (below arrows), showing that fluorescein was mainly found in the xylem tissue, possibly in the apoplast or xylem parenchyma cells. Scale bars: 5 mm (a-d), 1 mm (e) and 100 µm (f,g).

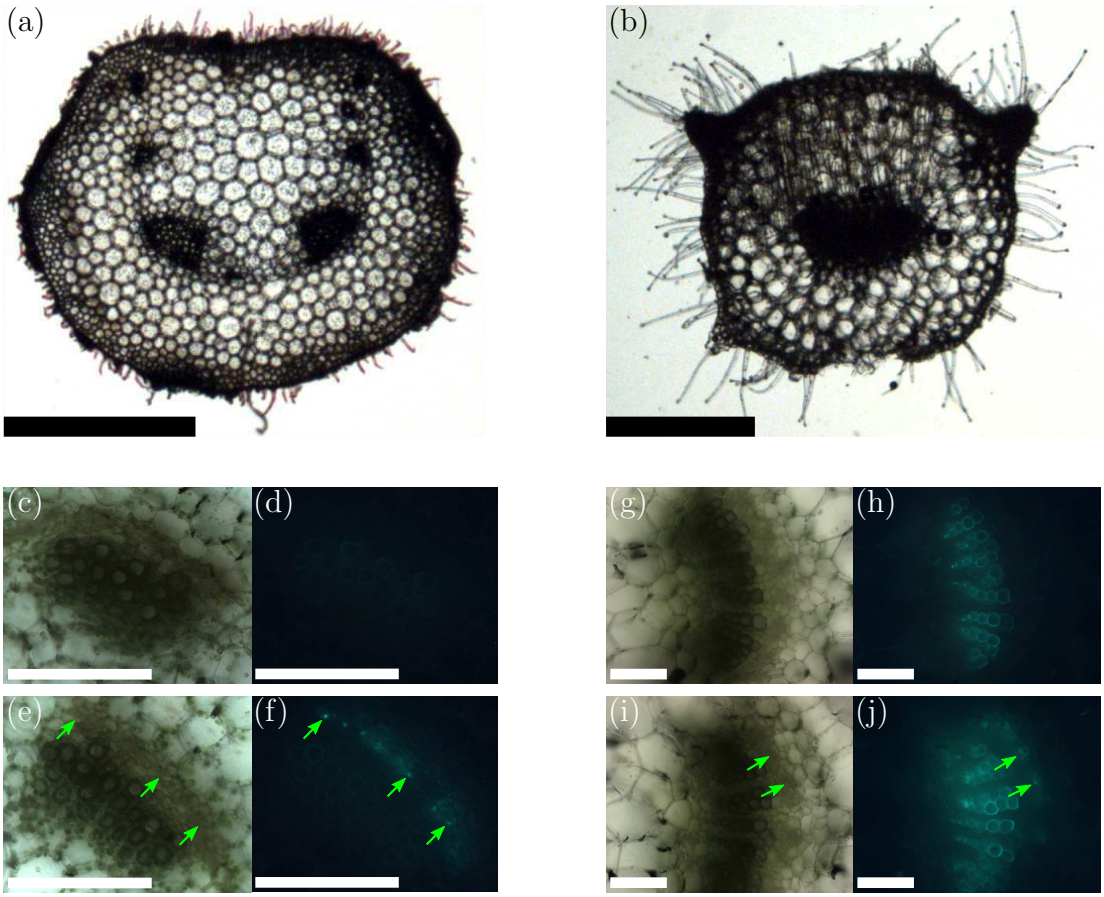

Figure 6.8: Mapping petiole sieve elements to regions on the leaf blade. (a,b): Cross sections of leaf petioles of *Coleus blumei* (a) with 7 vascular bundles and *Nicotiana benthamiana* (b) with a single vascular bundle. Control measurements for *C. blumei* and *N. benthamiana* with bright field image (c,g) and fluorescence microscopy image (d,h) show weak autofluorescence of the xylem vessels. After overnight incubation with fluorescein at a peeled spot on the leaf blade, the dye was found in the phloem of *C. blumei* (e,f) and *N. benthamiana* (i,j), indicated by the arrows. The phloem cell type (sieve element, companion cell or parenchyma) is not distinguishable in these images. Scale bars: 1 mm (a,b) and 100 µm (c-j).

Introduction In a first attempt we tried to map sieve elements inside the petiole to different regions on the leaf blade by introducing fluorescent dye at one spot on the blade and looking at sections of the petiole in the microscope the next day. The idea was to explore, if material loaded into the sieve elements at a certain location on the leaf blade (base/tip, left/right), would be transported in certain sieve elements in the petiole.

Materials and methods We used the tobacco relative *Nicotiana benthamiana* and painted nettle (*Coleus blumei*) plants. To introduce the fluorescent dye (fluorescein) into the leaf, we used either infiltration with a syringe or an epidermal peel. In the latter case, the epidermis on the lower side of the leaf was abraded/peeled off of an area of approximately $1\,cm^2$. A cotton patch soaked with fluorescein solution ($50\,\mu M$) was applied to the wounded area while the leaf was still attached to the plant. Plants were kept well-hydrated and in favourable lighting conditions, to ensure that the phloem was "running". 20 to 24 hours later the leaf was removed from the plant and the petiole was dissected for fluorescence microscopy.

Results From the images it was clear, that fluorescein had entered the veins around the wound in the epidermis (Fig. 6.7(a-d)). We also found fluorescein in major vein and petiole sections, although it was sometimes not associated with the phloem tissue (Fig. 6.7(e-g)). Furthermore, it was not possible to distinguish sieve elements and companion cells in the images. A correspondance of dye being on the same side (left/right) in blade and petiole could be observed in some samples, but the results were not reliably reproducible.

Fig. 6.8 shows one of the best results for each of the two plant species. While the control measurements in (d) and (h) only show some autofluorescence from the xylem vessels, the leaves treated with fluorescein in (f) and (j) showed also fluorescence in the phloem tissue of the petioles.

Discussion The experiments were discontinued due to insufficient reproducibility. The original plan was to take the studies to the confocal microscope once a reliable protocol for the uptake of fluorescein had been developed. Experiments on the confocal microscope are more time-taking, but would enable us to distinguish between the different cell types in the phloem. This would also allow us to count the sieve elements involved in the export of sap from a certain region of the leaf.

6.5.2 Branching of minor veins in 3 tree species

Introduction In this study we looked directly at the branching of sieve elements (SEs) in minor veins of broad leaves. We wanted to know, how the number and cross sectional area of sieve elements at a branching point changes.

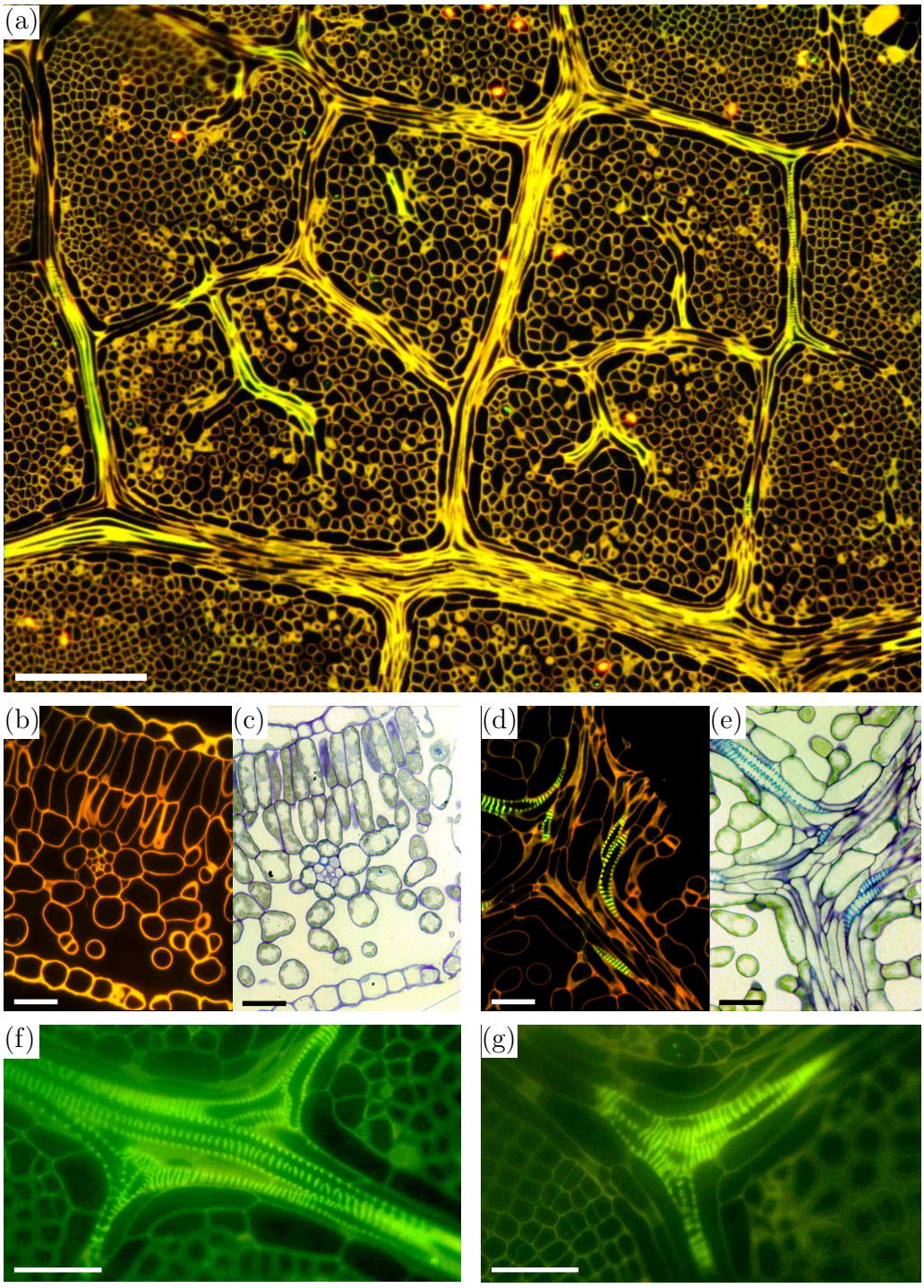

Figure 6.9: Semi-thin sections of venation in birch (a),(f) and apple (b-e),(g) leaves. The FM images (a,b,d,f,g) were stained with coriphosphine O, the bright field images (c,e) with toluidine blue. Details are given in the text. The image in (a) was submitted to the Gallery of Fluid Motion in 2015 [Rademaker et al., 2015]. Scale bars: 100 µm (a) and 25 µm (b-g).

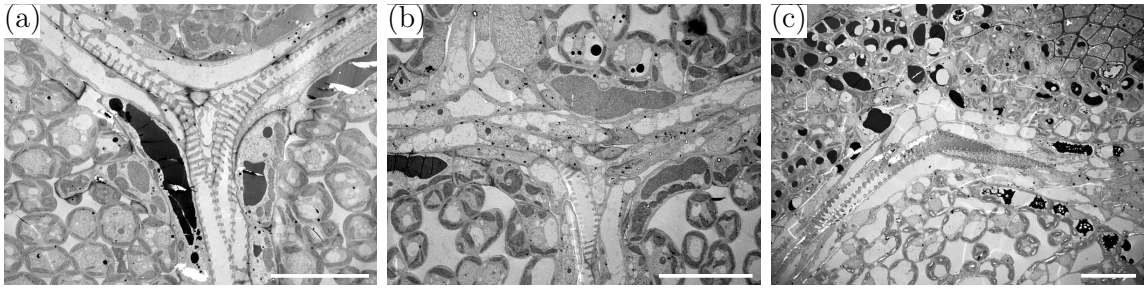

Figure 6.10: Transmission electron microscopy (TEM) images of ultra-thin, paradermal sections of leaves at branching points of minor veins. (a,b): white birch (*Betula pubescens*), (c): horse chestnut (*Aesculus hippocastanum*). For a cross section see Fig. 2.3. Xylem vessels are easily identified by their helical support structures. The leaves were rather young, which made it difficult to identify the phloem conduits. Scale bars: 20 µm.

Materials and methods For this study, we used young leaves of white birch (*Betula pubescens*), wild apple (*Malus sylvestris*) and horse chestnut (*Aesculus hippocastanum*). Pieces of leaves were cut excluding first and second order veins, fixed and embedded in Spurr's resin for paradermal and cross sections. Semi-thin sections (2 µm thick) were imaged using bright field or fluorescence microscopy (FM) (Fig. 6.9), stained with toluidine blue or coriphosphine O, respectively. Ultra-thin sections (40 nm thin) were used for transmission electron microscopy (TEM) (Fig. 6.10) with a standard contrast staining using osmium tetroxide, lead citrate and uranyl acetate. Two additional cross sections are shown in Fig. 2.3.

Results As all leaves were quite young, we did not find mature sieve elements in many of the specimens. SEs were difficult to identify, whereas xylem vessels were easily identified by their helical support structures (Fig. 6.9(a,d,e,f,g), Fig. 6.10(a-c)). Another issue was to achieve a paradermal section in plane with all three branches at a crossing (Fig. 6.9(a), Fig. 6.10(b,c)).

In cross sections, sieve elements were easier to identify (2.3(c), 6.9(b,c)). These sections can not give the desired information about branching points though.

Discussion The images obtained in this study gave a good impression of the complexity of the vascular tissue in broad leaves. Some qualitative information about phloem and xylem conduits can be extracted from the images. The intended quantitative information on numbers and cross sectional area of sieve elements was however not available obtained with this method.

6.5.3 Number and size of sieve elements along the mid-vein of a birch leaf

Introduction In order to compare the parallel venation found in needle-like leaves with broad leaves, we studied the number and size of sieve elements (SEs) along the mid-vein of a single birch (*Betula pubescens*) leaf. A similar study has been done for four conifer species [Ronellenfitsch et al., 2015b]. While they used fresh needles and fluorescein to mark the SEs, the pieces of birch leaf mid-vein in this study were fixed and embedded in resin. I prepared semi-thin sections from 10 logarithmically spaced locations along the mid-vein, and also ultrathin sections from one location close to the tip.

We are planning a joint publication (target journal: Tree Physiology) of the results of this study with results on minor veins in the same birch species obtained by Helle Juel Martens and Signe Randi Andersen (her Master student). This will allow for further conclusions (see Discussion below) on the branching behavior of SEs in birch leaves.

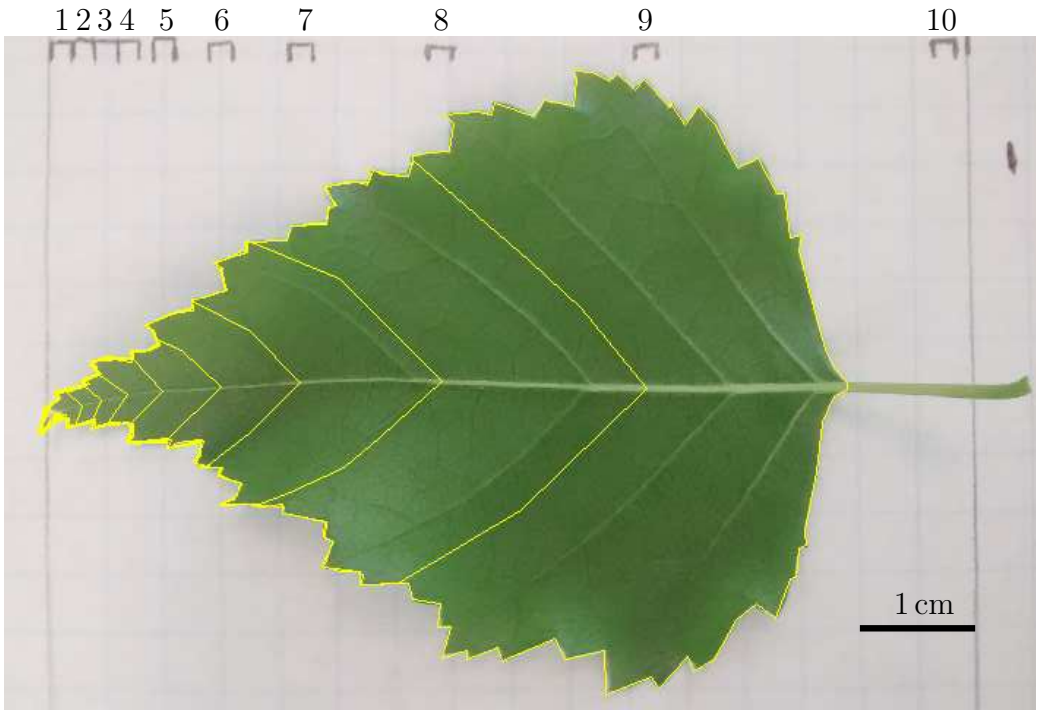

Figure 6.11: Birch (*Betula pubescens*) leaf. 10 pieces of the mid-vein were fixed, embedded in resin and sectioned. The yellow lines indicate the leaf area associated with a section point. They are chosen at an angle parallel to the second order veins. Section 10 was taken from the petiole as indicated in the image, but was treated as being at the end of the leaf blade in the evaluations shown in Fig. 6.14.

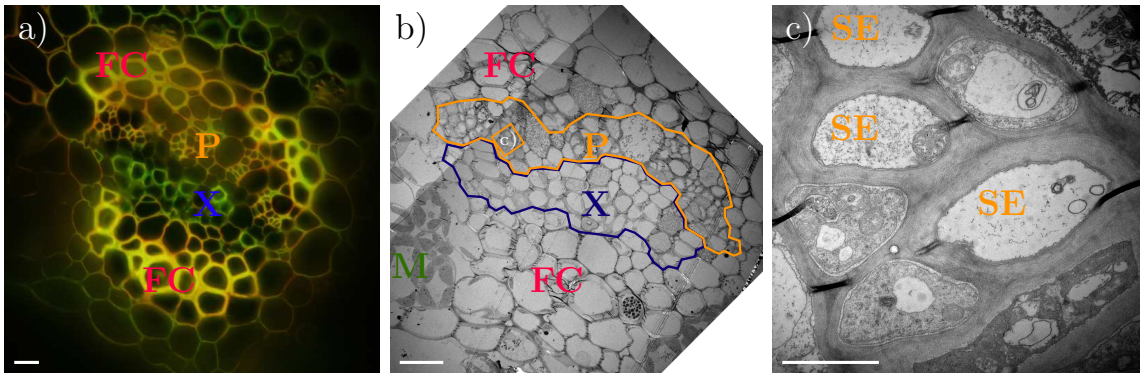

Figure 6.12: Comparison of fluorescence microscopy and transmission electron microscopy images of section 3. P: phloem, X: xylem, FC: fiber cells, M: mesophyll. a) FM image. b) TEM image with lines indicating the approximate areas of phloem (orange) and xylem (blue). c) Detailed view of sieve elements (SE) inside the orange square inside the phloem area of b). Scale bars: 10 µm (a,b) and 1 µm (c).

Material and methods The semi-thin sections were stained with the fluorescent dye Coriphosphine O for 5 minutes, rinsed with water, and imaged with a 100x oil immersion objective on a Nikon Eclipse 80i microscope. The fluorescence excitation wavelength was 450-490 nm, the emitted light was imaged with a 520 nm long-pass filter. For the larger sections, focus stacking and stitching of the images was necessary in order to show all phloem cells in focus. Phloem was easily identified by cell size and shape, as was confirmed by the ultra-thin section for TEM in one location. However, it was not always possible to unambigiously distinguish SEs and companion cells on the semi-thin sections. Thicker cell walls of the SEs was used as the primary indicator for identification of the SEs. It is further assumed, that there is one companion cell for every SE.

Results I determined the number and cross sectional area of the SEs. The evaluated images are shown in Fig. 6.13 and the results are summarized in Fig. 6.14. The number of SEs increased faster than linearly from tip to base (Fig. 6.14(a)). I found that the average SE radius r_a, calculated from the total area A_{tot} of N SEs assuming a circular cross section ($r_a = \sqrt{A_{tot}/(N\pi)}$), increases from 1.0 ± 0.1 µm close to the tip to 2.0 ± 0.2 µm in the petiole (Fig. 6.14(b)). There is a strong correlation between integrated leaf area and total SE cross sectional area (Fig. 6.14(c)). The integrated leaf area was measured from the point on the mid-vein, where the section was taken, to the tip of the leaf, choosing the boundary parallel to the second order veins, as indicated in Fig. 6.11. The underlying assumption for this choice is that photoassimilates will be taken up into a minor vein close to the site of production and then transported to higher order veins. Choosing a boundary perpendicular to the mid-vein would therefore overestimate the associated leaf area.

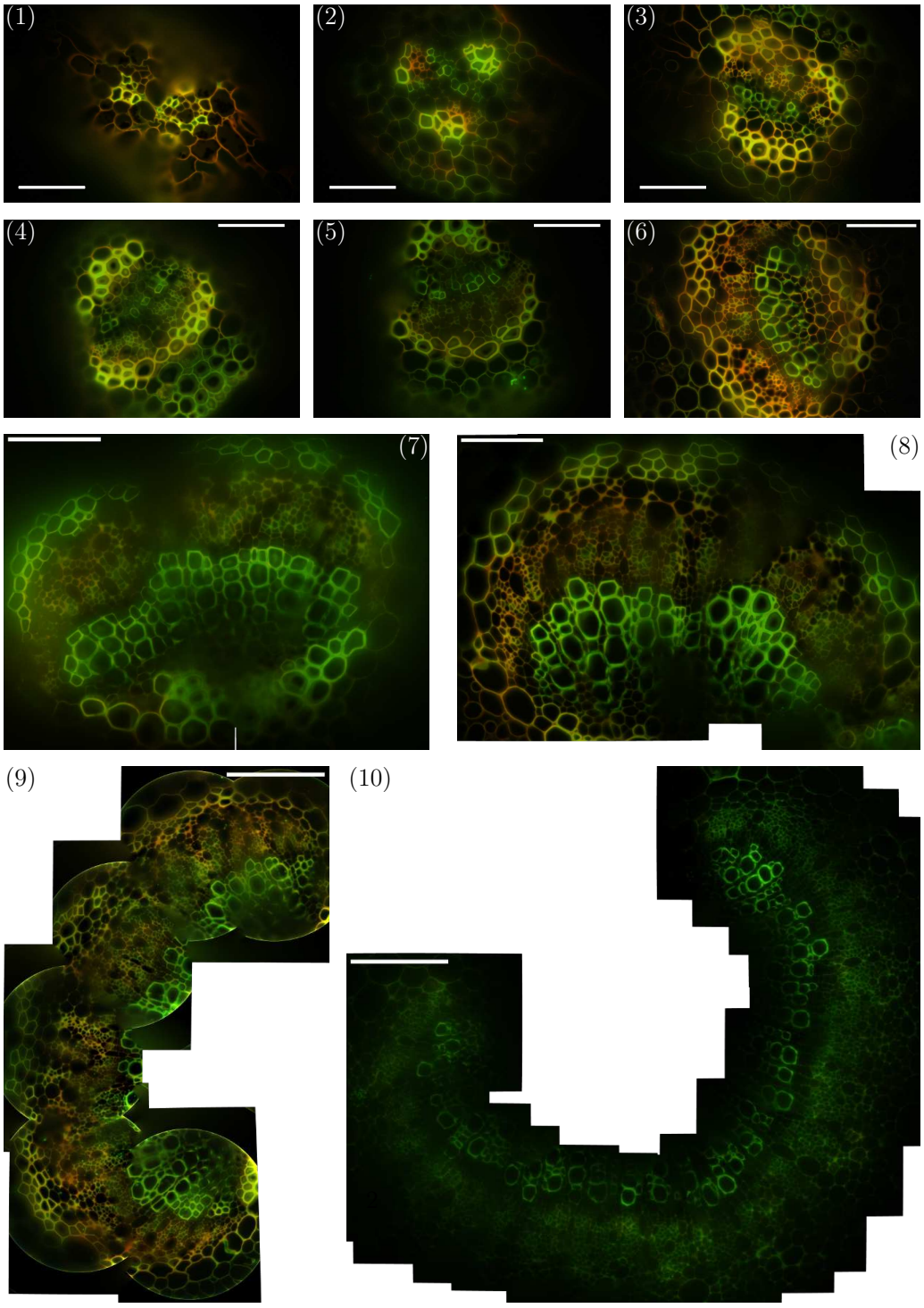

Figure 6.13: 10 cross sections of the midrib of a birch leaf. Semi-thin sections of fixed pieces of leaf mid-vein, stained with the fluorescent dye Coriphosphine O. Section 1 was omitted from further analysis, as the sieve elements could not be identified. Scale bars: 50 µm (1-8), 100 µm (9-10).

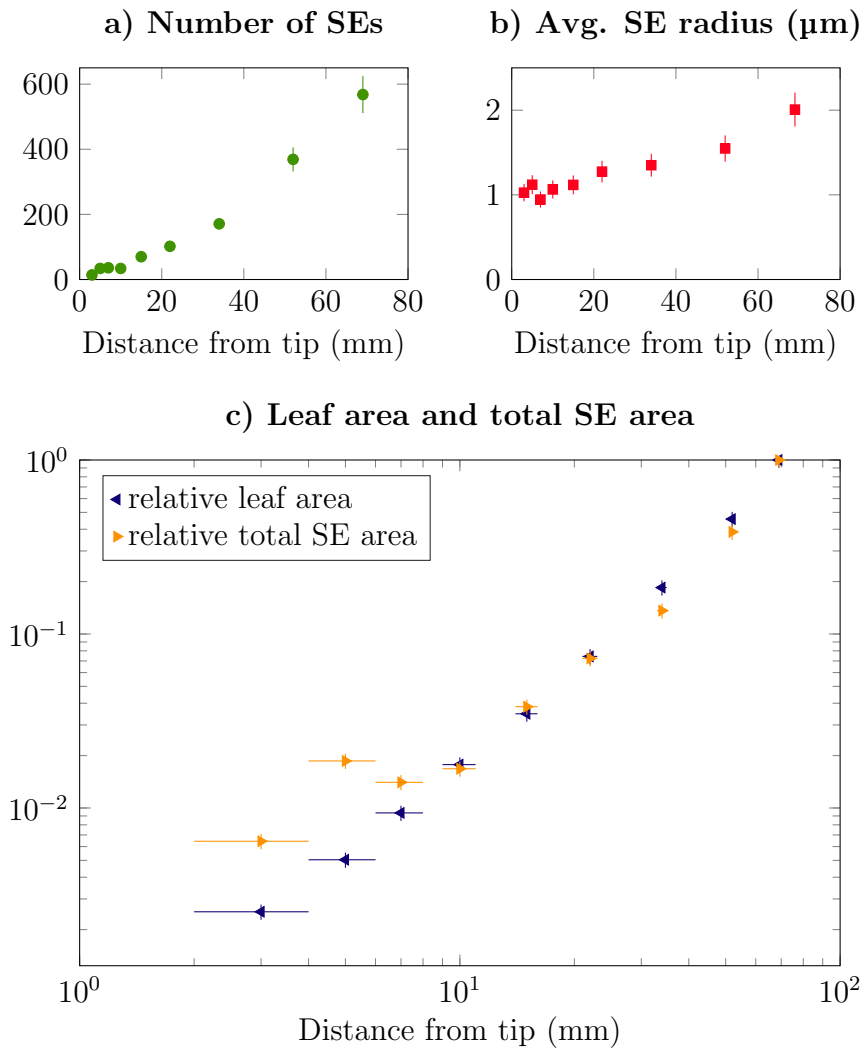

Figure 6.14: Evaluation of 9 sections along the midrib of a birch leaf. (Section 1 could not be evaluated and has been omitted from the analysis.) a) Number of sieve elements (SEs) in the mid-vein as a function of distance from the leaf tip. b) Average individual SE radius in µm, obtained by measuring the total SE area, dividing by the number of SEs and assuming a circular cross section. c) Comparison of leaf area and total SE area. The plot shows the integrated leaf area from the tip to the point of the section, evaluated at an angle parallel to the second order veins (see Fig. 6.11). Both leaf area and total SE area are devided by the maximum value, which is the total leaf area (21.1 cm^2) and the total SE area found in the petiole (section 10, 7188 μm^2), respectively. Error bars indicate 10% relative error for number and area of SEs and ± 1 mm for the distance from the tip.

Figs. 6.15 and 6.16 show the distribution of SE radii for every evaluated section (2 to 10). Fig. 6.15 shows the SE radius for every individual SE in the section, sorted ascending in size. The orange line indicates the mean of the distribution, and is also given numerically on each plot with the standard deviation. Here the mean is determined as the mean value of the individual SE radii r_1, inferred from the individual area A_1 by assuming a circular cross section ($r_1 = \sqrt{A_1/\pi}$). Fig. 6.16 shows the same data, only in the form of a histogram with bin width 0.2 µm. Again the mean and standard deviation are given and indicated by the orange line.

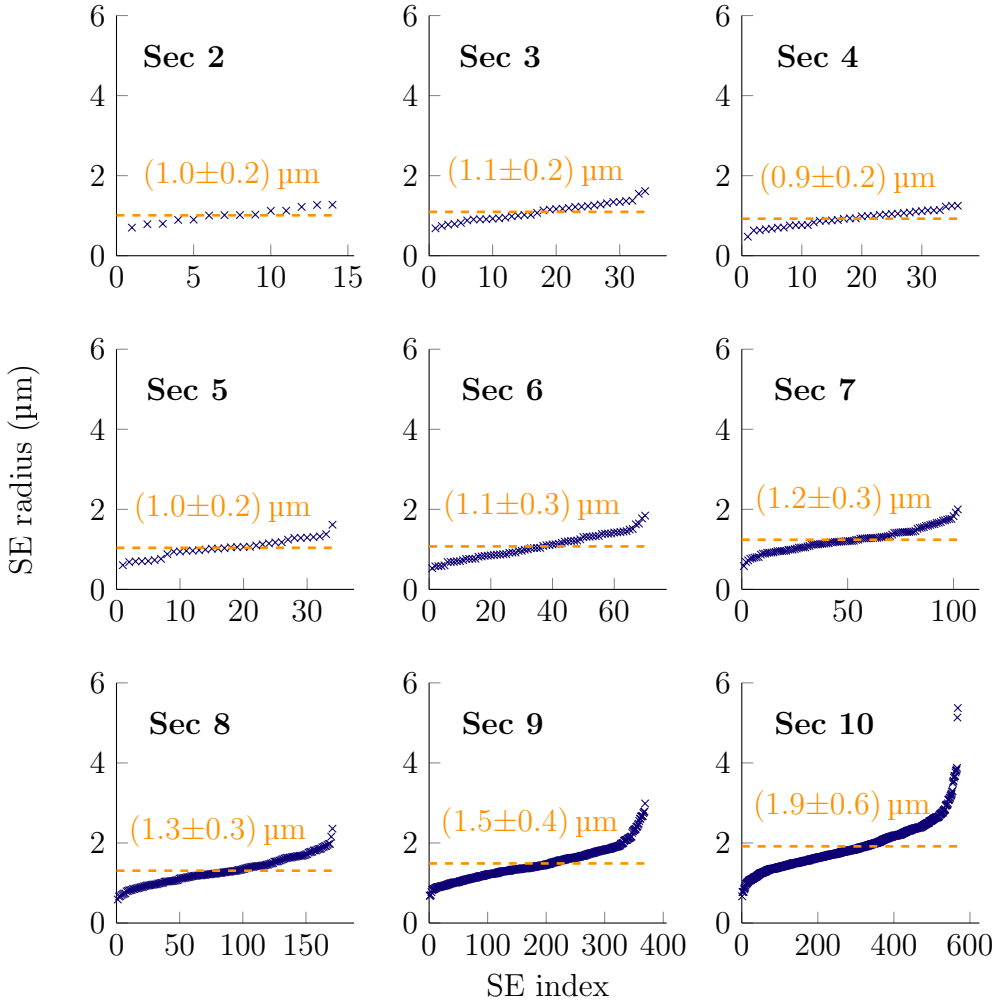

Figure 6.15: Distribution of sieve element (SE) radii for every evaluated section (2 to 10) along the midrib of a birch leaf. SE radii are sorted ascending in size. The orange line indicates the mean of the distribution, and is also given numerically on each plot together with the standard deviation.

Discussion In their study on conifer needles Ronellenfitsch et al. [2015b] found the number of SEs to increase sublinearly with distance from the tip, while in this study,

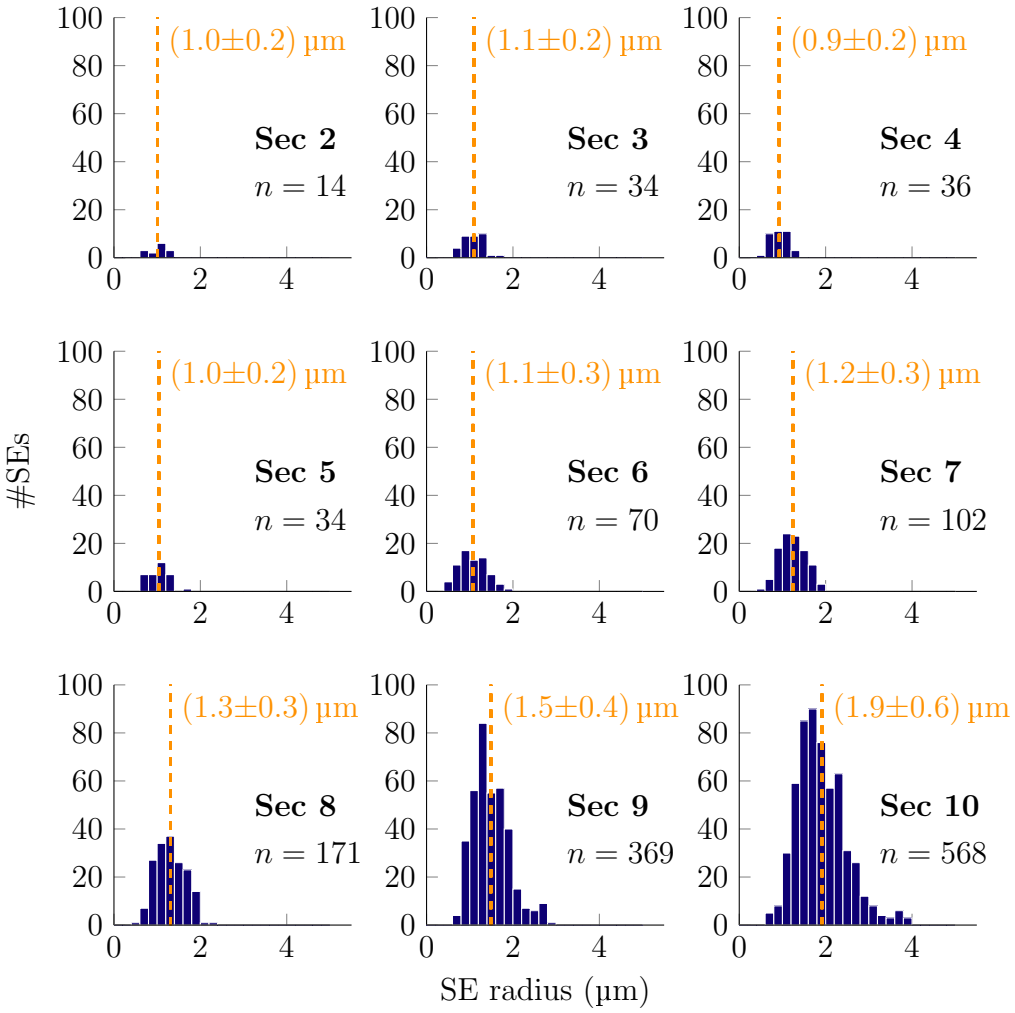

Figure 6.16: Distribution of sieve element (SE) radii for every evaluated section (2 to 10) along the midrib of a birch leaf. Bin width 0.2 µm. The orange line indicates the mean of the distribution, and is also given numerically on each plot together with the standard deviation.

the increase is superlinear. Another difference is, that the individual SE cross sectional area is constant in the needle study, while it was found to increase from tip to base in the birch leaf. It seems reasonable, that the shape of the leaf blade influences the size and/or number of sieve tubes. While the leaf area grows approximately linearly with distance from the tip in a needle, it grows like the distance squared in a triangular leaf like the birch leaf.

This study can further contribute to estimate the branching factor of sieve elements, that is the ratio of the number of SEs in the endings of the minor veins (MVs) to the number of SEs in the mid-vein. Using the data presented in Fig. 6.14 and assuming three SEs per minor vein (Helle Juel Martens, unpublished data), we would estimate the density of minor vein endings to be

$$\frac{\text{total number of SEs}}{\text{SEs per MV} \times \text{total leaf area}} = \frac{568}{3 \times 21.1\,\text{cm}^2} = 0.01 \text{ MV endings per mm}^2.$$

if there was no branching at all (branching factor equal to 1). Looking at Fig. 6.9(a), which shows a total area of $0.37\,\text{mm}^2$ and approximately 10 minor vein endings, the branching factor seems to be significantly larger than 1, on the order of 200. Since the leaf in Fig. 6.9(a) is a very young leaf and is the only image we can currently compare to, we do not have enough data on the density of minor vein endings yet in order to actually estimate the branching factor. We are currently in the process of measuring the density of MV endings in mature, cleared birch leaves.

We will further compare the total conductive area in the SEs of the minor veins with the SEs in the petiole. Fig. 6.17 and 6.18 show the distribution of individual SE radii in the petiole (data from section 10 above) and in the minor veins (data from Helle Juel Martens on a sample of 11 minor veins, each containing 3 SEs). The total number of SEs in all minor veins will be estimated once we know the density of minor vein endings.

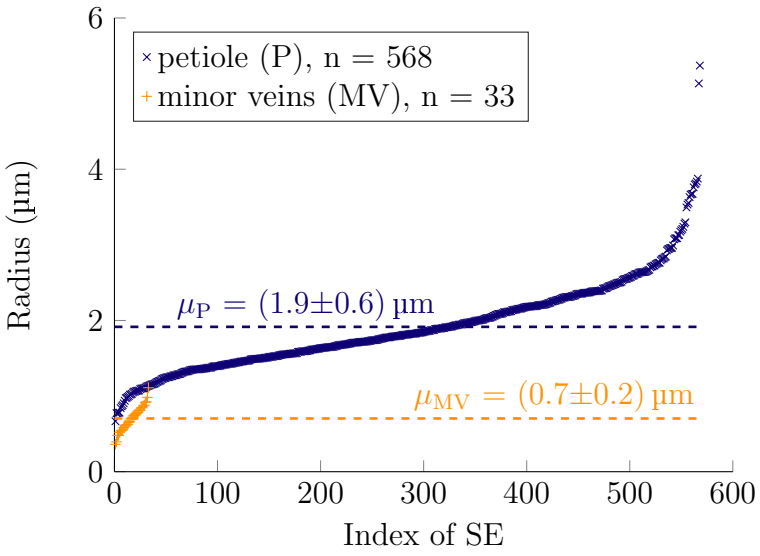

Figure 6.17: Comparing radii of individual sieve elements in minor veins (orange) and petiole (blue). SE radii are sorted ascending in size.

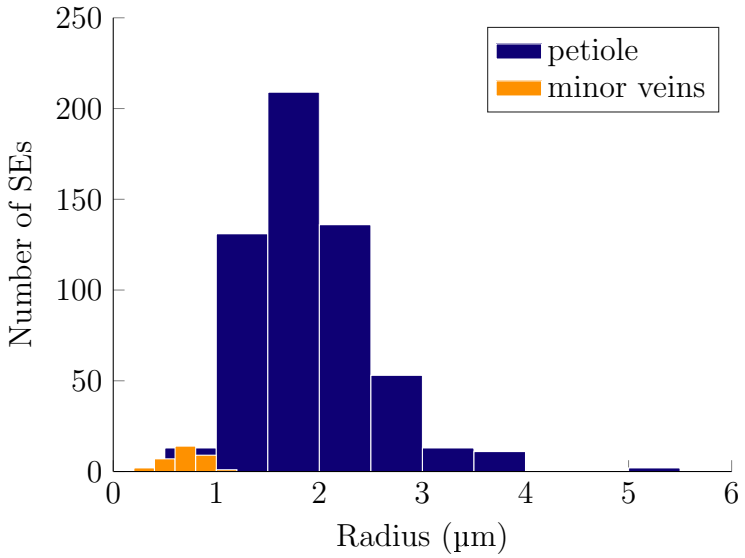

Figure 6.18: Comparing radii of individual sieve elements in minor veins (orange) and petiole (blue). Bin width 0.5 µm (petiole) and 0.2 µm (minor veins).

Bibliography

The nobel prize in chemistry 1901, nobelprize.org. Nobel Media AB. Web. `http://www.nobelprize.org/nobel_prizes/chemistry/laureates/1901/`, 2014. Accessed: 8 Mar 2016.

Geoffrey K Aldis. The unstirred layer during osmotic flow into a tubule. *Bulletin of mathematical biology*, 50(5):531–545, 1988.

C Kevin Boyce. The evolutionary history of roots and leaves. In N Michele Holbrook and Maciej A Zwieniecki, editors, *Vascular Transport in Plants*, chapter 23, pages 479–500. Elsevier, San Diego, CA, 2005.

Henrik Bruus. *Theoretical microfluidics*. Oxford University Press, New York, 2008.

Tessa M Burch-Smith and Patricia C Zambryski. Plasmodesmata paradigm shift: regulation from without versus within. *Annual review of plant biology*, 63:239–260, 2012.

Li-Qing Chen, Xiao-Qing Qu, Bi-Huei Hou, Davide Sosso, Sonia Osorio, Alisdair R Fernie, and Wolf B Frommer. Sucrose efflux mediated by sweet proteins as a key step for phloem transport. *Science*, 335(6065):207–211, 2012.

Maarten JM Christenhusz and James W Byng. The number of known plants species in the world and its annual increase. *Phytotaxa*, 261(3):201–217, 2016.

A Lawrence Christy and Jack M Ferrier. A mathematical treatment of munch's pressure-flow hypothesis of phloem translocation. *Plant Physiology*, 52(6):531–538, 1973.

Jean Comtet, Robert Turgeon, and Abraham D Stroock. Phloem loading through plasmodesmata: a biophysical analysis. *arXiv preprint arXiv:1603.04058*, 2016.

Joanne M Dannenhoffer, Wesley Ebert Jr, and Ray F Evert. Leaf vasculature in barley, Hordeum vulgare (poaceae). *American Journal of Botany*, pages 636–652, 1990.

Panadda Dechadilok and William M Deen. Hindrance factors for diffusion and convection in pores. *Industrial & Engineering Chemistry Research*, 45(21):6953–6959, 2006.

Sandra Díaz, Jens Kattge, Johannes HC Cornelissen, Ian J Wright, Sandra Lavorel, Stéphane Dray, Björn Reu, Michael Kleyer, Christian Wirth, I Colin Prentice, et al. The global spectrum of plant form and function. *Nature*, 529(7585):167–171, 2016.

Biao Ding, Robert Turgeon, and Mandayam V Parthasarathy. Substructure of freeze-substituted plasmodesmata. *Protoplasma*, 169(1-2):28–41, 1992.

Julia Dölger, Hanna Rademaker, Johannes Liesche, Alexander Schulz, and Tomas Bohr. Diffusion and bulk flow in phloem loading: a theoretical analysis of the polymer trap mechanism for sugar transport in plants. *Physical Review E*, 90(4): 042704, 2014.

Walter Eschrich, Ray F Evert, and John H Young. Solution flow in tubular semipermeable membranes. *Planta*, 107(4):279–300, 1972.

Ray F Evert. *Esau's plant anatomy: meristems, cells, and tissues of the plant body: their structure, function, and development*. John Wiley & Sons, 2006.

Christine Faulkner, Elena Petutschnig, Yoselin Benitez-Alfonso, Martina Beck, Silke Robatzek, Volker Lipka, and Andrew J Maule. Lym2-dependent chitin perception limits molecular flux via plasmodesmata. *Proceedings of the National Academy of Sciences*, 110(22):9166–9170, 2013.

Donald B Fisher. The estimated pore diameter for plasmodesmal channels in the abutilon nectary trichome should be about 4 nm, rather than 3 nm. *Planta*, 208(2): 299–300, 1999.

Yuri Gamalei. The symplastic connections in fraxinus minor veins. *Botan. Zhurn.(Leningrad)*, 59:980–988, 1974.

Yuri Gamalei. Structure and function of leaf minor veins in trees and herbs. *Trees*, 3 (2):96–110, 1989.

Yuri Gamalei. Phloem loading and its development related to plant evolution from trees to herbs. *Trees*, 5(1):50–64, 1991.

Thomas Graham. The bakerian lecture: on osmotic force. *Philosophical Transactions of the Royal Society of London*, 144:177–228, 1854.

Nicole Grignon, Bruno Touraine, and Monique Durand. 6 (5) carboxyfluorescein as a tracer of phloem sap translocation. *American Journal of Botany*, pages 871–877, 1989.

Louise S Haaning, Kaare H Jensen, Claus Hélix-Nielsen, Kirstine Berg-Sørensen, and Tomas Bohr. Efficiency of osmotic pipe flows. *Physical Review E*, 87(5):053019, 2013.

Edith Haritatos, Felix Keller, and Robert Turgeon. Raffinose oligosaccharide concentrations measured in individual cell and tissue types in cucumis melo l. leaves: implications for phloem loading. *Planta*, 198(4):614–622, 1996.

Leonard Horwitz. Some simplified mathematical treatments of translocation in plants. *Plant Physiology*, 33(2):81, 1958.

Kaare H Jensen and Maciej A Zwieniecki. Physical limits to leaf size in tall trees. *Physical review letters*, 110(1):018104, 2013.

Kaare H Jensen, Emmanuelle Rio, Rasmus Hansen, Christophe Clanet, and Tomas Bohr. Osmotically driven pipe flows and their relation to sugar transport in plants. *Journal of Fluid Mechanics*, 636:371–396, 2009.

Kaare H Jensen, Jonghwan Lee, Tomas Bohr, Henrik Bruus, N Michele Holbrook, and Maciej A Zwieniecki. Optimality of the Münch mechanism for translocation of sugars in plants. *Journal of the Royal Society Interface*, 8(61):1155–1165, 2011.

Kaare H Jensen, Kirstine Berg-Sørensen, Søren MM Friis, and Tomas Bohr. Analytic solutions and universal properties of sugar loading models in Münch phloem flow. *Journal of theoretical biology*, 304:286–296, 2012a.

Kaare H Jensen, Johannes Liesche, Tomas Bohr, and Alexander Schulz. Universality of phloem transport in seed plants. *Plant, cell & environment*, 35(6):1065–1076, 2012b.

Kaare H Jensen, Jessica A Savage, and N Michele Holbrook. Optimal concentration for sugar transport in plants. *Journal of The Royal Society Interface*, 10(83):20130055, 2013.

Kaare H Jensen, Kirstine Berg-Sørensen, Henrik Bruus, N Michele Holbrook, Johannes Liesche, Alexander Schulz, Maciej A Zwieniecki, and Tomas Bohr. Sap flow and sugar transport in plants. *Reviews of modern physics*, in press, 2016.

Kiyosada Kawai and Naoki Okada. How are leaf mechanical properties and water-use traits coordinated by vein traits? A case study in Fagaceae. *Functional Ecology*, 2015.

Ora Kedem and Aharon Katchalsky. Thermodynamic analysis of the permeability of biological membranes to non-electrolytes. *Biochimica et biophysica Acta*, 27:229–246, 1958.

Jan Knoblauch, Daniel L Mullendore, Kaare H Jensen, and Michael Knoblauch. Pico gauges for minimally invasive intracellular hydrostatic pressure measurements. *Plant physiology*, 166(3):1271–1279, 2014.

Michael Knoblauch, Jan Knoblauch, Daniel L Mullendore, Jessica A Savage, Benjamin A Babst, Sierra D Beecher, Adam C Dodgen, Kaare H Jensen, and N Michele Holbrook. Testing the münch hypothesis of long distance phloem transport in plants. *eLife*, 5:e15341, 2016. doi: 10.7554/eLife.15341.

Kirsten Knox, Pengwei Wang, Verena Kriechbaumer, Jens Tilsner, Lorenzo Frigerio, Imogen Sparkes, Chris Hawes, and Karl Oparka. Putting the squeeze on plasmodesmata: a role for reticulons in primary plasmodesmata formation. *Plant physiology*, 168(4):1563–1572, 2015.

Georges Kunstler, Daniel Falster, David A Coomes, Francis Hui, Robert M Kooyman, Daniel C Laughlin, Lourens Poorter, Mark Vanderwel, Ghislain Vieilledent, S Joseph Wright, et al. Plant functional traits have globally consistent effects on competition. *Nature*, 529(7585):204–207, 2016.

Michael LaBarbera. Principles of design of fluid transport systems in zoology. *Science*, 249(4972):992–1000, 1990.

André Lacointe and Peter EH Minchin. Modelling phloem and xylem transport within a complex architecture. *Functional Plant Biology*, 35(10):772–780, 2008.

Johannes Liesche and Alexander Schulz. Modeling the parameters for plasmodesmal sugar filtering in active symplasmic phloem loaders. *Frontiers in plant science*, 4: 207, 2013.

Johannes Liesche and Alexander Schulz. Quantification of plant cell coupling with live-cell microscopy. *Plasmodesmata: Methods and Protocols*, pages 137–148, 2015.

Johannes Liesche, Helle Juel Martens, and Alexander Schulz. Symplasmic transport and phloem loading in gymnosperm leaves. *Protoplasma*, 248(1):181–190, 2011.

Johannes Liesche, Carel Windt, Tomas Bohr, Alexander Schulz, and Kaare H Jensen. Slower phloem transport in gymnosperm trees can be attributed to higher sieve element resistance. *Tree physiology*, page tpv020, 2015.

William J Lucas and Robert L Gilbertson. Plasmodesmata in relation to viral movement within leaf tissues. *Annual review of phytopathology*, 32(1):387–415, 1994.

Christophe Maurel. Aquaporins and water permeability of plant membranes. *Annual review of plant biology*, 48(1):399–429, 1997.

Katherine A McCulloh, John S Sperry, and Frederick R Adler. Water transport in plants obeys murray's law. *Nature*, 421(6926):939–942, 2003.

Ernst Münch. *Die Stoffbewegungen in der Pflanze*. G. Fischer, Jena, 1930.

Cecil D Murray. The physiological principle of minimum work i. the vascular system and the cost of blood volume. *Proceedings of the National Academy of Sciences*, 12 (3):207–214, 1926.

Timothy Nelson and Nancy Dengler. Leaf vascular pattern formation. *The Plant Cell*, 9(7):1121, 1997.

Park S Nobel. *Physicochemical and environmental plant physiology*. Academic press, Boston, 4 edition, 2009.

Jean-Antoine Nollet. Recherches sur les causes du bouillonnement des liquides. *Histoire de l'Academie Royale des Sciences, Paris Annee*, 1748(57):1752, 1752.

Mark E Olson and Julieta A Rosell. Vessel diameter–stem diameter scaling across woody angiosperms and the ecological causes of xylem vessel diameter variation. *New Phytologist*, 197(4):1204–1213, 2013.

Soner Öner-Sieben and Gertrud Lohaus. Apoplastic and symplastic phloem loading in quercus robur and fraxinus excelsior. *Journal of experimental botany*, 65(7):1905–1916, 2014.

OpenSCAD. The Programmers Solid 3D CAD Modeller. `http://www.openscad.org`, 2016. Accessed: 31 Aug 2016.

John B Passioura. Translocation and the diffusion equation [of sugars in the phloem]. In *Transport and Transfer Processes in Plants, Canberra (Australia), Dec 1975*. Academic Press, 1976.

Kelly V Pescod, W Paul Quick, and Angela E Douglas. Aphid responses to plants with genetically manipulated phloem nutrient levels. *Physiological Entomology*, 32 (3):253–258, 2007.

David M Pharr and Harriet N Sox. Changes in carbohydrate and enzyme levels during the sink to source transition of leaves of cucumis sativus l., a stachyose translocator. *Plant science letters*, 35(3):187–193, 1984.

Jarmila Pittermann and John Sperry. Tracheid diameter is the key trait determining the extent of freezing-induced embolism in conifers. *Tree Physiology*, 23(13):907–914, 2003.

Hanna Rademaker, Kaare H Jensen, Helle J Martens, Alexander Schulz, and Tomas Bohr. The microfluidic network of a plant leaf. *Gallery of fluid motion. 68th annual meeting of the APS division of fluid dynamics*, 2015. doi: 10.1103/APS.DFD.2015.GFM.P0040.

Peter H Raven, Ray F Evert, and Susan E Eichhorn. *Biology of plants*. Macmillan, 7 edition, 2005.

Emilie A Rennie and Robert Turgeon. A comprehensive picture of phloem loading strategies. *Proceedings of the National Academy of Sciences*, 106(33):14162–14167, 2009.

Kay Robinson-Beers and Ray F Evert. Fine structure of plasmodesmata in mature leaves of sugarcane. *Planta*, 184(3):307–318, 1991.

Henrik Ronellenfitsch, Jana Lasser, Douglas C Daly, and Eleni Katifori. Topological phenotypes constitute a new dimension in the phenotypic space of leaf venation networks. *PLoS Comput Biol*, 11(12):e1004680, 2015a.

Henrik Ronellenfitsch, Johannes Liesche, Kaare H Jensen, N Michele Holbrook, Alexander Schulz, and Eleni Katifori. Scaling of phloem structure and optimality of photoassimilate transport in conifer needles. *Proceedings of the Royal Society of London B: Biological Sciences*, 282(1801):20141863, 2015b.

Sandra H Russell and Ray Franklin Evert. Leaf vasculature in zea mays l. *Planta*, 164 (4):448–458, 1985.

Lawren Sack, Christine Scoffoni, Athena D McKown, Kristen Frole, Michael Rawls, J Christopher Havran, Huy Tran, and Thusuong Tran. Developmentally based scaling of leaf venation architecture explains global ecological patterns. *Nature Communications*, 3:837, 2012.

Klaus Schmitz, Beate Cuypers, and Marianne Moll. Pathway of assimilate transfer between mesophyll cells and minor veins in leaves of Cucumis melo L. *Planta*, 171 (1):19–29, 1987.

Per F Scholander, Harold T Hammel, Edda D Bradstreet, and Edvard A Hemmingsen. Sap pressure in vascular plants. *Science*, 148(3668):339–346, 1965.

Alexander Schulz and Gary A Thompson. Phloem structure and function. *eLS*, 2009.

David Stephenson and Duncan A Lockerby. A generalized optimization principle for asymmetric branching in fluidic networks. 472(2191):20160451, 2016.

Abraham D Stroock, Vinay V Pagay, Maciej A Zwieniecki, and N Michele Holbrook. The physicochemical hydrodynamics of vascular plants. *Annual Review of Fluid Mechanics*, 46:615–642, 2014.

Tsun-kay Jackie Sze, Prashanta Dutta, and Jin Liu. Study of protein facilitated water and nutrient transport in plant phloem. *Journal of Nanotechnology in Engineering and Medicine*, 4(3):031005, 2013.

Tsun-kay Jackie Sze, Jin Liu, and Prashanta Dutta. Numerical modeling of flow through phloem considering active loading. *Journal of Fluids Engineering*, 136(2): 021206, 2014.

Lincoln Taiz, Eduardo Zeiger, Ian M Møller, and Angus S Murphy. *Plant physiology and development*. Sinauer, 6 edition, 2015.

Matthew V Thompson and N Michele Holbrook. Application of a single-solute non-steady-state phloem model to the study of long-distance assimilate transport. *Journal of Theoretical Biology*, 220(4):419–455, 2003a.

Matthew V Thompson and N Michele Holbrook. Scaling phloem transport: water potential equilibrium and osmoregulatory flow. *Plant, Cell & Environment*, 26(9): 1561–1577, 2003b.

Robert Turgeon. The sink-source transition in leaves. *Annual review of plant biology*, 40(1):119–138, 1989.

Robert Turgeon. The puzzle of phloem pressure. *Plant physiology*, 154(2):578–581, 2010a.

Robert Turgeon. The role of phloem loading reconsidered. *Plant physiology*, 152(4): 1817–1823, 2010b.

Robert Turgeon and Peter K Hepler. Symplastic continuity between mesophyll and companion cells in minor veins of mature cucurbita pepo l. leaves. *Planta*, 179(1): 24–31, 1989.

Robert Turgeon and Richard Medville. The absence of phloem loading in willow leaves. *Proceedings of the National Academy of Sciences*, 95(20):12055–12060, 1998.

Aart JE Van Bel, Wilhelmus JP Van Kesteren, and C Papenhuijzen. Ultrastructural indications for coexistence of symplastic and apoplastic phloem loading in commelina benghalensis leaves. *Planta*, 176(2):159–172, 1988.

Jacobus Van't Hoff. The function of osmotic pressure in the analogy between solutions and gases. *Proceedings of the Physical Society of London*, 9(1):307, 1887.

Kenneth L Webb and J William A Burley. Stachyose translocation in plants. *Plant physiology*, 39(6):973, 1964.

Leslie A Weisberg, Larry E Wimmers, and Robert Turgeon. Photoassimilate-transport characteristics of nonchlorophyllous and green tissue in variegated leaves of coleus blumei benth. *Planta*, 175(1):1–8, 1988.

Carel W Windt, Frank J Vergeldt, P Adrie De Jager, and Henk Van As. MRI of long-distance water transport: a comparison of the phloem and xylem flow characteristics and dynamics in poplar, castor bean, tomato and tobacco. *Plant, Cell & Environment*, 29(9):1715–1729, 2006.

Cankui Zhang, Lu Han, Thomas L Slewinski, Jianlei Sun, Jing Zhang, Zeng-Yu Wang, and Robert Turgeon. Symplastic phloem loading in poplar. *Plant physiology*, 166 (1):306–313, 2014.

Maciej A Zwieniecki, Howard A Stone, Andrea Leigh, C Kevin Boyce, and N Michele Holbrook. Hydraulic design of pine needles: one-dimensional optimization for single-vein leaves. *Plant, Cell & Environment*, 29(5):803–809, 2006.